Output-feedback design for non-smooth mechanical systems: Control synthesis and experiments

PROEFSCHRIFT

ter verkrijging van de graad van doctor aan de
Technische Universiteit Eindhoven,
op gezag van de Rector Magnificus, prof.dr.ir. C.J. van Duijn,
voor een commissie aangewezen door het College voor
Promoties in het openbaar te verdedigen op
dinsdag 11 september 2007 om 16.00 uur

door

Apostolos Doris

geboren te Thessaloniki, Griekenland

Dit proefschrift is goedgekeurd door de promotor:

prof.dr. H. Nijmeijer

Copromotoren:
dr.ir. N. van de Wouw
en
dr.ir. W.P.M.H. Heemels

A catalogue record is available from the Eindhoven University of Technology Library

Doris, Apostolos

Output-feedback feedback for non-smooth mechanical systems: Control synthesis and experiments / by
Apostolos Doris. – Eindhoven : Technische Universiteit Eindhoven, 2007.
Proefschrift. – ISBN: 978-90-386-1065-8
Subject headings: nonlinear systems/ output feedback/ disturbance attenuation / stabilization/ observer design/ convergent systems

Promotor: prof.dr. H. Nijmeijer

Copromotoren:

dr.ir. N. van de Wouw
dr.ir. W.P.M.H. Heemels

Kerncommissie:

dr. B. Brogliato
prof.dr.ir. D. Rixen
prof.dr.ir. M. Steinbuch

This Ph.D. work is supported by the SICONOS European project
(IST-2001-37172).

Contents

1

Introduction

1.1 Motivation

In the last decade, the modelling of non-smooth engineering systems has received wide attention. With the scope of mechanical systems, unilateral (flexible) constraints, friction and impact phenomena typically induce such non-smoothness. Depending on the degree of non-smoothness related models can be divided in three classes: 1) models described by differential equations with a continuous though non-smooth vectorfield; 2) models described by differential equations with a discontinuous right-hand side and 3) models with (discontinuous) jumps in the state variables. Many mathematical formalisms have been developed to describe these classes of systems such as piecewise affine (PWA) and switched systems [23; 40; 67; 82; 109; 119; 126; 131], differential inclusions [10; 19; 42; 116], complementarity systems [18; 49; 56; 89; 91; 105], measured differential inclusions [20; 48; 50; 90; 128] and hybrid systems [27; 68; 83; 117; 130]. The PWA and switched systems and DI are models of class 1 and 2, while measured differential inclusions and hybrid systems fit typically all three classes.

Examples of engineering systems that can be modelled by continuous, non-smooth differential equations are mechanical systems with one-sided supports. In this context, one can think of tower cranes, suspension bridges [33], snubbers on solar panels on satellites [127], floating platforms for oil exploration [124], safety stops in car suspensions, etc. In many cases, the one-sided support has affine or linear restoring characteristics and, consequently, these systems can be effectively described by piecewise smooth systems such as PWA or piecewise linear (PWL) systems. The second class of models consisting of differential equations with discontinuous right-hand sides can describe mechanical systems

with dry friction. More specifically, one can think of industrial robots, drilling rigs (see [78] and [129]), turbine blade dampers [107], curve squealing of railway vehicles [28], simple earthquake models, accurate mirror positioning systems on satellites and many more. The third class of models encompasses mechanical systems with unilateral constraints and impacts, [18; 48; 80; 89; 91; 106].

Non-smooth models within engineering are becoming more and more important. The reason is that these models have attractive properties as they can model many complex engineering systems accurately with fairly simple models. Recent work on the validation of non-smooth models show that relatively simple models for contact and friction result in accurate predictions of the system's behavior e.g. [88]. However, a consequence of adopting non-smooth modelling is the fact that also dedicated analysis and control synthesis techniques that can deal with the non-smoothness of the system, should be developed [18; 42; 80; 82; 130].

The analysis and control techniques to be developed for non-smooth mechanical systems have to be able to deal with disturbances as these are commonly present. In this context, one can think of road excitations of vehicle suspensions, wind exciting bridges, earthquakes exciting civil structures, mass-unbalance in rotor dynamics systems, acoustic noise perturbing sensitive measurement systems etc. These disturbances, are responsible for unwanted vibrations by exciting the systems resonances. It is well known, that resonating elements may exhibit responses with very high amplitudes. Such a resonance phenomenon often causes damage to the mechanical structure and is, therefore, unwanted. Another classical problem of mechanical systems is the material fatigue due to repetitive periodic excitations. Such periodic disturbances can cause significant damage, despite their relatively small amplitudes and frequencies far from the resonance frequencies of the system. Besides causing system damage or failure, vibrations are detrimental to the positioning performance in mechanical motion systems.

Besides external perturbations, also self-exciting mechanisms may cause unwanted vibrations. Well-known examples of causes for self-excited vibrations are the regenerative effect in milling [3], [125] or the presence of friction in motion systems [2; 60; 96; 128]. Indeed, the presence of friction in the moving elements of a mechanical system may lead to vibrations and other undesirable phenomena such as excessive wear of machine components, surface damage and kinetic energy dissipation into heat and noise.

Clearly, the attenuation of such vibrations, either caused by external or internal factors is of high interest to guarantee the safety of operation, positioning performance and high life cycle of a wide variety of mechanical systems. In general, one can attack vibrations by either passive means (e.g. dampers) and/or by active means (control). For instance, a classical way to attenuate the vibrations of a resonating element on a specific frequency range is by mounting an additional element on it such that the resonance is shifted out of this range,

see e.g. [14; 61]. An active approach to deal with vibrations in mechanical systems is the application of a control action in the system, see for instance [34; 62].

In the present thesis, the focus is on developing techniques for vibration attenuation in non-smooth mechanical systems by means of control. Firstly, we address the disturbance attenuation problem for PWL and PWA systems. Here, the application area of interest is perturbed flexible mechanical systems with PWL (one-sided) restoring characteristics. Secondly, the stabilization problem for systems with discontinuous vectorfields is examined. In the latter context, the focus is on applications of mechanical systems with set-valued friction characteristics, where the friction is non-collocated with the actuation.

1.2 Disturbance attenuation for continuous PWA systems

Disturbance attenuation for continuous PWA and PWL (mechanical) systems is an important control problem to be solved to ensure satisfactory performance of these systems and to avoid damage to the structures. Consider, for example, a suspension bridge as depicted in Figure 1.1(a). As mentioned before, such a bridge is a typical example of a mechanical system with PWL restoring characteristics and exogenous inputs. More specifically, the bridge in Figure 1.1(a) consists of a roadbed, three towers and a number of suspension cables that support the construction [22]. Commonly, the behavior of the suspension cables is assumed to be piecewise linear (see Figure 1.1(b)) and, consequently, the dynamics of the bridge can be described by a combination of linear regimes (PWL dynamics) that are mainly characterized by the stiffness of the roadbed and the cables under tension. Common excitations acting on the bridge are strong winds [110], earthquakes [21] and moving vehicles. Such excitations may lead to high amplitude vertical vibrations that can damage the bridge structure. Therefore, such vibrations should be attenuated.

In the recent literature related to PWA systems, many results are available for stability analysis and control synthesis. More specifically, in [67], a framework is developed, based on piecewise quadratic Lyapunov functions, to analyse the stability of piecewise affine (PWA) systems. In [109], this framework is extended for performance analysis and optimal control. In [54], a study related to the stability analysis and controller design for PWL systems is presented. This study uses common quadratic and piecewise quadratic Lyapunov functions for stability analysis purposes. In the case of a common quadratic Lyapunov function, both the stability analysis and the state-feedback synthesis can be expressed as a convex optimization problem based on constraints in linear matrix inequality (LMI) form. However, it has been pointed out that this is difficult in the case of a piecewise quadratic Lyapunov function. A solution for

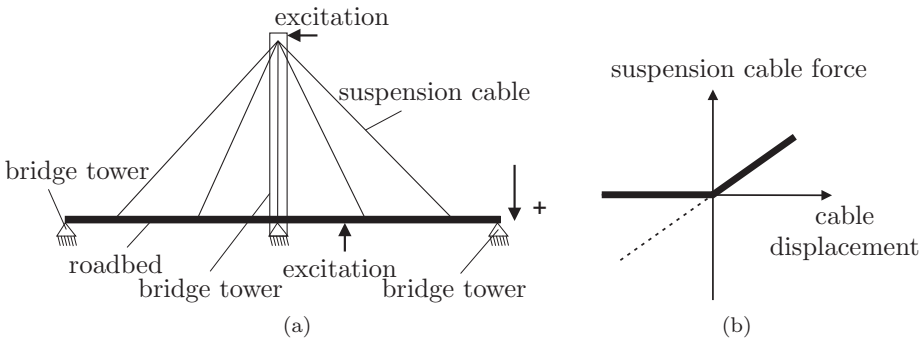

Figure 1.1: (a) Scheme of a suspension bridge. [35] (b) Suspension cable force vs roadbed displacement.

---

this problem has been given in [39] and [112]. In [39], a H_∞ controller synthesis method based on a piecewise quadratic Lyapunov function that can be cast in the form of solving a set of LMIs using standard LMI solvers is presented. In [112], a method used to design state- and output-feedback controllers with constraints on the smoothness and continuity of the piecewise quadratic Lyapunov function is shown. However, the controller design of [112] is restricted, as it is mentioned in [112], by two fundamental assumptions: 1) there are no sliding modes at the hyperplane boundaries between regions with different affine dynamics, 2) the examined PWL system and the controller are always in the same region. In [113], the case in which the assumptions in [112] are violated is examined and a general stability analysis of the closed-loop system for that case is presented.

A common characteristic of the papers [54; 67; 109; 112; 113] is that they study stability of the equilibrium of a PWL system for zero inputs. Work on the stability properties of the steady-state solutions of PWL/PWA systems with time-varying inputs (e.g disturbances) can be found in the literature based on the convergence property, see [100; 102; 103]. The concept of convergence was first introduced in [32] (see also [98]) for nonlinear systems with inputs. A system with the convergence property has a unique, bounded, globally asymptotically steady-state solution which is determined only by the system input and does not depend on the initial conditions. In [102], the notion of convergent systems is extended to the notion of (uniformly, exponentially) convergent systems and input-to-state convergent systems. Based on the extensions made in [102], the design of a controller that renders a non-convergent system convergent, is pursued as well.

So far, results related to the control design for PWL and PWA systems aiming at disturbance attenuation were given, among others, in [39; 54; 109]. The

performance results of these papers, which are based on a common quadratic or piecewise quadratic Lyapunov functions, provide an upper bound for the system output by bounding the $\mathcal{L}_2$ gain from the disturbance input to the system output. Nevertheless, these results lack generality in the sense that they have been derived under the assumption of zero initial conditions. A method to incorporate non-zero initial conditions in the $\mathcal{L}_2$ gain analysis is proposed in [47] for a class of nonlinear systems. This paper is based on the notion of incremental stability that is described in [4; 44]. All the aforementioned bounds can be used to evaluate the disturbance attenuation properties of different controllers to a certain extent. More specifically, for a class of disturbances satisfying a bound, a common bound on the (signal/norm) output can be given. However, as we will advocate in this thesis, this approach is rather conservative when one is interested in periodic disturbances. Note in this context, that many disturbances can be modeled as being periodic (such as e.g. mass-unbalance excitations, engine vibrations, etc). In this thesis, we will propose to explore the concept of convergence (guaranteeing unique bounded steady-state responses) to investigate the disturbance attenuation properties of controllers for PWA systems excited by periodic disturbances. In this manner, more specific and less conservative performance indications will be obtained for periodic disturbances.

Most of the aforementioned results have been successfully applied on simple simulation examples. However, often the experimental implementation and possible drawbacks remain to be explored. Therefore, the current work will also focus on the experimental implementation and validation of the developed control strategies.

1.3 Stabilization of systems with non-collocated friction and actuation

As already mentioned, a second commonly encountered cause for vibrations in mechanical motion systems is friction. In this thesis, we will address the stabilization problem of systems with friction in order to avoid such unwanted friction-induced vibrations.

In general, the stabilization of systems with friction is a complex control problem which needs to be solved to avoid damage to the system's structure and to ensure high positioning performance. The complexity of this control problem is due to the fact that friction is a very sensitive phenomenon. More specifically, changes in conditions such as humidity, contamination, temperature, etc., can cause significant changes to the friction characteristics. Therefore, to stabilize a system with friction by means of control, the controlled system should exhibits certain robustness properties with respect to changes in the friction characteristics.

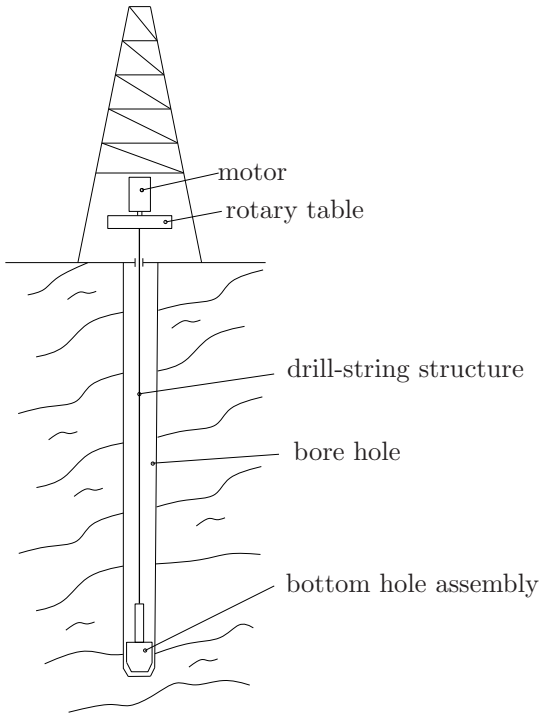

Figure 1.2: A rotary drilling system.

Control techniques focusing on mechanical systems with discontinuities due to friction and collocated actuation aim commonly at compensating the friction. Friction compensation techniques are, commonly, divided in two categories: non-model-based friction compensation and model-based friction compensation. Classical examples of non-model-based friction compensation are Dither and impulsive control, see [12] and [7], respectively. In [8; 26; 97], model-based-friction compensation techniques with adaptation mechanisms for the friction model parameters are presented. In [26], the proposed results are applicable for velocities around zero and are validated experimentally on a robot manipulator. An approach with friction compensation for a two-body system with, possibly discontinuous, load friction and joint flexibility and damping is discussed in [123]. A model reference adaptive control scheme is presented by using a controller that adapts the friction compensation based on friction changes. Some model-based friction compensation techniques based on Dahl and LuGre dynamic friction models are proposed in [75; 134] and in [25], respectively. Moreover, model-based-friction compensation techniques that do not require accurate velocity measurements as the aforementioned techniques

are given in [43; 121]. Finally, an observer-based friction compensation technique is proposed in [84; 108]. In [84], such technique is applied to a controlled one-link robot. It is shown that friction overcompensation leads the system to limit cycling and friction under-compensation leads the system to residual steady-state errors (an equilibrium set).

To stabilize a system with *non-collocated* friction and actuation around a chosen setpoint is an even more complex and difficult control problem. The additional complexity of this problem is due to the fact that the friction and actuation are non-collocated. As a consequence, direct cancellation (through friction compensation) of the friction is not possible. The stabilization of such systems can be particularly challenging because, on the one hand, we have to deal with a phenomenon such as friction and, on the other hand, in most of the cases there are dynamics (due to limited stiffness) between the actuated element and the element subject to friction. Classical examples of this type of systems are rotary drilling systems, printing systems and many more.

Consider, for example, the rotary drilling system which is schematically depicted in Figure 1.2. This system consists of a tower, a motor mounted to a rotary table, a drill-string structure and the bottom-hole assembly (including the drill-bit), see [65], [66], [78], [92]. The motor enforces a constant rotational speed to the rotary table that is used as a unit to store kinetic energy. The rotary table is, in turn, connected to the drill-string structure which is connected to the bottom-hole-assembly. The drill-string consists of pipes that can be as long as 11km. Due to the large length of the pipes, the drill-string is a low stiffness connection between the upper and lower part of the system. The bottom-hole-assembly consists of a drill-bit that creates the borehole. Due to the interaction of the drill-bit with the borehole the first is subject to contact forces with possibly discontinuous characteristics (for example friction and cutting forces). This interaction is responsible for complex and undesirable nonlinear dynamical phenomena, such as so-called stick-slip vibrations, whirl-type vibrations, bit bouncing and many more, see for example [66; 78; 88; 92].

There are several active and passive methods aiming at suppressing stick-slip vibrations in rotary drilling systems. In [104; 115], it is shown that by manipulating the different drilling parameters such as changing the rotational speed of the rotary table and the weight-on-bit, or by introducing an additional friction, the stick-slip motion can be suppressed. Similar alternatives for stick-slip vibration suppression are proposed in [1; 31; 52; 66; 93]. More specifically, in [1; 93; 104], the design of a PID controller for controlling the rotational speed is presented. In [52; 66; 115], the use of a vibration absorber at the top of the drill-string is proposed. Finally, in [31; 93], it is shown that the weight on the bit can significantly suppress the undesirable stick-slip behavior on a drilling system.

Another example of the considered type of systems is a printing system as depicted in Figure 1.3. This system consists of a motor, two wheels, a belt,

a printhead and a guidance for the printhead (see also [85]). The motor is connected to one of the wheels that drives the flexible belt. The two wheels are connected with each other by the belt. The printhead is mounted on the belt. The printhead guidance constrains the motion of the printhead in one dimension. Due to the presence of friction in the bearings of the wheels and between the printhead and the printhead guidance both the printhead speed and positioning accuracy are rather limited. Hence, a control design able to cope with the non-collocated friction (between the printhead and the printhead guidance) and actuation (applied by the motor in one of the wheels) and guarantee high accuracy in printhead positioning is desirable.

An approach to deal with the modeling of friction in general is the use of set-valued frictional force laws [48]. In literature, it has been shown that simple discontinuous, set-valued friction models have proven to capture the dynamics of many systems accurately, see for example [79; 84; 87; 88]. In this thesis we will also adopt a discontinuous (set-valued) modelling approach for friction, since, such an approach is able to describe real sticking behavior, it has proven to be predictive and it provides relatively simple models, which are favorable from analysis and control synthesis perspective. Note that the focus in our approach is in both low and high velocities while, for example, in [26] is only at low velocities. The choice for such set-valued frictional force laws in dynamics commonly leads to models in terms of differential inclusions, see [17; 80; 91; 106; 128]. In [42], [16], [10] and [111], an extensive analysis treatment of results for differential inclusions is presented. Stability theory for differential inclusions has received a lot of attention in [19; 42; 128]. Relevant results for control purposes are presented in [19; 51].

Due to the fact that direct friction compensation is not possible in the examined system, one may opt to exploit well-known control strategies for smooth nonlinear systems to tackle the system at hand. For systems with smooth nonlinear dynamics a vast amount of literature exists that covers the subject of the stability and stabilization of such systems. Some of the well known works in this field are [63; 72; 95; 116]. More specifically, a technique for stabilization of a class of nonlinear systems is so-called feedback linearization, see [72; 95]. By applying input-output linearization to a nonlinear system we can render its input-output behavior linear. Moreover, by using full-state linearization we can render the entire system linear after a suitable feedback and coordinate transformations. Then, standard linear control theory can be applied to stabilize the linearized system. However, both linearization methods are only applicable to smooth nonlinear systems (systems without discontinuities, e.g. due to friction). Another method for nonlinear system stabilization is back-stepping [72]. This method requires the existence of the derivatives of the system's nonlinearities with respect to the states and it is only applicable to smooth nonlinear systems. An extension to non-smooth systems is given in [122]. In [122], the proposed integrator back-stepping procedure is based on Lyapunov

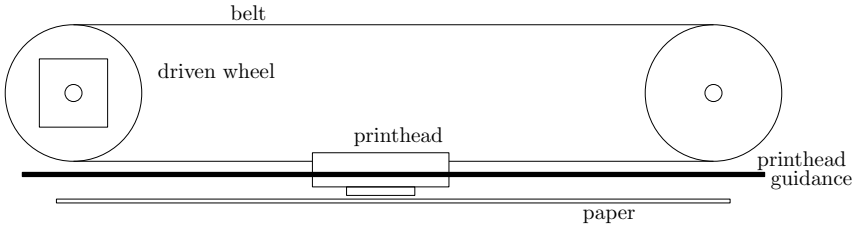

Figure 1.3: A printhead driven via a belt.

stability analysis for non-smooth systems. The drawback of this method is that it may lead to a complex control law that is difficult to implement in practice. An adapted back-stepping method suitable for systems with non-differentiable, bounded, uncertain nonlinearities is given in [76]. This method is called the multi-state back-stepping approach and it yields the design of a variable structure control in each step of the procedure. This control strategy consists of a sliding mode control and reaching control and it is applicable to a restricted class of systems with friction; namely, single-input-single-output systems where the friction forces are relatively small. Given the fact that in the systems we consider the friction will actually be one of the dominant forces this design procedure is not applicable. In [5; 6], stabilization techniques for locally Lipschitzian systems with slope-restricted nonlinearities are discussed. Due to the fact that the models for systems under study require large discontinuities to accurately describe the friction, these systems do not belong to the class of locally Lipschitzian systems. Hence we cannot apply the proposed designs.

1.4 Contribution of the thesis

This thesis presents observer-based output-feedback control designs for classes of non-smooth systems with (disturbance) inputs. We mainly focus on the disturbance rejection for continuous-time PWA systems and the stabilization problem for systems with discontinuous right-hand sides (in particular we study mechanical motion systems with non-collocated friction and actuation). Moreover, we implement the proposed control designs on experimental setups to show the strengths and weaknesses of the proposed output-feedback controllers beyond their theoretical importance and demonstrate the value of non-smooth modeling and observer-based controllers for engineering systems in practice.

For the experimental validation of the theoretical results for PWL systems, we have used an experimental setup as in Figure 1.4. This setup consists of a flexible steel beam, which is clamped on two sides and is supported at a location by a one-sided linear spring. Due to the one-sided spring, the beam exhibits complex steady-state dynamics, such as the co-existence of steady-state solu-

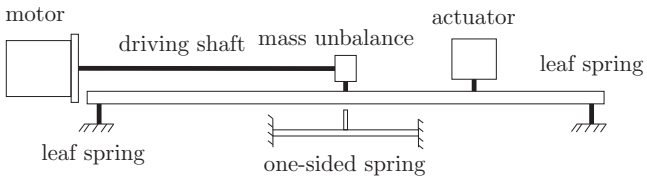

Figure 1.4: Schematic representation of the experimental PWL beam system.

tions (both harmonic and sub-harmonic) with high amplitude and bifurcations points, see e.g. [58]. The configuration of the examined setup can be recognized, for example, in mechanical systems in which the presence of one-sided restoring characteristics (such as one-sided supports, end-stops, snubbers, etc) renders the system dynamics highly nonlinear and non-smooth see Figure 1.1. More specifically, this system captures the basic dynamics of the aforementioned mechanical systems and reveals the fundamental practical problems that one faces when designing observers and controllers for such systems. Therefore, the examined system can be considered as benchmark for this type of systems.

The main contribution of this thesis in the field of PWA systems can be summarized as follows:

- An observer-based output-feedback control design that aims at disturbance attenuation for periodically excited PWA systems has been developed. This design includes a controller that renders the closed-loop system convergent. Since the convergence property guarantees unique globally asymptotically stable steady-state solutions, we can construct so-called generalized frequency response functions for nonlinear convergent systems [100]. Using such generalized frequency response functions, we can uniquely define the steady-state performance of the closed-loop PWA system in terms of disturbance attenuation for periodic disturbances. Moreover, based on the information contained in these generalized frequency response functions, we propose performance measures quantifying the disturbance attenuation properties. These performance measures can be used to evaluate the disturbance attenuation properties of different controllers and to design the 'best' controller.

- The proposed observer-based output-feedback control design has been implemented experimentally on the setup with PWL restoring characteristics. Based on the performed experiments, it is shown that the proposed observer-based output-feedback controller can render the setup convergent and attenuates the vibrations induced by the rotating mass-unbalance.

For the second class of systems addressed in this thesis, there are many analysis results available in the literature, as discussed in Section 1.3. However,

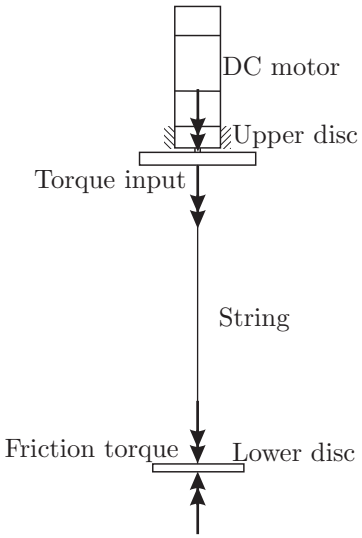

Figure 1.5: Schematic representation of the experimental rotor dynamic system.

only a limited number of works deals with the control synthesis for this type of systems and even less number deal with the actual implementation of these controllers in practice. Therefore, in this thesis the goal is not only to develop theoretical tools for control design for systems with discontinuous right-hand sides but the aim is also on the experimental validation of these designs for which a second experimental system is used, see Figure 1.5.

This system consists of two discs, connected through a low-stiffness string. The upper disc is driven by a motor. At the lower disc a brake is implemented to exert a friction torque on the disc. The presence of friction in the system gives rise to complex dynamical phenomena, such as co-existence of steady-state solutions, stick-slip limit cycling and discontinuous bifurcation points, see [129]. These vibrational phenomena are present in many mechanical motion systems with flexibilities and friction. In such engineering systems, limit cycling is an undesirable phenomenon because it causes kinetic energy dissipation, noise, excessive wear of machine parts and inferior positioning properties. Due to the fact that the examined system reproduces this kind of behavior, it can be considered as benchmark for this type of systems.

The main contribution of the thesis in the field of systems with non-collocated friction and actuation can be described as follows:

- An observer-based output-feedback control design for the stabilization of Lur'e type systems with set-valued nonlinearities in the feedback loop is proposed. We apply these results to solve the stabilization problem for

mechanical motion systems with non-collocated friction and actuation. It is shown that the control design is robust for uncertainties in the friction characteristics, which is an important characteristic in practice.

- The proposed observer-based output-feedback control design has been implemented on the experimental system. Based on the experimental results, the proposed controller is able to eliminated stick-slip limit cycling to a great extent and it is able to stabilize the system around an equilibrium point (constant velocity solution) for a large number of constant inputs applied by the motor.

1.5 Structure of the thesis

After the introductory Chapter 1, Chapter 2 gives basic theoretical preliminaries that we use throughout the thesis. In Section 2.1, the notions of Lyapunov stability and convergence are introduced. The latter concept will be used extensively in Chapters 3 and 4. In Section 2.2, the notions of passivity and positive realness are given. Finally, in Section 2.3, we recall the concept of absolute stability. In Chapters 5 and 6 controllers based on the absolute stability property will be proposed.

Chapter 3 is related to the design of an observer-based output-feedback controller for a class of PWA systems. In Section 3.2, a state-feedback control design strategy that is suitable for disturbance attenuation of PWA systems is described and, in Section 3.3, observer design strategies suitable for the considered PWA systems are given. In the same section, an output-feedback control design that consists of a state-feedback controller and an observer is introduced. Moreover, it is shown that the interconnection of the state-feedback controller with the observer and the plant is convergent. In Section 3.4, sufficient conditions for a bound for the control action are introduced and, in Section 3.5, a bound for the system output for bounded disturbance inputs is provided. In this section, also performance measures based on computed steady-state responses for periodic disturbances are proposed and a systematic approach towards high-performance control design for the attenuation of such disturbances is given. Finally, a discussion of the results presented in this chapter and directions for future work are given in Section 3.6.

Chapter 4 presents the implementation of the aforementioned output-feedback controller on an experimental setup involving a flexible beam with PWL restoring characteristics. In Section 4.2, a detailed description of the experimental setup is given and a model describing this setup is presented. In Section 4.3, we discuss an observer that will be used to estimate the state of the experimental system since we consider the case where the full state of the system is not available for feedback. In Section 4.4, output-feedback controllers are designed and implemented on this setup to validate the effectiveness of the proposed

approach in attenuating periodic disturbances. The disturbance attenuation properties of these output-feedback controllers are evaluated in Section 4.5 by using the theoretical tools developed in Chapter 3. This chapter is ended with a summary in Section 4.6.

Chapter 5 proposes two observer-based output-feedback control design strategies for a class of Lur'e-type systems with set-valued nonlinearities. Each of the resulting output-feedback controllers consist of a model-based observer and a state-feedback controller. In Section 5.2, the state-feedback controllers are discussed. These controllers are based on an extension of Popov's criterion for maximal monotone set-valued maps and guarantee absolute stability of the plant. The observers and the proposed output-feedback controllers are presented in Section 5.3. In that section, it is shown that the interconnection of the state-feedback controller with the observer and the plant are also absolutely stable. Finally, a discussion of the results presented in this chapter and directions for future work are given in Section 5.4.

In Chapter 6, one of the control design strategies presented in Chapter 5 is applied to the experimental setup of the dynamic rotor system to illustrate its practical use. This setup and a corresponding model are presented in Section 6.2. In Section 6.3, an output-feedback controller is designed for this system to stabilize its equilibria for different friction situations and, hence, to eliminate undesirable stick-slip limit-cycling. Finally, the obtained results are discussed in Section 6.4.

In Chapter 7, the conclusions of this thesis are given and recommendations for future work are discussed.

2

Preliminaries

In this chapter, we will present basic theoretical notions that are going to be used throughout the thesis. In Section 2.1, we provide the definitions of basic stability concepts, invariant sets and asymptotically ultimately bounded systems. Moreover, in this section we also introduce the notions of convergence, uniform convergence and input-to-state convergence. In Section 2.2, we recall the definitions of passivity and positive realness and, in Section 2.3, the notion of absolute stability is given. Theoretical results related to the absolute stability property, such as the circle criterion and the Popov criterion are also presented in this section. Both the notion of convergence and absolute stability will play an important role in the design of controllers for non-smooth systems, as presented in this thesis.

2.1 Lyapunov stability concepts and convergent systems

This sections starts with definitions related to Lyapunov stability concepts for non-autonomous systems. Consider the system

$$\dot{x} = f(x, t), \tag{2.1}$$

where state $x \in \mathbb{R}^n$, $t \in \mathbb{R}$ and $f(x,t)$ is locally Lipschitz in x and piecewise continuous in t.

Definition 2.1.1 [102] A solution $\bar{x}(t)$ of system (2.1), which is defined for $t \in (t_*, +\infty)$, is said to be

- stable if for any $t_0 \in (t_*, +\infty)$ and $\varepsilon > 0$ there exists $\delta = \delta(\varepsilon, t_0) > 0$ such that $|x(t_0) - \bar{x}(t_0)| < \delta$ implies $|x(t) - \bar{x}(t)| < \varepsilon$ for all $t \geq t_0$.
- uniformly stable if it is stable and the number δ in the definition of stability is independent of t_0.

- asymptotically stable if it is stable and for any $t_0 > 0$ there exists $\delta = \delta(t_0) > 0$ such that $|x(t_0) - \bar{x}(t_0)| < \delta$ implies $\lim_{t\to+\infty} |x(t) - \bar{x}(t)| = 0$.
- uniformly asymptotically stable if it is uniformly stable and there exists $\delta > 0$ (independent of t_0) such that for any $\varepsilon > 0$ there exists $T = T(\varepsilon) > 0$ such that $|x(t_0) - \bar{x}(t_0)| < \delta$ for $t_0 \in (t_*, +\infty)$ implies $|x(t) - \bar{x}(t)| < \varepsilon$ for all $t \geq t_0 + T$.
- exponentially stable if there exist $\delta > 0$, $C > 0$ and $\beta > 0$ such that $|x(t_0) - \bar{x}(t_0)| < \delta$ for $t_0 \in (t_*, +\infty)$ implies

$$|x(t) - \bar{x}(t)| \leq Ce^{-\beta(t-t_0)}|x(t_0) - \bar{x}(t_0)|, \qquad \forall t \geq t_0. \tag{2.2}$$

It is known that in case the solution $\bar{x}(t)$ is asymptotically stable this implies that $\bar{x}(t)$ attracts all the solutions that are near $\bar{x}(t)$. If one is interested in attractivity of the solution $\bar{x}(t)$ for all initial conditions $x(t_0) \in \mathbb{R}^n$, the following definitions are required.

Definition 2.1.2 [72] A solution $\bar{x}(t)$ of system (2.1), which is defined for $t \in (t_*, +\infty)$, is said to be

- globally asymptotically stable if it is asymptotically stable and any solution of the system (2.1) starting in $x(t_0) \in \mathbb{R}^n$, $t_0 \in (t_*, +\infty)$ satisfies $|x(t) - \bar{x}(t)| \to 0$ as $t \to +\infty$.
- globally uniformly asymptotically stable if it is uniformly asymptotically stable and it attracts solutions of system (2.1) starting in $x(t_0) \in \mathbb{R}^n$, $t_0 \in \mathbb{R}$ uniformly over t_0, i.e. for any compact set $K \subset \mathbb{R}^n$ and any $\varepsilon > 0$ there exists $T(\varepsilon, K) > 0$ such that if $x(t_0) \in K$, $t_0 \in (t_*, +\infty)$, then $|x(t) - \bar{x}(t)| < \varepsilon$ for all $t \geq t_0 + T(\varepsilon, K)$.
- globally exponentially stable if it is exponentially stable and there exist constant $C > 0$ and $\beta > 0$ such that any solution starting in $x(t_0) \in \mathbb{R}^n$, $t_0 \in \mathbb{R}$ satisfies

$$|x(t) - \bar{x}(t)| \leq Ce^{-\beta(t-t_0)}|x(t_0) - \bar{x}(t_0)|. \tag{2.3}$$

Next, we will define positively invariant (PI) sets and asymptotically ultimate boundedness of a system.

Definition 2.1.3 A set Ω is called positively invariant (PI) with respect to system (2.1), if for all initial times $t_0 \in \mathbb{R}$ and all initial states $x_0 \in \Omega$ the corresponding solution to (2.1) satisfies $x(t) \in \Omega$ for all $t \geq t_0$.

Definition 2.1.4 System (2.1) is called asymptotically ultimately bounded to a set $\Omega \subseteq \mathbb{R}^n$, if for all initial times $t_0 \in \mathbb{R}$ and all initial states $x_0 \in \mathbb{R}^n$, the corresponding solution trajectory $x(t)$ satisfies $\lim_{t\to\infty} d_\Omega(x(t)) = 0$, where $d_\Omega(x) := \inf_{z\in\Omega} \|z - x\|$ is the distance of the point x to the set Ω and z an element in Ω .

As we consider in Chapter 3 PWA systems with periodic exogenous inputs, it is useful to define the notion of convergence.

Definition 2.1.5 [102] System (2.1) is said to be

1. *convergent* if there exists a solution $\bar{x}(t)$ satisfying the following conditions:
   (a) $\bar{x}(t)$ is defined and bounded for all $t \in \mathbb{R}$,
   (b) $\bar{x}(t)$ is globally asymptotically stable for all $t \in \mathbb{R}$.
2. *uniformly convergent* if it is convergent and $\bar{x}(t)$ is globally uniformly asymptotically stable.
3. *exponentially convergent* if it is convergent and $\bar{x}(t)$ is globally exponentially stable.

The solution $\bar{x}(t)$ is called a steady-state solution. As follows from the definition of convergence, any solution of a convergent system 'forgets' its initial condition and converges to some steady-state solution. In general, the steady-state solution $\bar{x}(t)$ may be non-unique. But for any two steady-state solutions $\bar{x}_1(t)$ and $\bar{x}_2(t)$ it holds that $|\bar{x}_1(t) - \bar{x}_2(t)| \to 0$ as $t \to +\infty$. At the same time, for uniformly convergent systems the steady-state solution is unique, as formulated below.

Property 2.1.6 [102] If system (2.1) is uniformly convergent, then the steady-state solution $\bar{x}(t)$ is the only solution defined and bounded for all $t \in \mathbb{R}$.

In our problem setting, the time-dependency of (2.1) is due to some time-dependent exogenous input $w(t)$. As such, we will consider convergence properties for systems with inputs. So, instead of systems of the form (2.1), we consider systems of the form

$$\dot{x} = f(x, w(t)), \tag{2.4}$$

with state $x \in \mathbb{R}^n$ and input $w \in \mathbb{R}^d$, where $f(x, w)$ is locally Lipschitz in x and continuous in w. In the sequel, we will consider the class $\mathbb{P}\bar{\mathbb{C}}_d$ of piecewise continuous inputs $w(t) : \mathbb{R} \to \mathbb{R}^d$ which are bounded on $\mathbb{R}$. Below we define the convergence property for suchsystems with inputs.

Definition 2.1.7 [102] System (2.4) is said to be uniformly (exponentially) convergent if it is uniformly (exponentially) convergent for every input $w(t) \in \mathbb{P}\bar{\mathbb{C}}_d$. In order to emphasize the dependency on the input $w(t)$, the steady-state solution is denoted by $\bar{x}_w(t)$.

The uniform convergence property can now be extended to the input-to-state stability framework. Hereto, we need to define class $\mathcal{K}$ and class $\mathcal{KL}$ functions.

Definition 2.1.8 [72] A function $\alpha : [0, \infty) \to [0, +\infty)$ is said to belong to class $\mathcal{K}$ if it is continuous, strictly increasing and $\alpha(0) = 0$. It is said to belong to class $\mathcal{K}_\infty$ if it belongs to class $\mathcal{K}$ and $\alpha(r) \to +\infty$ as $r \to +\infty$.

Definition 2.1.9 [72] A function $\beta : [0, a) \times [0, +\infty) \to [0, +\infty)$ is said to belong to class $\mathcal{KL}$ if it is continuous and, for each fixed s, the mapping $r \mapsto \beta(r, s)$ belongs to class $\mathcal{K}$ and, for each fixed r, the mapping $s \mapsto \beta(r, s)$ is decreasing and $\beta(r, s) \to 0$ as $s \to +\infty$.

With these definitions the uniform convergence property can be extended to the input-to-state stability framework [120] as follows.

Definition 2.1.10 [102] System (2.4) is said to be input-to-state convergent if it is globally uniformly convergent and for every input $w(t) \in \mathbb{P}\bar{\mathbb{C}}_d$ system (2.4) is input-to-state (ISS) stable [120] along the steady-state solution $\bar{x}_w(t)$, i.e. there exist a $\mathcal{KL}$-function $\beta(r, s)$ and a class $\mathcal{K}$-function $\gamma(r)$ such that any solution of this system corresponding to some input $\tilde{w}(t) := w(t) + \Delta w(t)$ satisfies

$$|x(t) - \bar{x}_w(t)| \leq \beta(|x(t_0) - \bar{x}_w(t_0)|, t - t_0) + \gamma(\sup_{t_0 \leq \tau \leq t} |\Delta w(\tau)|). \tag{2.5}$$

In general, the functions $\beta(r, s)$ and $\gamma(r)$ may depend on the particular input $w(t)$.

For more information on ISS, see [120].

2.2 Passivity and positive realness

In this section, we will begin with a definition of passivity for nonlinear systems [72]. Consider the dynamical system

$$\begin{aligned} \dot{x} &= f(x, w) \\ z &= h(x, w), \end{aligned} \tag{2.6}$$

with $x \in \mathbb{R}^n$ the state of the system and $w \in \mathbb{R}^d$ the input of the system, $z \in \mathbb{R}^p$ the output of the system. The system is assumed to have the same number of

inputs and outputs ($d = p$). Moreover, we assume that an equilibrium point of the system (2.6) for $z = 0$ is $x = 0$ with zero output z (i.e. $f(0,0) = 0$ and $h(0,0) = 0$).

Definition 2.2.1 [72] The system (2.6) is said to be passive if there exists a continuous differentiable positive semidefinite function $V(x)$ (called the storage function) such that

$$w^T z \geq \dot{V} = \frac{\partial V}{\partial x} f(x,w), \quad \forall (x,w) \in \mathbb{R}^n \times \mathbb{R}^d. \tag{2.7}$$

Moreover, the system (2.6) is said to be strictly passive if

$$w^T z > \dot{V}, \quad \forall (x,w) \neq (0,0). \tag{2.8}$$

In Chapter 5, we will use the notion of passivity together with the notion of absolute stability (we will introduce this notion in the following section) to synthesize controllers for a class of Lur'e type of systems. For this purpose, we will introduce now some theoretical tools, strongly related to passivity, that are useful for the control design for this class of systems. More specifically, we will provide definitions of a positive real transfer function and a strictly positive real transfer function. Moreover, we will recall two lemmas for a class of linear systems that give algebraic characterizations of (strictly) positive real transfer functions. Finally, we will relate a (strictly) positive real transfer function with a (strictly) passive system by using an additional lemma.

Definition 2.2.2 [72] A $p \times p$ proper rational transfer function matrix $G(s)$ is called positive real if

- the poles of $G(s)$ are in $Re[s] \leq 0$,
- for all real ω for which $j\omega$ is not a pole of $G(s)$, the matrix $G(j\omega) + G^T(-j\omega)$ is positive semidefinite, and
- any pure imaginary pole $j\omega$ of $G(s)$ is a simple pole and the residue matrix $\lim_{s \to j\omega}(s - j\omega)G(s)$ is positive semidefinite Hermitian.

Definition 2.2.3 [72] Let $G(s)$ be a $p \times p$ proper rational transfer function matrix, and suppose $\det[G(s) + G^T(-s)]$ is not identically zero. Then, $G(s)$ is strictly positive real if and only if

- $G(s)$ is Hurwitz; that is, poles of all elements of $G(s)$ have negative real parts,
- $G(j\omega) + G^T(-j\omega)$ is positive definite for all $\omega \in \mathbb{R}$, and

- either $G(\infty) + G^T(\infty)$ is positive definite or it is semi-definite and $\lim_{\omega\to\infty} \omega^2 M^T[G(j\omega)+G^T(-j\omega)]M$ is positive definite for any $p\times(p-q)$ full rank matrix M such that $M^T[G(\infty) + G^T(\infty)]M = 0$, where $q = \text{rank}[G(\infty) + G^T(\infty)]$.

At this point, we will recall the so-called Positive real Lemma and the Kalman-Yakubovich-Popov Lemma. Consider linear time-invariant systems of the form

$$\begin{array}{l} \dot{x} = Ax + Bw \\ z = Cx + Dw, \end{array} \tag{2.9}$$

where the equilibrium point of the system (2.9) for $w = 0$ is $x = 0$ and

$$G(s) = C(sI - A)^{-1}B + D \tag{2.10}$$

is the proper rational transfer function matrix from input w to output z of system (2.9). Now, the Positive real Lemma and the Kalman-Yakubovich-Popov, respectively, reads as follows:

Definition 2.2.4 [72] The $p \times p$ transfer function matrix $G(s)$, where (A, B) is controllable and (A, C) is observable, is positive real if and only if there exist matrices $P = P^T > 0$, L and W such that

$$\begin{array}{ll} PA + A^T P & = -L^T L \\ PB & = C^T - L^T W \\ W^T W & = D + D^T. \end{array} \tag{2.11}$$

Definition 2.2.5 [72] The $p \times p$ transfer function matrix $G(s)$, where (A, B) is controllable and (A, C) is observable, is strictly positive real if and only if there exist matrices $P = P^T > 0$, L, W and a positive constant ε such that

$$\begin{array}{ll} PA + A^T P & = -L^T L - \varepsilon P \\ PB & = C^T - L^T W \\ W^T W & = D + D^T. \end{array} \tag{2.12}$$

Finally, we introduce a lemma that shows the fact that a (strictly) positive real transfer function $G(s)$, as in (2.10), represents a (strictly) passive system (2.9).

Definition 2.2.6 [72] The linear time-invariant system (2.9) with $G(s)$ given in (2.10), (A, B) controllable and (A, C) observable, is

- passive if $G(s)$ is positive real;
- strictly passive if $G(s)$ is strictly positive real.

2.3 Absolute stability

Consider the following feedback interconnection of a linear dynamical system and a nonlinear element given by

$$\begin{aligned} \dot{x} &= Ax + Bw \\ z &= Cx + Dw, \\ w &= -\varphi(t, z), \end{aligned} \tag{2.13}$$

where $x \in \mathbb{R}^n$, $w, z \in \mathbb{R}^p$, φ locally Lipschitz in x, (A, B) is controllable, (A, C) is observable. We assume that the feedback connection has a well-defined state model, which is the case when

$$w = -\varphi(t, Cx + Dw) \tag{2.14}$$

has a unique solution u for every (t, x) in the domain of interest. The nonlinearity φ is required to satisfy a sector condition[1]. For all nonlinearities satisfying a sector condition, the origin $x = 0$ is an equilibrium point of the system (2.13). Then, the system (2.13) is said to be absolutely stable for sector $[K_\alpha,\ K_\beta]$ if the origin is globally uniformly asymptotically stable for any nonlinearity φ satisfying the sector condition $[K_\alpha,\ K_\beta]$ [72]. In the thesis, we will consider extensions to the case of set-valued nonlinearities. Moreover, to prove absolute stability for system (2.13) we use a particular case of the so-called circle criterion. In this particular case, the circle criterion guarantees absolute stability if the transfer function of the linear part of system (2.13) is strictly positive real and the nonlinearity in the feedback loop is passive. The circle criterion will be used in Chapter 5 for observer and control design purposes. The circle criterion is given as follows

Theorem 2.3.1 *[72] Consider system* (2.13) *with* (A, B) *controllable and* (A, C) *observable. Then the following statements hold:*

- *System* (2.13) *is absolutely stable for sector* $[K_1,\ \infty]$*, with* K_1 *a positive semi-definite matrix, if* $\varphi \in [K_1,\ \infty]$ *and* $G(s)[I + K_1G(s)]^{-1}$ *is strictly positive real (strictly passive).*
- *System* (2.13) *is absolutely stable for sector* $[K_1,\ K_2]$*, with* $K = K_2 - K_1 = K^T$ *positive definite, if* $\varphi \in [K_1,\ K_2]$ *and* $[I + K_2G(s)][I + K_1G(s)]^{-1}$ *is strictly positive real.*

[1] A memoryless function $w = \varphi(t, z) : \mathbb{R} \times \mathbb{R}^p \to \mathbb{R}^p$ belongs to the sector $[K_\alpha,\ K_\beta]$ for the matrices $K_\alpha, K_\beta \in \mathbb{R}^{p\times p}$ and $K_{\alpha,\beta} = K_\alpha - K_\beta = K_{\alpha,\beta}^T$ positive definite matrix, if $[\varphi(t, z) - K_\alpha z]^T [\varphi(t, z) - K_\beta z] \leq 0,\ \forall (t, z)$, with $K_\alpha = \text{diag}(k_{\alpha,1}, \ldots, k_{\alpha,p})$ and $K_\beta = \text{diag}(k_{\beta,1}, \ldots, k_{\beta,p})$.

By using an additional theorem, the so-called Popov criterion, we can relax the condition of strict positive realness for the transfer function of the linear part of system (2.13) by a loop transformation with a dynamic multiplier. In Chapter 5, the Popov criterion is also used for control design purposes.

Consider a linear system with a nonlinearity in the feedback loop,

$$\begin{aligned} \dot{x} &= Ax + Bw \\ z &= Cx \\ w_i &= -\varphi_i(z_i),\ 1 \leq i \leq p \end{aligned} \tag{2.15}$$

where $x \in \mathbb{R}^n$, $w, z \in \mathbb{R}^p$, (A, B) is controllable, (A, C) is observable and $\varphi_i : \mathbb{R} \to \mathbb{R}$ is a locally Lipschitz memoryless nonlinearity that belongs to the sector $[0,\ k_i]$, with $0 < k_i < \infty$. In this specific case, the transfer function $G(s)$ in (2.10) is strictly proper and φ is time-invariant and decoupled meaning that $\varphi_i(y) = \varphi_i(y_i)$. The Popov criterion is stated as follows:

Theorem 2.3.2 *[72] The system* (2.13) *is absolutely stable if, for* $1 \leq i \leq p$, $\varphi_i \in [0,\ k_i],\ 0 < k_i \leq \infty$ *and there exists a constant* $\gamma_i \geq 0$, *with* $(1 + \lambda\gamma_i) \neq 0$ *for every eigenvalue* λ *of* A, *such that* $M + (I + s\Gamma)G(s)$ *is strictly positive real, where* $\Gamma = diag(\gamma_1, ..., \gamma_p)$ *and* $M = diag(1/k_1, ..., 1/k_p)$.

3

Convergence-based controller design for disturbance attenuation in PWA systems

3.1 Introduction

In this chapter, we propose a control design strategy for a class of PWA systems based on the notion of convergence [32], uniform convergence and input-to-state convergence [102] (see Chapter 2 for the definition of these concepts). Next to analyzing and synthesizing controllers for PWA systems, we also aim at showing the potential of the control design strategy in practice by implementing the controllers on an experimental mechanical system with PWA characteristics. A successful implementation requires that the controller design strategy has to guarantee stability, disturbance attenuation and limited control effort. Therefore, to be useful for practical implementation, the proposed controller design strategy has also to include theoretical tools to analyze input bounds, output bounds and performance measures in terms of disturbance attenuation to evaluate different controllers. Moreover, since the entire state of the system will not be available for feedback, an output-feedback design is needed.

The uniform convergence and input-to-state convergence properties are beneficial in the scope of stability and performance analysis of PWA systems. Firstly, they ensure that these systems exhibit unique steady-state solutions for any bounded disturbance and, secondly, they ensure the asymptotic ultimate boundedness of the state, which can be related to input and output bounds.

In order to support the practical applicability of the proposed control design strategy, we propose a control design procedure that guarantees a bound on the control input of the system. This bound guarantees that the control action required to render a system convergent within a given class of disturbances, stays below a predefined value for a given set of initial conditions of interest. This is very important for applications, because there are always limitations on the control action that an actuation mechanism can provide. The basic idea that we will use to guarantee an upper bound on the control input of a system was first introduced in [15] for linear systems and extended in [74] for discrete-time uncertain linear systems. In [94], similar developments are given for discrete-time PWA systems. The main idea consists of constructing a positively invariant set and showing that on this set the control bound holds. These conditions will be expressed in terms of linear matrix inequalities (LMIs). In this work, we will extend these ideas to continuous-time PWA systems and give an explicit constructive form of the positively invariant set. Moreover, we show for the class of convergent PWA systems how a positively invariant set can be obtained in a computational manner.

Due to the fact that we will employ so-called quadratic convergence, i.e. convergence based on a quadratic Lyapunov function, we can readily provide an upper bound for the system state (in steady-state) given a class of bounded piecewise continuous inputs and initial conditions. This bound is more general than that presented in [39], [54] and [109], since these bounds only hold for zero initial condition. The bound presented here is similar to the bound presented in [47] with the only difference that the bound considered here is based on the notion of convergence, while the bound in [47] is based on the notion of incremental stability [4], [44].

The fact that uniformly convergent systems have unique steady-state responses allows for a more accurate evaluation of the performance (in terms of disturbance attenuation) based on computed responses. Actually, one can provide Bode-like plots for nonlinear systems, using uniform convergence, although these plots do not have the favorable properties that 'linear' Bode plots have (due to the absence of the super-position principle). In particular, this leads to the introduction of performance evaluation techniques based on computed steady-state responses applicable to convergent systems with bounded periodic disturbances. The motivation for this choice lies in the fact that in engineering practice many disturbances can be approximated by harmonic signals. One can think of periodic vibrations in vehicles [53], unbalance phenomena in optical storage drives [57] and many more. Next to the Bode-like plots, we provide performance measures on specific characteristics of the system responses, e.g. the maximum 'amplitude' or the total energy of a response, over a frequency range of the periodic disturbances. This allows to design high performance controllers for applications in which periodic disturbances are dominant and this also allows to account for frequency weighting. In [57], a similar approach

towards performance assessment is proposed for a class of Lur'e systems with slope restricted nonlinearities. Here, a different perspective is taken in the sense that we consider general PWA systems.

Using such performance evaluation techniques, we can promote controllers for a PWA system that are favorable in terms of disturbance attenuation. Based on these techniques, we evaluate the class of controllers that render the system convergent and result in a control input that satisfies the saturation bound. Within this class of controllers, the performance assessment is used as a discriminating tool to steer the design towards controllers with 'optimal' disturbance attenuation properties.

Another practical problem of concern is that, generally, the entire state of a PWA system will not be available for feedback. Therefore, an additional goal is to construct an output-based feedback controller that renders the PWA system under study convergent. The output-feedback controller is a combination of a model-based observer and a state-feedback controller. Based on a result on the input-to-state convergence of a feedback interconnection of an input-to-state convergence system and a uniformly stable system [102], we guarantee that this combination will yield a convergent closed-loop system. Hence, the 'certainty equivalence' or 'separation principle' is valid within this context. The observers that are used for this design are based on [99] for continuous PWA systems and based on [35] and [70] for bi-modal piecewise linear (PWL) systems.

In this chapter, we first describe a state-feedback control design strategy that is suitable for disturbance attenuation of PWA systems in Section 3.2. Furthermore, in Section 3.3, we present observer design strategies that are suitable for the considered PWA and bi-modal PWL systems. Moreover, we introduce the output-feedback control design and we prove that the interconnection of the state-feedback controller with the observer and the plant is uniformly convergent. In Section 3.4, we analyze the bound for the control action and in Section 3.5 we derive a bound for the system output for bounded piecewise continuous disturbances. Moreover, we also provide performance measures based on computed steady-state responses for periodic disturbances and a systematic approach towards high-performance control design (within the class of controllers that render the closed-loop system convergent). Finally, a discussion of the results presented in this chapter and directions for future work are given in Section 3.6.

3.2 Convergence-based state-feedback control design

We consider the class of PWA systems:

$$\dot{x} = A_i x + b_i + Bw(t) + B_1 u \text{ for } \ x \in \Lambda_i,\ i = 1, ..., l \tag{3.1a}$$

$$y = Cx, \tag{3.1b}$$

where $x \in \mathbb{R}^n$, $w \in \mathbb{R}^m$, $u \in \mathbb{R}^k$ and $y \in \mathbb{R}^p$ are the state, the exogenous input, the control input and the output of the system, respectively, depending on time $t \in \mathbb{R}$. The matrices $A_i,\ b_i,\ i = 1, ..., l,\ B,\ B_1$ and C are constant matrices of appropriate dimensions. The sets Λ_i are polyhedral and form a partitioning of the state-space $\mathbb{R}^n$ in the sense that the sets Λ_i have disjoint interiors and $\bigcup_i \Lambda_i = \mathbb{R}^n$. The cells Λ_i are divided by hyperplanes given by equations of the form $H_j^T x + h_j = 0$, for some $H_j \in \mathbb{R}^n$ and $h_j \in \mathbb{R},\ j = 1, ..., k_1$. Hence, the hyperplanes $H_j^T x + h_j = 0,\ j = 1, ..., k_1$, are the switching surfaces. The time varying input $w(t)$ acts as a disturbance on the system and it is considered to be bounded. In the sequel, we will deal with PWA systems that have continuous right-hand sides. This continuity requirement on the right-hand side of system (3.1a) can be characterized by a simple algebraic condition as in [102]. Due to the continuity on the right-hand side, the right-hand side is globally Lipschitz continuous with linear growth bounds and thus global existence and uniqueness of solution trajectories is guaranteed for any bounded piecewise continuous w and u.

In the control design, we start with a static state-feedback as the input for the system (3.1a):

$$u = -Kx, \tag{3.2}$$

where $K \in \mathbb{R}^{k \times n}$ is the controller gain. Consequently, the dynamics of the closed-loop system (3.1) and (3.2) can be written as:

$$\dot{x} = (A_i - B_1 K)x + b_i + Bw(t) \text{ for } \ x \in \Lambda_i,\ i = 1, ..., l \tag{3.3a}$$

$$y = Cx. \tag{3.3b}$$

Note that the closed-loop system described by (3.3a) is also a continuous PWA system due to the continuity of the feedback law (3.2). The control goal can be formally stated as:

> Determine, if possible, the controller gain K in (3.2) such that the closed-loop system (3.3a) is uniformly convergent for piecewise continuous inputs $w : \mathbb{R} \longrightarrow \mathbb{R}^m$.

This problem can be solved by using a result in [100], which states conditions under which a linear static state-feedback law as in (3.2) renders a PWA system as in (3.1a) input-to-state convergent and thus uniformly convergent for all

piecewise continuous disturbances w. The conditions, that are formalized in the following theorem, are only sufficient (not necessary) for input-to-state convergence.

Theorem 3.2.1 *[100] Consider the continuous PWA system* (3.1a). *Suppose that the right-hand side of* (3.1a) *is continuous in x and there exist matrices $P_c \in \mathbb{R}^{n\times n}$ and $P_s \in \mathbb{R}^{k\times n}$ satisfying the linear matrix inequalities*

$$P_c = P_c^T > 0 \tag{3.4a}$$

$$P_c A_i^T + A_i P_c - B_1 P_s - P_s^T B_1^T < 0,\ i = 1, ..., l. \tag{3.4b}$$

Then, system (3.1a) *in closed-loop with the controller* (3.2) *where $K := P_s P_c^{-1}$ and w as external input is input-to-state convergent.*

The conditions provided in [100] are in linear matrix inequality (LMI) form and these LMIs can be solved easily by the use of standard LMI solvers (such as LMITOOL for MATLAB [38]). It should be noted that Theorem 3.2.1 is based on a quadratic Lyapunov function and that input-to-state convergence implies uniform convergence. Furthermore, we should also note that the LMIs in (3.4b) originate from the bi-linear matrix inequalities (BMI):

$$P(A_i - B_1 K) + (A_i - B_1 K)^T P < 0,\ i = 1, ..., l, \tag{3.5}$$

where $P = P_c^{-1}$. We can derive (3.4b) if we pre- and post- multiply (3.5) by P^{-1}.

An important observation is that the proposed design has robustness properties against unmodelled inaccuracies. Namely, if the conditions of Theorem 3.2.1 hold, then the BMIs (3.5) will be satisfied, which due to strictness imply that the BMIs

$$P(A_i+\Delta A_i-(B_1+\Delta B_1)K)+(A_i+\Delta A_i-(B_1+\Delta B_1)K)^T P < 0, \text{ for } i = 1, ..., l, \tag{3.6}$$

will still be satisfied for sufficiently small model uncertainties ΔA_i, $i = 1, ..., l$, and ΔB_1 (provided that the uncertainties do not destroy the continuity of the system) and hence, input-to-state convergence is maintained.

3.3 Output-feedback convergence-based control design

In the control law proposed in Section 3.2, all the state variables are used for feedback. In practice, the entire state of system (3.1) is in general not measured and thus not available for feedback. Indeed, in some cases, physical constraints do not allow the measurement of certain state variables and, in other cases,

the high costs of sensors prohibit such measurements. Therefore, the goal of this section is to construct an output-based feedback controller that solves this problem and renders the PWA system (3.1) input-to-state convergent using output measurements only. This output-feedback controller consists of a state-feedback controller as in (3.2) and a model-based observer. The observer will reconstruct the full state of the system based on only the measurement of the output (and input).

3.3.1 Strategies for observer design

In this subsection, we will discuss two observer design strategies that are suitable for the state estimation of continuous PWA systems of the form (3.1). One of the strategies is based on the notion of convergence and is applicable to continuous PWA systems and the other strategy focuses on a class of PWL systems, but allows for possible extension to discontinuous PWL systems.

Convergence-based observer design strategy for PWA systems

Consider the following model-based observer for the continuous PWA system (3.1):

$$\dot{\hat{x}} = A_i\hat{x} + b_i + Bw(t) + B_1u + L(y(t) - \hat{y}) \text{ for } \hat{x} \in \Lambda_i,\ i = 1, ..., l, \tag{3.7a}$$

$$\hat{y} = C\hat{x}, \tag{3.7b}$$

with $L \in \mathbb{R}^{n\times p}$ and $\hat{x} \in \mathbb{R}^n$ the observer gain and the observed state, respectively.

The following theorem, proved in [100], formalizes conditions under which the observer (3.7) asymptotically recovers the state of system (3.1).

Theorem 3.3.1 *[100] Consider system* (3.1)*. Suppose that the right-hand side of* (3.1) *is continuous in x and there exist matrices $P_o \in \mathbb{R}^{n\times n}$ and $X \in \mathbb{R}^{n\times p}$ solving the LMI*

$$P_o = P_o^T > 0, \tag{3.8a}$$

$$P_oA_i + A_i^TP_o - XC - C^TX^T < 0,\ i = 1, ..., l, \tag{3.8b}$$

is feasible. Then, system (3.7) *with $L := P_o^{-1}X$ is an observer for system* (3.1) *with globally exponentially stable error dynamics. The observer error $\Delta x := x - \hat{x}$ satisfies the dynamics*

$$\dot{\Delta x} = g(x, u, w) - g(x + \Delta x, u, w), \tag{3.9}$$

where $g(x, u, w) = A_ix + b_i + Bw + B_1u + LCx$ for $x \in \Lambda_i, i = 1, ..., l$. Moreover, for any bounded $x(t)$ and $w(t)$ and any feedback $u = u(\Delta x, x, t)$ all solutions of system (3.9) *satisfy*

$$|\Delta x(t)| \leq ce^{-a(t-t_0)}|\Delta x(t_0)|, \tag{3.10}$$

where the numbers $c > 0$ and $a > 0$ are independent of $x(t)$, $w(t)$ and u.

Note that the LMIs in (3.8b) originate from the bi-linear matrix inequalities (BMI)

$$P_o(A_i - LC) + (A_i - LC)^T P_o < 0,\ i = 1, ..., l. \tag{3.11}$$

From (3.11), we can derive (3.8b) by straightforward substitution.

The basic reasoning behind this convergence-based observer design is that the satisfaction of the LMIs in (3.8b) or the BMIs in (3.11) guarantees that the observer (3.7) is an exponentially convergent system with inputs $u, w, y \in \mathcal{PC}$. Moreover, $x(t)$ is a solution of (3.1) and it is easy to see that it is also a solution to (3.7). Due to exponential convergence of (3.7), $\hat{x}(t) = x(t)$ is a GES solution of (3.7). In general, (quadratic) convergence of observers implies that all solutions of a convergence-based observer converge to each other for $t \to \infty$. Note that quadratic convergence implies also quadratic incremental stability see [4; 44].

Observer design strategy for bi-modal PWL systems

Consider a bi-modal PWL system that can be described by (3.1) with $l = 2$ and $b_i = 0$, $i = 1, 2$. In this system, Λ_1 is defined by $H^T x \geq 0$ and Λ_2 by $H^T x \leq 0$, with $H^T \in \mathbb{R}^n$. Since the vector-field of (3.1) is continuous, it holds that $A_1 x = A_2 x$ on the switching boundary $H^T x = 0$. Consider the following switching model-based observer

$$\dot{\hat{x}} = \begin{cases} A_1\hat{x} + Bw(t) + B_1 u + L_1(y(t) - \hat{y}) \text{ for } \hat{x} \in \Lambda_1 \\ A_2\hat{x} + Bw(t) + B_1 u + L_2(y(t) - \hat{y}) \text{ for } \hat{x} \in \Lambda_2, \end{cases} \tag{3.12a}$$

$$\hat{y} = C\,\hat{x}, \tag{3.12b}$$

where $\hat{x}(t)$ is the observer state and $L_1,\ L_2 \in \mathbb{R}^{n \times p}$ are observer gain matrices. Consequently, the dynamics of the observer error $\Delta x = x - \hat{x}$ is described by

$$\Delta\dot{x} = \begin{cases} (A_1 - L_1 C)\Delta x, & x \in \Lambda_1, \quad \hat{x} \in \Lambda_1 \\ (A_2 - L_2 C)\Delta x + \Delta A x, & x \in \Lambda_1, \quad \hat{x} \in \Lambda_2 \\ (A_1 - L_1 C)\Delta x - \Delta A x, & x \in \Lambda_2, \quad \hat{x} \in \Lambda_1 \\ (A_2 - L_2 C)\Delta x, & x \in \Lambda_2, \quad \hat{x} \in \Lambda_2, \end{cases} \tag{3.13}$$

where $\Delta A = A_1 - A_2$, x satisfies (3.1) (for $l = 2$ and $b_i = 0$) and $\hat{x}$ satisfies (3.12a). By substituting $\hat{x} = x - \Delta x$ in (3.13), we see that the right-hand side of the observer error dynamics is piecewise linear in $[\Delta x^T \quad x^T]^T$.

The following theorem guarantees that the observer (3.12) exponentially reconstructs the state of system (3.1) (for $l = 2$ and $b_i = 0$, $i = 1, 2$).

Theorem 3.3.2 *[35; 70] The observer error dynamics* (3.13) *is globally exponentially stable (in the sense of Lyapunov), for all $x : \mathbb{R}^+ \longrightarrow \mathbb{R}^n$ satisfying*

(3.1) *(for $l = 2$ and $b_i = 0$, $i = 1, 2$) for an arbitrary locally integrable input function $w : \mathbb{R}^+ \longrightarrow \mathbb{R}^m$, if there exist matrices $P = P^T > 0$, L_1, L_2 and constants $\lambda_1, \lambda_2 \geq 0$, $\alpha > 0$ such that the following set of matrix inequalities is satisfied:*

$$\begin{bmatrix} (A_2 - L_2C)^T P + P(A_2 - L_2C) + \alpha P & P\Delta A + \lambda_1 \frac{1}{2} HH^T \\ \Delta A^T P + \lambda_1 \frac{1}{2} HH^T & -\lambda_1 HH^T \end{bmatrix} \leq 0 \tag{3.14a}$$

$$\begin{bmatrix} (A_1 - L_1C)^T P + P(A_1 - L_1C) + \alpha P & -P\Delta A + \lambda_2 \frac{1}{2} HH^T \\ -\Delta A^T P + \lambda_2 \frac{1}{2} HH^T & -\lambda_2 HH^T \end{bmatrix} \leq 0. \tag{3.14b}$$

Moreover, the observer error is upper bounded by

$$\|\Delta x(t)\| \leq 1/\sqrt{\lambda_{min}(P)}\, \|\Delta x(t_0)\|_P e^{-\frac{\alpha(t-t_0)}{2}}, \tag{3.15}$$

with $\Delta x(t_0)$ the initial estimation error at time t_0.

The inequalities (3.14a)-(3.14b) are nonlinear matrix inequalities in $\{P, L_1, L_2, \lambda_1, \lambda_2, \alpha\}$. By choosing α a priori, these can formulated as LMIs in $\{P, L_1^T P, L_2^T P, \lambda_1, \lambda_2\}$ and thus can be efficiently solved using LMI solvers (such as LMI-TOOL for MATLAB [38]).

Both observers in (3.7) and (3.12) do not require information on which linear dynamics of the system is currently active. Furthermore, in case we consider bi-modal PWL systems, we note that the observer (3.12) is more general than (3.7) in the sense that it provides different gains L_1 and L_2 for each mode of the system in contrast to (3.7) that only allows a common gain L for both system modes. Moreover, if $L_1 = L_2 = L$, the LMIs (3.8) and (3.14) are equivalent to each other.

3.3.2 Observer/controller combination

The choice of the observer/controller combination that renders the interconnected system uniformly convergent and input-to-state convergent is based on the following results presented in [100].

Property 3.3.3 [100] Consider the system

$$\begin{cases} \dot{z} = F(z, y, w),\ z \in \mathbb{R}^d \\ \dot{y} = G(z, y, w),\ y \in \mathbb{R}^q. \end{cases} \tag{3.16}$$

Suppose that the z-subsystem is input-to-state convergent with respect to y and w. Assume that there exists a class $\mathcal{KL}$ function $\beta_y(r, s)$ such that for any

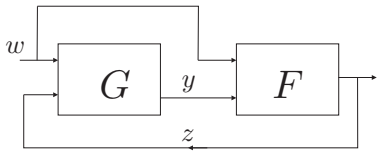

Figure 3.1: Schematic representation of the interconnected system (3.16).

piecewise continuous input $(w,\ z)$, any solution of the y-subsystem satisfies

$$|y(t)| \leq \beta_y(|y(t_0)|, t - t_0). \tag{3.17}$$

Then, the interconnected system (3.16) is input-to-state convergent.

A schematic representation of the interconnected system (3.16) is depicted in Figure 3.1.

The following theorem combines Theorem 3.2.1, Theorem 3.3.1, Theorem 3.3.2 and Property 3.3.3 and shows how to design an output-feedback controller that renders a continuous PWA system input-to-state convergent. The output-feedback controller consists of an observer with exponentially stable observer error dynamics and a state-feedback controller that renders the considered PWA system input-to-state convergent with respect to the observer error dynamics and an exogenous input. This theorem represents an adapted version of Theorem 2 in [100].

Theorem 3.3.4 *Consider the continuous PWA system* (3.1). *Suppose that the LMIs* (3.4) *and either* (3.8) *or* (3.14) *are feasible. Denote* $K = P_s P_c^{-1}$ *and let* $L = P_o^{-1} X$ *be the observer gain* L *for observer* (3.7) *or* L_1, L_2 *for observer* (3.12). *Then, system* (3.1) *in closed-loop with the dynamic controller* $u = -K\hat{x}$, *where* $\hat{x}$ *is generated by either observer* (3.7) *or* (3.12) *is input-to-state convergent, with respect to the input* $w(t)$.

Proof Denoting the observer error $\Delta x := x - \hat{x}$, we can write the system (3.1) in closed loop with the observer-based controller (3.7) (or (3.12)) and $u = -K\hat{x}$ as

$$\dot{x} = (A_i - B_1 K)x + b_i - B_1 K \Delta x + Bw(t) \text{ for } \ x \in \Lambda_i, \tag{3.18a}$$

$$\Delta\dot{x} = g(x, u, w) - g(x + \Delta x, u, w), \tag{3.18b}$$

$$u = -K(x + \Delta x), \tag{3.18c}$$

where (3.18b) reflects either the observer error dynamics (3.9) or (3.13). Since the LMIs (3.4) are feasible, system (3.18a) with $(\Delta x, w)$ as inputs is input-to-state convergent by Theorem 3.2.1. Due to the fact that the LMIs (3.8)

or the matrix inequalities (3.14) are feasible, the corresponding observer error dynamics are globally exponentially stable and Δx satisfies

$$|\Delta x(t)| \leq ce^{-\beta(t-t_0)}|\Delta x(t_0)|, \tag{3.19}$$

where the numbers $c > 0$ and $\beta > 0$ are independent of $x(t)$, $w(t)$. Applying Property 3.3.3 we obtain that the interconnected system (3.18) is input-to-state convergent with respect to the input $w(t)$. □

3.4 Bound on the control input

In this section, the previous design procedure is adapted to guarantee that the control action required to render a system convergent stays below a predefined value, given a class of bounded disturbances and a compact set of initial conditions. To bound the control action one needs, first, a restricted set in which the system state resides irrespective of the effect of disturbance (i.e. a positively invariant (PI) set for the system state). Secondly, one should relate this PI set to a bound on the control input. These conditions should preferably have an LMI form in order to facilitate the computationally efficient combination with the previous LMIs.

We will provide such a computational characterization of a PI set and an LMI formalism for the control input bound. We will do this following three important technical lemmas, that will be proven next, and will be used to obtain the main result (Theorem 3.4.5) of this section. This theorem provides conditions under which there exists a PI set for the state of system (3.1)-(3.2) and a saturation bound for the control input u while the system is input-to-state convergent. The proof of the existence of the PI set for the system state is based on a quadratic Lyapunov function V. The first lemma provides an analytical (lower) bound on the rate of decay of V along solutions of system (3.1)-(3.2) (towards their steady-state solution). The second lemma provides conditions under which the control action of a system remains bounded given the fact that the state lives in a bounded set at all times. The third lemma shows how such a PI set can be obtained based on the quadratic Lyapunov function V.

Lemma 3.4.1 *Consider system* (3.1a) *and the linear static state-feedback law* (3.2). *If there exists a feedback gain matrix* K *and a matrix* $P = P^T > 0$ *that satisfy* (3.5), *then there exists a constant* $\alpha > 0$ *such that*

$$P(A_i - B_1K) + (A_i - B_1K)^T P \leq -2\alpha P, \quad \text{for} \quad i = 1, ..., l, \tag{3.20}$$

where

$$\alpha = \min_i\{\alpha_i\} > 0 \tag{3.21}$$

and

$$\alpha_i = -\frac{1}{2}\lambda_{max}(P^{\frac{1}{2}}(A_i - B_1K)P^{-\frac{1}{2}} + P^{-\frac{1}{2}}(A_i - B_1K)^T P^{\frac{1}{2}}) > 0, \quad \textit{for} \quad i = 1, ..., l, \tag{3.22}$$

where $\lambda_{max}(\cdot)$ represents the maximum eigenvalue of a symmetric matrix.

Proof Since the matrices K and P satisfy (3.5), it holds that

$$P(A_i - B_1K) + (A_i - B_1K)^T P < 0, \quad \text{for} \quad i = 1, ..., l. \tag{3.23}$$

By pre- and post-multiplying (3.23) by $P^{-\frac{1}{2}}$ we derive the following inequality

$$P^{\frac{1}{2}}(A_i - B_1K)P^{-\frac{1}{2}} + P^{-\frac{1}{2}}(A_i - B_1K)^T P^{\frac{1}{2}} < 0, \quad \text{for} \quad i = 1, ..., l. \tag{3.24}$$

Hence, it holds that

$$\begin{array}{l} P^{\frac{1}{2}}(A_i - B_1K)P^{-\frac{1}{2}} + P^{-\frac{1}{2}}(A_i - B_1K)^T P^{\frac{1}{2}} \leq \\ \lambda_{max}(P^{\frac{1}{2}}(A_i - B_1K)P^{-\frac{1}{2}} + P^{-\frac{1}{2}}(A_i - B_1K)^T P^{\frac{1}{2}})I, \end{array} \tag{3.25}$$

for $i = 1, ..., l$ where I is a unity matrix of appropriate dimensions. Note that $\lambda_{max}(P^{\frac{1}{2}}(A_i - B_1K)P^{-\frac{1}{2}} + P^{-\frac{1}{2}}(A_i - B_1K)^T P^{\frac{1}{2}}) < 0$ since $P^{\frac{1}{2}}(A_i - B_1K)P^{-\frac{1}{2}} + P^{-\frac{1}{2}}(A_i - B_1K)^T P^{\frac{1}{2}}$ is negative definite for any $i \in \{1, ..., l\}$. Hence, by pre- and post-multiply (3.25) by $P^{\frac{1}{2}}$, we obtain

$$P(A_i - B_1K) + (A_i - B_1K)^T P \leq -2\alpha_i P, \quad \text{for} \quad i = 1, ..., l, \tag{3.26}$$

where α_i as in (3.22). By choosing $\alpha = \min_i\{\alpha_i\}$ inequality (3.20) holds. This completes the proof. □

Lemma 3.4.2 *Consider $x \in \mathbb{R}^n$, $u_{max} > 0$, $\rho > 0$, the matrix $P \in \mathbb{R}^{n\times n}$ with $P = P^T > 0$ and the matrix $P_s \in \mathbb{R}^{k\times n}$ such that*

$$\begin{bmatrix} u_{max}^2/\rho I & P_s \\ P_s^T & P^{-1} \end{bmatrix} \geq 0, \tag{3.27}$$

with $K := P_sP$. Then $x \in \Theta_\rho := \{\xi | \xi^T P \xi \leq \rho\}$ implies that $\|Kx\| \leq u_{max}$.

Proof We need to show that for all $x \in \mathbb{R}^n$ it holds that

$$x^T Px \leq \rho \Rightarrow \|Kx\| \leq u_{max}. \tag{3.28}$$

The right-hand side of (3.28), $\|Kx\| \leq u_{max}$, is equivalent to

$$x^T K^T Kx = x^T PP_s^T P_s Px \leq u_{max}^2. \tag{3.29}$$

Thus, we need to show that

$$x^T Px \leq \rho \Rightarrow x^T PP_s^T P_s Px \leq u_{max}^2. \tag{3.30}$$

Substituting the coordinate transformation $x = P^{-1}v$ in (3.30), shows that (3.30) is equivalent to

$$v^T P^{-1} v \leq \rho \Rightarrow v^T P_s^T P_s v \leq u_{max}^2. \tag{3.31}$$

Clearly, the implication in (3.31) holds if

$$\frac{P_s^T P_s}{u_{max}^2} \leq \frac{P^{-1}}{\rho}. \tag{3.32}$$

Using Schur complements (see [15]) on (3.32), we obtain the requirement in (3.27), which completes the proof. □

Remark 3.4.3 Note that the variables of (3.27) are P^{-1}, P_s, which are the same as in the LMIs (3.4) that guarantee convergence of the considered PWA system. Moreover, in (3.27) we can choose $\rho = 1$ without loss of generality, because the LMIs scale with ρ, i.e. if P^{-1}, P_s is a solution to (3.27) for $\frac{P}{\rho}$, ρP_s is a solution to (3.27) for $\rho = 1$ (resulting in the same K).

Note that Θ_ρ is a subset of the safe set $S := \{x \in \mathbb{R}^n | \|Kx\| \leq u_{max}\|$ largest set for which $\|Kx\| \leq u_{max}$. However, in general, S is not a PI set for the closed-loop (3.1a)-(3.2). As such, one often searches for the maximal positively invariant set inside S for the closed-loop system (3.1a)-(3.2). As this maximal PI set might be hard to construct, we will use Θ_ρ instead, because we have an approach to guarantee PI for this set.

This approach will be shown in the next lemma, where we use the norm $\|x\|_P = \sqrt{x^T P x}$ for a positive definite matrix P.

Lemma 3.4.4 *Consider system* (3.1) *and the linear static state-feedback law* (3.2). *Suppose there exist matrices* $P \in \mathbb{R}^{n\times n}$ *with* $P = P^T > 0$ *and* $P_s \in \mathbb{R}^{k\times n}$ *that satisfy the matrix inequalities*

$$-P^{-1}A_i^T + P_s^T B_1^T - A_i P^{-1} + B_1 P_s > 0,\ i = 1, ..., l, \tag{3.33}$$

and define $K := P_s P$. *Then the following statements hold:*

- *Let an external input* $w(t) : \mathbb{R} \to \mathbb{R}$ *be given. The set*

$$\Theta_\gamma = \{x \in \mathbb{R}^n | \|x\|_P^2 \leq \gamma\}, \tag{3.34}$$

with

$$\gamma = \frac{1}{\alpha^2}(\max_i\{\|b_i\|_P\} + \|B\|_P \sup_{t\in\mathbb{R}} \|w(t)\|_P)^2 \tag{3.35}$$

and α *as in* (3.22), *is a PI set for system* (3.1)-(3.2) *with disturbance* $w(t)$. *Moreover,* Θ_γ *characterizes an asymptotic ultimate upper bound for the state of system* (3.1)-(3.2) *with disturbances* $w(t)$;

- *Any set*
$$\Theta_\rho = \{\xi | \|\xi\|_P^2 \leq \rho\}, \tag{3.36}$$
with $\Theta_\gamma \subseteq \Theta_\rho$ *(i.e.* $\gamma \leq \rho$*) is a positively invariant set for system* (3.1)-(3.2) *with external input* $w(t)$*.*

Proof We will show that the ellipsoid Θ_γ is a PI set for the input-dependent closed-loop system (3.1), (3.2) if the LMI (3.33) is feasible. Consider hereto the closed-loop system (3.1), (3.2), as described in (3.3a), the quadratic Lyapunov function $V(x) = x^T P x$ and the time-derivative of V that satisfies for $x \in \Lambda_i$

$$\dot{V}(x,t) = 2x^T P \dot{x} = 2x^T P(A_i - BK)x + 2x^T P(Bw(t) + b_i). \tag{3.37}$$

The matrix inequality (3.33) implies that the matrix inequality (3.20) is satisfied for α as is Lemma 3.4.1.

Substitution of (3.20) in (3.37) yields

$$\begin{array}{rcl} \dot{V}(x,t) & \leq & -2\alpha x^T P x + 2x^T P(b_i + Bw(t)) \\ & = & -2\alpha \|x\|_P^2 + 2(P^{\frac{1}{2}}x)^T [P^{\frac{1}{2}}(b_i + Bw(t))] \\ & \leq & -2\alpha \|x\|_P^2 + 2\|P^{\frac{1}{2}}x\| \|P^{\frac{1}{2}}(b_i + Bw(t))\|, \end{array} \tag{3.38}$$

for $x \in \Lambda_i$. Note that $\|P^{\frac{1}{2}}x\| = \sqrt{(P^{\frac{1}{2}}x)^T P^{\frac{1}{2}}x} = \sqrt{x^T P x} = \|x\|_P$. Therefore, (3.38) can be dominated as

$$\begin{array}{rcl} \dot{V}(x,t) & \leq & -2\alpha \|x\|_P^2 + 2\|x\|_P \|b_i + Bw(t)\|_P \\ & \leq & -2\alpha \|x\|_P^2 + 2\|x\|_P \sup_{t\in\mathbb{R}} \|b_i + Bw(t)\|_P \\ & = & -2\|x\|_P \{\alpha \|x\|_P - \sup_{t\in\mathbb{R}} \|b_i + Bw(t)\|_P\}. \end{array} \tag{3.39}$$

Since it holds that

$$\begin{array}{rcl} \sup_{t\in\mathbb{R}} \|b_i + Bw(t)\|_P & \leq & \max_i\{\|b_i\|_P\} + \sup_{t\in\mathbb{R}} \|Bw(t)\|_P \\ & \leq & \max_i\{\|b_i\|_P\} + \|B\|_P \sup_{t\in\mathbb{R}} \|w(t)\|_P, \end{array} \tag{3.40}$$

we obtain that $\dot{V}(x,t) \leq 0$ as long as

$$\|x\|_P \geq \alpha^{-1}(\max_i\{\|b_i\|_P\} + \|B\|_P \sup_{t\in\mathbb{R}} \|w(t)\|_P)$$

or

$$\|x\|_P^2 \geq \alpha^{-2}(\max_i\{\|b_i\|_P\} + \|B\|_P \sup_{t\in\mathbb{R}} \|w(t)\|_P)^2.$$

Consequently, the ellipsoid Θ_γ as defined in (3.21), (3.22), (3.34), (3.35) is a PI set and characterizes an asymptotic ultimate bound to which all solutions converge.

To prove the second statement, note that Θ_ρ is a level set of V and $\Theta_\gamma \subseteq \Theta_\rho$ by the hypothesis. If $x(t_0) \in \Theta_\rho$ and $x(t_0) \notin \Theta_\gamma$, then $\dot{V}(x(t)) < 0$ for

$t_0 < t < t_1$, with $t_1 := \inf\{t \geq t_0 | x(t) \in \Theta_\gamma\}$ (possibly $t_1 = \infty$). Hence, for all $t \in [t_0,\ t_1]$ $x(t) \in \Theta_\rho$. If $x(t_1) \in \Theta_\gamma$ (possibly for $t_1 = t_0$) then $x(t) \in \Theta_\gamma$, $\forall t \geq t_1$ since Θ_γ is a positively invariant set. Consequently, $x(t)$ can not leave Θ_ρ for $t \geq t_0$, which proves the second statement. □

Now, we combine Lemmas 3.4.1, 3.4.2 and 3.4.4 to prove a result that provides conditions under which 1) the closed loop system (3.1a), (3.2) is rendered uniformly convergent; 2) the controlled input is guaranteed to satisfy the bound $\|u\| \leq u_{max}$ for a given bound on the disturbances and a bounded set of initial conditions.

Theorem 3.4.5 *Consider system* (3.1). *Suppose there exist* $P_s \in \mathbb{R}^{k\times n}$ *and a matrix* $P \in \mathbb{R}^{n\times n}$ *with* $P = P^T > 0$ *that satisfy the matrix inequalities* (3.33) *and* (3.27) *for a given* $u_{max} > 0$ *and* $\rho > 0$ *and define* $K := P_s P$. *Then,*

- *the closed-loop system* (3.1), (3.2) *is uniformly convergent and input-to-state convergent with respect to the input* $w(t)$*;*
- $x(t)$ *is asymptotically ultimately bounded to the set* Θ_γ *for specific bounded disturbances, with* Θ_γ *and* γ *as in* (3.34) *and* (3.35)*, respectively, and* $x(t)$ *denotes the solution of* (3.1) *with initial state* $x_0 = x(t_0) \in \Theta_\rho$*;*
- *Suppose* Θ_ρ *given in* (3.36) *satisfies* $\Theta_\gamma \subseteq \Theta_\rho$*, then for any* $x(t) \in \Theta_\rho$*, it holds that* $\|u(t)\| \leq \|Kx(t)\| \leq u_{max}$ *for all* $t \geq t_0$ *and bounded disturbance* $w(t)$.

Proof The LMI (3.33) guarantees uniform convergence and input-to-state convergence of the considered closed-loop system based on Theorem 3.2.1.

Based on Lemma 3.4.4, it is obvious that for the input-dependent closed-loop system (3.1)-(3.2) the ellipsoid Θ_γ as defined in (3.34)-(3.35), (3.22) is PI if the LMI (3.33) is feasible. Based on Lemma 3.4.4, if $\Theta_\gamma \subseteq \Theta_\rho$ then Θ_ρ is PI. Thus, if $x(t_0) \in \Theta_\rho$ then $x(t) \in \Theta_\rho$ $\forall t \geq t_0$. Moreover, based on Lemma 3.4.2 and the feasibility of the LMI (3.27) we conclude that $\|u(t)\| = \|Kx(t)\| \leq u_{max}$ as $x(t) \in \Theta_\rho$ for all $t \geq t_0$. Hence, the proof is complete. □

Under the hypothesis $x(t) \in \Theta_\rho$ for all $t \geq t_0$ of Theorem 3.4.5 the saturated closed-loop system is still convergent in the compact set Θ_ρ (see [101] for an exact definition on convergent systems in compact sets) with the same steady-state solution as the unsaturated system.

At this point, we will provide the procedure one has to follow to compute the control gain K for the state-feedback law (3.2). As a first step, we choose u_{max}, an upper bound ($R_{max} := \sup_{t\in\mathbb{R}} \|w(t)\|$) for the disturbances w and we set $\rho = 1$. As a second step, we compute P^{-1} and P_s by solving the LMIs (3.27) and (3.33). Next, we compute $K = P_s P$, γ and α (for γ and α we use (3.35) and (3.21), (3.22), respectively). Finally, we check whether $\gamma \leq 1$ (in

other words $\Theta_\gamma \subseteq \Theta_\rho$). If this is the case, then we know from Lemma 3.4.4 that Θ_ρ is PI and from Lemma 3.4.2 that the control input u is bounded by u_{max} for initial state in Θ_ρ and all disturbances with $\|w(t)\| \leq R_{max}$. In case $\gamma > 1$, then we cannot conclude whether Θ_ρ is PI or not. Moreover, in that case we cannot conclude that the system can be rendered (quadratic) convergent for the given disturbances and initial states and satisfying the control bound u_{max}. Note that γ in (3.35) scales the bound R_{max} on the disturbances. Therefore, in case $\gamma > 1$ the satisfaction of the conditions of Theorem 3.4.5 can still be satisfied for some smaller bound $\bar{R}_{max} < R_{max}$ on disturbances.

We studied here only the case of state-feedback. We postpone the discussion on the applicability of the proposed bound for the output-feedback controller to the end of Section 3.5.1.

3.5 Output bounds and performance measures

Using Theorem 3.4.5 and the fact that the input w is bounded, we will introduce an asymptotic ultimate bound for the output of the considered class of PWA systems in the following section. Such an asymptotic ultimate bound for the system output can readily be used to asses the closed-loop attenuation performance of PWA systems for a wide class of piecewise continuous disturbances.

3.5.1 Asymptotic ultimate boundedness of the output

The asymptotic ultimate bound on the system output that we introduce here is valid for general piecewise continuous disturbances and applies to continuous PWA systems.

Consider the 2-norm of the output y as defined in (3.1b):

$$\|y\| = \|Cx\| \leq \|C\|\|x\|. \tag{3.41}$$

Since $P = P^T > 0$, it holds that

$$\begin{array}{lll} & \lambda_{min}(P)x^Tx & \leq x^TPx \\ \Leftrightarrow & \lambda_{min}(P)\|x\|^2 & \leq \|x\|_P^2 \\ \Leftrightarrow & \|x\|^2 & \leq \lambda_{min}^{-1}(P)\|x\|_P^2 \\ \Leftrightarrow & \|x\| & \leq \frac{1}{\sqrt{\lambda_{min}(P)}}\|x\|_P. \end{array} \tag{3.42}$$

Due to (3.41), (3.42) we have that

$$\|y\| \leq \frac{1}{\sqrt{\lambda_{min}(P)}}\|C\|\|x\|_P. \tag{3.43}$$

In Theorem 3.4.5, we have shown that if the LMI (3.33) is feasible and $w(t)$ is bounded for all $t \in \mathbb{R}$ ($R_{max} := \sup_{t\in\mathbb{R}} \|w(t)\|$), then the following inequality

provides an asymptotic ultimate bound on the state:

$$\|x\|_P \leq \frac{1}{\alpha}(\max_i\{\|b_i\|_P\} + \|B\|_P \sup_{t\in\mathbb{R}} \|w(t)\|_P). \tag{3.44}$$

Using (3.43) yields an asymptotic ultimate bound on the system output:

$$\begin{array}{rcl} \|y\| & \leq & \frac{1}{\alpha\sqrt{\lambda_{min}(P)}}\|C\|(\max_i\{\|b_i\|_P\} + \|B\|_P\|P^{\frac{1}{2}}\|R_{max}) \\ & \leq & \frac{\|C\|\max_i\{\|b_i\|_P\}}{\alpha\sqrt{\lambda_{min}(P)}} + \frac{\|C\|\|B\|_P\|P^{\frac{1}{2}}\|}{\alpha\sqrt{\lambda_{min}(P)}}R_{max} =: Y_b, \end{array} \tag{3.45}$$

It is obvious that (3.45) provides an ultimate asymptotic bound for output y for any disturbance $w(t)$ that satisfies $\|w(t)\| \leq R_{max}$ for all t. This bound can be used, for example, to evaluate the performance of different controllers in terms of disturbance attenuation. However, it can be conservative since it is based on a quadratic Lyapunov function and it is applicable to the wide class of piecewise continuous bounded disturbances. Therefore, for particular disturbances of interest, it can be important to find more specific and tighter bounds.

So far, we have developed bounds for the PWA system (3.1) in closed-loop with the state-feedback law $u = -Kx$. In order to use the control input bound as proposed in Section 3.4 and the ultimate bound on the output as proposed in Section 3.5.1 in the output-feedback case, one can activate first the observer and then, after Δx has converged to zero, switch on the controller. In such a situation, we can still apply the control input bounds and the outputs in the output-feedback case.

As harmonic disturbances are very common in engineering practice, we focus in the next section on this class of periodic disturbances.

3.5.2 Performance measures for periodic disturbances

Periodic (or in particular harmonic) disturbances arise in many mechanical systems. For instance, in the specific application of the PWL beam they are caused by mass unbalance excitation. In many of these systems the attenuation of the response to this specific class of disturbances is of great concern for the performance of these systems. Indeed, the presence of periodic disturbances in mechanical systems is inevitable and disturbance amplification, especially when the disturbance frequencies are close to the resonance frequencies of one or more system's elements, is undesirable. Indeed, it is well known that resonating elements exhibit responses with very high amplitudes. This phenomenon very often causes violent damages in the structure of a mechanical system and as such is unwanted.

A bound on the system state or output, as introduced in the previous section, provides a non-discriminating view on the disturbance attenuation for

harmonic disturbances (and all other specific classes of disturbances satisfying the amplitude bound), because this bound is uniform over all disturbances. Accounting for the specific responses to these harmonic disturbances, which may vary significantly over the disturbance frequency range, allows for a dedicated performance assessment in terms of disturbance attenuation for this type of disturbances (Bode-like plot for convergent systems). Obviously, such exact response evaluation only makes sense if the steady-state solution is asymptotically unique (otherwise the performance could not be uniquely defined in terms of these steady-state responses). It is exactly the uniform convergence property, which we induce in the closed-loop system by means of feedback, that ensures the existence, uniqueness and global asymptotic stability of the steady-state solution for every given bounded disturbance. Moreover, convergent systems exhibit the favorable property that the steady-state response to periodic disturbances is also periodic with the same period time, see Chapter 2. This allows the introduction of so-called frequency-response functions (the Bode-like plots we mentioned earlier) for nonlinear but convergent systems, see [101], [102].

Now, let us illustrate the reasoning above by means of an example. Consider system (3.1) and the control law (3.2) for the case that we have scalar output $y \in \mathbb{R}$. For a class of bounded disturbances $w(t)$ (in this case harmonic with constant amplitude) we compute the steady-state solution for the open- and closed-loop system. For the open-loop system we consider the 'worst' stable steady-state solution ('worst' in the sense of largest maximum value of $\sup_{t\in\mathbb{R}} \|y(t)\|$). For the closed-loop system we use two different linear controllers ($u = -K_a x$, $u = -K_b x$) characterized by two feedback gains K_a, K_b that render the closed-loop convergent.

For this example, let us define the disturbance attenuation performance as the attenuation of the output response in steady-state $\bar{y}^w$ to harmonic disturbances w with frequency ω and fixed amplitude R in a given frequency interval $[\omega_{min} \quad \omega_{max}]$, with $0 < \omega_{min} < \omega_{max}$, (see also Figure 3.2). For sake of simplicity, we assume that the open-loop system is also uniformly convergent. Next, we evaluate the performance of the closed-loop system, with controllers with gains K_a and K_b. As a performance measure, we first use the ultimate bound Y_b in (3.45) or one of the bounds introduced in the papers [39], [47], [54], [109] which predict the output bound for a general class of piecewise continuous disturbances. Note that these bounds might very well be (almost) equal for both control gains K_a and K_b, i.e. $Y_b(K_a) = Y_b(K_b) = Y_b$. In Figure 3.2, we depict this bound (thick solid line). Moreover, we plot the maximum absolute value of the steady-state open-loop periodic output responses $\max_{t\in[0,\ T]} \|\bar{y}^w_{ol}(t)\|$ over one period $T = \frac{2\pi}{\omega}$ (solid curve) and a similar measure for closed-loop periodic output response $\max_{t\in[0,\ T]} \|\bar{y}^w_{cl}(t)\|$ (dashed and dashed-dotted curves). The dashed curve corresponds to the controller with gain K_a and the dashed-dotted curve to the controller with gain K_b. Consequently, based on the asymptotic

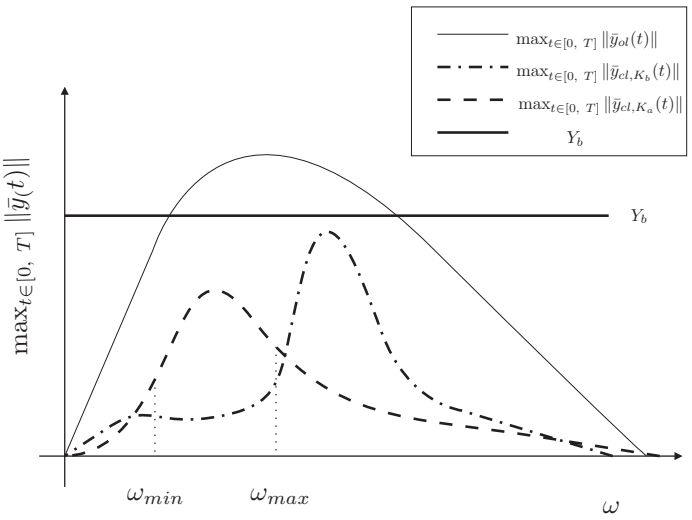

Figure 3.2: Asymptotic ultimate bound based on (3.45) *(thick solid line), open-loop periodic response* $\max_{t\in[0,\ T]} \|\bar{y}_{ol}(t)\|$ *(solid curve), closed-loop periodic response* $\max_{t\in[0,\ T]} \|\bar{y}_{cl}(t)\|$ *(dashed and dashed-dotted curves).*

ultimate bound $Y_b(K_a) = Y_b(K_b)$, the controllers perform equally well. Nevertheless, based on Figure 3.2, it is obvious that the controller with gain K_b performs better than the controller with gain K_a for disturbances in the frequency range $\omega \in [\omega_{min}, \quad \omega_{max}]$. The comparison of K_a and K_b based on the ultimate bound Y_b cannot reveal such differences. Therefore, in the following we propose performance measures based on computed steady-state solutions for harmonic disturbances.

In general, responses with large amplitudes and high energy content result in premature material fatigue of a mechanical system. Therefore, it is very interesting to study control designs for mechanical systems that result in systems with small amplitudes and low energy content responses given periodic disturbances. The foregoing motivates the need for performance measures that reflect either or both the magnitude or energy of such periodic responses. These performance measures can subsequently be used to evaluate and compare the 'disturbance attenuation' performance of different control designs. As already mentioned, for uniformly convergent systems the steady-state response to a given harmonic disturbance exists, is unique and has the same period as the disturbance.

Using these unique steady-state responses, we propose a performance measure that is based on the maximum value of the L_p-norm (signal norm) of these steady-state responses $\bar{y}^{\omega,R}(t)$ for system (3.1)-(3.2) and disturbances $w(t) = R\sin\omega t$ over a range of frequencies $\omega \in [\omega_{min},\ \omega_{max}]$ and amplitudes

$R \in [R_{min},\ R_{max}]$. This 'worst case' performance measure is denoted by Π_1^p, $p \in \mathbb{N}$ including $p = \infty$, and it is defined according to

$$\Pi_1^p = \frac{\pi_1^p}{\pi_{1,ref}^p}, \quad 1 \leq p \leq \infty, \tag{3.46}$$

with

$$\pi_1^p = \max_{R \in [R_{min}\ R_{max}]} \{ \max_{\omega \in [\omega_{min}\ \omega_{max}]} \{ \|\bar{y}^{\omega,R}\|_{L_p} \} \} \quad \text{for} \quad 1 \leq p \leq \infty, \tag{3.47}$$

and

$$\pi_{1,ref}^p = \max_{R \in [R_{min}\ R_{max}]} \{ \max_{\omega \in [\omega_{min}\ \omega_{max}]} \{ \|\bar{y}_{ref}^{\omega,R}\|_{L_p} \} \} \quad \text{for} \quad 1 \leq p \leq \infty. \tag{3.48}$$

The steady-state output response of system (3.1)-(3.2) for a certain reference controller is denoted as $\bar{y}_{ref}^{\omega,R}$ in (3.48). Note that the denominator in (3.46) is used to provide a means of scaling. The L_p-norm of $\bar{y}$ is defined as

$$\|\bar{y}\|_{L_p} = \begin{cases} \frac{1}{T} \int_0^T \|\bar{y}(t)\|^p dt)^{1/p} & \text{for } 1 \leq p < \infty \\ \max_{t \in [0,\ T]} \|\bar{y}(t)\| & \text{for } p = \infty \end{cases} \tag{3.49}$$

because $\bar{y}(t)$ is periodic with period T. Note that a value of Π_1^p less than 1 indicates that the current controller performs better than the reference controller. Note that, Π_1^∞ is a hint of 'worst case' output 'amplitude' or peak value and that Π_1^2 is a performance measure accounts for the 'worst case' output energy.

Besides a 'worst case' performance measure such as Π_1^p, we also propose a measure that uses a more averaged summed quantity. We denote this measure by Π_2^p and define it as

$$\Pi_2^p = \frac{\int_{w_{min}}^{w_{max}} \int_{\omega_{min}}^{\omega_{max}} \|\bar{y}^{\omega,R}\|_{L_p} d\omega dR}{\int_{w_{min}}^{w_{max}} \int_{\omega_{min}}^{\omega_{max}} \|\bar{y}_{ref}^{\omega,R}\|_{L_p} d\omega dR} \quad \text{for} \quad 1 \leq p \leq \infty. \tag{3.50}$$

In (3.50), ω_{min} and ω_{max} denote the lower and upper bound of the excitation frequency interval of interest and, similarly, R_{min} and R_{max} denote the lower and upper bound of the excitation amplitude interval of interest. As Π_1^p, $\Pi_2^p \in \mathbb{R}^+$ is also a relative measure with respect to a reference controller.

These performance measures together with the frequency response functions form a systematic way to study the performance of control designs that aim at attenuating the amplitude of the steady-state system responses.

3.5.3 Performance-based control design for disturbance attenuation of periodic disturbances

In this section, we consider the convergence-based controllers proposed in Section 3.2 and 3.3 and the performance measures proposed in Section 3.5.2, in

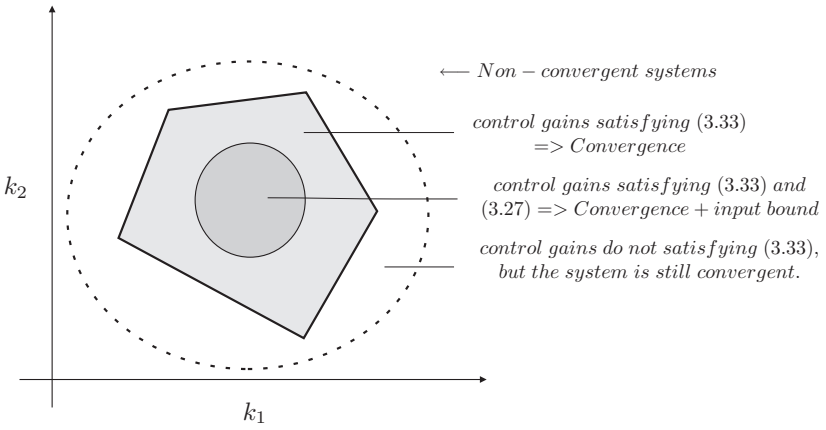

Figure 3.3: Convergent and non-convergent systems.

order to develop a systematic approach for disturbance attenuation of PWA systems in the face of harmonic disturbances.

By solving the LMIs (3.27) and (3.33) we guarantee, firstly, that the system (3.1) in closed-loop with the resulting linear static state-feedback law (3.2) is uniformly convergent. Secondly, we guarantee that the control input $u(t)$ is bounded using Theorem 3.4.5, i.e. $\|u(t)\| \leq u_{max}$ for $t \geq t_0$ and for all disturbances $w(t)$ with $\|w(t)\| \leq R_{max},\ t \in \mathbb{R}$ and initial states $x(t_0)$ in the set $\Theta_\rho = \{x | \|x\|_P^2 \leq \rho\}$ at time t_0. Last but not least, we desire to design a controller, satisfying the above two properties, that attenuates periodic disturbances acting on a PWA system adequately. In the present work, we follow a brute force approach that just generates many controllers satisfying (3.27) and (3.33) and evaluate their performance using the measures in Section 3.5.2. We aim at finding the controller that has the best performance (among the considered controllers) for the given disturbance attenuation problem. Of course, a more structured approach would be to make the proposed performance measures objective functions in an optimization problem in which the LMIs (3.27) and (3.33) are constraints. Since Π_1^p and Π_2^p are not analytically available, this is not a straightforward task. However, it is of interest and certainly a topic for future research.

To make our approach a bit more specific, consider a PWA system (3.1) with $x \in \mathbb{R}^2$ and with control gain $K = [k_1,\ k_2]$. By solving the LMIs (3.27) and (3.33) we guarantee that this system is uniformly convergent and that $\|u(t)\| \leq u_{max}$ for $t \geq t_0$, for all $w(t)$ with $\|w(t)\| \leq R_{max},\ t \in \mathbb{R}$ and $x(t_0) \in \Theta_\rho$ as outlined in Lemma 3.4.4. The control gain elements k_1 and k_2 satisfying these conditions are depicted in Figure 3.3 by the set with dark grey color. Note that in this figure the axes are related to the elements k_1 and k_2 of the controller gain

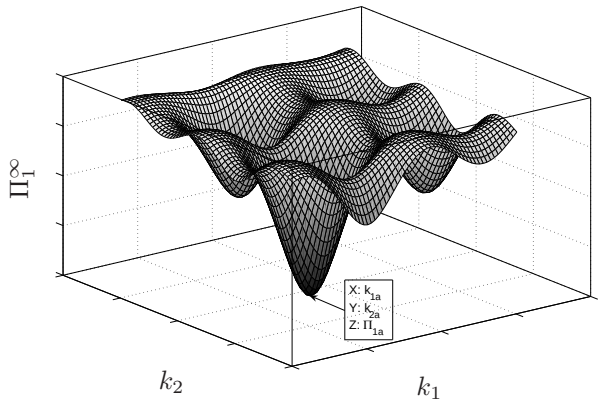

Figure 3.4: Performance measure illustration.

K. The set with the light grey color in Figure 3.3 includes the control gains that satisfy only the LMI (3.33). As we have already mentioned in Section 3.2, the LMI (3.33) is only a sufficient condition for quadratic convergence. These control gains assure that the closed-loop system is uniformly convergent by using a control action that may be larger than u_{max}. The set within the dashed curve includes control gains that render the closed-loop system convergent, but do not satisfy LMI (3.33). Finally, the set outside the dashed curve includes control gains that do not render the closed-loop system convergent. We do not have a full characterization of the set of controllers indicated by the dashed curve.

The dark grey region is actually the region of interest. Moreover, to select the 'best' controller in terms of disturbance attenuation in this region we will use the performance measure introduced in (3.46). A graphical representation of this evaluation is given in Figure 3.4. In this figure, we depict the performance measure Π_1^∞. Based on the measure in Figure 3.4, we would promote the control gain $K_a = [k_{1a},\ k_{2a}]$ because it gives the minimum value for Π_1^∞. This approach will be adopted in Chapter 4 in order to evaluate the disturbance attenuation properties of different controllers for an experimental application with PWL characteristics.

3.6 Discussion

We have proposed a convergence-based control design strategy for perturbed PWA systems in order to achieve disturbance attenuation. The uniform convergence property was exploited for various reasons. More specifically, the

uniform convergence property guarantees stabilization, it was used to develop bounds for the system's input and output and several performance measures. Moreover, it was also used for observer-based output-feedback control design. In particular, the fact that a nonlinear system has a unique globally asymptotically stable steady-state solution when it is uniformly convergent for bounded disturbance signals was core to our design.

First, we used state-feedback controllers to render the closed-loop of a PWA system convergent and to attain disturbance attenuation. However, as often in practice the whole state is not available for feedback, we have also developed output-based controllers. These output-based controllers consist of an interconnection of model-based observers and a state-feedback that uses the estimated state of the observers as its input. We also showed that the 'separation principle' holds in this case in the sense that we are able to obtain input-to-state convergent closed-loop systems. In this way, we are able to separate the observer design from the controller design.

Moreover, we provided additional conditions under which the control action induced by these controllers can be bounded for a given bound on the disturbances and for a compact set of initial conditions. Such a guaranteed bound on the control action is very important for the implementation of the proposed control design strategy on real mechanical systems as we always have to deal with actuation limitations in practice.

To compare the disturbance attenuation properties of different control laws, we have proposed performance measures. These performance measures consist of 1) asymptotic ultimate bounds on the output for all disturbance signals that have the same upper bound. This measure does not discriminate between particular shapes or classes of disturbances, such as harmonic functions, 2) frequency response functions that provide Bode-like plots for the class of harmonic disturbances, 3) certain quantitative characterizations (Π_1^p and Π_2^p) that capture 'worst case' or 'averaged' information of the steady-state responses in one number.

An interesting extension of this work is the formulation of the presented performance-based control design strategy in terms of an optimization problem. In such a problem setting, the proposed performance measures (Π_1^p or Π_2^p) can be used as objective functions and the convergence property together with the control input saturation as LMI-based constraints for the optimization problem. Such an approach may be more efficient in constructing a high performance controller, although at the moment it is open how to tackle such complex optimization problem.

4

Convergence-based controller design implementation on a PWL beam system

4.1 Introduction

In this chapter, the controller design strategy presented in Chapter 3 is implemented on an experimental setup of a mechanical beam system with piecewise linear restoring characteristics. This experimental setup consists of two flexible steel beams. One of them behaves as a one-sided spring and the other is periodically excited by a rotating mass unbalance mechanism. A typical system model can be cast in the form of a PWA system with exogenous perturbations, see Section 4.2. The presence of periodic excitations and the one-sided spring creates complex dynamical phenomena [58] such as the coexistence of steady-state solutions and bifurcations. These nonlinear dynamic phenomena are present in many mechanical motion systems with one-sided flexibilities when they are excited by periodic disturbances. In such engineering systems, the coexistence of steady-state solutions in combination with high amplitude responses, due to 'nonlinear' resonances, is an undesirable phenomenon because it limits the system's performance and leads to early material failure of machine parts. Due to the fact that the examined setup produces this kind of behavior, it can be considered as a benchmark for this type of systems. In this chapter, we aim to eliminate the coexistence of multiple steady-state solutions in order to be able to uniquely assess the 'magnitude' of the closed-loop vibrations. Moreover, we aim to attenuate the effect of the periodic disturbances (induced by the mass unbalance) on the vibrations of the beam system. Thereby, we illustrate the applicability of the control synthesis results developed in Chapter 3.

In Section 4.2, the experimental setup is given and a model describing this setup is presented. The accuracy of the model with respect to the real system is studied based on simulations and experiments. Due to the fact that the full state of the system is not available for feedback, in Section 4.3, we briefly discuss the observer that will be used to estimate the system state. A more extensive discussion of the observer design and its performance in both simulations and experiments is presented in Appendix B. In Section 4.4, a number of output-feedback controllers are designed for and implemented on this system to attenuate periodic disturbances (using the results of Chapter 3). The structure of these output-feedback controllers, as proposed in Section 3.3, consists of an observer and a state-feedback controller. We use a state-feedback that is based on the notion of input-to-state convergence. More specifically, in Section 4.4.1, it is studied whether the examined state-feedback controllers render the PWL system convergent and in Section 4.4.2, it is studied whether these controllers render the PWL system convergent given a saturation constraint, introduced in Section 3.4, in the control input. The ability of the controllers to achieve disturbance attenuation is studied in Sections 4.5.1 and 4.5.2 based on bounds and performance measures for the system's output, as proposed in Sections 3.5.1 and 3.5.2, respectively. Finally, in Section 4.5.3 the controller with the 'best' disturbance attenuation properties is applied to the real experimental system. Its performance is evaluated based on extensive experimental tests.

4.2 Experimental setup

In order to evaluate experimentally the controller design strategy proposed in Chapter 3, we will use an experimental setup that is available in the Dynamics and Control Technology Laboratory at Eindhoven University of Technology. In the remainder of this thesis we will call this setup the PWL beam system.

4.2.1 Description of the PWL beam system

The experimental setup (see Figures 4.1 and 4.2) consists of a steel beam supported at both ends by two leaf springs. A second beam, that is clamped at both ends, is located parallel to the first one and acts as a one-sided spring. This one-sided spring represents a non-smooth nonlinearity in the dynamics of the beam system (beam and one-sided spring). The beam is excited by a force generated by a rotating mass-unbalance, that is mounted at the middle of the beam. A tacho-controlled motor, that enables a constant rotational speed, drives the mass-unbalance. An actuator is mounted on the beam in order to control the beam dynamics. In the experimental setup two positions can be measured by using linear voltage displacement transducers and the acceleration of the middle of the beam by using an accelerometer. For further information on the experimental setup the reader is referred to [58] and [132].

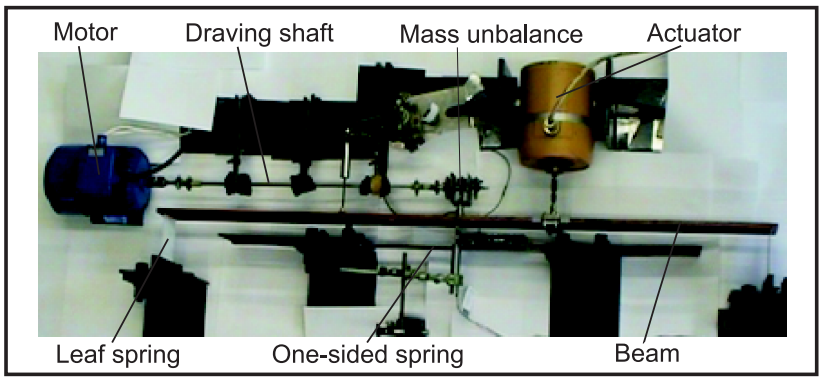

Figure 4.1: Photo of the experimental setup.

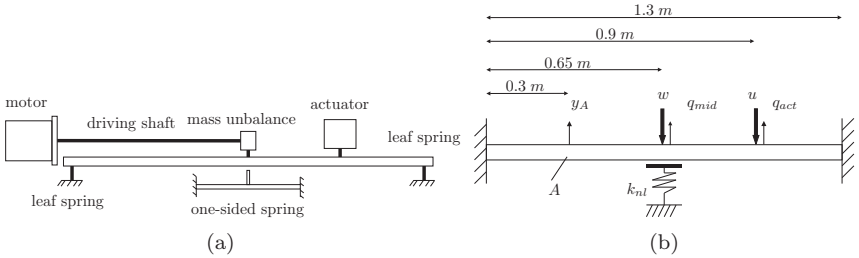

Figure 4.2: (a) Schematic representation of the experimental PWL beam setup (b) characteristic lengths and variables of the experimental PWL beam system.

When the beam moves from its rest point towards the one-sided spring, the spring is active. Therefore, the system has different dynamics on this side than on the opposite side. In the first case, the system dynamics is determined by the stiffness of the beam and the spring and, in the second case, only by the beam stiffness. The switching boundary between the two dynamic regimes is present at zero displacement of the middle of the beam. In case the one-sided spring has linear restoring characteristics, the beam system can be described as a PWL system.

4.2.2 Model of the PWL beam system

In order to describe the behavior of the PWL beam system accurately, a finite element model (FEM) has been developed, see [14]. Due to the large number of

the model DOFs, the simulation of the nonlinear responses is computationally expensive. In order to decrease the computation time we develop a reduced model, which is based on FEM, by using a dynamic component mode synthesis reduction method, the so-called Rubin method [30]. The full order model has 111 degree-of-freedom (DOF), and the reduced model will have four degrees of freedom (see later). The relation between the DOF of the FEM and the reduced model is given by

$$p = Tq, \tag{4.1}$$

where $p \in \mathbb{R}^{111}$ denotes the DOFs of the FEM model and $q \in \mathbb{R}^4$ the DOFs of the reduced model. The transformation matrix $T \in \mathbb{R}^{111\times 4}$ obtained from the model reduction procedure has the following structure:

$$T = [\tau_1 \mid \tau_2 \mid \cdots \mid \tau_{111}]^T, \tag{4.2}$$

where $\tau_i \in \mathbb{R}^4$. For further details of the reduction method the reader is referred to [14]. The dynamics of the system described by the 4DOF model is given by

$$M_r\ddot{q} + B_r\dot{q} + K_r q + f_{nl}(q) = h_1\, w(t) + h_2\, u, \tag{4.3}$$

where $h_1 = [1 \quad 0 \quad 0 \quad 0]^T$, $h_2 = [0 \quad 1 \quad 0 \quad 0]^T$ and
$q = [q_{mid} \quad q_{act} \quad q_{\xi,1} \quad q_{\xi,3}]^T$. Herein, q_{mid} is the displacement of the middle of the beam and q_{act} is the displacement of the point where the actuator is mounted at the beam, see Figure 4.2(b). Note that the actuator does not act in the middle of the beam. Moreover, $q_{\xi,1}$, $q_{\xi,2}$ reflect the contribution of the first and third eigenmode of the beam that occur at 21Hz and 55Hz, respectively. The contribution of the second eigenmode occurs at 23Hz and is neglected because it hardly contributes to the transversal system dynamics, see [14]. M_r, B_r and K_r are the mass, damping and stiffness matrices of the reduced model, respectively. We apply a periodic excitation force

$$w(t) = R(\omega)\sin\omega t, \tag{4.4}$$

which is generated by the rotating mass-unbalance at the middle of the beam. Herein, ω is the excitation frequency and $R(\omega)$ the amplitude of the excitation force. The amplitude $R(\omega)$ has the form

$$R(\omega) = m_a\omega^2, \tag{4.5}$$

where $m_a = m_e r_e$, with m_e and r_e the mass unbalance and the distance of m_e with respect to the center of mass of the mass-unbalance mechanism, respectively. The frequency dependency of $R(\omega)$ is due to the rotating mass-unbalance. More specifically, the higher the rotational velocity of the mass unbalance is, the higher the centrifugal forces due to the mass unbalance, hence the excitation amplitude $R(\omega)$. The numerical values of m_a, m_e and r_e are:

$1.014 \cdot 10^{-3} \frac{kg}{m^2}$, 0.078 kg, 0.013 m, respectively. The range of excitations is 10-60 Hz. Below 10 Hz the model accuracy is rather limited, while the frequency of 60 Hz is the maximum excitation frequency that the motor can provide to the system. Moreover, in (4.3) f_{nl} is the restoring force of the one-sided spring:

$$f_{nl}(q) = k_{nl}\ h_1\ \min(0, h_1^T q) = k_{nl}\ h_1\ \min(0, q_{mid}), \tag{4.6}$$

where $k_{nl} = 1.6 \cdot 10^5 \frac{N}{m}$ is the stiffness of the one-sided spring.

In state space form, the model (4.3), (4.4), (4.6) can be written as in (3.1) for $l = 2$ and $b_i = 0$ (bi-modal PWL system):

$$\dot{x} = \begin{cases} A_1 x + Bw + B_1 u \text{ for } \ H^T x \leq 0 \\ A_2 x + Bw + B_1 u \text{ for } \ H^T x > 0 \end{cases} \tag{4.7a}$$

$$u = Kx, \tag{4.7b}$$

with $A_1 x = A_2 x$ on $H^T x = 0$, $x = [q^T \quad \dot{q}^T]^T \in \mathbb{R}$, $H = [h_1^T \quad 0_{4\times 1}^T]$,

$$A_1 = \begin{bmatrix} 0_{4\times 4} & I_{4\times 4} \\ -M_r^{-1}(K_r + k_{nl}\ h_1\ h_1^T) & -M_r^{-1} B_r \end{bmatrix},$$

$$A_2 = \begin{bmatrix} 0_{4\times 4} & I_{4\times 4} \\ -M_r^{-1} K_r & -M_r^{-1} B_r \end{bmatrix},$$

$$B = \begin{bmatrix} 0_{4\times 1} \\ M_r^{-1} h_1 \end{bmatrix}, \quad B_1 = \begin{bmatrix} 0_{4\times 1} \\ M_r^{-1} h_2 \end{bmatrix}.$$

The numerical values of the matrices M_r $[kg]$, K_r $[N/m]$ and B_r $[Ns/m]$ are:

$$M_r = \begin{bmatrix} 3.38062 & 1.2961 & 2.0957 & -0.4958 \\ 1.2961 & 38.6548 & 16.3153 & -14.6109 \\ 2.0957 & 16.3153 & 8.6864 & -6.2413 \\ -0.4958 & -14.6109 & -6.2413 & 6.5893 \end{bmatrix},$$

$$K_r = 10^6 \begin{bmatrix} 2.4151 & 0.0521 & 1.1445 & -0.0199 \\ 0.0521 & 6.3914 & 2.6420 & -2.4342 \\ 1.1445 & 2.6420 & 1.6270 & -1.0107 \\ -0.0199 & -2.4342 & -1.0107 & 1.0542 \end{bmatrix},$$

$$B_{ext} = \begin{bmatrix} 109.3370 & 25.8569 & 61.4792 & -9.8913 \\ 25.8569 & 294.2009 & 128.7864 & -108.5757 \\ 61.4792 & 128.7864 & 85.1265 & -49.2662 \\ -9.8913 & -108.5757 & -49.2662 & 55.5620 \end{bmatrix}.$$

The output of the model (4.3), (4.4), (4.6) will be the transversal displacement of a point on the beam. This displacement is one of the 111 DOFs of the model. The state-space form of this output is

$$y = p_i = \tau_i q = [\ \tau_i^T \quad \underline{0}^T] x = Cx, \tag{4.8}$$

where p_i is the i^{th} DOF of the 111DOF model, ${\tau_i}^T$ is the i^{th} row of the transformation matrix T and $C = [{\tau_i}^T \quad \underline{0}^T]$ is the output matrix for the system (4.7a).

4.2.3 Evaluation of the model for the PWL beam system

In this section, we will use, following earlier work presented in [14], simulation and experimental results to show that the model of the PWL beam system captures with accuracy the dynamics of the real system. In addition to that, we will numerically show that the considered system is not convergent since it exhibits multiple coexisting steady-state solutions. For this purpose, we present periodic responses of the open-loop PWL beam system ((4.7a) with $u = 0$) for harmonic disturbances, as in (4.4). These responses correspond to the transversal displacements y_A and q_{mid} of two points on the beam (point A and middle of the beam, see Figure 4.2(b)) and they are based on numerical computations and measurements. For the numerical computation of these responses the collocation method [9] is used. Note that q_{mid} is the first element of the system state x and y_A is a system output. In general, the state elements and the output of system (4.7a) depend on both the excitation frequency ω and the excitation amplitude R. Therefore, x and y can be expressed as $x^{\omega,R}$ and $y^{\omega,R}$, respectively. As we have mentioned in the previous section, the excitation amplitude is a function of ω, see (4.5). Therefore, $x^{\omega,R}$ and $y^{\omega,R}$ can be written as x^{ω} and y^{ω}, respectively.

In Figures 4.3(a), 4.3(b), the plots of

$$\max_{t\in[0\ T]} |\bar{q}^{\omega}_{mid}(t)|/R(\omega) \text{ and } \max_{t\in[0\ T]} |\bar{y}^{\omega}_{A}(t)|/R(\omega)$$

for the open-loop system are depicted for the excitation frequency range [10, 60] Hz, where $\bar{q}^{\omega}_{mid}(t)$ and $\bar{y}^{\omega}_{A}(t)$ are the displacements q_{mid} and y_A in steady-state for an excitation frequency ω and an excitation amplitude $R(\omega)$. Note that these plots denote every value of

$$\max_{t\in[0\ T]} |\bar{q}^{\omega}_{mid}(t)|/R(\omega) \text{ and } \max_{t\in[0\ T]} |\bar{y}^{\omega}_{A}(t)|/R(\omega)$$

for each $\frac{\omega}{2\pi} \in [10,\ 60]$Hz. Moreover, for the PWL beam system the state solutions $\bar{x}^{\omega}(t)$ scale with $R(\omega)$, i.e. $\bar{x}_{\omega}(t)|/R(\omega)$ is independent of $R(\omega)$, as shown in [58] and [41]. By comparing the curves that correspond to measurements (thick solid curves) with those that correspond to numerical computations (thin solid and dashed curves), we can conclude that the model of the open-loop PWL beam system describes the steady-state dynamics of the real system accurately. Note that a time domain validation in the form of a comparsion between these measurements and the numerical computations is available in Appendix B. Based on both measurements and numerical computations, we showed that q_{mid} and y_A exhibit stable harmonic steady-state

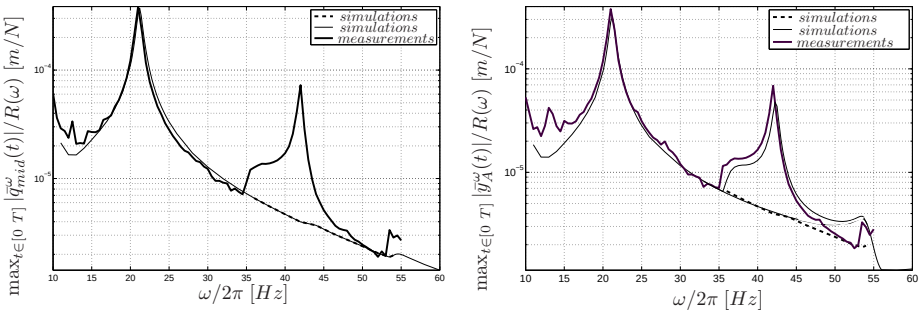

Figure 4.3: (a) $\max_{t\in[0\ T]} |q^{\omega}_{mid}(t)|/R(\omega)$; (b) $\max_{t\in[0\ T]} |y^{\omega}_{A}(t)|/R(\omega)$, based on the open-loop model of the PWL beam system (thin solid and dashed curves) and measurements of the real system (thick solid curve).

responses in the frequency range of [10, 36]Hz and stable 1/2-subharmonic steady-state responses in [36, 54]Hz. Based on numerical computations, we also notice that in the excitation frequency range [36, 54]Hz there also exist unstable harmonic steady-state responses (dashed curve in Figures 4.3(a), 4.3(b)). It is obvious that these responses cannot be measured in practice. Note that for $\frac{\omega}{2\pi} \in [34, 47]$Hz the experimental results are slightly shifted to the lower frequencies. The differences in the simulated and measured results in the latter frequency range are caused by model inaccuracies and noise in the measurements. Furthermore, for frequencies around 55Hz one can notice, in both simulations and measurements, the contribution of the third eigenmode in the system. From the aforementioned analysis, it is clear that the PWL beam system is not convergent since it exhibits multiple coexisting steady-state solutions given certain harmonic excitation signals.

4.3 Observer design implementations on the PWL beam system

We will use the switching observer (3.12) presented in Section 3.3.1 to estimate the state of the PWL beam system as we consider the situation where we can only measure the transversal displacement of one point on the beam (this implies that the full state is not available for feedback). In Appendix B, we design an observer based on the results of Theorem 3.3.1 and an observer based on the results of Theorem 3.3.2. Both observers are implemented on the PWL beam system. It is shown that these observers are able to estimate

the system state adequately and that the observer error dynamics is globally exponentially stable for both observers. Note that the observer error is defined as the difference between the real state of the system and the estimated state of the system. Moreover, the performance of these observers is investigated for different observer gain settings in both simulations and experiments. Herein, both the transients convergence speed and the steady-state sensitivity of the observer error to modelling errors and measurement noise are taken into account to support a choice for a particular gain setting. The observer gain with the best performance is the switching observer (3.12) with observer gains:

$$L_1 = [98.475\ 88.090\ -284.05\ -5.254\ 386.35\ 4626.0\ -18411.0\ 766.50]\,,$$

$$L_2 = [98.781\ 88.212\ -284.35\ -5.2469\ 1910.2\ 5031.8\ -19635.0\ 627.17]\,.$$

In the following section, we will use the switching observer (3.12) for the PWL beam system in an output-feedback control design and we will show that the interconnection of the observer with a state-feedback controller and the PWL system is stable. This is essential, due to the fact that a successful design of an observer and a state feedback controller does not necessarily imply a successful output-feedback design.

4.4 Output-feedback controller design for the PWL beam system

In the first part of this section, we will show that output-feedback controllers, with the structure proposed in Section 3.3, can attenuate periodic disturbances acting on the PWL beam system. More specifically, we will show that the proposed output-feedback controllers are stable, are able to render the PWL beam system convergent and are suitable for disturbance attenuation for periodic disturbances within a given frequency range. These output-feedback controllers consist of a state-feedback controller that uses the state estimates (derived from the switching observer (3.12)) of the PWL beam system. In the second part of this section, we will account for a bound for the control input, as proposed in Section 3.4, in the aforementioned output-feedback controllers and we will study the controller performance for disturbance attenuation in the face of this bound.

4.4.1 Output-feedback controller: Ideal case

To render the model of the PWL beam system globally uniformly convergent we use, firstly, a high gain controller, secondly, a controller based on experience and engineering insight for the PWL beam system and, finally, two controllers with a bound on the control action, based on Theorem 3.4.5.

Consider the system (4.7a), and the control law

$$u = K\hat{x} \tag{4.9}$$

with $\hat{x}$ the state estimate based on the observer (3.12). The observer gains are computed based on the LMIs in (3.14) and they are equal to those used in Appendix B.

High gain controller

The control gain K (denoted as K_{HG}) of a controller that guarantees convergence for the system (4.7) is computed by solving LMI (3.33) using the LMITOOL for MATLAB [38]. The numerical values of K_{HG} are

$$K_{HG} = 10^7 \cdot [6.4257\ 0.1538\ -1.8210\ 0.0576\ 0.0042\ -0.0002\ 0.0002\ 0.0001].$$

As we will show below these values are significantly larger than the values we obtain for the other control gains and they also lead to high control action (as will be shown in Figure 4.8). For the numerical values of the corresponding P matrix (P_{HG}), see Appendix A.

Controller based on engineering insight

Clearly, a whole range of control gains K satisfy condition (3.33). Based on engineering insight, we choose a control gain K (denoted as K_{EI} for this case) that adds damping to the nonlinear resonances of the system. Using the LMI condition (3.33) we check whether the resulting closed-loop system is convergent. Based on trial and error, we notice that by adding damping in q_{mid}, we render the system convergent and reduce the contributions of the first two resonances to all elements of the system state. Hereto, we choose K_{EI} of the form

$$K_{EI} = [0\ 0\ 0\ 0\ k_{EI}\ 0\ 0\ 0],\ \text{with}\ k_{EI} > 0;$$

i.e we add damping at the middle of the beam. The value of K_{EI} that is selected is

$$K_{EI} = 10^3 \cdot [0\ 0\ 0\ 0\ 32.0\ 0\ 0\ 0].$$

For the corresponding numerical values of P (from now on denoted as P_{EI}), see Appendix A.

Controllers based on constructive LMI conditions for an input saturation bound

A more constructive way to choose control gains K that do not lead to high control values is by using the LMI condition (3.33) together with the LMI condition (3.27) that ensures bounds on the control action u (we will provide

further information on these controllers in Section 4.4.2). For the present case, we compute two control gains denoted as $K_{IS,1}$ and $K_{IS,2}$ based on these LMIs. In order to compute these gains we add a component of the form μI, with $\mu > 0$ and I a unity matrix of proper dimension, to the right-hand side of (3.33). Subsequently, we choose different values for μ and solve the resulting LMI together with the LMI (3.27). The control gains derived in this way also satisfy the LMI (3.33). The obtained numerical values of $K_{IS,1}$, $K_{IS,2}$ and μ are

$$K_{IS,1} = [-7524.4\ 4831.3\ -16196.0\ 499.03\ 26.791\ 54.566\ -236.63\ -0.2323],$$

$$\mu_{IS,1} = 1.5$$

and

$$K_{IS,2} = [-36723.0\ 1389.0\ -38083.0\ 1068.5\ 15.589\ 3.7828\ -276.22\ -1.1345],$$

$$\mu_{IS,1} = 10.$$

The numerical values of the P matrices corresponding to $K_{IS,1}$ and $K_{IS,2}$ (denoted by $P_{IS,1}$ and $P_{IS,2}$, respectively) are given in Appendix A.

By using numerical analysis, we compute the steady-state responses of system (4.7) (with K being either K_{HG}, K_{EI}, $K_{IS,1}$ or $K_{IS,2}$). Based on this analysis, there is only one steady-state solution of (4.7) for every exogenous input $R(\omega)\sin\omega t$. This fact implies that indeed system (4.7) is uniformly convergent, as guaranteed by the theory. In Figures 4.4(a), 4.4(b) and 4.5, we plot $\max_{t\in[0\ T]}|\bar{q}^{\omega}_{mid}(t)|/R(\omega)$, $\max_{t\in[0\ T]}|\bar{q}^{\omega}_{act}(t)|/R(\omega)$ and $\max_{t\in[0\ T]}|\bar{y}^{\omega}_{A}(t)|/R(\omega)$ for the open- and closed-loop system, with $T = \frac{2\pi}{\omega}$. The symbol $\bar{\cdot}$ in $\max_{t\in[0\ T]}|\bar{q}^{\omega}_{mid}(t)|/R(\omega)$, $\max_{t\in[0\ T]}|\bar{q}^{\omega}_{act}(t)|/R(\omega)$ and $\max_{t\in[0\ T]}|\bar{y}^{\omega}_{A}(t)|/R(\omega)$ denotes the fact that we consider a steady-state solution. In these figures, the thin solid line and the dotted lines correspond to open-loop responses, while the thin dashed, the thin dash-dotted, the thick dash-dotted and the thick solid curves correspond to closed-loop responses. The frequency range of interest is $\frac{\omega}{2\pi} \in [10,\ 60]$Hz.
For a better understanding of these results also time responses of q_{mid} and y_A are shown in Figures 4.6 and 4.7 for the control gain $K_{IS,1}$. In these figures, $q_{mid}(t)$ and $y_A(t)$ are depicted for three different initial conditions $x_{0,i},\ i = 1, 2, 3$:

$$x_{0,1} = 10^{-4}[-8.529\ -328.4\ 24.70\ 56.72\ -226.0\ 234.8\ 234.4\ -7.413],$$

$$x_{0,2} = 10^{-4}[-11.51\ -44.33\ 3.335\ 7.658\ -30.51\ 31.70\ 31.65\ -1.000],$$

$$x_{0,3} = 2\cdot 10^{-3}[-11.51\ -44.33\ 3.335\ 7.658\ -30.51\ 31.70\ 31.65\ -1.000].$$

The excitation frequencies and the force amplitudes for the examined cases are $\frac{\omega}{2\pi} = 20$Hz, $A = 18$N and $\frac{\omega}{2\pi} = 43$Hz and $A = 50$N, respectively.

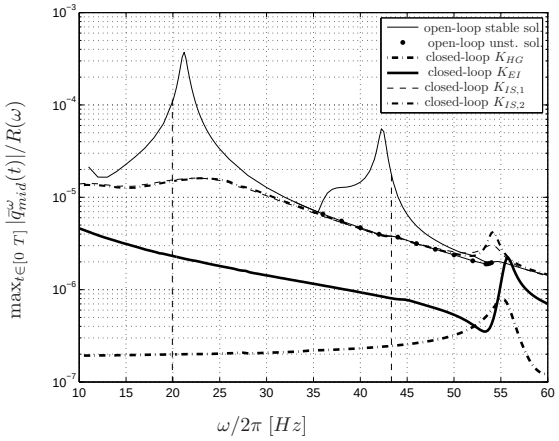

(a) $\max_{t\in[0\ T]} |\bar{q}^{\omega}_{mid}(t)|/R(\omega)$

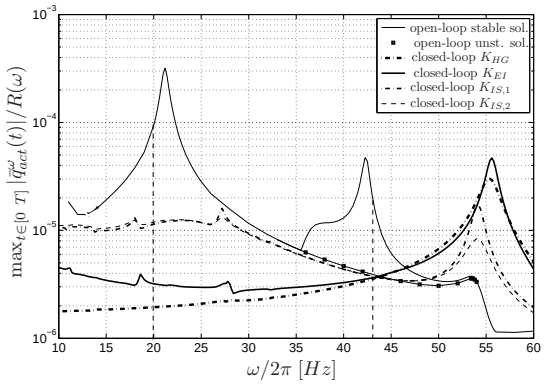

(b) $\max_{t\in[0\ T]} |\bar{q}^{\omega}_{act}(t)|/R(\omega)$

Figure 4.4: (a) $\max_{t\in[0\ T]} |\bar{q}^{\omega}_{mid}(t)|/R(\omega)$*; (b)* $\max_{t\in[0\ T]} |\bar{q}^{\omega}_{act}(t)|/R(\omega)$*, based on the open-loop (thin solid and thick dashed lines) and the closed-loop system* (4.7) *(dashed, thin dash-dotted, thick dash-dotted and thick solid lines).*

Based on Figures 4.4, 4.5 and 4.6-4.7, we can conclude that the closed-loop PWL beam system exhibits a unique steady-state solutions for all four control gains K_{HG}, K_{EI}, $K_{IS,1}$, $K_{IS,2}$. This fact indicates that the controlled system is indeed uniformly convergent and allows for a unique performance assessment in terms of disturbance attenuation.

Figures 4.4, 4.5 also provide a lot of insight in the disturbance attenuation properties of the controllers. Note that here under the term disturbance attenuation we define the suppression of the vibrations in the generalized co-

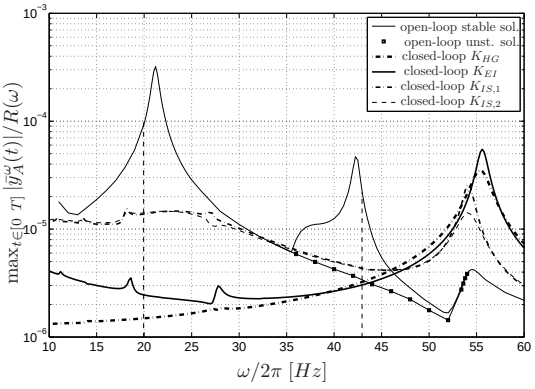

Figure 4.5: $\max_{t\in[0\ T]} |\bar{y}_A^{\omega}(t)|/R(\omega)$*, based on the open-loop (thin solid and thick dashed lines) and the closed-loop system* (4.7) *(dashed, thin dash-dotted, thick dash-dotted and thick solid lines).*

---

ordinates q_{mid}, q_{act} and in the output y_A. More specifically, in these figures we show that the control gain K_{HG} significantly suppresses the first two resonance peaks while it amplifies the third one (especially visible in Figures 4.4(b) and 4.5). The fact that the amplitudes of q_{mid}, q_{act} and y_A are increased in the third resonance frequency is remarkable because it shows that the 'fixation' (due to high gain control K_{HG}) of the beam in an additional position (the actuator location) is not enough for overal disturbance attenuation. More specifically, the beam fixation in an additional position only decreases the amplitude of the transversal displacements of the points that are near the additional fixation and does not achieve attenuation of the amplitude of the transversal displacement of every point on the beam. On the contrary, it may even give rise to new resonances that deteriorate the system performance in terms of disturbance attenuation. Furthermore, the application of the high-gain controller K_{HG} in the experimental PWL beam system is not favorable from a practical point of view, because, firstly, it leads to measurement noise amplification which is undesirable for the system performance and, secondly, it leads to control input saturation. In addition to that, a high control gain implies large control efforts for the suppression of the system resonance peaks. This is also illustrated in Figure 4.8. In this figure, we notice that the control force $u_{HG}(t)$ that corresponds to the control gain K_{HG} is significantly larger than that for the other control gains (we will provide detailed information about this figure in Section 4.4.2). A more sophisticated way to overcome such high gain control design is the control design based on engineering insight of the experimental PWL beam system. Nevertheless, based on Figures 4.4, 4.5, we see that the control gain

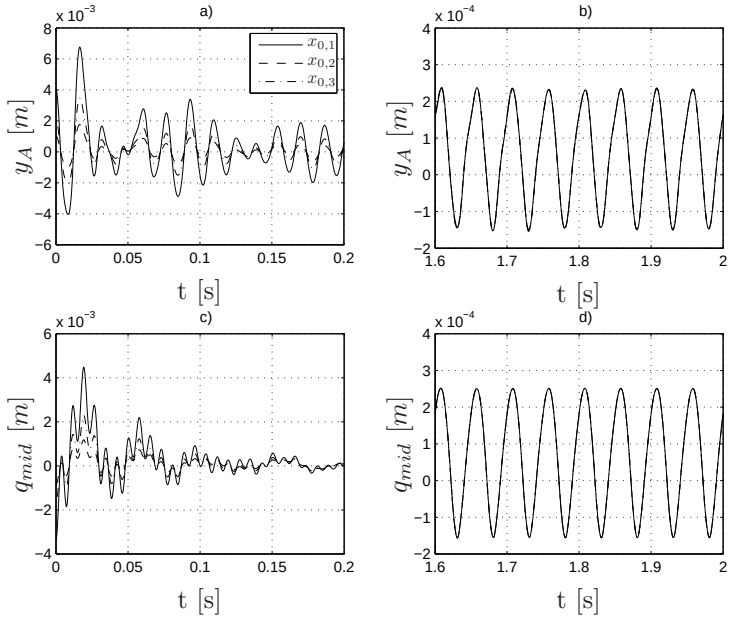

Figure 4.6: $q_{mid}(t)$ *and* $y_A(t)$ *for different initial conditions and* $\frac{\omega}{2\pi}$*=20Hz and R=18N and control gain* $K_{IS,1}$*.*

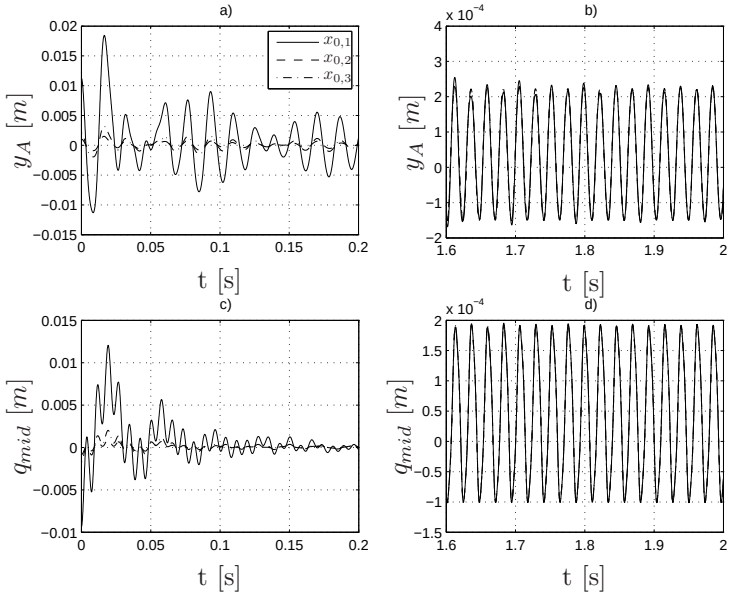

Figure 4.7: q_{mid} *and* y_A *for different initial conditions and for* $\frac{\omega}{2\pi}$*=43Hz and R=50N and control gain* $K_{IS,1}$*.*

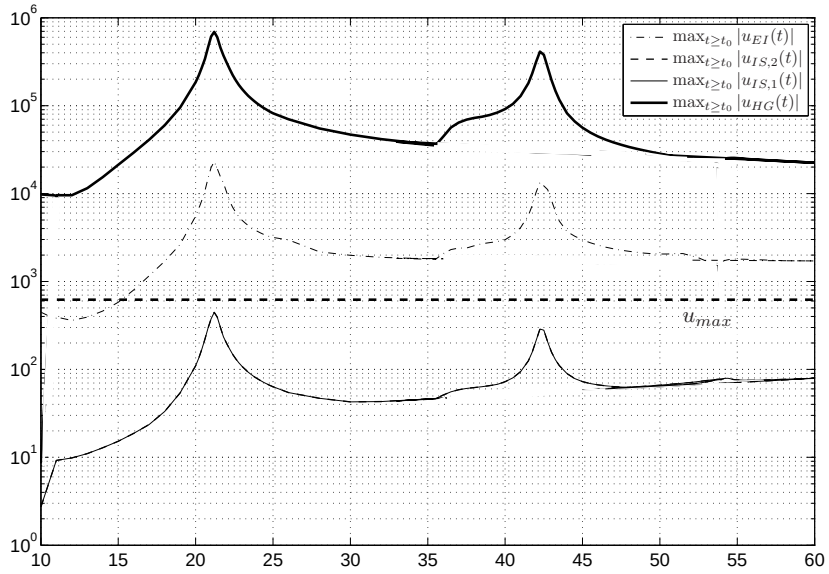

Figure 4.8: Control constraint u_{max} (thick dash line) and $\max_{t\geq t_0}|u(t)|$ for all frequencies $\frac{\omega}{2\pi} \in [10\ 60]Hz$ for K_{HG} (thin solid curve), K_{EI} (dash-dotted curve), $K_{IS,1}$ (thick solid curve) and $K_{IS,2}$ (thin dash curve).

K_{EI} leads to similar system behavior as in the case of K_{HG} (suppression of the responses in the first two resonance frequencies, though significant amplification of the responses in the third resonance frequency). Finally, based on Figures 4.4, 4.5 and 4.8, we notice that the control gains $K_{IS,1}$, $K_{IS,2}$ lead to a good performance of the closed-loop system in terms of disturbance attenuation since the responses of q_{mid}, q_{act} and y_A are significantly suppressed in the first two dominant resonances. Moreover, the responses in the third resonance (although they are larger than in open-loop) they are smaller than those related to the control gains K_{HG} and K_{EI}. Furthermore, the control action related to the control gains $K_{IS,1}$, $K_{IS,2}$ is much smaller than for the gains K_{HG} and K_{EI}. Finally, as we have already mentioned before, by adding damping in q_{mid} we reduce the contributions of the first two resonances to all elements of the system state. This is also shown in the Figures 4.4, 4.5. More specifically, in these figures we show that indeed the closed-loop responses related to the control gains K_{HG}, K_{EI} (with damping in q_{mid} equal to 42000 and 32000, respectively) are significant smaller than those related to the control gains $K_{IS,1}$,

$K_{IS,2}$ (with damping in q_{mid} equal to 26.791 and 15.589, respectively).

The aforementioned analysis based on the Figures 4.4, 4.5 can only give a qualitative feeling on the controller's performance, although it provides a lot of insight in the disturbance attenuation properties of the controllers. Therefore, in Section 4.5 we will quantify the disturbance attenuation properties of the controllers by using the quantitative performance measures presented in Section 3.5.3. More specifically, we will relate the disturbance attenuation definition with the performance measures given in Section 3.5.2 and we will evaluate the disturbance attenuation properties of the controllers by using these performance measures (Π_1^p, Π_2^p), the ultimate asymptotic bounds and the saturation bounds presented in Chapter 3.

In the following section, we evaluate the controllers that render the PWL beam system convergent while respecting the input saturation bound. This bound is specified by the maximum control effort that the actuator, used in the examined system, can provide to the system (see Section 4.4.2).

4.4.2 Output-feedback controller: Input saturation

In the experimental setup, we have to deal with a maximum control effort of 75N and also with fixed amplitudes of the harmonic disturbances (due to available fixed mass-unbalance and the excitation frequency range under study). So, given the fixed setup specifications, we would have to enforce 75N as a control input bound. Although it will turn out later (see Appendix C and Section 4.5.3) that some of the developed controllers will perform well using this bound, theoretically (using the synthesis techniques based on the control input constraints LMIs for a specified set of initial conditions) we cannot guarantee the satisfaction of the control bound. Therefore, we will start by assuming a maximum control effort of $u_{max} = 650$N for which the LMIs are feasible and analyze the resulting controllers later when $u_{max} = 75$N is used. Note that the situation of $u_{max} = 650$N is still realistic and practical. Namely, if we would implement a different actuator that can provide the 650N (or we could lower the amplitude of the disturbances, i.e. consider the case of a smaller mass unbalance), the theoretical developments would result directly in well functioning controllers without saturation. This indicates the practical value of the developed machinery. We return to these issues later.

The controllers that render the PWL beam system convergent by using control action $u(t)$, with $|u(t)| \leq u_{max}$, are considered to be suitable for practical implementation. Other controllers are rejected. As such, we will compute the maximum value $\max_{t \geq t_0} |u(t)|$ of the control input u for all $\frac{\omega}{2\pi} \in [10\ 60]$Hz for the aforementioned controllers, with t_0 the moment that the controller is engaged. The control inputs that correspond to K_{HG}, K_{EI}, $K_{IS,1}$ and $K_{IS,2}$ are denoted by u_{HG}, u_{EI}, $u_{IS,1}$ and $u_{IS,2}$, respectively. For a given excitation frequency ω and control gain K, the maximum absolute value of the controller

action $\max_{t\geq t_0}|u(t)|$ can be assessed by performing closed-loop simulations for a set X_0 of initial conditions. The set X_0 is selected such that it contains all initial conditions for which we desire to converge to the unique (closed-loop) steady state solution without saturating the actuator. Such simulation-based assessment, although computationally expensive, can be carried out for all four controllers K_{HG}, K_{EI}, $K_{IS,1}$ and $K_{IS,2}$.

Before we provide the control inputs for the controllers with gains K_{HG}, K_{EI}, $K_{IS,1}$ and $K_{IS,2}$ (using simulations), it will be shown that Theorem 3.4.5 can be used in the examined system to bound the control action u for the gains $K_{IS,1}$ and $K_{IS,2}$ ($|u_{IS,1}(t)|$, $|u_{IS,2}(t)| \leq u_{max}$). Based on that theorem, it is known that if the LMIs (3.27), (3.33) are feasible and, given a bound R_{max} on the disturbances, there exist sets Θ_ρ and Θ_γ, as defined in the theorem, with $\Theta_\gamma \subseteq \Theta_\rho$, then $|u(t)| \leq u_{max}\ \forall\ t \geq t_0$, as long as $x_0 \in \Theta_\rho$. Therefore, the main concern here is, firstly, to find a feasible solution for the LMIs (3.27), (3.33) and, secondly, to examine whether the designed set of initial conditions X_0 is a subset of Θ_ρ. To find a feasible solution for the LMIs (3.27), (3.33), we choose, first, u_{max}, R_{max} and set $\rho = 1$ (see also the procedure described in Chapter 3). Next, we solve the LMIs (3.27), (3.33), we compute P_s, P^{-1}, K and, then, we compute γ from (3.35). In case $\gamma \leq \rho = 1$ (i.e. $\Theta_\gamma \subseteq \Theta_\rho$ is satisfied) the results of Theorem 3.4.5 can be applied to the given system for the chosen values of the parameters u_{max}, R_{max}, ρ and for any set of initial conditions X_0 satisfying $X_0 \subseteq \Theta_\rho$. When $\gamma > 1$, we can scale the variables u_{max} and ρ in the upper left entry of LMI (3.33) such that for the new values of these variables (u_{max}^{new} and ρ_{new}) the results of Theorem 3.4.5 are applicable (i.e $\Theta_\gamma \subseteq \Theta_{\rho_{new}}$) as long as $X_0 \subseteq \Theta_{\rho_{new}}$. This is the case when we consider larger u_{max}^{new}. Alternatively, in case u_{max} is fixed and $\gamma > \rho = 1$, we can also opt to reduce the set of considered disturbance inputs leading to a smaller γ_{new}. Indeed, if we would set $\gamma_{new} = 1$, then this leads to (using (3.35)):

$$\sup_{t\in\mathbb{R}} \|w(t)\|_P = \frac{\alpha - \max_i\{\|b_i\|_P\}}{\|B\|_P}, \tag{4.10}$$

which is a bound for the disturbances for which we can guarantee the avoidance of actuator saturation for the given control gain matrix. Let us now provide a concise form of the aforementioned procedure for applying Theorem 3.4.5:

- Choose values for u_{max}, R_{max} and set $\rho = 1$;
- Solve the LMIs (3.27), (3.33), and compute P_s, P^{-1}, K and γ;
- check the value of γ,
  1. if $\gamma \leq 1$ apply the results of Theorem 3.4.5 for $X_0 \subseteq \Theta_\rho$,
  2. if $\gamma > 1$

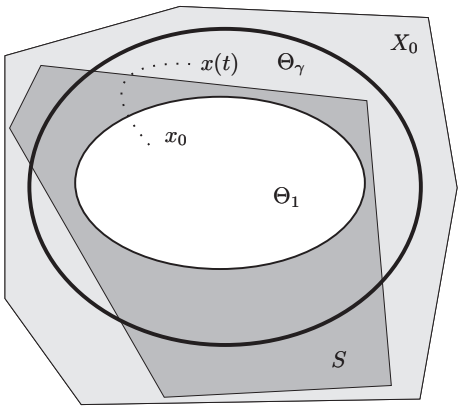

Figure 4.9: Graphical illustration of the situation where $\rho < \gamma$ for the PWL beam system for $u_{max} = 75N$ and $R_{max} = 144N$.

I. (Changing control bound) either, compute ρ_{new} and u_{max}^{new} from

$$\frac{(u_{max}^{new})^2}{\rho_{new}} = \frac{u_{max}^2}{1}, \tag{4.11}$$

such that $\rho_{new} \geq \gamma$ and then apply the results of Theorem 3.4.5 for $X_0 \subseteq \Theta_{\rho_{new}}$;

II. (Changing the magnitude of the disturbances) or set $\gamma_{new} = 1$ and compute $\sup_{t\in\mathbb{R}} \|w(t)\|_P$ for the given u_{max} from (4.10) and then apply the results of Theorem 3.4.5 for $X_0 \subseteq \Theta_\rho$ with $\rho = 1$.

In the considered study, we choose as R_{max} the maximum amplitude of the disturbances acting on the PWL beam system. Namely, $R_{max} = \max_{\omega\in[20\pi,\ 120\pi]}\{m_a\omega^2\}$ (see also (4.5)). The numerical value of R_{max} is equal to 144N. Moreover, the available control action for the PWL beam system is $u_{max} = 75$N. The values of γ related to the control gains $K_{IS,1}$ and $K_{IS,2}$ are $\gamma_{IS,1} = 53.48$ and $\gamma_{IS,2} = 61.30$, respectively. Due to the fact that $\gamma_{IS,1},\ \gamma_{IS,2} > 1$, the results of Theorem 3.4.5 cannot be applied for the given system for a control action that is limited to 75N and for $\rho = 1$. In other words, for $u_{max} = 75$N, we cannot guarantee that actuator saturation is avoided.

Let us now illustrate this situation by means of a graphical example depicted in Figure 4.9. Consider initial conditions satisfying $x_0 \in X_0$. In Figure 4.9, X_0 is depicted by a polyhedral (light grey color) and Θ_1 is denoted by an ellipsoid (white color). The fact that $\gamma > 1 = \rho$ implies that the ellipsoid Θ_γ lies outside Θ_1 ($\Theta_\gamma \nsubseteq \Theta_1$). Therefore, in Figure 4.9, we depict Θ_γ by an ellipsoid (thick solid line) that includes Θ_1. Note that Θ_γ is PI (for the closed-loop system without actuator bounds). The set S, as defined in Section 3.4

and reflecting the set of states for which $|u| \leq u_{max}$, with $u = Kx$ is depicted by the polyhedral with the dark grey color. In this particular case, $\Theta_1 \subseteq S$ (guaranteed by LMI) but $\Theta_\gamma \nsubseteq S$. Since Θ_ρ is not shown to be PI, there might be initial states $x_0 \in \Theta_1$ for which the trajectory leaves Θ_1 (but remains in Θ_γ) and also leaves S. Hence, saturation of the control bound can occur.

In the sequel, we will 1) choose a 'desirable set' of initial conditions X_0, 2) compute a set $\Theta_{\rho_{new}}$ such that it includes the sets Θ_γ and X_0, 3) compute the new bound on the control action u_{max}^{new} using (4.11). This procedure guarantees that $\Theta_\gamma \subseteq \Theta_{\rho_{new}}$ and $X_0 \subseteq \Theta_{\rho_{new}}$ and saturation can be avoided for initial conditions $x_0 \in X_0$.

A 'realistic set' of initial conditions should include the state values that the system can have at the moment we activate the controller. This set can be chosen as follows. It is assumed either that the controller is switched on when the observer error dynamics has converged to zero and the open-loop PWL beam system is in steady-state (this can be easily achieved in practice by operating the system with the observer switched on for few seconds before we switch on the controller) or that the closed-loop system starts at rest (i.e the controller is on when the disturbance starts acting). This assumption implies either that x_0 is on a steady-state solution of the open-loop system ($\bar{x}_{ol}$) or that $x_0 = 0$. We define X_0 as $X_0 = \{\bar{x}_{ol}^{\omega}(t) | \frac{\omega}{2\pi} \in [10,\ 60]Hz,\ t \in [0,\ \frac{2\pi}{\omega}]\} \cup \{0\}$. This set is a subset of a set $\Theta_{\mu_{max}}$ that has the form of Θ_γ and Θ_ρ and is defined as follows:

$$\Theta_{\mu_{max}} = \{x_0 | x_0^T P x_0 \leq \mu_{max}\},$$

with

$$\mu_{max} = \{\max_{\omega \in [20\pi,\ 120\pi]} \{\max_{t \in [0,\ 2\pi/\omega]} \|\bar{x}_{ol}^{\omega}(t)\|_P\}\}. \tag{4.12}$$

The values of μ_{max} for $P_{IS,1}$ and $P_{IS,2}$ are $\mu_{max}^{IS,1} = 72.26$ and $\mu_{max,}^{IS,2} = 73.95$, respectively. Note that $\mu_{max}^{IS,i}$, for $i = 1, 2$, are computed by using extensive open-loop simulations (simulations as used to compute the open-loop part of Figure 4.8). Now, we would like to guarantee that if we activate the controller, while the system resides in one of its open-loop steady-state periodic solutions or while the system is at rest (i.e. $x_0 \in X_0 \subseteq \Theta_{\mu_{max}}$), then the control input constraints is satisfied.

Let us now compute a set that can be chosen to represent $\Theta_{\rho_{new}}$. In order to apply Theorem 3.4.5 for the given system, $\Theta_{\rho_{new}}$ should include Θ_γ and $\Theta_{\mu_{max}}$. Any $\Theta_{\rho_{new}}$ with $\rho_{new} \geq \max\{\gamma, \mu_{max}\}$ is suitable. Let us choose $\rho_{new}^{K_{IS,1}} = 72.5$ and $\rho_{new}^{K_{IS,2}} = 74$.

The numerical values of u_{max}^{new} related to the control gains $K_{IS,1}$ and $K_{IS,2}$ can now be computed using (4.11) and are given by $u_{max,IS,1}^{new} = 637.5$N and $u_{max,IS,2}^{new} = 645$N, respectively. Based on Theorem 3.4.5 we can now guarantee that in the examined system the control action u is bounded by $u_{max}^{IS,1}$ and

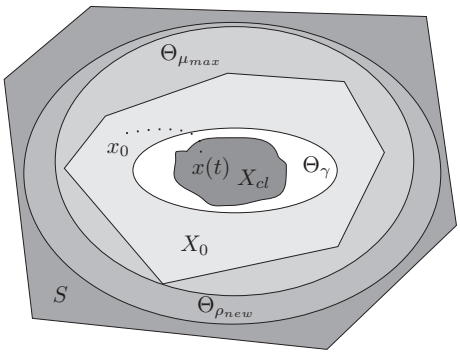

Figure 4.10: Graphical illustration of the results presented in Theorem 3.4.5 for the PWL beam system for $u_{max} = 650N$ and $R_{max} = 144N$.

$u_{max}^{IS,2}$ as long as we use the control gains $K_{IS,1}$ and $K_{IS,2}$, respectively, and take initial conditions in X_0.

Let us now illustrate the aforementioned situation by means of a graphical example depicted in Figure 4.10 (for the case of $u_{max} = 650$N). Consider initial conditions satisfying $x_0 \in X_0$. In Figure 4.10, X_0 is denoted by a polyhedral (light grey color). The fact that $\Theta_\gamma \subseteq \Theta_{\rho_{new}}$, $\Theta_{\mu_{max}} \subseteq \Theta_{\rho_{new}}$ and $X_0 \subseteq \Theta_{\mu_{max}}$ implies that the ellipsoid depicts $\Theta_{\rho_{new}}$ (grey color) includes the ellipsoids that depict Θ_γ (white color), $\Theta_{\mu_{max}}$ (light grey color) and the polyhedral that depicts X_0 (light grey color), respectively. We also depict the set S (largest polyhedral in Figure 4.10) which includes both $\Theta_{\rho_{new}}$ and Θ_γ. Moreover, the fact that $\Theta_\gamma \subseteq \Theta_{\rho_{new}}$ also implies that $\Theta_{\rho_{new}}$ is PI. Due to the fact that $\Theta_{\rho_{new}}$ is PI and $x_0 \in X_0$, the solution $x(t)$ will stay in $\Theta_{\rho_{new}}$ at all times. Since $\Theta_{\rho_{new}} \subseteq S$, the control action u will not saturate when starting in X_0. In addition to that, $x(t)$ will converge to the set X_{cl} that includes the steady-state solution of the closed-loop system. By definition, X_{cl} (depicted by the smallest set in Figure 4.10) is a subset of Θ_γ.

Next, we will present simulation results for the PWL beam system for $u_{max} = 650$N and for a large number of initial conditions taken from the set X_0. In Figure 4.8, $\max_{t\geq t_0} |u(t)|$ for all $\frac{\omega}{2\pi} \in [10\ 60]$Hz for K_{HG}, K_{EI}, $K_{IS,1}$ and $K_{IS,2}$ are depicted together with the bound u_{max}. In this figure, it is shown that the curves related to $\max_{t\geq t_0} |u_{IS,1}(t)|$ (thin dashed curve), $\max_{t\geq t_0} |u_{IS,2}(t)|$ (thick solid curve) are below the line that represents u_{max} (thick dashed line). Note that the curves related to $\max_{t\geq t_0} |u_{IS,1}(t)|$ and $\max_{t\geq t_0} |u_{IS,2}(t)|$ almost coincide with each other. Moreover, the curves representing $\max_{t\geq t_0} |u_{HG}(t)|$ (thin solid curve) and $\max_{t\geq t_0} |u_{ES}(t)|$ (dash-dotted curve) are above the line corresponding to u_{max} for almost all ω. Consequently, the control gains $K_{IS,1}$ and $K_{IS,2}$ are suitable for practical implementation (given $u_{max} = 650$N), while

K_{HG}, K_{EI} are not.

4.5 Performance evaluation

In this section, we will study the performance of the controllers with control gains $K_{IS,1}$ and $K_{IS,2}$ in terms of disturbance attenuation for periodic excitations for two different cases. In the first case, we use an upper bound $u_{max} = 650$N for the control input and the controllers guarantee the satisfaction of the control input constraints. In the second case, we use an upper bound $u_{max} = 75$N for the control input and the controllers do not guarantee the satisfaction of the control input constraints (this is the case in the experimental PWL beam system). Firstly, we will more precisely define what we mean with the term disturbance attenuation. Next, we will use the asymptotic ultimate upper bound for the system output, as is presented in 3.5.1 and the performance measures presented in Section 3.5.2 for the case of $u_{max} = 650$N to quantitatively asses disturbance attenuation properties of the controllers. Based on this output bound and these performance measures we will promote the controller with the 'best' disturbance attenuation properties. Finally, we will apply the 'best' controller on the experimental PWL beam system and we will study its disturbance attenuation properties based on experimental results and the proposed performance measures (in the fase of actuator constraints).

4.5.1 Controller evaluation based on an asymptotic ultimate upper bound for the system output

As motivated in Section 4.4.1, we consider as output for system (4.7) the first two elements of x ($x_1 = q_{mid}$, $x_2 = q_{act}$) and the system output y_A.

$$y_1 = C_{x_1}x = x_1, \quad y_2 = C_{x_2}x = x_2, \quad y_3 = C_A x = y_A. \tag{4.13}$$

The numerical values of the output matrices are given by

$$C_{x_1} = [1\ 0\ 0\ 0\ 0\ 0\ 0\ 0],$$

$$C_{x_2} = [0\ 1\ 0\ 0\ 0\ 0\ 0\ 0],$$

$$C_A = [-0.317\ \ -0.334\ \ -0.667\ \ -0.3069\ 0\ 0\ 0\ 0].$$

According to Theorem 3.4.5, in order to apply the ultimate bound (3.45) for each element $y_i,\ i = 1, 3$ of the output, the following constraints have to be satisfied:

- Boundedness of the disturbances w;
- Feasibility of the LMIs (3.33) for the numerical parameter values of the system;

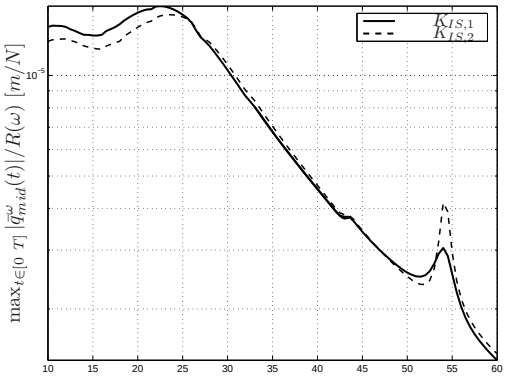

(a) $\max_{t\in[0\ T]} |\bar{q}^{\omega}_{mid}(t)|/R(\omega)$.

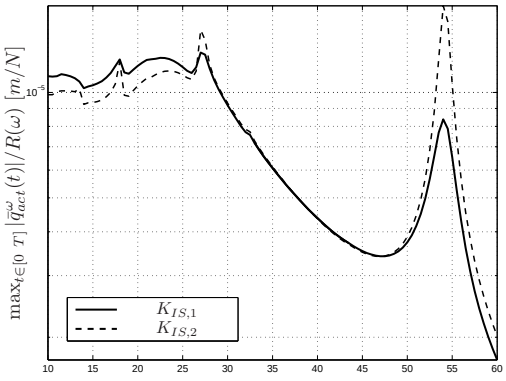

(b) $\max_{t\in[0\ T]} |\bar{q}^{\omega}_{act}(t)|/R(\omega)$.

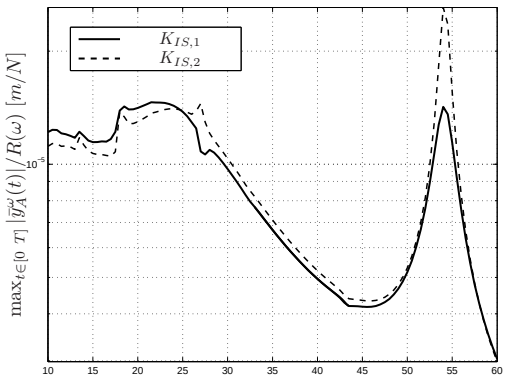

(c) $\max_{t\in[0\ T]} |\bar{y}^{\omega}_{A}(t)|/R(\omega)$.

Figure 4.11: (a) $\max_{t\in[0\ T]} |\bar{q}^{\omega}_{mid}(t)|/R(\omega)$*; (b)* $\max_{t\in[0\ T]} |\bar{q}^{\omega}_{act}(t)|/R(\omega)$*; (c)* $\max_{t\in[0\ T]} |\bar{y}^{\omega}_{A}(t)|/R(\omega)$ *of the closed-loop system* (4.7) *for* $K_{IS,1}$ *(solid curve) and* $K_{IS,2}$ *(dashed curve).*

- Satisfaction of the condition $\Theta_\gamma \subseteq \Theta_\rho$ $(\gamma \leq \rho)$.

It is easy to show that w is bounded by a constant $R_{max} = \max_\omega\{R(\omega)\}$, where $R(\omega)$ is given in (4.5). As it was shown in the previous section, the closed-loop system for the control gains $K_{IS,1}$ and $K_{IS,2}$ is uniformly convergent since the LMIs (3.33) are feasible. Moreover, the condition $\Theta_\gamma \subseteq \Theta_{\rho_{new}}$ is satisfied for the ρ_{new} and γ values given in Section 4.4.2 (for the case that $u_{max} = 650$N).

The asymptotic ultimate bound (3.45) for $y_1 = q_{mid}$, $y_2 = q_{act}$ and $y_3 = y_A$ has the form

$$Y_b^{q_{mid}} = \|C_{x_1}\|G_b,\ Y_b^{q_{act}} = \|C_{x_2}\|G_b\ Y_b^{y_A} = \|C_A\|G_b \tag{4.14}$$

with

$$G_b = \frac{\|B\|_P\|P^{\frac{1}{2}}\|}{\alpha\sqrt{\lambda_{min}(P)}}R_{max}, \tag{4.15}$$

since $b_1,\ b_2 = 0$. In other words,

$$\lim_{t\to\infty}\|y_{1,2,3}(t)\| \leq \|C_{x_1,x_2,y_A}\|G_b. \tag{4.16}$$

Here, we denote $Y_{b,(IS,1)}^{q_{mid}}$, $Y_{b,(IS,1)}^{q_{act}}$, $Y_{b,(IS,1)}^{y_A}$ and $Y_{b,(IS,2)}^{q_{mid}}$, $Y_{b,(IS,2)}^{q_{act}}$, $Y_{b,(IS,2)}^{y_A}$ to be the $Y_b^{q_{mid}}$, $Y_b^{q_{act}}$ and $Y_b^{y_A}$ bounds, as in (4.14), related to $K_{IS,1}$ and $K_{IS,2}$, respectively. The numerical values of these bounds are $Y_{b,(IS,1)}^{q_{mid}} = Y_{b,(IS,1)}^{q_{act}} = 0.152$, $Y_{b,(IS,1)}^{y_A} = 0.131$ and $Y_{b,(IS,2)}^{q_{mid}} = Y_{b,(IS,2)}^{q_{act}} = 0.164$, $Y_{b,(IS,2)}^{y_A} = 0.141$, respectively.

In Figures 4.11(a)-4.11(c), the graphs of

$$\max_{t\in[0\ T]}|\bar{q}_{mid}^{\omega}(t)|/R(\omega),$$

$$\max_{t\in[0\ T]}|\bar{q}_{act}^{\omega}(t)|/R(\omega)$$

and

$$\max_{t\in[0\ T]}|\bar{y}_A^{\omega}(t)|/R(\omega)$$

are plotted for the closed-loop system for $K_{IS,1}$, $K_{IS,2}$. In these figures, the solid curve corresponds to $K_{IS,1}$, while the dashed curve corresponds to $K_{IS,2}$. The frequency range of interest is $\frac{\omega}{2\pi} \in [10,\ 60]$Hz. The scaled values of the ultimate asymptotic output bounds are:

$$Y_{b,(IS,1)}^{q_{mid}}/R_{max} = Y_{b,(IS,1)}^{q_{act}}/R_{max} = 0.00105,\ Y_{b,(IS,1)}^{y_A}/R_{max} = 9.1\cdot 10^{-4}$$

and

$$Y_{b,(IS,2)}^{q_{mid}} = Y_{b,(IS,2)}^{q_{act}} = 0.0013,\ Y_{b,(IS,2)}^{y_A}/R_{max} = 9.81\cdot 10^{-4}.$$

Based on these numerical values and the Figures 4.11(a)-4.11(c), we notice that

$$\max_{t\in[0\ T]} |\bar{q}_{mid}^{\omega,(IS,1)}(t)|/R(\omega) < Y_{b,(IS,1)}^{q_{mid}}/R_{max},$$

$$\max_{t\in[0\ T]} |\bar{q}_{act}^{\omega,(IS,1)}(t)|/R(\omega) < Y_{b,(IS,1)}^{q_{act}}/R_{max},$$

$$\max_{t\in[0\ T]} |\bar{y}_{A}^{\omega,(IS,1)}(t)|/R(\omega) < Y_{b,(IS,1)}^{y_A}/R_{max}$$

and

$$\max_{t\in[0\ T]} |\bar{q}_{mid}^{\omega,(IS,2)}(t)|/R(\omega) < Y_{b,(IS,2)}^{q_{miq}}/R_{max},$$

$$\max_{t\in[0\ T]} |\bar{q}_{act}^{\omega,(IS,2)}(t)|/R(\omega) < Y_{b,(IS,2)}^{q_{act}}/R_{max},$$

$$\max_{t\in[0\ T]} |\bar{y}_{A}^{\omega,(IS,2)}(t)|/R(\omega) < Y_{b,(IS,2)}^{y_A}/R_{max},$$

which is guaranteed by the theory. If one is interested in general disturbance signals then the asymptotic ultimate output bounds $Y_b^{q_{mid},q_{act},y_A}$ may very well be a good indication for performance. However, if one is interested in harmonic disturbances, then this might be a far too conservative measure; e.g. in the case under study

$$\max_{t\in[0\ T]} |\bar{q}_{mid}^{\omega}(t)|/R(\omega),\ \max_{t\in[0\ T]} |\bar{q}_{act}^{\omega}(t)|/R(\omega),\ \max_{t\in[0\ T]} |\bar{y}_{A}^{\omega}(t)|/R(\omega)$$

are in the order of 10^{-5} while $Y_b^{q_{mid},q_{act},y_A}/R_{max}$ are in the order of 10^{-3}. Additionally, these asymptotic ultimate bounds do not discriminate in terms of the different steady-state behaviors for different excitation frequencies. Consequently, we cannot compare which of these controllers performs better in terms of disturbance attenuation for specific disturbances (such as harmonic ones). In order to overcome this problem, we are going to study the performance measures presented in Section 3.5.2, which are based on computed periodic, asymptotically unique, steady-state responses of the system.

4.5.2 Controller evaluation based on performance measures

In the sequel, a definition of the term disturbance attenuation for this work is given and the performance measures presented in Section 3.5.2 are used, with minor adaptations based on the knowledge on the experimental setup, to promote the controller with the 'best' disturbance attenuation properties.

The attenuation of

$$\max_{\omega\in[20\pi\ \ 120\pi]} \max_{t\in[0\ T]} |\bar{q}_{mid}^{\omega}(t)|, \tag{4.17}$$

$$\max_{\omega\in[20\pi\ \ 120\pi]}\ \max_{t\in[0\ \ T]} |\bar{q}^{\omega}_{act}(t)|, \tag{4.18}$$

$$\max_{\omega\in[20\pi\ \ 120\pi]}\ \max_{t\in[0\ \ T]} |\bar{y}^{\omega}_{A}(t)|, \tag{4.19}$$

and

$$\int_{20\pi}^{120\pi} \max_{t\in[0\ \ T]} |\bar{q}^{\omega}_{mid}(t)|d\omega, \tag{4.20}$$

$$\int_{20\pi}^{120\pi} \max_{t\in[0\ \ T]} |\bar{q}^{\omega}_{act}(t)|d\omega \tag{4.21}$$

$$\int_{20\pi}^{120\pi} \max_{t\in[0\ \ T]} |\bar{y}^{\omega}_{A}(t)|d\omega \tag{4.22}$$

are together defined as disturbance attenuation. The reason for choosing q_{mid}, q_{act} and y_A as system outputs and, consequently, as disturbance attenuation variables is that they represent physical entities (transversal displacements of the middle of the beam, of the point where the actuator is mounted on the beam and of the point A in Figure 4.2(b)) and these variables can be easily measured. In general, one can choose as output any displacement on the beam. Since, both in experiments and simulations, we only have knowledge on the steady-state solutions on a discrete set of frequencies, we will approximate the integrals by their corresponding Riemmann sums.

Consider now the performance measures Π_1^p, Π_2^p, defined in (3.46), (3.50), for $p = \infty$ and outputs q_{mid}, q_{act} and y_A. As we have already mentioned in Section 4.2.3, in the examined system, the excitation amplitude is a function of ω, see (4.5). Therefore, the steady-state output response $\bar{y}^{\omega,R}$ in (3.46) and (3.50) only depends on ω and therefore $\bar{y}^{\omega,R}$ can be written as $\bar{y}^{\omega}$. For the same reason, the maximization over the disturbance amplitude R in Π_1^∞ and the integration over a range in R in Π_2^∞ can be omitted.

Using the aforementioned remarks, the performance measures Π_1^∞ and Π_2^∞ for q_{mid}, q_{act} and y_A can be written as:

$$\Pi_1^{\infty,q_{mid}} = \frac{\max_{\omega\in[\omega_{min}\ \ \omega_{max}]} \|\bar{q}^{\omega}_{mid}(t)\|_{L_\infty}}{\max_{\omega\in[\omega_{min}\ \ \omega_{max}]} \|\bar{q}^{\omega}_{mid,ref}(t)\|_{L_\infty}}, \tag{4.23}$$

$$\Pi_1^{\infty,q_{act}} = \frac{\max_{\omega\in[\omega_{min}\ \ \omega_{max}]} \|\bar{q}^{\omega}_{act}(t)\|_{L_\infty}}{\max_{\omega\in[\omega_{min}\ \ \omega_{max}]} \|\bar{q}^{\omega}_{act,ref}(t)\|_{L_\infty}}, \tag{4.24}$$

$$\Pi_1^{\infty,y_A} = \frac{\max_{\omega\in[\omega_{min}\ \ \omega_{max}]} \|\bar{y}^{\omega}_{A}(t)\|_{L_\infty}}{\max_{\omega\in[\omega_{min}\ \ \omega_{max}]} \|\bar{y}^{\omega}_{A,ref}(t)\|_{L_\infty}}, \tag{4.25}$$

$$\Pi_2^{q_{mid},\infty} = \frac{\int_{\omega_{min}}^{\omega_{max}} \|\bar{q}^{\omega}_{mid}(t)\|_{L_\infty} d\omega}{\int_{\omega_{min}}^{\omega_{max}} \|\bar{q}^{\omega}_{mid,ref}(t)\|_{L_\infty} d\omega}, \tag{4.26}$$

$$\Pi_2^{q_{act},\infty} = \frac{\int_{\omega_{min}}^{\omega_{max}} \|\bar{q}_{act}^{\omega}(t)\|_{L_\infty} d\omega}{\int_{\omega_{min}}^{\omega_{max}} \|\bar{q}_{act,ref}^{\omega}(t)\|_{L_\infty} d\omega}, \tag{4.27}$$

$$\Pi_2^{y_A,\infty} = \frac{\int_{\omega_{min}}^{\omega_{max}} \|\bar{y}_{A}^{\omega}(t)\|_{L_\infty} d\omega}{\int_{\omega_{min}}^{\omega_{max}} \|\bar{y}_{A,ref}^{\omega}(t)\|_{L_\infty} d\omega}. \tag{4.28}$$

The values of ω_{min} and ω_{max} are $20\pi\frac{rad}{s}$ and $120\pi\frac{rad}{s}$, respectively (see also in Section 4.2.2). It is obvious that the performance measures in (4.23)-(4.28) are directly related to the disturbance attenuation definition for the PWL beam system and, consequently, is a sensible choice to evaluate different controllers for their disturbance attenuation properties.

At this point, the controllers $K_{IS,1}$ and $K_{IS,2}$ will be compared by using these performance measures. As a reference control gain we choose $K_{IS,2}$. By computing the values of the performance measures in (4.23)-(4.28) for q_{mid}, q_{act}, y_A and for control gains $K_{IS,1}$ and $K_{IS,2}$ we derive the following numerical values: $\Pi_1^{\infty,q_{mid}} = 1.007$, $\Pi_1^{\infty,q_{act}} = 0.767$, $\Pi_1^{\infty,y_A} = 0.651$, $\Pi_2^{\infty,q_{mid}} = 1.013$, $\Pi_2^{\infty,q_{act}} = 0.991$, $\Pi_2^{\infty,y_A} = 0.993$. These computations are based on the information on the closed-loop steady-state responses as depicted in Figure 4.11. These performance measures clearly show that the control gain $K_{IS,1}$ suppresses the vibrations in q_{act} and y_A to a higher extent than the control gain $K_{IS,2}$, since the performance measures $\Pi_1^{\infty,q_{act}} = 0.767$, $\Pi_2^{\infty,q_{act}} = 0.991$ and $\Pi_1^{\infty,y_A} = 0.651$, $\Pi_2^{\infty,y_A} = 0.993$ are smaller than 1. On the other hand, the control gain $K_{IS,2}$ suppresses the vibrations in q_{mid} to a higher extent than the control gain $K_{IS,1}$ since $\Pi_1^{\infty,q_{mid}} = 1.007$ and $\Pi_2^{\infty,q_{act}} = 1.013$. The aforementioned conclusion also agrees with the observations based on Figures 4.11(a)-4.11(c). More specifically, in these figures $\max_{t\in[0\ T]} |\bar{q}_{mid}^{\omega}(t)|/R(\omega)$, $\max_{t\in[0\ T]} |\bar{q}_{act}^{\omega}(t)|/R(\omega)$ and $\max_{t\in[0\ T]} |\bar{y}_{A}^{\omega}(t)|/R(\omega)$ are plotted for the closed-loop system for $K_{IS,1}$ and $K_{IS,2}$. In these figures, the solid curve corresponds to $K_{IS,1}$, while the dashed curve corresponds to $K_{IS,2}$. The frequency range of interest is [10, 60]Hz. Based on these figures, it is concluded, once again, that $K_{IS,1}$ suppresses q_{act} and y_A more than $K_{IS,2}$ does, while the situation is opposite in q_{mid}. Note that in an integral sense (see value of the Π_2-measures) the performance difference between $K_{IS,1}$ and $K_{IS,2}$ is rather small. However, when considering peak values (see values of the Π_1-measures), $K_{IS,1}$ performs significantly better; especially with respect to q_{act} and y_A.

At this point, we will study the level of disturbance attenuation achieved in the closed-loop system based on the performance measures in (4.23)-(4.28) by comparing it to the open-loop behaviour. For the computation of these measures we will consider the stable steady-state solutions of the open-loop system. As a reference controller we choose $K_{IS,1}$. By computing the values of the proposed performance measures, denoted here as $\Pi_{1,ol}^{\infty,q_{mid}}$, $\Pi_{1,ol}^{\infty,q_{act}}$, $\Pi_{1,ol}^{\infty,y_A}$, $\Pi_{2,ol}^{\infty,q_{mid}}$, $\Pi_{2,ol}^{\infty,q_{act}}$ and $\Pi_{2,ol}^{\infty,y_A}$, it is concluded that the periodic disturbances acting on the PWL beam are considerably suppressed in the closed-loop system

since,

$$\Pi_{1,ol}^{\infty,q_{mid}},\ \Pi_{1,ol}^{\infty,q_{act}},\ \Pi_{1,ol}^{\infty,y_A},\ \Pi_{2,ol}^{\infty,q_{mid}},\ \Pi_{2,ol}^{\infty,q_{act}},\ \Pi_{2,ol}^{\infty,y_A} > 1.$$

The numerical values of the considered performance measures are:

$$\Pi_{1,ol}^{\infty,q_{mid}} = 22.961,\ \Pi_{1,ol}^{\infty,q_{act}} = 24.043,\ \Pi_{1,ol}^{\infty,y_A} = 22.586,$$

$$\Pi_{2,ol}^{\infty,q_{mid}} = 13.038,\ \Pi_{2,ol}^{\infty,q_{act}} = 15.221,\ \Pi_{2,ol}^{\infty,y_A} = 14.894.$$

These results also agree with the observations based on Figures 4.4, 4.5, where it is shown that the open-loop responses are considerably larger than the closed-loop responses for almost all $\frac{\omega}{2\pi} \in [10\ 60]$Hz.

4.5.3 Experiments

In this section, we will implement the observer/controller combination of (3.12), (4.9) with

$$L_1 = [98.475\ 88.090\ -284.05\ -5.254\ 386.35\ 4626.0\ -18411.0\ 766.50]\,,$$

$$L_2 = [98.781\ 88.212\ -284.35\ -5.2469\ 1910.2\ 5031.8\ -19635.0\ 627.17]$$

(see also Appendix B) and $K = K_{IS,1}$ on the experimental PWL beam system. We will show, based on experimental results and the performance measures presented in Section 4.5.2, that this observer/controller combination is able to render this system convergent and significantly attenuate the vibrations caused by the periodic disturbances acting on it. Note that for the remainder of this section we will use only the responses of q_{mid} and y_A because there are no available measurements of the response q_{act}, since there are only two linear variable displacement transducers on the setup (one is located in q_{mid} and the other in y_A).

As it has been mentioned before, the available actuator in the experimental PWL beam system, can only provide a control action limited to $u_{max} = 75$N for frequencies in the range of $\frac{\omega}{2\pi} \in [10\ 60]$Hz. It is obvious that in this case the control input will be saturated even when using control gains $K_{IS,1}$ and $K_{IS,2}$, see Figure 4.8. However, in Appendix C, it is shown based on simulations that the control gain $K_{IS,1}$ results in a closed-loop system with a unique steady-state solution ($\bar{x}_{cl}(t)$) and a control action in steady-state that is smaller than 75N. Consequently, no saturation occurs in that case. Moreover, the resulting closed-loop steady-state solution is exactly the same with the steady-state solution of the closed-loop system of the non-saturated control input. Therefore, we achieve the same disturbance attenuation level as in the non-saturated case. Finally, due to the fact that on $\bar{x}_{cl}(t)$ no saturation occurs the case that the controller is turned on before the perturbation will work.

In Figures 4.12 and 4.13, we depict the measured and simulated steady-state transversal displacements q_{mid} and y_A. By comparing the measured and

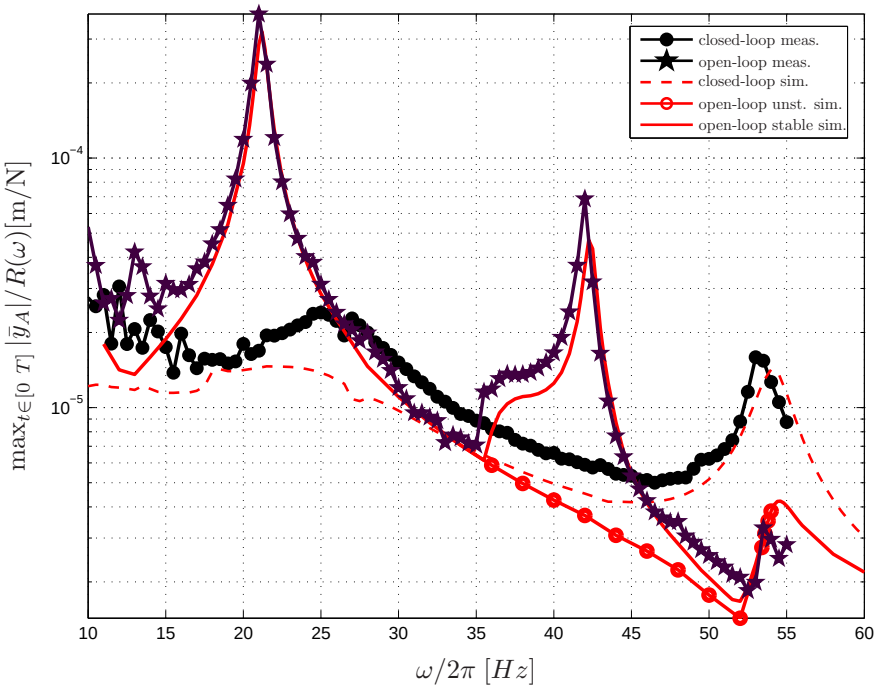

Figure 4.12: Open- and closed-loop steady-state responses of $\bar{y}_A$ using simulations and measurements.

simulated displacements, it is concluded that the model of the interconnected system can reconstruct with high accuracy the steady-state dynamics of the real PWL beam system (see also Section 4.2.3 for the open-loop model validation). In these figures, it is shown that the closed-loop system exhibits unique steady-state solutions $\forall \frac{\omega}{2\pi} \in [10,\ 60]$Hz. This confirms that the experimental closed-loop PWL beam system is (locally) uniformly convergent. The difference between simulations and measurements is due to measurement noise and model uncertainties, as in the case of the open-loop system. Around 53Hz, in both simulations and measurements, one can notice the contribution of the third eigenmode to the system. Based on these figures, it is obvious that this contribution is larger in the closed-loop system than the open-loop system. Nevertheless, the related resonance peaks of the closed-loop response are very small (maximum peak response of both q_{mid} and y_A around $2 \cdot 10^{-5}\ m$) with respect to the open-loop resonance peaks at $\frac{\omega}{2\pi} = 19$Hz and $\frac{\omega}{2\pi} = 43$Hz (maximum peak response of q_{mid} around $4 \cdot 10^{-4}\ m$ and of y_A around $3.5 \cdot 10^{-4}\ m$).

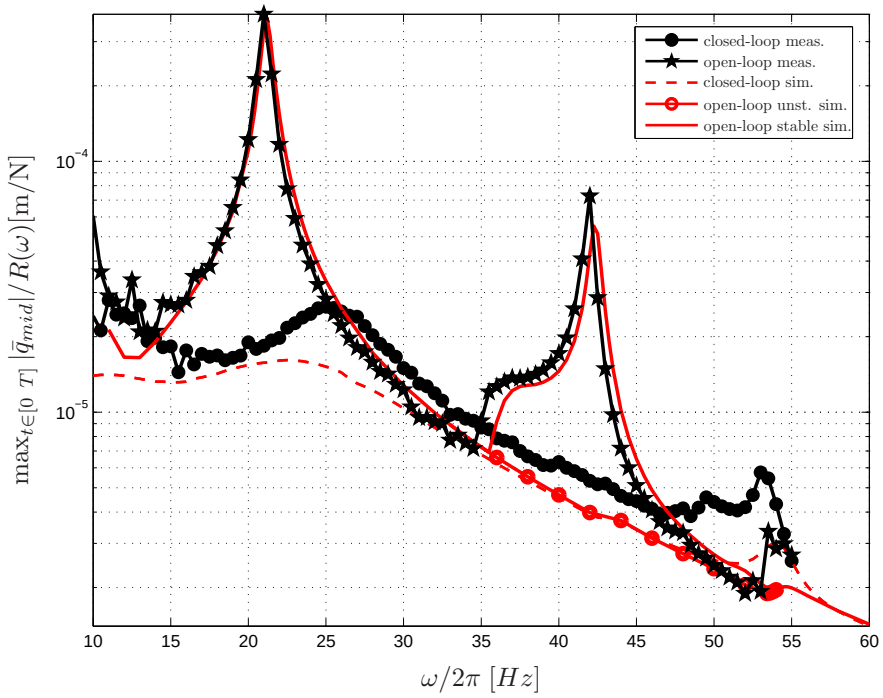

Figure 4.13: Open- and closed-loop steady-state responses of $\bar{q}_{mid}$ using simulations and measurements.

Moreover, the performance measures

$$\int_{20\pi}^{120\pi} \max_{t\in[0\ T]} |\bar{q}^{\omega}_{mid}(t)|d\omega,\ \int_{20\pi}^{120\pi} \max_{t\in[0\ T]} |\bar{q}^{\omega}_{act}(t)|d\omega \text{ and } \int_{20\pi}^{120\pi} \max_{t\in[0\ T]} |\bar{y}^{\omega}_{A}(t)|d\omega$$

of the closed-loop system are also significantly smaller than those in the open-loop system. Therefore, we can say that significant disturbance attenuation is achieved.

In Figure 4.14, u_{max} and $\max_{t\in[0\ T]} |\bar{u}(t)|$ (i.e. the maximum (absolute value of the) actuator force in steady-state) for the interconnected system are depicted using measurements and simulations. Based on this figure, the results based on simulations (solid curve) and measurements (dashed curve) are similar and $\max_{t\in[0\ T]} |\bar{u}(t)| \leq u_{max}$ at all times, for both cases. In these figures, $u_{max} = 75$N is depicted with a dash-dotted line. The small differences between the simulated and measured results are, most probably, due to model inaccuracies and measurement noise.

For a better understanding of the results shown in Figures 4.12 and 4.13, also time responses of q_{mid} and y_A are given in Figures 4.15-4.18. In these

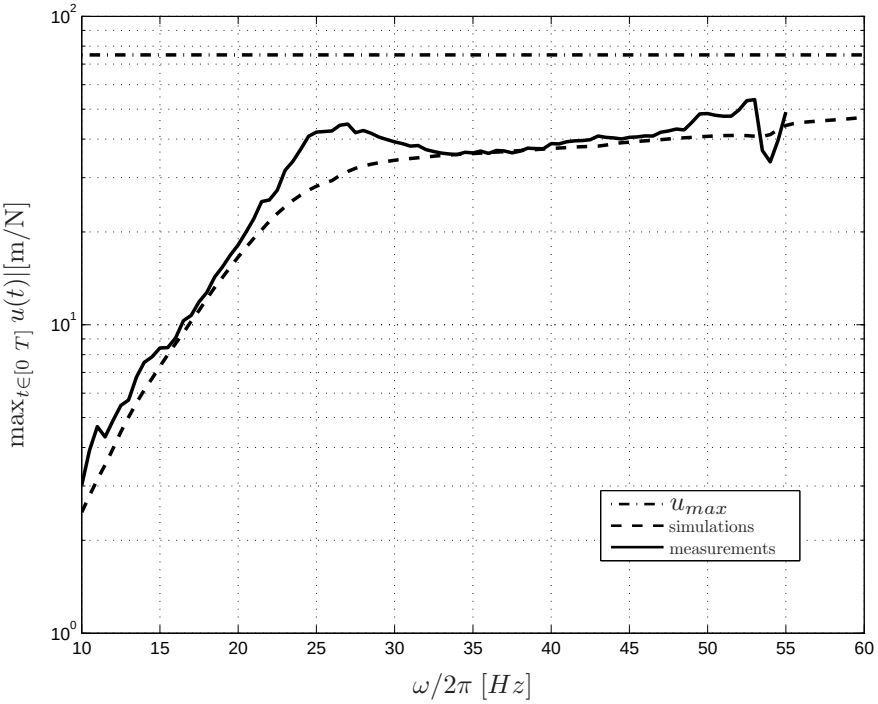

Figure 4.14: The actuator force in steady-state; simulations and measurements.

---

figures, the time responses of q_{mid} and y_A are depicted for three different initial conditions $x_{0,i},\ i = 1, 2, 3$ and two excitation frequencies. More specifically, in the main plot of these figures the measured responses of q_{mid} and y_A are depicted (for $x_{0,3}$) from the moment the observer is switched on until the moment the system reaches its steady-state. In the left-hand subplots, the transient of these responses is shown for $x_{0,i},\ i = 1, 2$. Finally, in the right-hand subplots, the steady-state responses are presented for $x_{0,i},\ i = 1, 2, 3$. Based on these subplots, once again, it is confirmed that the system is convergent since all solutions converge to a unique steady-state solution with period T equal to the excitation period. The frequencies and amplitudes of the periodic disturbances in Figures 4.15, 4.16 and in Figures 4.17, 4.18 are $\frac{\omega}{2\pi} = 20$Hz, $R = 16\ N$ and $\frac{\omega}{2\pi} = 43$Hz, $R = 74\ N$, respectively. The values of the initial conditions $x_{0,i},\ i = 1, 2, 3$ for $\frac{\omega}{2\pi} = 20$Hz and $\frac{\omega}{2\pi} = 43$Hz are:

$$
\begin{aligned}
x_{0,1} &= [1.7845 \cdot 10^{-3}, \quad 2.0815 \cdot 10^{-3}, \quad 5,1631 \cdot 10^{-5}, \quad 1.0761 \cdot 10^{-4}] \\
x_{0,2} &= [6.7622 \cdot 10^{-4}, \quad 8.7611 \cdot 10^{-4}, \quad 7.1132 \cdot 10^{-4}, \quad 9.3131 \cdot 10^{-4}] \\
x_{0,3} &= [6.4401 \cdot 10^{-6}, \quad 3.4354 \cdot 10^{-6}, \quad 3,6317 \cdot 10^{-6}, \quad -8.8223 \cdot 10^{-6}]
\end{aligned}
$$

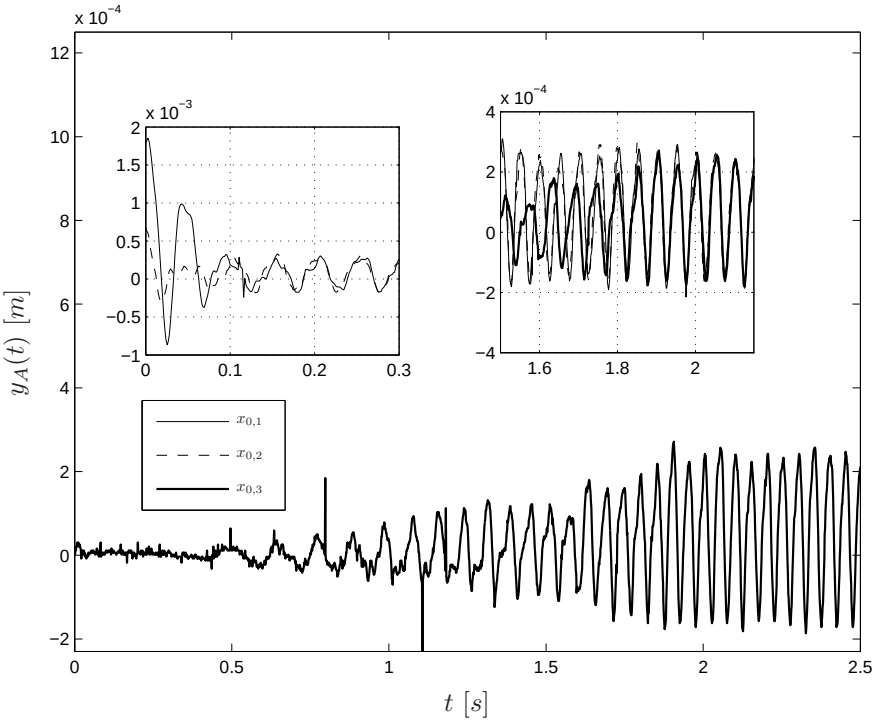

Figure 4.15: Measured $y_A(t)$ for $R = 16N$ and $\frac{\omega}{2\pi} = 20Hz$ for $x_{0,i},\ i = 1, 2, 3$.

---

and

$$\begin{aligned} x_{0,1} &= [9.5569 \cdot 10^{-4}, \quad 1.0931 \cdot 10^{-3} \quad -5.6771 \cdot 10^{-5}, \quad -9.0715 \cdot 10^{-5}] \\ x_{0,2} &= [-6.6816 \cdot 10^{-4}, \quad -7.1977 \cdot 10^{-4} \quad -6.9195 \cdot 10^{-4}, \quad -7.2106 \cdot 10^{-4}] \\ x_{0,3} &= [6.4401 \cdot 10^{-6}, \quad -1.3860 \cdot 10^{-6} \quad 2.0495 \cdot 10^{-6}, \quad 2.2913 \cdot 10^{-6}], \end{aligned}$$

respectively.

The initial conditions are obtained by doing the following three experiments:

1. $x_{0,1}$: the disturbance $w(t)$ is acting on the beam, the beam is in steady-state and the observer and controller are switched off. Subsequently, the observer and the controller are switched on simultaneously at the initial time corresponding to $x_{0,1}$.

2. $x_{0,2}$: the disturbance $w(t)$ is acting on the beam, the beam is in steady-state, the observer is switched on and the controller is still switched off. Subsequently, the controller is switched on at the initial time corresponding to $x_{0,2}$.

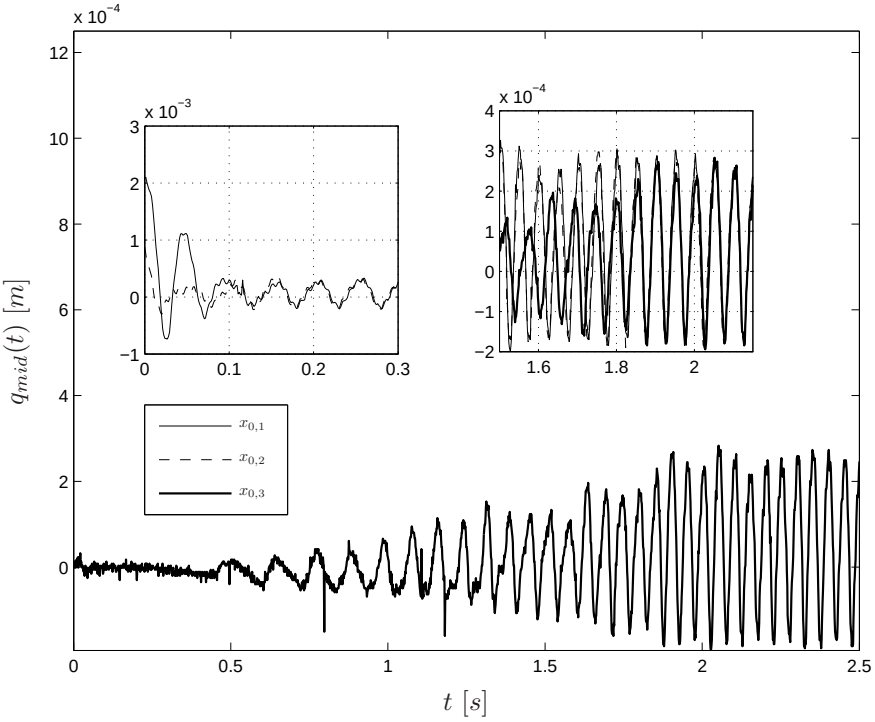

Figure 4.16: Measured $q_{mid}(t)$ for $R = 16N$ and $\frac{\omega}{2\pi} = 20Hz$ for $x_{0,i},\ i = 1, 2, 3$.

3. $x_{0,3}$: the disturbance $w(t)$ is not acting on the beam and the observer and controller are switched on. Subsequently, the disturbance $w(t)$ is activated at the initial time corresponding to $x_{0,3}$.

The comparison of the plots calculated for the open- and closed-loop system, depicted in Figure 4.12 and 4.13, shows that for the frequency ranges where the open-loop exhibits resonance peaks with high amplitudes, the closed-loop system responses are significantly smaller than those of the open-loop system. Based on this comparison, it is concluded that the effect of the disturbances $w(t)$ to the PWL beam is attenuated due to the control force u. Note that especially the resonances are suppressed. This can also be noticed in Figure 4.19, where the time response of q_{mid} and y_A in steady-state are shown. In these figures, the dashed line is the open-loop steady-state solution, while the solid line is the closed-loop steady-state solution. The excitation frequencies for these cases are 20Hz and 43Hz, respectively.

At this point we will study the level of disturbance attenuation achieved in the closed-loop system based on the performance measures in (4.23)-(4.28). For

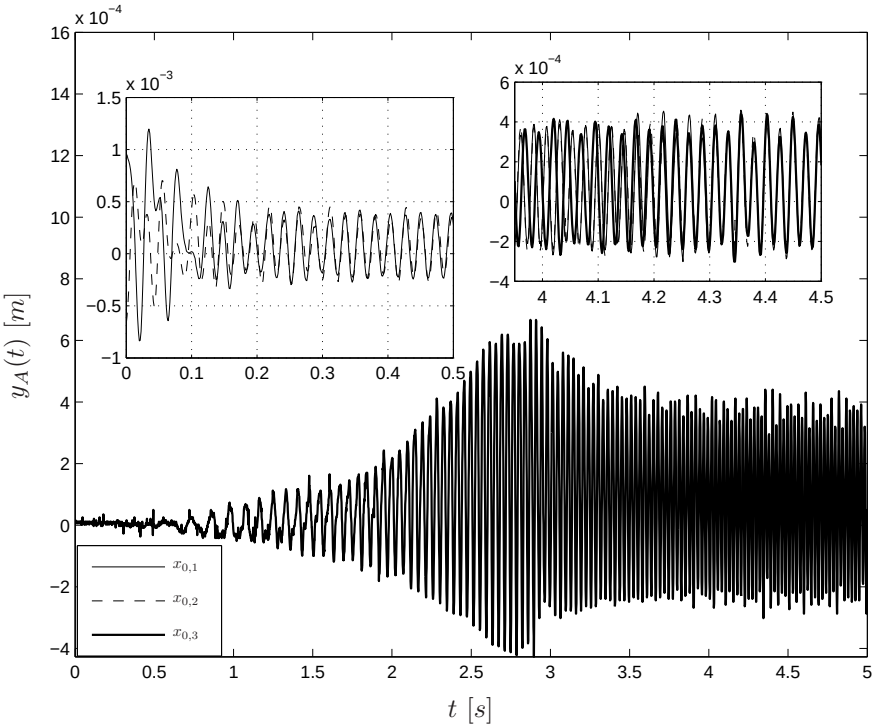

Figure 4.17: Measured $y_A(t)$ for $R = 74N$ and $\frac{\omega}{2\pi} = 43Hz$ for $x_{0,i},\ i = 1, 2, 3$.

---

the computation of these measures we will consider the steady-state open-loop responses and the steady-state closed-loop responses. As a reference controller we choose $K_{IS,1}$. By computing the values of the proposed performance measures, denoted here as $\Pi^{\infty,q_{mid}}_{1,ol,exp}$, $\Pi^{\infty,y_A}_{1,ol,exp}$, $\Pi^{\infty,q_{mid}}_{2,ol,exp}$ and $\Pi^{\infty,y_A}_{2,ol,exp}$, it is concluded that the periodic disturbances acting on the PWL beam are considerably suppressed in the closed-loop system since

$$\Pi^{\infty,q_{mid}}_{1,ol} = 14.00,\ \Pi^{\infty,y_A}_{1,ol} = 12.50,$$

$$\Pi^{\infty,q_{mid}}_{2,ol} = 8.613,\ \Pi^{\infty,y_A}_{2,ol} = 6.193.$$

The conclusion derived based on the performance measures agrees with those derived from the observations of Figures 4.12 and 4.13. Namely, significant disturbance attenuation is achieved.

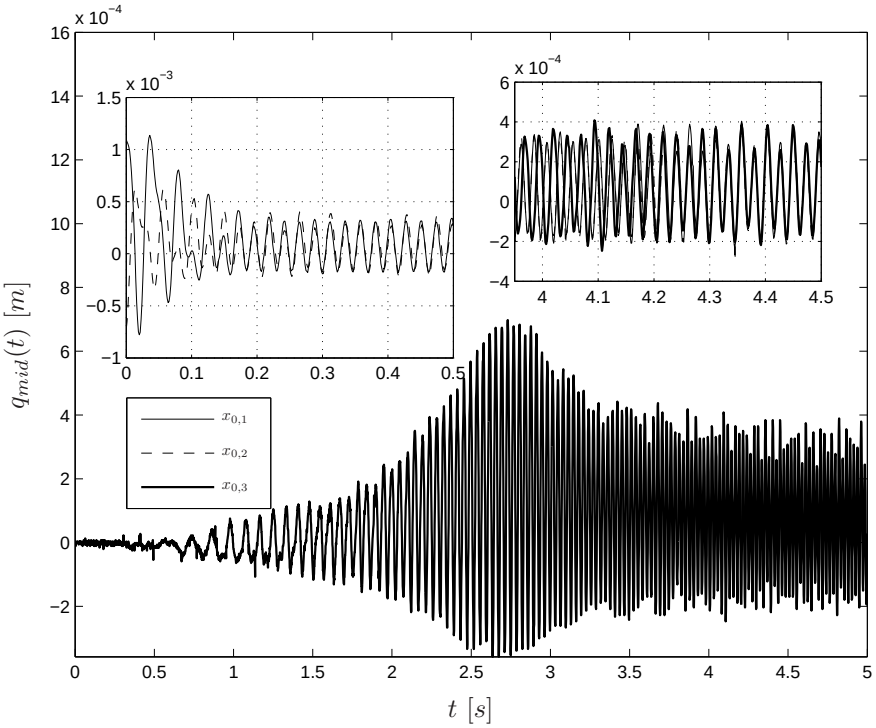

Figure 4.18: Measured $q_{mid}(t)$ for $R = 74N$ and $\frac{\omega}{2\pi} = 43Hz$ for $x_{0,i},\ i = 1, 2, 3$.

4.6 Summary

In this chapter, we implemented a convergence-based output-feedback control design on a real PWL system and evaluated the performance of this controller in terms of disturbance attenuation. This performance evaluation is based on ultimate bounds and performance measures for the system's (measured) periodic responses. The evaluation shows that the proposed design is able to significantly attenuate the influence of periodic disturbance to the system. The output-feedback controller is a combination of a state-feedback controller and a model based switching observer. This observer exponentially recovers the state of the experimental setup.

More specifically, in Section 4.2 we have presented an experimental setup that can be modeled as a PWL system and we showed that a four degree-of-freedom model can accurately describe the dynamics of the experimental setup. In Section 4.3 we have used a switching observer to estimate the state of the experimental system as the full state of the system is measured. In Section

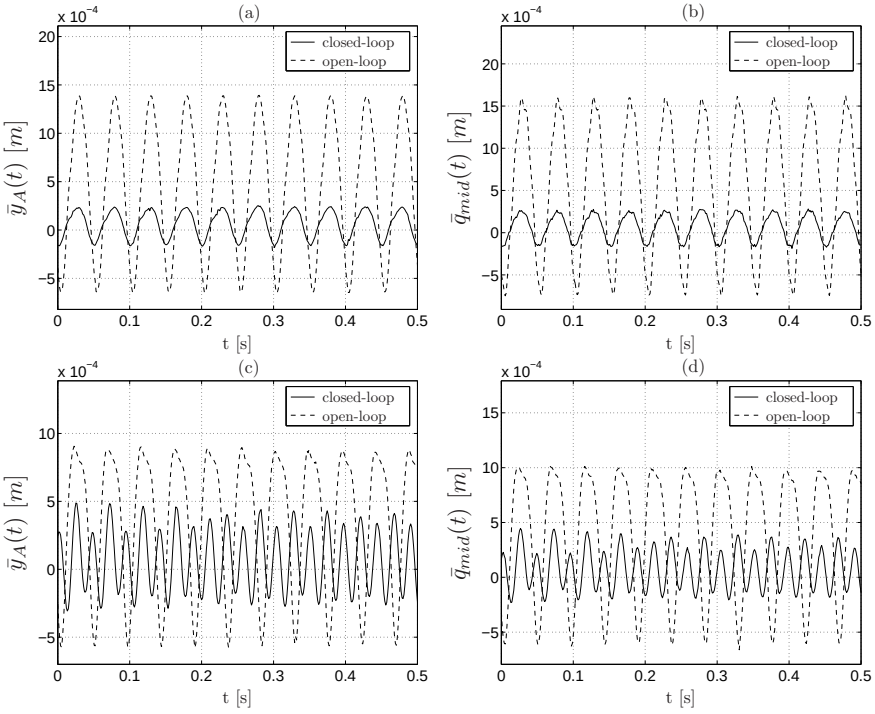

Figure 4.19: Experimental open- and closed-loop time responses of $y_A(t)$, $q_{mid}(t)$, in steady-state, for (a), (b) $R = 16N$, $\frac{\omega}{2\pi} = 20Hz$ and (c), (d) $R = 74N$, $\frac{\omega}{2\pi} = 43Hz$.

4.4, we have designed four different output-feedback controllers that render the PWL beam system convergent and we have studied, on a model level, their applicability to the system and their performance in terms of disturbance attenuation. Moreover, in that section we have also studied the case in which the control action is bounded. In Section 4.5, we have evaluated the disturbance attenuation properties of different controllers by using a bound in the control action and performance measures based on computed periodic responses. The controller with the best performance in terms of disturbance attenuation was promoted for implementation on the experimental setup. Finally, we have also applied the promoted controller to the experimental setup. Based on experimental results and the aforementioned performance measures, it is shown that this controller renders the system convergent and exhibits high performance in terms of disturbance attenuation.

5

Controller design for stabilization of Lur'e-type systems with set-valued nonlinearities

5.1 Introduction

In this chapter, we propose two observer-based output-feedback controller design strategies for a class of Lur'e type systems based on the notions of passivity and absolutely stability [72; 81; 137] (see Chapter 2). This class of systems consists of a linear part in the forward path and decoupled, set-valued nonlinearities in the feedback path. The aim of the controller designs is to guarantee the stabilization of the origin of such systems. It will be shown that passivity properties of the (controlled) linear part of the system are beneficial to ensure that these systems are asymptotically stable as long as the nonlinearities in the feedback path are sector bounded.

The ultimate test for the developed controllers is their implementation on an experimental mechanical system with non-collocated actuation and set-valued friction characteristics. In order to support such practical applicability, the controller designs will be designed such that they render the closed-loop system absolutely stable meaning that global asymptotic stability of the equilibrium of the closed-loop system is guaranteed for all the set-valued nonlinearities in the sector $[0,\ \infty]$. This property is favorable in terms of the robustness as uncertainties in the set-valued nonlinearities do not destroy the stability of the closed-loop system as long as the nonlinearities remain in the sector $[0,\ \infty]$. This is very important for applications, because there are, for example, always changes in the friction characteristics between the elements of a mechanical system due to temperature changes, humidity, lubrication conditions etc.

The proposed controller designs are based either on the circle criterion or the Popov criterion, which are discussed for sector bounded Lipschitz nonlinearities, for instance, in [5; 6; 64; 72]. Especially in [5], [6] a circle criterion controller design for Lur'e type systems with such nonlinearities is proposed and feasibility conditions are given. One of the main differences with the work here is that we do not constrain ourselves to Lipschitz continuous mappings but allow general *set-valued* maps (such as set-valued friction laws). The controller designs that we propose are discussed in Section 5.2 and aim to render the system absolutely stable. For the controller design based on the circle criterion a specific form of the circle criterion is used. This specific form guarantees that the system is absolutely stable as long as the linear part is strictly passive and the set-valued nonlinearities in the feedback loop are passive i.e. belong to the sector $[0, \infty]$, and this form of the circle criterion is related to the well known passivity theorems (see e.g. [72]). For the case of linear complementarity systems an extension of this form of the circle criterion to set-valued nonlinearities was given in [24].

In the controller design based on the Popov criterion the requirement of strict passivity of the linear part of the closed-loop system is relaxed by using a dynamic multiplier. More specifically, the multiplication of the transfer function of the linear part with a dynamic multiplier and the multiplication of the inverse of this multiplier with the set-valued nonlinearities in the feedback loop results in a new linear system and new set-valued nonlinearities. The requirements for absolute stability for the new system are the strict passivity of the new linear part and the passivity of the new system in the feedback path (which is now a dynamical system with a set-valued output map). In this manner, we will derive a generalization of the Popov criterion that applies to Lur'e type systems with set-valued nonlinearities (instead of only Lipschitz continuous maps). The main difficulty to apply the Popov criterion to this type of systems is the non-smoothness of the Popov-inspired Lyapunov function.

In practice, the entire state of Lur'e type systems with set-valued nonlinearities is often not available for feedback. Therefore, an additional goal is to construct output-feedback controllers based on the aforementioned criteria that overcome this problem and render a Lur'e type system of the considered class absolutely stable. The proposed output-feedback controllers are a combination of a model-based observer and a state-feedback controller and are presented in Section 5.3. Based on the theoretical results presented in this chapter we guarantee that this combination yields globally asymptotically stable closed-loop systems for both controller designs. The observer design is based on [36], [55] where a constructive procedure for the considered type of systems is given. Under certain passivity-related assumptions the observer is shown to asymptotically recover the state of the observed system. Finally, a discussion of the results presented in this chapter and directions for future work are given in Section 5.4.

5.2 State-feedback controller design for Lur'e type systems with set-valued nonlinearities

Consider a Lur'e system described by the following differential inclusion (see also Figure 5.1(a)):

$$\dot{x} = Ax + Gw + Bu \tag{5.1a}$$
$$w \in -\varphi(z) \tag{5.1b}$$
$$z = Hx \tag{5.1c}$$
$$y = Cx, \tag{5.1d}$$

where $x \in \mathbb{R}^n$ is the system state, $w \in \mathbb{R}^p$, $z \in \mathbb{R}^p$ is the input of a set-valued mapping $\varphi(z)$, $u \in \mathbb{R}^m$ is the control input and $y \in \mathbb{R}^\kappa$ is the system output. Moreover, the matrices $A \in \mathbb{R}^{n\times n}$, $B \in \mathbb{R}^{n\times m}$, $H \in \mathbb{R}^{p\times n}$, $C \in \mathbb{R}^{\kappa\times n}$ are given and the matrix $G \in \mathbb{R}^{n\times p}$ has full column rank.

We use the following assumptions on the properties of the set-valued mapping $\varphi(z)$.

Assumption 5.2.1 The set-valued map $\varphi(z) : \mathbb{R}^p \hookrightarrow \mathbb{R}^p$ satisfies

- $0 \in \varphi(0)$;
- φ is upper semicontinuous (see [10]) and locally integrable with respect to z;
- φ is decomposed as $\varphi(z) = [\varphi_1(z_1), ..., \varphi_p(z_p)]^T$, $z = [z_1, ..., z_p]^T$ and $\varphi_i(z_i) : \mathbb{R} \hookrightarrow \mathbb{R}$, for $i = 1, ...p$;
- for all $v \in \mathbb{R}$ the set $\varphi_i(v) \subseteq \mathbb{R}$, $i = 1, ..., p$, is non-empty, convex, closed and bounded;
- each φ_i satisfies the $[0,\ \infty]$ sector condition in the sense that

$$z_i w_i \leq 0 \text{ for all } w_i \in \varphi_i(z_i) \text{ for } i = 1, ..., p; \tag{5.2}$$

- there exist positive constants γ_1 and γ_2 such that for any $w \in \varphi(v)$ it holds that

$$\|w\| \leq \gamma_1 \|v\| + \gamma_2. \tag{5.3}$$

Remark 5.2.2 Note that the property in the last bullet in Assumption 5.2.1 is not needed for the state-feedback design that we will present in this section. This property will be used for observer design (see Section 5.3.1) and for output-feedback design (see Section 5.3.2).

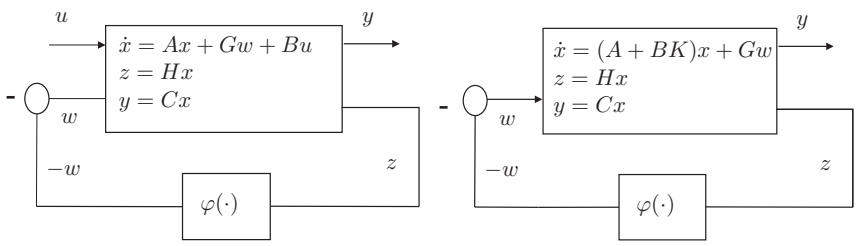

(a) Open-loop system. (b) Closed-loop system.

Figure 5.1: Block diagrams of the open-loop system and the closed-loop system.

The input functions u are assumed to be in the space of piecewise continuous[1] bounded functions from $[0, \infty)$ to $\mathbb{R}^m$, denoted by $\mathbb{PC}$. Clearly, the mapping $(t, x) \mapsto Ax - G\varphi(Hx) + Bu(t)$ is upper semicontinuous on intervals where u is continuous and attains non-empty, convex, closed and bounded set-values. From [10, p. 98] or [42, § 7], it follows that local existence of solutions[2] is guaranteed given an initial state x_0 at initial time 0. Due to the growth condition of $\varphi(v)$ it holds that $\|\dot{x}(t)\| \leq \tilde{\gamma}_1\|x\| + \tilde{\gamma}_2$, which prevents finite escape times and thus any solution to (5.1) is globally defined on $[0, \infty)$. Hence, solutions $x(t)$ and also $z(t) = Hx(t)$ are absolutely continuous functions. Note that $0 \in \varphi(0)$ implies that the origin $x = 0$ is an equilibrium of system (5.1) for input $u = 0$. The fourth bullet in Assumption 5.2.1 means that we have p 'decoupled' nonlinearities in the sense that the i-th component of φ only depends on z_i. If φ is a piecewise continuous map with only countably many 'discontinuities' (i.e. points z at which $\varphi(z)$ is not a singleton), then the integrability assumption of bullet two is satisfied.

To control the system, we propose the linear static state-feedback law

$$u = Kx, \tag{5.4}$$

where $K \in \mathbb{R}^{m\times n}$ is the control gain matrix. Consequently, the resulting closed-loop system is described by the following differential inclusion (see also Figure 5.1(b)):

$$\dot{x} = (A + BK)x + Gw \tag{5.5a}$$
$$w \in -\varphi(z) \tag{5.5b}$$
$$z = Hx. \tag{5.5c}$$

[1] We call a function u defined on $[0, \infty)$ piecewise continuous, if any bounded interval contains at most a finite number of discontinuity points of u.

[2] We call a function $x : [a, b] \to \mathbb{R}^n$ a solution to the differential inclusion $\dot{x}(t) \in F(t, x(t))$, if x is absolutely continuous and satisfies $\dot{x}(t) \in F(t, x(t))$ for almost all $t \in (a, b)$.

The transfer function $G_{cl}(s)$ of the linear part of system (5.5) is

$$G_{cl}(s) = H(sI - (A + BK))^{-1}G, \ s \in \mathcal{C}. \tag{5.6}$$

The control goal here is to render the closed-loop system (5.5) absolutely stable by means of a proper choice for the control gain K. For the considered closed-loop system, absolute stability means that the origin is globally asymptotically stable for any set-valued nonlinearity in the feedback loop belonging to the $[0, \infty]$ sector. In the following sections, we will introduce two controller design methods that are able to achieve this goal by exploiting the notion of passivity.

5.2.1 Popov and circle criterion controller design

In this section, we will provide sufficient conditions for the absolute stability of the equilibrium point $x = 0$ of the closed-loop system (5.5). Loosely speaking, the conditions are as follows: the linear part of this system should be passive and the set-valued nonlinearities should belong to the sector $[0, \infty]$ (this implies that the nonlinearity is passive). In these results, the passivity of the linear part will be expressed in a matrix inequality form based on the Kalman-Yakubovich-Popov lemma, see [72] and Chapter 2.

Consider system (5.5) with the related transfer function $G_{cl}(s)$ given in (5.6) and satisfying Assumption 5.2.1. We choose the transfer function of a so-called dynamic multiplier $M(s)$ which is given by

$$M(s) = I + \Gamma s, \ s \in \mathbb{C}, \tag{5.7}$$

where $\Gamma = \text{diag}(\eta_1, \dots \eta_p) \in \mathbb{R}^{p \times p}$, with $\eta_i > 0$ for $i = 1, \dots, p$. This choice is common for the case with a Lipschitz continuous nonlinearity, see [72]. The inverse of $M(s)$ will be chosen to be (strictly) passive, because (as we will explain later) the multiplication of the set-valued nonlinearity in (5.5) with the inverse of the dynamic multiplier must yield a passive system.

A cascade that represents system (5.5) is shown in Figure 5.2(a). In this figure, both the post-multiplication of the linear part of system (5.5) with the dynamic multiplier $M(s)$ and the pre-multiplication of the nonlinear (feedback) part of system (5.5) with the inverse of $M(s)$ are depicted. Using the dynamic multiplier $M(s)$ we aim to transform the original system into a feedback interconnection of two passive systems, as is done in [72]. In this figure, Σ_1 represents a new linear system in the forward path and Σ_2 is the new system in the feedback path.

In state-space formulation, the interconnected system Σ_1, Σ_2 takes the following form:

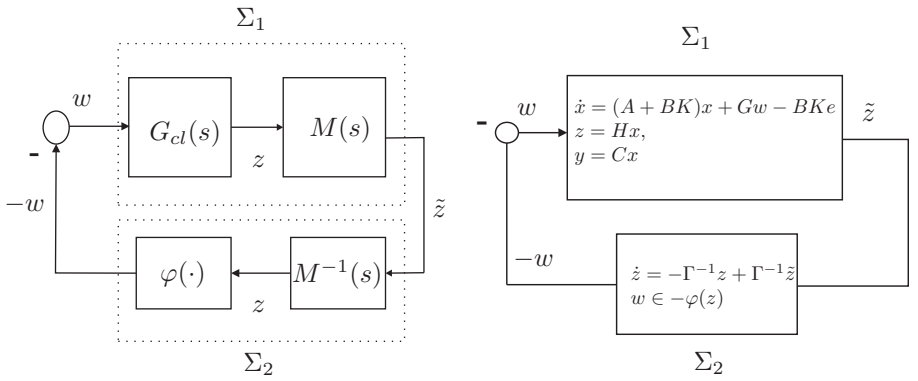

(a) Cascade representation of system (5.5) using the dynamic $M(s)$.

(b) Closed-loop system after transformation with dynamic multiplier $M(s)$.

Figure 5.2: Block diagrams of the open-loop system and the closed-loop system.

$$\Sigma_1 = \begin{cases} \dot{x} &= (A + BK)x + Gw \\ \tilde{z} &= \tilde{H}x + \tilde{D}w \end{cases} \tag{5.8a}$$

$$\Sigma_2 = \begin{cases} \dot{z} &= -\Gamma^{-1}z + \Gamma^{-1}\tilde{z} \\ w &\in -\varphi(z). \end{cases} \tag{5.8b}$$

Herein, $\tilde{z} \in \mathbb{R}^p$ and the matrices $\tilde{H} \in \mathbb{R}^{p\times n}$, $\tilde{D} \in \mathbb{R}^{p\times p}$ can be derived from the fact that $\tilde{z} = z + \Gamma\dot{z}$ (as a consequence of the choice of the multiplier $M(s)$ in (5.7)):

$$\begin{aligned} \tilde{z} &= z + \Gamma\dot{z} \\ &= Hx + \Gamma H\dot{x} \\ &= Hx + \Gamma H[(A + BK)x + Gw] \\ &= [H + \Gamma H(A + BK)]x + \Gamma HGw \\ &= \tilde{H}x + \tilde{D}w. \end{aligned} \tag{5.9}$$

Hence,

$$\tilde{H} = H + \Gamma H(A + BK) \quad \text{and} \quad \tilde{D} = \Gamma HG. \tag{5.10}$$

At this point we are going to formulate conditions that guarantee that the equilibrium point $x = 0$ of the system (5.1), (5.4) (i.e. the closed-loop system (5.5)) is absolutely stable. The following theorem states sufficient conditions for the global asymptotic stability of the origin of (5.1). The analysis of that theorem is based on a Lyapunov function inspired by the Popov criterion. In [137], a result on the Popov criterion for systems with discontinuous nonlinearities is given. Here, we formulate a stability result, based on the Popov

criterion, for the more general class of integrable, set-valued nonlinearities (and an alternative proof is presented).

Theorem 5.2.3 *Consider system* (5.1)*, with $\varphi(z)$ satisfying Assumption 5.2.1 and the linear static state-feedback law* (5.4) *with $K \in \mathbb{R}^{m\times n}$. If there exists a diagonal matrix $\Gamma = diag(\eta_1, \quad ..., \quad \eta_p) \in \mathbb{R}^{p\times p}$, with $\eta_i > 0$ for $i = 1, ..., p$ and a matrix $P = P^T > 0$ that satisfy*

$$\begin{bmatrix} (A+BK)^T P + P(A+BK) & PG - \tilde{H}^T \\ G^T P - \tilde{H} & -\tilde{D} - \tilde{D}^T \end{bmatrix} < 0, \tag{5.11}$$

with $\tilde{H}$ and $\tilde{D}$ given in (5.10)*, then the origin $x = 0$ is a globally asymptotically stable equilibrium of the closed-loop system* (5.1) *and* (5.4)*.*

Proof Consider the following Lyapunov candidate function:

$$V(x) = V_1(x) + V_2(Hx), \tag{5.12}$$

with

$$V_1(x) = \frac{1}{2} x^T P x, \quad P = P^T > 0, \tag{5.13}$$

and

$$V_2(Hx) = \sum_{i=1}^{p} V_{2,i}(H_i x) = \sum_{i=1}^{p} V_{2,i}(z_i) = V_2(z), \quad \text{for} \quad i = 1, ..., p, \tag{5.14}$$

where H_i is the i^{th} row of H and

$$V_{2,i}(z_i) = \eta_i \int_0^{z_i} \varphi_i(s) ds \quad \text{for} \quad i = 1, ..., p. \tag{5.15}$$

We aim to prove that along solutions $x(t)$ of the system (5.1)-(5.4) we have that V is strictly decreasing, i.e. when $x(t_1) \neq 0$

$$V(x(t_2)) - V(x(t_1)) < 0, \ \forall t_2 > t_1, \ t_1, t_2 \in \mathbb{R}. \tag{5.16}$$

For the V_1 contribution with V_1 as in (5.13), we have that:

$$V_1(x(t_2)) - V_1(x(t_1)) = \int_{t_1}^{t_2} \dot{V}_1(s) ds, \tag{5.17}$$

where the derivative of V_1 with respect to time is computed as follows:

$$\begin{aligned} \dot{V}_1 &= \tfrac{1}{2}\{\dot{x}^T P x + x^T P \dot{x}\} \\ &= \tfrac{1}{2}\{[(A+BK)x + Gw]^T P x + x^T P[(A+BK)x + Gw]\} \\ &= \tfrac{1}{2}\{x^T[(A+BK)^T P + P(A+BK)]x + w^T G^T P x + x^T P G w\}. \end{aligned} \tag{5.18}$$

At this point we add and subtract $\frac{1}{2}[\tilde{z}^T w + w^T \tilde{z}]$ from the above equation and use (5.9):

$$\begin{aligned} \dot{V}_1 &= \dot{V}_1 + \tfrac{1}{2}[-\tilde{z}^T w - w^T \tilde{z} + \tilde{z}^T w + w^T \tilde{z}] \\ &= \dot{V}_1 + \tfrac{1}{2}[-(\tilde{H}x + \tilde{D}w)^T w - w^T(\tilde{H}x + \tilde{D}w) + 2\tilde{z}^T w] \\ &= \dot{V}_1 + \tfrac{1}{2}[-x^T \tilde{H}^T w - w^T \tilde{D}^T w - w^T \tilde{H}x - w^T \tilde{D}w + 2\tilde{z}^T w] \\ &= \tfrac{1}{2}\rho_1 + \tilde{z}^T w. \end{aligned} \tag{5.19}$$

with ρ_1 given by:

$$\begin{aligned} \rho_1 &= x^T[(A+BK)^T P + P(A+BK)]x + w^T G^T P x + x^T P G w - x^T \tilde{H}^T w \\ &\quad -w^T \tilde{D}^T w - w^T \tilde{H}x - w^T \tilde{D}w \\ &= \begin{bmatrix} x \\ w \end{bmatrix}^T \begin{bmatrix} (A+BK)^T P + P(A+BK) & PG - \tilde{H}^T \\ G^T P - \tilde{H} & -\tilde{D} - \tilde{D}^T \end{bmatrix} \begin{bmatrix} x \\ w \end{bmatrix} \\ &= \begin{bmatrix} x \\ w \end{bmatrix}^T F(P,K) \begin{bmatrix} x \\ w \end{bmatrix}, \end{aligned} \tag{5.20}$$

where

$$F(P,K) := \begin{bmatrix} (A+BK)^T P + P(A+BK) & PG - \tilde{H}^T \\ G^T P - \tilde{H} & -\tilde{D} - \tilde{D}^T \end{bmatrix}. \tag{5.21}$$

Using (5.20) in the expression for $\dot{V}_1$ in (5.19), we obtain

$$\dot{V}_1 = \tfrac{1}{2}\begin{bmatrix} x \\ w \end{bmatrix}^T F(P,K) \begin{bmatrix} x \\ w \end{bmatrix} + \tilde{z}^T w. \tag{5.22}$$

By substituting (5.22) in (5.17), we obtain that

$$V_1(x(t_2)) - V_1(x(t_1)) = \int_{t_1}^{t_2} \left(\frac{1}{2} \begin{bmatrix} x(s) \\ w(s) \end{bmatrix}^T F(P,K) \begin{bmatrix} x(s) \\ w(s) \end{bmatrix} + \tilde{z}^T(s) w(s) \right) ds. \tag{5.23}$$

For the V_2 contribution with V_2 as in (5.14), (5.15) and $z(t) = Hx(t)$, we have that:

$$V_2(Hx(t_2)) - V_2(Hx(t_1)) = \sum_{i=1}^{p} (V_{2,i}(z_i(t_2)) - V_{2,i}(z_i(t_1))), \tag{5.24}$$

with

$$V_{2,i}(z_i(t_2)) - V_{2,i}(z_i(t_1)) = \eta_i \int_{z_i(t_1)}^{z_i(t_2)} \varphi_i(z_i) dz_i, \text{ for } i = 1, ..., p. \tag{5.25}$$

The integral $\int_{z_i(t_1)}^{z_i(t_2)} \varphi_i(z_i)dz_i$ equals the integral $\int_{t_1}^{t_2} \varphi_i(z_i(s))dz_i(s)$, which can be interpreted as a Lebesgue-Stieltjes integral, see [73]. For this Lebesgue-Stieltjes integral we can use the following result, see page 364 in [73],

$$\int_{t_1}^{t_2} \varphi_i(z_i(s))dz_i(s) = \int_{t_1}^{t_2} (\varphi_i \circ z_i)(s)\frac{dz_i(s)}{ds}ds. \tag{5.26}$$

Using this fact in (5.25) and using that $w_i(t) = -(\varphi_i \circ z_i)(t)$, for $i = 1, ..., p$, almost everywhere and $\dot{z}_i = \frac{1}{\eta_i}(\tilde{z}_i - z_i)$ we obtain

$$V_{2,i}(z_i(t_2)) - V_{2,i}(z_i(t_1)) = \eta_i \int_{t_1}^{t_2} (\varphi_i \circ z_i)(s)\frac{dz_i(s)}{ds}ds = \int_{t_1}^{t_2} -w_i(s)\left(\tilde{z}_i(s) - z_i(s)\right)ds, \tag{5.27}$$

for $i = 1, ..., p$. Combining (5.17), (5.24) and (5.27) yields

$$\begin{aligned} V(x(t_2)) - V(x(t_1)) &= \int_{t_1}^{t_2} \left(\frac{1}{2}\begin{bmatrix} x(s) \\ w(s) \end{bmatrix}^T F(P,K) \begin{bmatrix} x(s) \\ w(s) \end{bmatrix} + \tilde{z}^T(s)w(s) \right) ds \\ &\quad - \sum_{i=1}^{p} \int_{t_1}^{t_2} w_i(s)\left(\tilde{z}_i(s) - z_i(s)\right)ds \\ &= \int_{t_1}^{t_2} \frac{1}{2}\begin{bmatrix} x(s) \\ w(s) \end{bmatrix}^T F(P,K) \begin{bmatrix} x(s) \\ w(s) \end{bmatrix} ds + \sum_{i=1}^{p} \int_{t_1}^{t_2} w_i(s)z_i(s)ds \\ &= \int_{t_1}^{t_2} \frac{1}{2}\begin{bmatrix} x(s) \\ w(s) \end{bmatrix}^T F(P,K) \begin{bmatrix} x(s) \\ w(s) \end{bmatrix} ds + \int_{t_1}^{t_2} z^T(s)w(s)ds. \end{aligned} \tag{5.28}$$

The satisfaction of the matrix inequality in (5.11) guarantees that $F(P,K) < 0$ and, consequently, that

$$\frac{1}{2}\begin{bmatrix} x \\ w \end{bmatrix}^T F(P,K) \begin{bmatrix} x \\ w \end{bmatrix} < 0. \tag{5.29}$$

Furthermore, due to (5.2) in Assumption 5.2.1 we have that $z^T w \leq 0$. Therefore, we can conclude that (5.16) is satisfied, which proves global asymptotic stability of the closed-loop system 5.5. □

In case we take $\eta_i = 0$ for $i = 1, ..., p$, we can derive the following corollary from Theorem 5.2.3, which actually leads to a controller design based on a particular case of the circle criterion (see also the passivity theorem in [72]) with sector bounds $[0, \infty]$. In this corollary, we provide conditions that express strict passivity of the linear part of system (5.1) from the input z to the output w and passivity of the nonlinearity $\varphi(z)$.

Corollary 5.2.4 *Consider system* (5.1)*, with* $\varphi(z)$ *satisfying Assumption 5.2.1 and the linear static state-feedback law* (5.4) *with* $K \in \mathbb{R}^{m \times n}$*. If* K *is such that* $(A + BK, G, H)$ *is strictly passive, i.e. there exists a matrix* $P = P^T > 0$ *that satisfy such that*

$$\begin{array}{cc} (A+BK)^T P + P(A+BK) & < 0 \\ PG & = H^T, \end{array} \tag{5.30}$$

then the origin $x = 0$ *is a globally asymptotically stable equilibrium of the closed-loop system* (5.1) *and* (5.4)*.*

Theorem 5.2.3 and Corollary 5.2.4 state sufficient conditions for the absolute stability of Lur'e type systems with sector bounded set-valued nonlinearities in the feedback loop. As such, Theorem 5.2.3 is a generalized Popov criterion and Corollary 5.2.4 is a generalized circle criterion, in the sense that set-valued mappings are allowed. Both results have favorable properties from the perspective of robustness with respect to changes in these nonlinearities. Indeed, for any nonlinearity satisfying Assumption 5.2.1, closed-loop stability is guaranteed. In addition to that, absolute stability is also useful for designing controllers for a range of set-points using a common control gain K as will be shown in Chapter 6. In Corollary 5.2.4, in order to achieve global asymptotic stability of the equilibrium $x = 0$ for all the sector bounded nonlinearities in the sector $[0, \infty]$, strict passivity of the linear part of the system is required (see (5.30)). This may be rather restrictive for some control applications. Note that this work on the circle criterion is similar to the work in [19] for the general setup and similiar to the work in [24] for the particular case of linear complementarity systems. The main contribution of our work is in the generalization of the Popov criterion to set-valued nonlinearities as formulated in Theorem 5.2.3.

5.3 Output-feedback controller design for Lur'e systems with set-valued nonlinearities

In the previous sections, we proposed a state-feedback design for Lur'e type systems with set-valued sector bounded nonlinearities. In this section, we will construct an output-based controller using these state-feedbacks together with an observer that recovers the system state exponentially by using only the

information of the system output, see also [36], [55]. After that, we show that the interconnection of this observer, the state-feedback controller and the original plant yields a stable closed-loop system, which can be considered as a hind of separation principle.

In general, the separation principle does not hold for nonlinear systems. Even though the proposed observers will exhibit the property that the observer error converges to zero exponentially, this is not sufficient in general to guarantee stability of the interconnected system. Indeed, the observer error may destabilize the closed-loop system before it converges to the equilibrium (finite escape time of the controlled system perturbed by the observer error). However, we can prove that the interconnection of the observer/controller combination with the Lur'e type system is a cascade feedback system of an input-to-state-stable system and a globally exponentially stable (GES) system. This fact implies that the origin of the total closed-loop system is globally asymptotically stable (GAS).

In the following sections, the observer design and the output-feedback controller designs based on the circle and Popov criteria are presented. For both the observer design and the stability of the interconnected system, the linear boundedness of the set-valued nonlinearities in Assumption 5.2.1 in the system's feedback loop will be used as an additional condition.

5.3.1 Observer design for Lur'e type systems with set-valued nonlinearities

Consider system (5.1) (see Figure 5.1(a)) with the following additional assumption,

Assumption 5.3.1 The set-valued map $\varphi : \mathbb{R}^p \hookrightarrow \mathbb{R}^p$ is such that

- φ is monotone, i.e. for all $x_1 \in \mathbb{R}^p$ and $x_2 \in \mathbb{R}^p$ it holds that $x_1^* \in \varphi(x_1)$ and $x_2^* \in \varphi(x_2)$ implies that $\langle x_1^* - x_2^*, x_1 - x_2 \rangle \geq 0$, where $\langle \cdot, \cdot \rangle$ denotes the inner product.

As an observer for the system (5.1), we propose the following differential inclusion:

$$\dot{\hat{x}} = (A - LC)\hat{x} + Gw + Bu + Ly \tag{5.31a}$$
$$\hat{w} \in -\varphi(\hat{z}) \tag{5.31b}$$
$$\hat{z} = (H - NC)\hat{x} + Ny \tag{5.31c}$$
$$\hat{y} = C\hat{x}. \tag{5.31d}$$

with $N \in \mathbb{R}^{p \times \kappa}$ and $L \in \mathbb{R}^{n \times \kappa}$.

Since the right-hand side of (5.31a)-(5.31d) is again upper semicontinuous in (t, x) due to continuity of y and piecewise continuity of u, using Assumption

5.2.1 of φ it can be shown that global solutions exist of (5.31). Knowing that both the plant and the observer have global solutions, the observer error $e := x - \hat{x}$ has as dynamics:

$$\dot{e} = (A - LC)e + G(w - \hat{w}) \tag{5.32a}$$
$$w \in -\varphi(Hx) \tag{5.32b}$$
$$\hat{w} \in -\varphi(H\hat{x} + N(y(t) - \hat{y})). \tag{5.32c}$$

The problem of the observer design is finding the gains L, N such that all solutions to the observer error dynamics converge exponentially to the origin, which implies that $\lim_{t\to\infty} |\hat{x}(t) - x(t)| = 0$.

The following theorem presents a method for the observer design that requires the concept of positive realness (see Chapter 2) and states sufficient conditions for the global exponential stability of the origin $e = 0$ of the observer error dynamics (5.32).

Theorem 5.3.2 *[36; 55] Consider the observed system* (5.1)*, the observer* (5.31) *with* $(A - LC, G, H - NC)$ *strictly passive and the observer error dynamics* (5.32)*. Then, the point* $e = 0$ *is globally exponentially stable as long as* $\varphi(\cdot)$ *satisfies Assumptions 5.2.1 and 5.3.1. Moreover, the following bound holds:*

$$\frac{1}{2}\lambda_{min}(P_o)e^T(t)e(t) \leq e^T(0)P_o e(0)\exp\left(-\frac{\lambda_{min}(Q)}{\lambda_{min}(P_o)}t\right), \tag{5.33}$$

where $\lambda_{min}(\cdot)$ *denotes the minimal eigenvalue, and matrices* P_o *and* Q *are given by*

$$P_o = P_o^T > 0, \quad (A-LC)^T P_o + P_o(A-LC) + Q < 0, \quad G^T P_o = H - NC. \tag{5.34}$$

To compute the gains L and N such that $(A - LC, G, H - NC)$ is strictly passive, one can solve the following matrix inequalities (see also in [55; 69]):

$$P_o = P_o^T > 0, \quad (A - LC)^T P_o + P_o(A - LC) + \nu I < 0, \quad G^T P_o = H - NC, \tag{5.35}$$

where we substituted $Q = \nu I$ for some $\nu > 0$. For a given ν, inequality (5.35) is a linear matrix inequality in P_o, N and $L^T P_o$. According to the equation (5.33) the rate of convergence depends on ν and the eigenvalues of the matrix P_o, which in turn depend on the system parameters. When solving the LMIs for observer design, the size of the entries of the matrix P_o can be 'controlled'. For example, by tuning ν or by adding the constraint $P_o < I$ and by including scalar variables in the optimization objective. The computed output feedback gains will then guarantee the rate of convergence as in (5.33). For details on numerical schemes for computing the solutions to the observer dynamics (being differential inclusion) we refer the reader to [80].

5.3.2 Output-feedback based on the Popov and circle criterion

Consider the following control law for the system (5.1):

$$u = K\hat{x}, \tag{5.36}$$

with $K \in \mathbb{R}^{m\times n}$ and $\hat{x}$ the state estimation provided by the observer (5.31). Using the circle and the Popov criteria, we will aim to render the interconnected system (5.1), (5.31), (5.36) absolutely stable. In a state-space formulation, the controlled system (5.1), (5.31), (5.36) can be written in the following form:

$$\dot{x} = (A + BK)x + Gw - BKe \tag{5.37a}$$
$$\dot{e} = (A - LC)e + G(w - \hat{w}) \tag{5.37b}$$
$$w \in -\varphi(z) \tag{5.37c}$$
$$\hat{w} \in -\varphi(\hat{z}) \tag{5.37d}$$
$$z = Hx \tag{5.37e}$$
$$\hat{z} = H\hat{x} + N(y - \hat{y}), \tag{5.37f}$$

with $\varphi(\cdot)$ satisfying the Assumptions 5.2.1 and 5.3.1. Remark that the observer error e can be considered to be an input to the closed-loop system (5.37a), (5.37c), (5.37e). A cascade that represents system (5.1), (5.31), (5.36) or system (5.37) is shown in Figure 5.3.

We want to prove global asymptotic stability (GAS) of the equilibrium (x, e)=(0,0) of system (5.37). The approach we will take is a Lyapunov-based one and the Lyapunov function we will adopt for the closed-loop system is inspired by the Popov criterion.

In the proof of Theorem 5.2.3, it is shown that the origin of system (5.1), (5.36) for $e = 0$ (i.e. $\hat{x} = x$) is GAS. Moreover, in the proof of Theorem 5.3.2 it is shown that $e = 0$ is a GES equilibrium point of the observer error dynamics (5.32). In the sequel, we will provide sufficient conditions under which the system (5.1), (5.31), (5.36) or the equivalent system (5.37) is a cascade feedback system of an ISS system and a GES system, which implies that the origin of the total closed-loop system is GAS.

As far as the right part of Figure 5.3 is concerned (i.e. the system described by (5.37a), (5.37c), (5.37e)) we apply the transformation using a dynamic multiplier as proposed before in Section 5.2.1 (see Figure 5.4). In this figure, we post-multiply the linear part of system (5.1) with the dynamic multiplier $M(s)$ given in (5.7) and pre-multiply the nonlinear (feedback) part of system (5.1) with the inverse of $M(s)$. Using the dynamic multiplier $M(s)$ we aim to transform the original system into a feedback interconnection of two passive systems, see [6] and [72]. Now, Σ_1 represents a new linear system, in the forward path, with the transfer function between w and $\tilde{z}$ given by $\Sigma_1(s) = M(s)G_{cl}(s)$, with $G_{cl}(s)$ as in (5.6) and Σ_2 represents the new system in the feedback path.

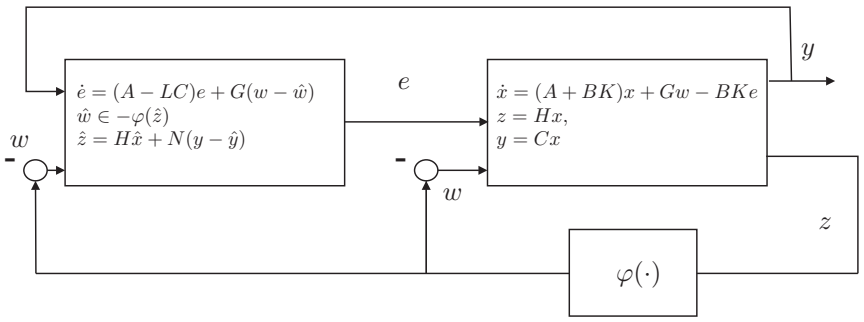

Figure 5.3: Combination of the observer design and the controller design.

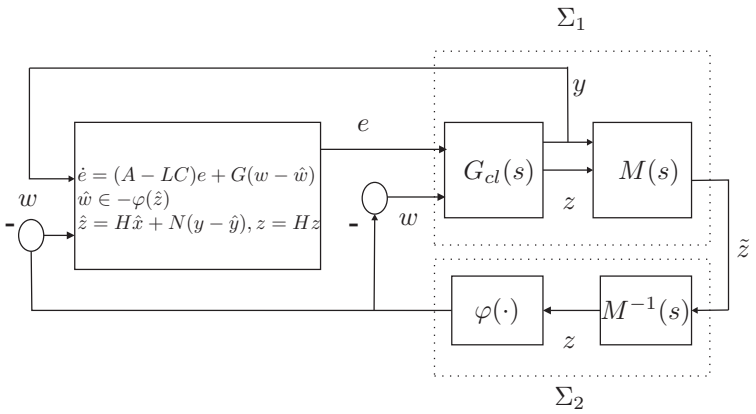

Figure 5.4: Cascade representation of system (5.1), (5.31), (5.36) *using the dynamic multiplier* $M(s)$.

In state-space formulation the transformed controlled system (5.1), (5.31), (5.36), i.e. system (Σ_1, Σ_2), has the following form:

$$\Sigma_1 = \begin{cases} \dot{x} &= (A + BK)x + Gw - BKe(t) \\ \tilde{z} &= \tilde{H}x + \tilde{D}w + Ze(t) \end{cases} \tag{5.38a}$$

$$\Sigma_2 = \begin{cases} \dot{z} &= -\Gamma^{-1}z + \Gamma^{-1}\tilde{z} \\ w &\in -\varphi(z). \end{cases} \tag{5.38b}$$

Herein, the matrices $\tilde{H}$, $\tilde{D}$ and Z can be derived from:

$$\begin{aligned}\tilde{z} &= z + \Gamma\dot{z} \\ &= Hx + \Gamma H\dot{x} \\ &= Hx + \Gamma H[(A+BK)x + Gw - BKe] \\ &= [H + \Gamma H(A+BK)]x + \Gamma HGw - \Gamma HBKe \\ &= \tilde{H}x + \tilde{D}w + Ze,\end{aligned} \tag{5.39}$$

with

$$\tilde{H} = H + \Gamma H(A+BK), \qquad \tilde{D} = \Gamma HG, \qquad Z = -\Gamma HBK. \tag{5.40}$$

The following result proposes conditions under which system (5.38) is input-to-state stable (ISS) with respect to the observer error $e(t)$.

Theorem 5.3.3 *Consider system* (5.38) *with φ satisfying the Assumptions 5.2.1 and 5.3.1. Suppose there exists $\Gamma = diag(\eta_1, ..., \eta_p) \in \mathbb{R}^{p\times p}$, with $\eta_i > 0$ for $i = 1, ..., p$, a matrix $P = P^T > 0$ and a feedback gain matrix $K \in \mathbb{R}^{m\times n}$ that satisfy the following matrix inequality*

$$\begin{bmatrix} (A+BK)^T P + P(A+BK) & PG - \tilde{H}^T \\ G^T P - \tilde{H} & -\tilde{D} - \tilde{D}^T \end{bmatrix} < 0, \tag{5.41}$$

with $\tilde{H}$ and $\tilde{D}$ defined in (5.40). *Then system* (5.38) *is ISS with respect to the input $e(t)$.*

Proof Consider the Lyapunov candidate function defined by (5.12), (5.13), (5.14), (5.15) for the system (5.38). Similar to the proof of Theorem 5.2.3, we study the evolution of time V in time along solutions of (5.38).
For the V_1 contribution with V_1 as in (5.13), we have that

$$V_1(x(t_2)) - V_1(x(t_1)) = \int_{t_1}^{t_2} \dot{V}_1(s)ds. \tag{5.42}$$

Herein, the time derivative of V_1 can be written as follows:

$$\begin{aligned}\dot{V}_1 &= \tfrac{1}{2}\{\dot{x}^T Px + x^T P\dot{x}\} \\ &= \tfrac{1}{2}\{[(A+BK)x + Gw - BKe]^T Px + x^T P[(A+BK)x + Gw - BKe]\} \\ &= \tfrac{1}{2}\{x^T[(A+BK)^T P + P(A+BK)]x + w^T G^T Px + x^T PGw + \rho_2\},\end{aligned} \tag{5.43}$$

with $\rho_2 = -e^T K^T B^T P x - x^T P B K e$. At this point we add and subtract $\frac{1}{2}\{\tilde{z}^T w + w^T \tilde{z}\}$ from the above equation and use (5.39):

$$\begin{aligned}
\dot{V}_1 &= \dot{V}_1 + \tfrac{1}{2}\{-\tilde{z}^T w - w^T \tilde{z} + \tilde{z}^T w + w^T \tilde{z}\} \\
&= \dot{V}_1 + \tfrac{1}{2}\{-(\tilde{H}x + \tilde{D}w + Ze)^T w - w^T(\tilde{H}x + \tilde{D}w + Ze) \\
&\quad +2\tilde{z}^T w\} \\
&= \dot{V}_1 + \tfrac{1}{2}\{-x^T \tilde{H}^T w - w^T \tilde{D}^T w - e^T Z^T w - w^T \tilde{H}x - w^T \tilde{D}w - w^T Ze \\
&\quad +2\tilde{z}^T w\} \\
&= \tfrac{1}{2}\begin{bmatrix} x \\ w \end{bmatrix}^T F(P,K) \begin{bmatrix} x \\ w \end{bmatrix} - \tfrac{1}{2}e^T K^T B^T P x - \tfrac{1}{2}x^T P B K e - \tfrac{1}{2}e^T Z^T w \\
&\quad -\tfrac{1}{2}w^T Z e + \tilde{z}^T w,
\end{aligned} \tag{5.44}$$

with $F(P,K)$ defined in (5.21).
Based on the proof of Theorem 5.2.3 the contribution of V_2 to V, with V_2 as in (5.14), (5.15) obeys

$$V_2(Hx(t_2)) - V_2(Hx(t_1)) = \int_{t_1}^{t_2} w^T(s)(z(s) - \tilde{z}(s))ds \ \forall t_2 > t_1 \text{ and } t_1, t_2 \in \mathbb{R}, \tag{5.45}$$

along a solution $x(t)$ with input $w(t)$ and output $z(t)$. Combining (5.12), (5.42), (5.44) and (5.45) we can derive that

$$\begin{aligned}
V(x(t_2)) - V(x(t_1)) &= \textstyle\int_{t_1}^{t_2} \big\{ \frac{1}{2}\begin{bmatrix} x(s) \\ w(s) \end{bmatrix}^T F(P,K) \begin{bmatrix} x(s) \\ w(s) \end{bmatrix} + z^T(s)w(s) \\
&\quad -\tfrac{1}{2}e(s)^T K^T B^T P x(s) - \tfrac{1}{2}x^T(s) P B K e(s) \\
&\quad -\tfrac{1}{2}e^T(s) Z^T w(s) - \tfrac{1}{2}w^T(s) Z e(s) \big\}\, ds \ \forall t_2 > t_1 \text{and } t_1 \in \mathbb{R}.
\end{aligned} \tag{5.46}$$

Hence, the derivative of V with respect to time, for all $x \in \mathbb{R}^n$ and $z_i \in \mathbb{R}$, $i = 1, ..., p$, can be written as

$$\begin{aligned}
\dot{V} &= \tfrac{1}{2}\begin{bmatrix} x \\ w \end{bmatrix}^T F(P,K) \begin{bmatrix} x \\ w \end{bmatrix} + z^T w - \tfrac{1}{2}e^T K^T B^T P x - \tfrac{1}{2}x^T P B K e \\
&\quad -\tfrac{1}{2}e^T Z^T w - \tfrac{1}{2}w^T Z e,
\end{aligned} \tag{5.47}$$

with

- $z^T w \leq 0$, see Assumption 5.2.1
- $F(P,K) < 0$ (due to (5.41)) and thus we have that $\frac{1}{2}\begin{bmatrix} x \\ w \end{bmatrix}^T F(P,K) \begin{bmatrix} x \\ w \end{bmatrix} < -\varepsilon\|x\|^2 - \varepsilon\|w\|^2 \leq -\varepsilon\|x\|^2$, for some $\varepsilon > 0$.

Consequently, the first two components in the right-hand side of (5.47) satisfy

$$\frac{1}{2}\begin{bmatrix} x \\ w \end{bmatrix}^T F(P,K)\begin{bmatrix} x \\ w \end{bmatrix} + z^T w \leq -\varepsilon\|x\|^2. \tag{5.48}$$

In the sequel, we will use the following inequality

$$2y^T z \leq y^T G y + z^T G^{-1} z \text{ for any } G = G^T > 0 \text{ and for all vectors } y, z. \tag{5.49}$$

More specifically, using (5.49) and the definitions $X := K^T B^T P$ and $\bar{G} := XG^{-1}X^T$ we have that

$$\begin{array}{rcl} -\frac{1}{2}e^T K^T B^T P x - \frac{1}{2}x^T P B K e & = & -e^T K^T B^T P x \\ & = & -e^T X x \\ & \leq & \frac{1}{2}e^T X G^{-1} X^T e + \frac{1}{2}x^T G x \\ & = & \frac{1}{2}e^T \bar{G} e + \frac{1}{2}x^T G x. \end{array} \tag{5.50}$$

Based on (5.48) and (5.50) and by choosing $G = \varepsilon I$, $\dot{V}$ in (5.47) takes the form

$$\dot{V} \leq -\frac{\varepsilon}{2}\|x\|^2 + \frac{1}{2}e^T \bar{G} e - e^T Z w. \tag{5.51}$$

Next, we use the following linear growth condition on w (see (5.3) in Assumption 5.2.1):

$$\|w\| \leq \gamma_1\|z\| + \gamma_2. \tag{5.52}$$

With $z = Hx$ it holds that $\|z\| \leq \|H\|\|x\|$ and thus

$$\|w\| \leq \gamma_1\|H\|\|x\| + \gamma_2 = \bar{\gamma}_1\|x\| + \bar{\gamma}_2, \tag{5.53}$$

where $\bar{\gamma}_1 := \gamma_1\|H\|$ and $\bar{\gamma}_2 := \gamma_2$.
Using (5.53), we derive the following equality for the term $-e^T Z w$ in (5.51):

$$-e^T Z w \leq \|e^T Z w\| \leq \|e\|\|Z\|w\| \leq \|Z\|\|e\|(\bar{\gamma}_1\|x\| + \bar{\gamma}_2) = \hat{\gamma}_1\|e\|\|x\| + \hat{\gamma}_2\|e\|, \tag{5.54}$$

with $\hat{\gamma}_1 := \|Z\|\bar{\gamma}_1$ and $\hat{\gamma}_2 := \|Z\|\bar{\gamma}_2$.
Using (5.54) in (5.51) gives

$$\dot{V} \leq -\frac{\varepsilon}{2}\|x\|^2 + \frac{1}{2}e^T \bar{G} e + \hat{\gamma}_1\|e\|\|x\| + \hat{\gamma}_2\|e\|. \tag{5.55}$$

Since inequality (5.49) holds for any y, z, it also holds that (using $G = \alpha I$) in the inequality (5.49)

$$2\|y\|\|z\| \leq \alpha\|y\|^2 + \frac{1}{\alpha}\|z\|^2 \text{ for any } \alpha > 0. \tag{5.56}$$

Therefore,

$$\hat{\gamma}_1\|x\|\|e\| \leq \frac{\hat{\gamma}_1}{2}(\alpha\|x\|^2 + \frac{1}{\alpha}\|e\|^2) \text{ for any } \alpha > 0. \tag{5.57}$$

Using (5.57) in (5.55) and choosing $\alpha = \frac{\varepsilon}{2\hat{\gamma}_1}$ yields

$$\begin{array}{rcl} \dot{V} & < & -\frac{\varepsilon}{2}\|x\|^2 + \frac{\hat{\gamma}_1}{2}\alpha\|x\|^2 + \frac{1}{2}e^T\bar{G}e + \hat{\gamma}_2\|e\| + \frac{\hat{\gamma}_1}{2\alpha}\|e\|^2 \\ \Rightarrow \dot{V} & < & -\frac{\varepsilon}{4}\|x\|^2 + \frac{1}{2}[\lambda_{max}(\bar{G}) + 2\frac{\hat{\gamma}_1^2}{\varepsilon}]\|e\|^2 + \hat{\gamma}_2\|e\|. \end{array} \tag{5.58}$$

From (5.58) it follows that

$$\begin{array}{rcl} \dot{V} & < & -\frac{\varepsilon}{8}\|x\|^2 \text{ if } \frac{\varepsilon}{8}\|x\|^2 > \frac{1}{2}[\lambda_{max}(\bar{G}) + 2\frac{\hat{\gamma}_1^2}{\varepsilon}]\|e\|^2 + \hat{\gamma}_2\|e\| \\ \Rightarrow \dot{V} & < & -\frac{\varepsilon}{8}\|x\|^2 \text{ if } \|x\| > \sqrt{\frac{4}{\varepsilon}([\lambda_{max}(\bar{G}) + 2\frac{\hat{\gamma}_1^2}{\varepsilon}]\|e\|^2 + 2\hat{\gamma}_2\|e\|)}. \end{array} \tag{5.59}$$

We define

$$\beta_2(\|e\|) := \sqrt{\frac{4}{\varepsilon}([\lambda_{max}(\bar{G}) + 2\frac{\hat{\gamma}_1^2}{\varepsilon}]\|e\|^2 + 2\hat{\gamma}_2\|e\|)}$$

and

$$\beta_1(\|x\|) := \frac{\varepsilon}{8}\|x\|^2,$$

where $\beta_1(\|x\|)$ is a positive definite function and $\beta_2(\|e\|)$ is a class K-function. Consequently, the conditions for input-to-state stability, as formulated in Theorem 4.19 in [72], are satisfied. This concludes the proof. □

Now, we combine Theorem 5.3.2 and Theorem 5.3.3 and use the fact that a feedback interconnection of an ISS system with GES system yields an asymptotic stable interconnection (see Lemma 4.7 in [72] which can be viewed as special version of Property 3.3.3 in this thesis). The latter line of reasoning is adopted in the following theorem, regarding the observer-based output-feedback design for system (5.1).

Theorem 5.3.4 *Consider system* (5.1)*, observer* (5.31) *and control law* (5.36) *with φ satisfying the Assumptions 5.2.1 and 5.3.1. Suppose there exists $\Gamma = diag(\eta_1, ..., \eta_p) \in \mathbb{R}^{p\times p}$, with $\eta_i > 0$ for $i = 1, ..., p$, a matrix $P = P^T > 0$ and a feedback gain matrix $K \in \mathbb{R}^{m\times n}$ that satisfy the matrix inequality* (5.41) *with $\tilde{H}$ and $\tilde{D}$ defined in* (5.40)*. Suppose, $(A - LC, G, H - NC)$ is strictly passive. Then, $(x, e) = (0, 0)$ is a globally asymptotically stable equilibrium point of the closed-loop system* (5.1), (5.31), (5.36).

Proof The closed-loop system (5.1), (5.31), (5.36) can be written as a feedback interconnection of system (5.37a), (5.37c), (5.37e) and the observer error dynamics (5.37b), (5.37d), (5.37f).

According to Theorem 5.3.3, under the conditions of the current theorem, system (5.1), (5.31), (5.36) is ISS with respect to the observer $e(t)$. Moreover, according to Theorem 5.3.2, the observer error dynamics is globally exponentially stable for any $w(t)$, $x(t)$. Using Lemma 4.7 in [72] or, alternatively, Property 3.3.3 in this thesis, we can conclude that $(x, e) = (0, 0)$ is a globally asymptotically stable equilibrium point of system (5.1), (5.31), (5.36). □

In case we take $\eta_i = 0$ for $i = 1, ..., p$, in the definition of the Lyapunov function in (5.12)-(5.15), i.e. $V(x) = x^T P x,\ P = P^T > 0$, we can derive the corollary below from Theorem 5.3.3, which yields an output-feedback design based on the circle criterion.

Corollary 5.3.5 *Consider system* (5.1), *observer* (5.31) *and the control law* (5.36) *with φ satisfying the Assumptions 5.2.1 and 5.3.1. Suppose there exists a matrix $P = P^T > 0$ and a feedback gain matrix K that satisfy the matrix inequality in* (5.30). *Suppose, $(A - LC, G, H - NC)$ is strictly passive. Then, $(x, e) = (0, 0)$ is a globally asymptotically stable equilibrium point of the closed-loop system* (5.1), (5.31), (5.36).

5.4 Discussion

In this chapter, we proposed two passivity-based controller designs for Lur'e type systems with a linear part in the forward path and set-valued sector bounded nonlinearities in the feedback loop to achieve absolute stability of the closed-loop system. To obtain this goal, we extended the common reasoning based on the well known circle criterion and Popov criterion towards set-valued nonlinearities that two interconnected passive systems of the Lur'e type form again a passive system.

In the state-feedback controller design based on the circle criterion (using a quadratic Lyapunov function), we guarantee that the closed-loop system is absolutely stable under the condition that the linear part of the system is strictly passive and the set-valued nonlinearities in the feedback loop are passive. In the controller design based on the Popov criterion, the requirement of strict passivity of the linear part of the closed-loop system is relaxed by using a dynamic multiplier. More specifically, by multiplying the transfer function of the linear part with a dynamic multiplier and by multiplying the set-valued nonlinearities in the feedback loop by the inverse of this multiplier we derive a new linear system in the forward path and new dynamic system with a set-valued output map in the feedback path. For the interconnection of these subsystems to be absolutely stable we require strict passivity of the new linear part and passivity of the new set-valued nonlinearities.

For the case that not all states are available (measured), we also developed a design method for output-feedback controllers that consist of a model-based observer and a state-feedback controller. The state-feedback controller used herein is based either on the (extended) circle or on the (extended) Popov criterion, as mentioned before. We derived conditions under which the adopted model-based observer recovers the system state exponentially by using only the information of the system output. Moreover, conditions have been provided under which the separation principle holds for the systems under study. More specifically, the stability of the interconnected system is achieved if the observer

error converges to zero exponentially and the controlled system is input-to-state stable with respect to the observer error.

An interesting extension of this work is to relax the requirements of strict passivity for the new linear system to requirements for passivity by using another multiplier than the first order multiplier used in this chapter. This would extend the applicability of the Popov criterion design to a broader class of systems. Moreover, the Popov criterion controller design is only applicable to Lur'e systems with time-independent nonlinearities. The extension of this design for time-dependent nonlinearities could be of interest (see [13]), although it still has to be generalized to set-valued mappings. This might be a topic of future research.

6

Passivity-based controller design implementation on a rotor dynamic system

6.1 Introduction

In this chapter, we evaluate the practical use of the controller design strategy presented in Chapter 5, using an experimental setup that describes a dynamic rotor system with set-valued friction and non-collocated actuation. This experimental setup consists of two discs coupled by a low stiffness spring (see Figure 6.1(a)). Both discs are subject to friction and one of them (the upper disc) is driven by an actuator. The friction that acts on the upper disc is modeled as dry friction and the friction that acts on the other disc (lower) is modeled as dry friction with Stribeck effect [26]. The presence of negative damping in one of the friction models leads to complex dynamical phenomena such as the coexistence of steady-state solutions, discontinuous bifurcation points and stick-slip limit cycling [86–88]. These vibrational phenomena are present in many mechanical motion systems with flexibilities and friction. In such engineering systems, especially limit cycling is an undesirable phenomenon because it causes kinetic energy dissipation, noise, excessive wear of machine parts and inferior positioning properties. Due to the fact that the examined setup reproduces this kind of behavior it can be considered as benchmark for this type of systems. The goal of this chapter is the elimination of this limit-cycling behavior in the setup. Common friction compensation techniques such as, for instance, the ones proposed in [8; 26; 97] that deal with system subject to friction cannot be applied in the present system due to the fact that the control action is non-collocated with the set-valued friction.

The model of the rotor dynamic system can be written as a Lur'e type system with monotone sector bounded set-valued nonlinearities in the feedback

loop. Since the model of the rotor dynamic system can be expressed as a Lur'e type system, the output-feedback controller designs proposed in Chapter 5 can be applied. In the present chapter, we will apply the controller designs that are based on the circle and Popov criterion, respectively, to the rotor dynamic system. It will be shown that the circle criterion design cannot render this system absolutely stable while the Popov criterion design can. Absolute stability implies a favorable robustness property for the elimination of limit cycling because it guarantees the stabilization of a unique equilibrium for any friction model satisfying a sector condition. Moreover, it will be shown that the robustness with respect to changes in set-valued nonlinearities (i.e. the friction) also allows to stabilize a range of set-points (equilibria) using a single controller design.

This chapter is organized as follows. In Section 6.2, the experimental setup is described and a model for this setup is presented. The predictive quality of the model with respect to the real system is studied based on simulations and experiments. In Section 6.3, an output-feedback controller is designed for this system to stabilize its equilibria for different friction situations, thereby eliminating undesirable stick-slip limit-cycling. This output-feedback controller consists of an observer and a state-feedback controller as discussed in Chapter 5. In this section, we also examine whether the closed-loop system is absolutely stable based on experiments and simulations. At the end of this section, we investigate the effect of controller saturation on the closed-loop performance. Finally, a discussion of the results presented in this chapter is given in Section 6.4.

6.2 Experimental setup

In order to evaluate experimentally the controller design strategies proposed in Chapter 5, an experimental setup that consists of two inertias coupled by a flexibility and subject to friction has been built. This setup is available in the Dynamics and Control Technology Laboratory at Eindhoven University of Technology. For the remainder of this thesis we will call this setup the rotor dynamic system.

6.2.1 Description of the rotor dynamic system

The experimental setup is shown in Figures 6.1(a)-6.1(b). The input voltage from the computer, which is between $-5\,\mathrm{V}$ and $5\,\mathrm{V}$, is fed into the DC-motor via the current-controlled amplifier. The DC-motor is connected to the upper steel disc, via the gear box. The upper and lower discs are connected through a low-stiffness steel string. Both discs can rotate around their geometric centers and the related angular positions are measured using incremental encoders. Moreover, a brake is applied at the lower disc and induces a friction torque that

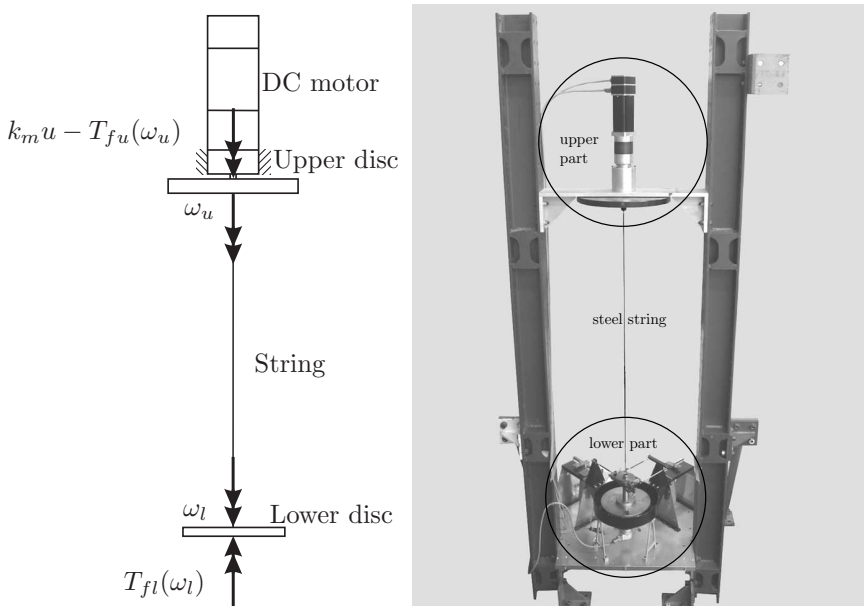

Figure 6.1: (a) Schematic representation of the experimental dynamic rotor system (b) Photo of the experimental dynamic rotor system.

causes limit cycling in the system. More detailed photographs and descriptions of the lower part of the setup and the brake are given in Figures 6.2 and 6.3, respectively.

6.2.2 Model of the rotor dynamic system

In order to derive a simple, though predictive, model for the dynamic rotor system we assume that

- the DC motor dynamics does not influence the system dynamics (the inductance of the rotor circuit and the back electromagnetic phenomenon (EMF) are neglected),
- the lower disc always remains horizontal and does not move in vertical and lateral direction,
- the torsional damping in the string is negligible compared to the damping of the bearings of the discs,

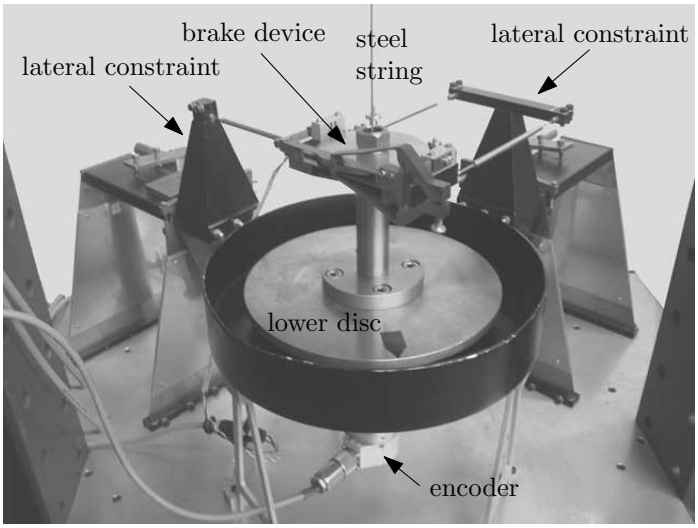

Figure 6.2: Lower part of the experimental rotor dynamic set-up.

- the string is massless.

For more details on these modelling assumptions see [86], [87], [88]. The experimental dynamic rotor system can then be described by the following model:

$$\begin{aligned} J_u\ddot{\theta}_u + k_\theta(\theta_u - \theta_l) + T_{fu}(\dot{\theta}_u) - k_m u = 0 \\ J_l\ddot{\theta}_l - k_\theta(\theta_u - \theta_l) + T_{fl}(\dot{\theta}_l) = 0, \end{aligned} \tag{6.1}$$

where θ_u and θ_l are the angular positions of the upper and lower discs, respectively. Moreover, u is the input voltage to the power amplifier of the motor, J_u and J_l are the moments of inertia of the upper and lower discs about their respective centers of mass, k_θ is the torsional spring stiffness and k_m is the motor constant. The friction torques T_{fu} and T_{fl} act on the upper and lower disc, respectively. The friction torque at the upper disc T_{fu} is caused by the friction in the bearings of the upper disc and the electro-magnetic effect in the DC-motor. The friction torque at the lower disc T_{fl} comprises the friction in the bearings of the lower disc and the friction induced by the brake-mechanism.

The dynamics of the system (6.1) can be described by a third-order state-space system since the dynamics only depends on the difference between the velocities of the discs and the angular positions. Therefore, by choosing the state variables as $x_1 = \alpha = \theta_u - \theta_l$, $x_2 = \dot{\theta}_u$ and $x_3 = \dot{\theta}_l$, the following

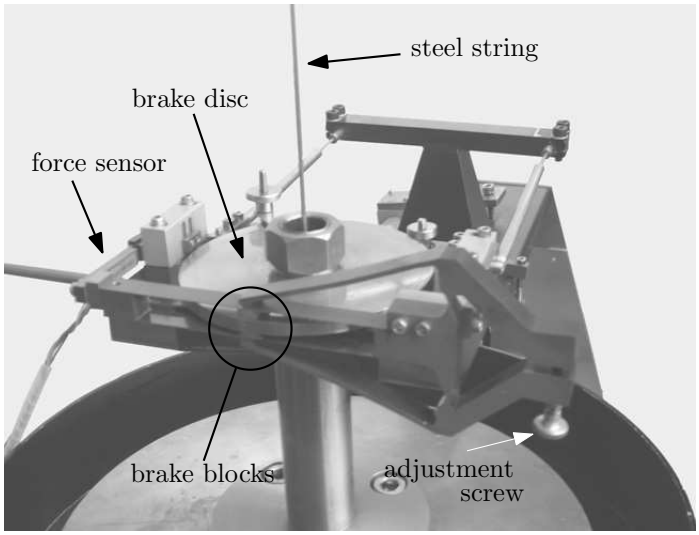

Figure 6.3: Brake device.

state-space model is obtained:

$$\begin{aligned} \dot{x}_1 &= x_2 - x_3 \\ \dot{x}_2 &= \tfrac{1}{J_u}[-k_\theta x_1 - T_{fu}(x_2) + k_m u] \\ \dot{x}_3 &= \tfrac{1}{J_l}[k_\theta x_1 - T_{fl}(x_3)]. \end{aligned} \tag{6.2}$$

Both friction torques T_{fu} and T_{fl} are modelled by set-valued force laws to account for the sticking effect of the real friction. Moreover, $x = [x_1\ x_2\ x_3]^T$ is the state and $x_{eq} = [\alpha_{eq}\ \omega_{eq}\ \omega_{eq}]^T$ denotes an equilibrium of (6.2). Note that the equilibrium x_{eq} corresponds to the situation where both discs rotate with the same constant velocity ($x_2 = x_3 = \omega_{eq}$) and a fixed distance α_{eq} is maintained between the angular positions of upper and lower disc.

The friction torque acting on the upper disc can be described by the set-valued map:

$$T_{fu}(x_2) \in \begin{cases} T_{cu}(x_2)\mathrm{sgn}(x_2) & \text{for } x_2 \neq 0 \\ [-T_{su} + \Delta T_{su}, T_{su} + \Delta T_{su}] & \text{for } x_2 = 0, \end{cases} \tag{6.3}$$

where the function $T_{cu}(x_2)$ is given by

$$T_{cu}(x_2) = T_{su} + \Delta T_{su}\mathrm{sgn}(x_2) + b_u|x_2| + \Delta b_u x_2. \tag{6.4}$$

The constants T_{su}, ΔT_{su}, b_u, Δb_u are the parameters of the friction model related to the friction at the upper disc. Moreover, $-T_{su} + \Delta T_{su}$ and $T_{su} + \Delta T_{su}$ represent the minimum and the maximum static friction levels, respectively,

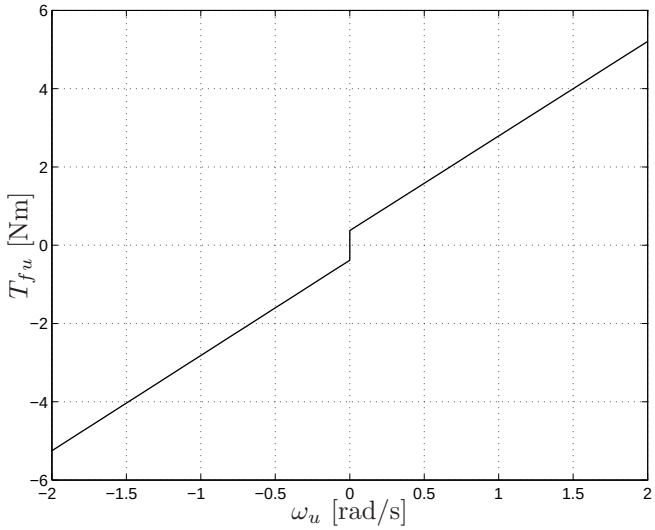

Figure 6.4: Upper friction model T_{fu}.

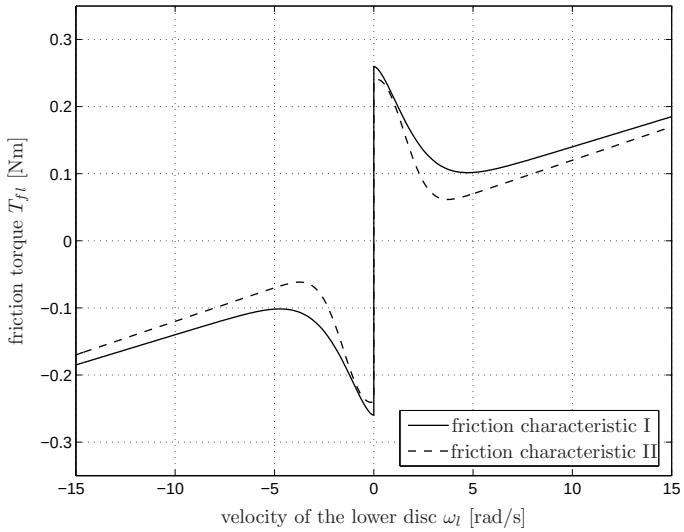

Figure 6.5: Friction torque of the lower disc for friction characteristic I and II.

---

and b_u is the viscous friction coefficient of the friction in the upper disc. Furthermore, the friction at the lower disc can be modeled accurately with an algebraic inclusion that includes a dry friction model including the Stribeck

effect [26] and viscous friction:

$$T_{fl}(x_3) \in \begin{cases} T_{cl}(x_3)\mathrm{sgn}(x_3) & \text{for } x_3 \neq 0 \\ [-T_{sl}, T_{sl}] & \text{for } x_3 = 0, \end{cases} \tag{6.5}$$

where the continuous function $T_{cl}(x_3)$ is given by

$$T_{cl}(x_3) = T_{cl} + (T_{sl} - T_{cl})e^{-|\frac{x_3}{\omega_{sl}}|^{\delta_{sl}}} + b_l|x_3|. \tag{6.6}$$

The constants T_{sl}, δ_{sl} and b_l are the parameters of the friction model related to the friction at the lower disc. Moreover, $-T_{sl}$ and T_{sl} represent the minimum and the maximum static friction levels, respectively, and b_l is the viscous friction coefficient. Note that the system (6.2)-(6.6) is a differential inclusion due to the set-valued nature of the friction models (6.3)-(6.4) and (6.5)-(6.6). The parameters k_m, J_u, J_l and k_θ are identified experimentally in [86–88]. Moreover, the parameters of the friction model are identified using an approach as described in [86; 87]. The identified parameters of the model (6.2)-(6.6) are given in Tables 6.1 and 6.2 for different settings of the brake blocks. Indeed, we can obtain different friction characteristics for the friction at the lower disc by changing the normal force acting in the contact between the brake blocks and the brake disc by using the adjustment screw (see Figure 6.3). This results in two different friction characteristics with different parameters as in Table 6.1 for friction characteristic I and in Table 6.2 for friction characteristic II. The nominal force for friction characteristic I is 17N and for friction characteristic II is 25N. The resulting friction laws (6.3)-(6.4) and (6.5)-(6.6) are depicted in Figures 6.4 and 6.5, respectively.

6.2.3 Nonlinear dynamics of the rotor dynamic system

In this section, we consider the case of constant inputs (i.e. constant voltage inputs to the DC motor), since in this dynamic rotor system the steady-state behavior to constant inputs is of great interest. Constants inputs are commonly used to excite several mechanical motion systems such as drill-string systems, printers, shafts in ship engines and many more. Equilibria, represented by constant velocities, are considered desirable, whereas stick-slip limit-cycling is considered to be an unwanted vibrational phenomenon as discussed in Section 6.1.

First of all, we will use simulations and experimental results to show that the model of the rotor dynamic system, given in the previous section, captures with accuracy the dynamics of the real system. In addition to that, we will show that both the model and the considered system exhibits complex dynamical phenomena such as the coexistence of steady-state solutions, bifurcations, stable and unstable equilibria and periodic solutions. To validate the model of the considered system two bifurcation diagrams are constructed. These diagrams represent properties of the steady-state trajectories versus a properly

Table 6.1: Parameter values of the model (6.2)-(6.6) *for friction characteristic I.*

parameter	**estimated value**	**unit**
k_m	4.3228	[Nm/V]
J_u	0.4765	[kg m^2]
T_{su}	0.3797	[Nm]
ΔT_{su}	-0.0057	[Nm]
b_u	2.4245	[kg m^2/rad s]
Δb_u	-0.0084	[kg m^2/rad s]
k_θ	0.075	[Nm/rad]
J_l	0.035	[kg m^2]
T_{sl}	0.26	[Nm]
T_{cl}	0.05	[Nm]
ω_{sl}	2.2	[rad/s]
δ_{sl}	1.5	[-]
b_l	0.009	[kg m^2/rad s]

Table 6.2: Parameter values of the model (6.2)-(6.6) *for friction characteristic II.*

parameter	**estimated value**	**unit**
k_m	4.3228	[Nm/V]
J_u	0.4765	[kg m^2]
T_{su}	0.37975	[Nm]
ΔT_{su}	-0.00575	[Nm]
b_u	2.4245	[kg m^2/rad s]
Δb_u	-0.0084	[kg m^2/rad s]
k_θ	0.075	[Nm/rad]
J_l	0.035	[kg m^2]
T_{sl}	0.24	[Nm]
T_{cl}	0.02	[Nm]
ω_{sl}	2.0	[rad/s]
δ_{sl}	2.2	[-]
b_l	0.01	[kg m^2/rad s]

chosen bifurcation parameter. Furthermore, the period of the periodic solutions is computed and measured. For all these diagrams together with time responses, comparisons are made between the results obtained via the model

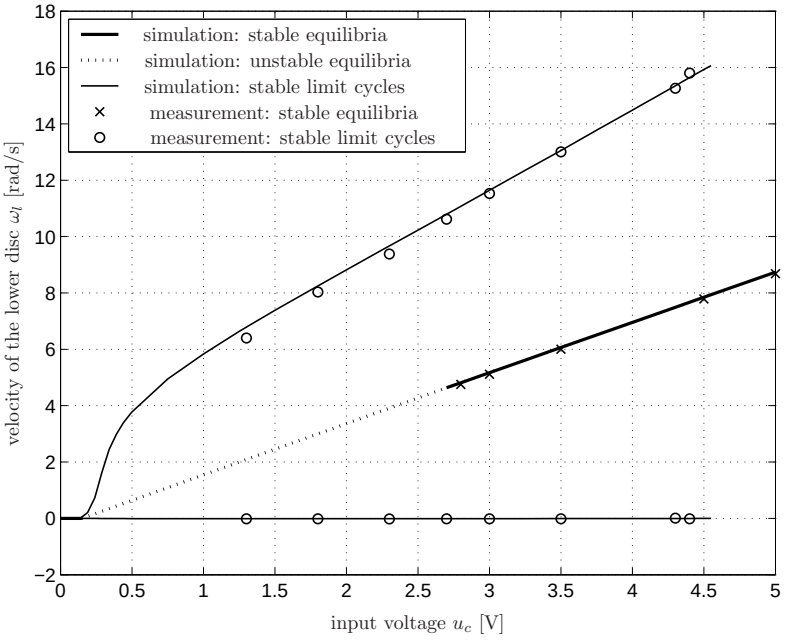

Figure 6.6: Bifurcation diagram with the velocity of the lower disc for positive constant input voltages.

---

and the measurements obtained from the setup.

Consider the system given by the differential inclusions (6.2)-(6.6) with parameter values taken from Table 6.1. By using numerical computations, the periodic steady-state solutions of the system state x for constant inputs $u = u_c$ in the range $[0,\ 5]V$ are derived. Moreover, we compute the equilibria $x_{eq} = [\alpha_{eq}\ \omega_{eq}\ \omega_{eq}]^T$ by solving the algebraic inclusions originating from setting $\dot{x}_1 = \dot{x}_2 = \dot{x}_3 = 0$ is (6.2). It is proven in [86] that there exists an input voltage $u_{\mathcal{E}q} > 0$ ($u_{\mathcal{E}q} = 0.151$V) such that for $u_c < u_{\mathcal{E}q}$ (for which $\omega_{eq} = 0$ there is an equilibrium set (i.e. multiple equilibrium) and for $u_c > u_{\mathcal{E}q}$ a unique isolated equilibrium exists for the given parameter set, see [88]. The technique used for the numerical computation of solutions of the system (6.2)-(6.6) is based on the switch model (see [80]). This algorithm is able to solve differential inclusions with a limited number of discontinuities. Details on the switch model are given in [80].

In Figures 6.6 and 6.7, two bifurcation diagrams of the rotor dynamic system are given. The bifurcation diagram in Figure 6.6 depicts the steady-state response of the velocity of the lower disc ω_l versus the constant input voltage u_c, which is chosen as the bifurcation parameter. To be precise, the dotted

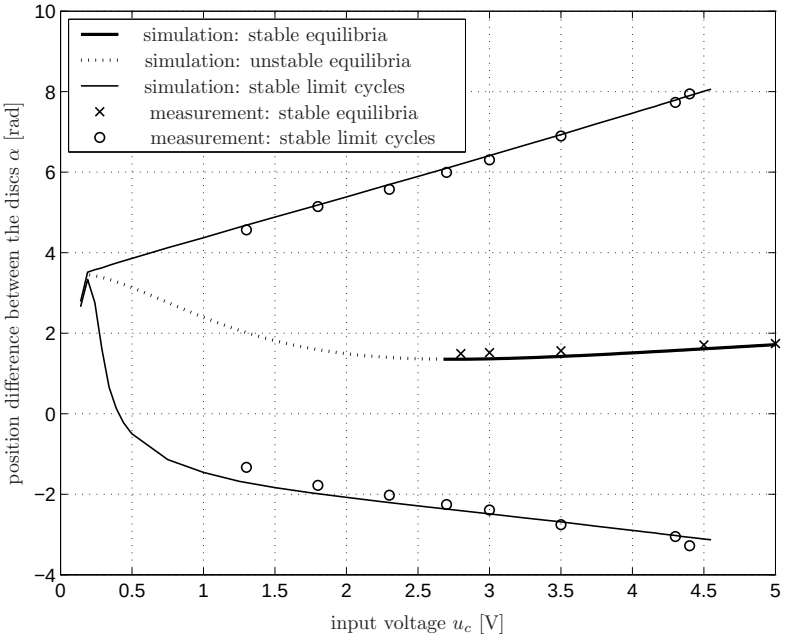

Figure 6.7: Bifurcation diagram with the position difference between the upper and the lower disc for positive constant input voltages.

line represents a region of unstable equilibria and the thick solid line a region of stable equilibria. The thin solid curves correspond to the maximum and minimum value, i.e. $\max_{t\in[0,\ T]}\omega_l(t)$ and $\min_{t\in[0,\ T]}\omega_l(t)$, respectively, of the steady-state periodic solutions (limit cycles) with period time T. In Figure 6.6, the experimental results[1] of ω_l in steady-state are depicted with the marks $\times$ and $\circ$. The marks $\times$ correspond to stable equilibria and the marks $\circ$ correspond to stable limit cycles.

Similarly, the bifurcation diagram in Figure 6.7 depicts the steady-state response of the difference in displacements between the upper and lower disc α versus the bifurcation parameter u_c (for $u_c > u_{\mathcal{E}q}$). Once again, the dotted line represents a region of unstable equilibria and the thick solid line a region of stable equilibria. The thin solid curves correspond to the maximum and minimum value of α, i.e. $\max_{t\in[0,\ T]}\alpha(t)$ and $\min_{t\in[0,\ T]}\alpha(t)$, respectively. By using the two incremental encoders, located at the upper and the lower disc, the system variable α is measured. The measurements of α are taken when the system is in steady-state. The measured values of α are depicted in Figure 6.7

[1]Note that the experimental velocity signal is obtained by numerical differentiation (and by using a low pass filter) of the measured position signals.

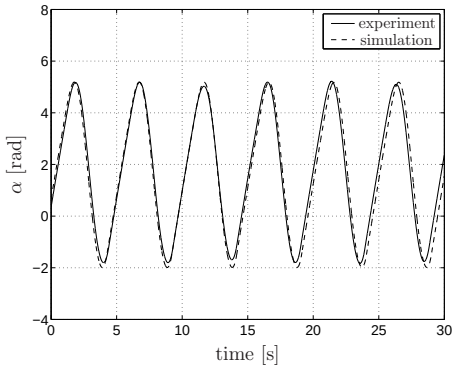

(a) $\alpha(t)$.

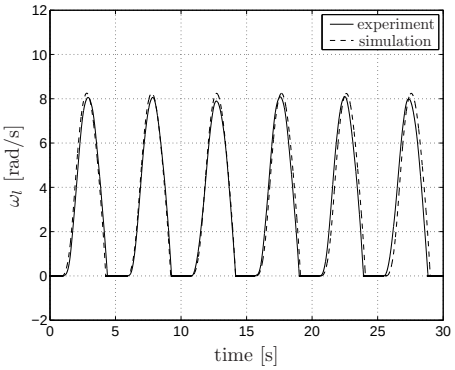

(b) $\omega_l(t)$.

Figure 6.8: Measured and simulated limit cycle responses of the rotor dynamic system for $u_c = 1.8$ V.

with the marks $\times$ and $\circ$. The marks $\times$ correspond to stable equilibria and the marks $\circ$ correspond to stable limit cycles.

In order to gain a better understanding of the presented bifurcation diagrams, time responses of $\alpha(t)$ and $\omega_l(t)$ are studied. In Figures 6.8, 6.9 and 6.10, $\alpha(t)$ and $\omega_l(t)$ are depicted for constant input voltages of 1.8V, 2.8V and 3.8V, respectively. The dashed curves correspond to simulations and the solid curves to measurements. In Figure 6.8, a limit cycle response is shown for $u_c = 1.8V$, while in Figures 6.9 and 6.10, equilibria are depicted for $u_c = 2.8$V and 3.5V, respectively.

Based on Figure 6.8, we notice that the stick-slip limit cycling is predicted accurately by the model. From Figures 6.9 and 6.10, we notice that in principle the system's equilibria are also predicted well. However, there are some

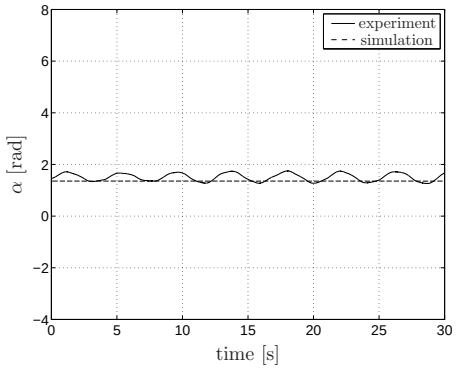

(a) $\alpha(t)$.

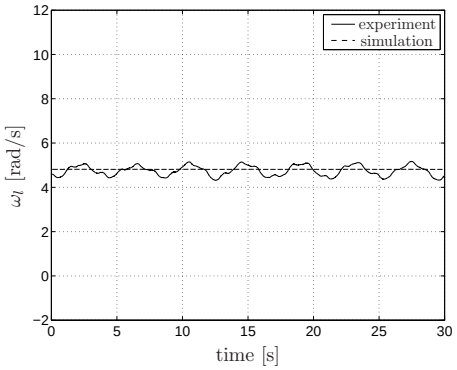

(b) $\omega_l(t)$.

Figure 6.9: Measured and simulated equilibrium responses of the rotor dynamic system for $u_c = 2.8$ V.

fluctuations that remain in the experimental signals. Note that in Figures 6.6 and 6.7, both $\times$ and $\circ$ represent the average of ω_l and α, respectively. This implies that the considered model does not entirely capture the dynamics of the real rotor dynamic system. Nevertheless, the error induced from this unmodeled dynamics is not significant. To study the origin of these fluctuations, a frequency-domain analysis is performed on the time responses of w_l for input voltages of 2.8V and 3.5V, see Figure 6.11. Figures 6.11(a) and 6.11(b) correspond to the responses depicted in Figure 6.9(b) and Figure 6.10(b), respectively. The rotational equilibrium velocity (in Hz) is plotted with a vertical dashed line in the diagrams. The power spectral density diagrams in these figures show that there exists a dominant spectral component at 0.24 Hz for both $u_c = 2.8$V and $u_c = 3.5$V. This frequency is due to the mechanical resonance

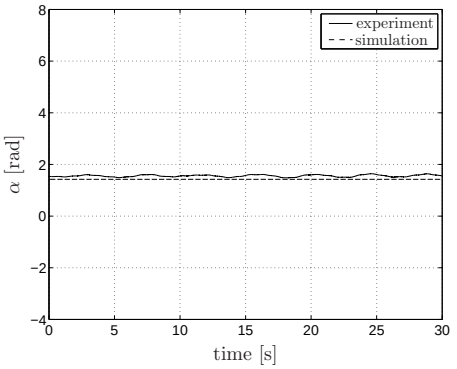

(a) $\alpha(t)$.

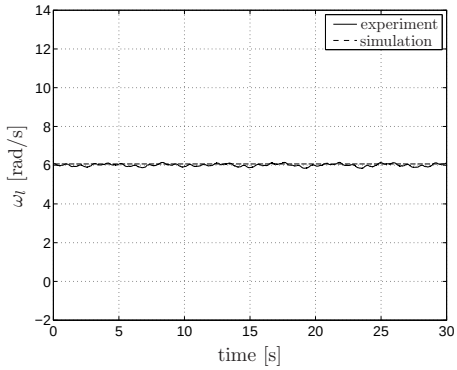

(b) $\omega(t)$.

Figure 6.10: Measured and simulated equilibrium responses of the rotor dynamic system for $u_c = 3.5$ V.

frequency of the brake disc mechanism, which is independent of the rotational frequency. This mechanical resonance frequency is also observed in [86]. For all the constant input voltages u_c, the rotational equilibrium velocity (in Hz) represents another dominant spectral component. The fact that there are such peaks in the power spectral density diagrams of the experimental steady-state 'equilibrium' responses indicates that there is unmodeled dynamics in the experimental system. Specifically, the presence of the frequency corresponding to the rotational speed of the lower disc may indicate the presence of position-dependent friction.

Finally, in Figure 6.12, we depict the period time T of the periodic solutions of system (6.2)-(6.6). The solid curve represents simulations and the marks $\circ$ represent measurements.

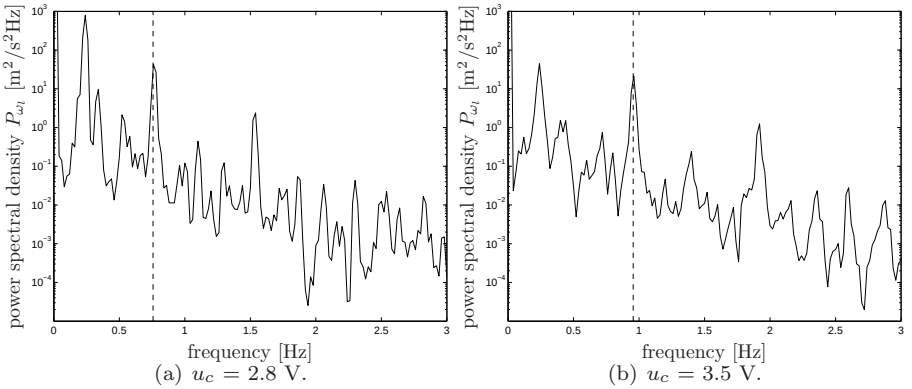

(a) $u_c = 2.8$ V. (b) $u_c = 3.5$ V.

Figure 6.11: Spectral analysis of responses of rotor dynamic system for different input voltages.

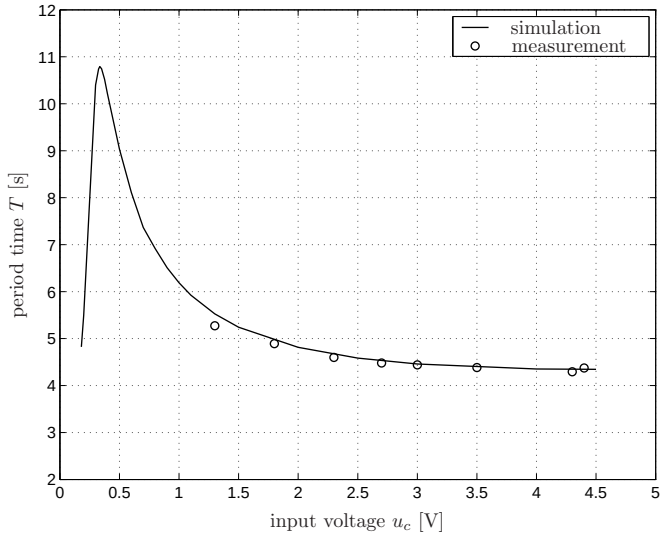

Figure 6.12: Diagram with the period times of the periodic solutions for positive input voltages.

Based on Figures 6.6-6.10 and 6.12, we conclude that the model with the estimated parameters describes the steady-state dynamics of the rotor dynamic system with high accuracy. Some unmodeled dynamics are present in the experimental system, especially influencing the equilibria for the lower input voltages. Nevertheless, these unmodeled dynamics are not dominating the modeled

dynamics for 'higher' input voltages (and that is the range of our interest). The accurate prediction of the equilibria is crucial within the controller design since these will be the set-points provided to the feedback controller in Section 6.3.

6.3 An output-feedback controller

In this section, we will show that an output-feedback controller can eliminate the limit cycle responses of the rotor dynamic system by stabilizing it over a range of given set-points (corresponding to the open-loop equilibria for varying, though constant, input voltages u_c). Firstly, we will use the observer presented in Section 6.3.1 to estimate the system state with high accuracy. Secondly, we will use two output-feedback controllers with the goal to render the rotor dynamic system absolutely stable. One of them is based on the circle criterion and the other is based on the Popov criterion as presented in Section 5.3.2. It will be shown that the closed-loop stability condition of the circle criterion-based design (see Corollary 5.2.4) is not feasible for the rotor dynamic system. However, the conditions imposed by Popov-based approach (see Theorem 5.2.3) will turn out to be feasible. The absolute stability of the resulting closed-loop system is studied both in simulations and in experiments. More specifically, by studying two different friction situations (friction characteristics I and II) that lead to two different nonlinearities in the feedback-loop we check whether the resulting closed-loop system indeed has a unique asymptotically stable equilibrium for any contant input u_c within a given range and whether the design is robust for such friction changes. This will be done both in numerical simulations and experimental measurements. It has already been mentioned in the beginning of Section 6.2.1 that the control action provided by the motor (see Figure 6.1(a)) to the rotor dynamic system may saturate (the maximum control input is $5V$). Therefore, we will also examine the influence of this input saturation on the stabilization and limit cycle elimination of the closed-loop system.

Consider the system (6.2)-(6.6) with parameter values taken from Table 6.1. In order to apply the observer and controller designs presented in Chapter 5, this system is presented as a Lur'e type system with monotone set-valued nonlinearities in the feedback loop. For system (6.2)-(6.6) these set-valued nonlinearities are formed by the friction torques T_{fu} and T_{fl}, see Figures 6.4 and 6.5. Figure 6.5 shows that T_{fl} is not monotone. Nevertheless, it can be transformed into a monotone mapping using the technique of loop transformation [133]. The transformed system takes the form

$$\begin{aligned} \dot{x} &= A_{tr}x + Bu + G\bar{w} \\ z &= Hx \\ \bar{w} &\in -\bar{\varphi}(z) \\ y &= Cx, \end{aligned} \tag{6.7}$$

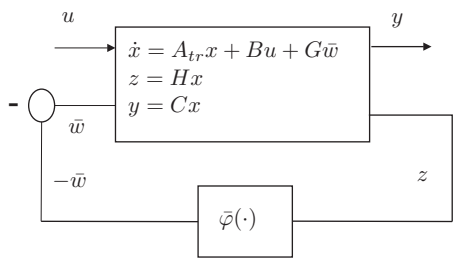

Figure 6.13: Transformation of the rotor dynamic system.

where $\bar{w}, z \in \mathbb{R}^2$, the input $u \in \mathbb{R}$, the measured output $y \in \mathbb{R}$, and $\bar{\varphi}_i : \mathbb{R} \to \mathbb{R}$ for $i = 1, 2$. Note that both mappings $\bar{\varphi}_i, i = 1, 2$, are maximally monotone. The system (6.7) is depicted schematically in Figure 6.13.

The system matrices in (6.7) are given by

$$A_{tr} = \begin{bmatrix} 0 & 1 & -1 \\ -\frac{k_\theta}{J_u} & -\frac{b}{J_u} & 0 \\ \frac{k_\theta}{J_l} & 0 & \frac{m}{J_l} \end{bmatrix}, \quad B = \begin{bmatrix} 0 \\ \frac{k_m}{J_u} \\ 0 \end{bmatrix}, \quad G = \begin{bmatrix} 0 & 0 \\ \frac{1}{J_u} & 0 \\ 0 & \frac{1}{J_l} \end{bmatrix}, \tag{6.8}$$

$$H = \begin{bmatrix} 0 & 1 & 0 \\ 0 & 0 & 1 \end{bmatrix}, \qquad \bar{\varphi}(z) = \begin{bmatrix} \bar{\varphi}_1(z_1) \\ \bar{\varphi}_2(z_2) \end{bmatrix} = \begin{bmatrix} T_{fu}(z_1) - bz_1 \\ T_{fl}(z_2) + mz_2 \end{bmatrix}, \tag{6.9}$$

with $b = b_u - \Delta b_u$. Note that the loop transformation removes some viscous friction from the friction model T_{fu} and creates a new friction model $T_{fu}(z_1) - bz_1$ which thereby becomes monotone. Moreover, it adds viscous friction to the friction model T_{fl} to create a new friction model, $T_{fl}(z_2) + mz_2$, which thereby is monotone. m is the maximal negative slope of the friction curve (at the lower disc). Herein,

$$m = \min\{\frac{\partial}{\partial z_2} T_{fl}(z_2) | z_2 \geq 0\}, \tag{6.10}$$

with numerical value $m = 0.1$Nms/rad. The changes in the friction models are compensated by changes in the linear system. In the present application it has been noticed that by adding viscous damping (bx_2) in the transformed linear part of the system it becomes strictly passive.

6.3.1 Observer design implementations on the rotor dynamic system

We will use the observer (5.31) presented in Section 5.3.1 to estimate the state of the rotor dynamic system, described in (6.7), as we consider the situation where we can only measure the difference of the displacement between the two discs (this implies that the full state is not available for feedback). In

Appendix E, an observer is designed, based on the results of Theorem 5.3.2, and implemented on the rotor dynamic system. It is shown that this observer is able to estimate the system state adequately and that the observer error dynamics is globally exponentially stable. Note that the observer error is defined as the difference between the real state of the system and the estimated state of the system. Moreover, the performance of this observer is investigated for different observer gain settings in both simulations and experiments. Herein, both the transient convergence speed and the steady-state sensitivity of the observer error to modelling errors and measurement noise are taken into account to support a choice for a particular gain setting. The observer gain settings with the best performance is:

$$L_2 = [195 \ -312 \ -9080 \ 98.475]\,, \ N_2 = [-2.22 \ -37.8]\,.$$

In the following section, we will use the proposed observer with gains L_2, N_2 for the rotor dynamic system in an output-feedback controller design and we will show that the interconnection of the observer with a state-feedback controller and the rotor dynamic system is stable. This is essential, due to the fact that a successful design of an observer and a state feedback controller does not necessarily imply a successful output-feedback design.

6.3.2 Feedback controller based on the circle criterion

In the present section, we aim to render the rotor dynamic system absolutely stable by means of feedback. Since we consider the situation in which we can only measure one state variable (the difference in displacement of the upper and lower disc) we use an output-feedback controller to render the rotor dynamic system absolutely stable. This output-feedback controller consists of a state-feedback controller that uses the observer estimates of the rotor dynamic system state. These estimates are based on the observer as proposed in the previous section. Both the state- and the output-feedback controllers are based on the circle criterion (see Corollaries 5.2.4 and 5.3.5, respectively). Finally, the proposed controllers use a single control gain to stabilize the system around its entire equilibrium branch. In order to do so, we transform the system (6.7) (i.e. system (6.2)-(6.6)) to a new system that has, for every constant input, the origin as equilibrium.

The transformed system takes the form

$$\begin{aligned} \dot{\xi} &= A_{tr}\xi + Bv + G\tilde{w} \\ z &= H\xi \\ \tilde{w} &\in -\varphi_{tr}(z) \\ y &= C\xi, \end{aligned} \tag{6.11}$$

where the state $\xi \in \mathbb{R}^3$ with $\xi = x - x_{eq}$ and $x_{eq} = [\alpha_{eq} \ \omega_{eq} \ \omega_{eq}]^T$. Herein, x_{eq} is an equilibrium of system (6.7) (i.e. system (6.2)-(6.6)). Furthermore,

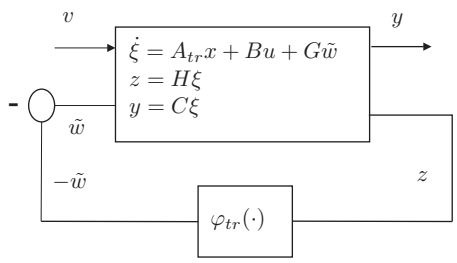

Figure 6.14: Transformation of the rotor dynamic system.

$\tilde{w}, z \in \mathbb{R}^2$, the transformed input $v = u - u_c$ with $v \in \mathbb{R}$, the measured output $y \in \mathbb{R}$, and $\varphi_{tr,i} : \mathbb{R} \to \mathbb{R}$ for $i = 1, 2$. For the definition of the system matrices see (6.8), (6.9). For further information related to the loop transformation the reader is referred to Appendix D. Note that both mappings $\varphi_{tr,i}, i = 1, 2$, are maximally monotone. The system (6.11) is depicted schematically in Figure 6.14.

The system matrices A_{tr}, B, G and H are given as in (6.8) and (6.9). The column $\varphi_{tr}(z)$ is given by

$$\varphi_{tr}(z) = \begin{bmatrix} \varphi_{tr,1}(z_1) \\ \varphi_{tr,2}(z_2) \end{bmatrix} = \begin{bmatrix} T_{fu,tr}(z_1) - bz_1 - T_{fu}(\omega_{eq}) \\ T_{fl,tr}(z_2) + mz_2 - T_{fl}(\omega_{eq}) \end{bmatrix}, \tag{6.12}$$

where, once again, b is the damping coefficient of the viscous friction bz_1 that is taken out from the friction model related to the upper disc. Moreover, m is the maximal negative slope (see in (6.10)) of the viscous friction mz_2 that is added in the friction model related to the lower disc. In addition to that,

$$T_{fu,tr}(z_1) \in \begin{cases} T_{cu,tr}(z_1)\mathrm{sgn}(z_1 + \omega_{eq}) & \text{for } z_1 \neq -\omega_{eq} \\ [-T_{su} + \Delta T_{su}, T_{su} + \Delta T_{su}] & \text{for } z_1 = -\omega_{eq}, \end{cases} \tag{6.13}$$

with

$$T_{cu,tr}(z_1) = T_{su} + \Delta T_{su}\mathrm{sgn}(z_1 + \omega_{eq}) + b_u|z_1 + \omega_{eq}| + \Delta b_u(z_1 + \omega_{eq}). \tag{6.14}$$

Note that for $\omega_{eq} > 0$ both $T_{fu}(\omega_{eq})$ and $T_{fl}(\omega_{eq})$ are single-valued functions. The function $T_{fl,tr}(z_2)$ is given by

$$T_{fl,tr}(z_2) \in \begin{cases} T_{cl,tr}(z_2)\mathrm{sgn}(z_2 + \omega_{eq}) & \text{for } z_2 \neq -\omega_{eq} \\ [-T_{sl}, T_{sl}] & \text{for } z_2 = -\omega_{eq}, \end{cases} \tag{6.15}$$

where

$$T_{cl,tr}(z_2) = T_{cl} + (T_{sl} - T_{cl})e^{-|\frac{z_2 + \omega_{eq}}{\omega_{sl}}|^{\delta_{sl}}} + b_l|z_2 + \omega_{eq}|. \tag{6.16}$$

The transformed friction torques $\varphi_{tr,1}$ and $\varphi_{tr,2}$ are plotted in Figure 6.15 for the constant input voltage $u_c = 1.0\mathrm{V}$ and $\omega_{eq} = 1.6\mathrm{rad/s}$.

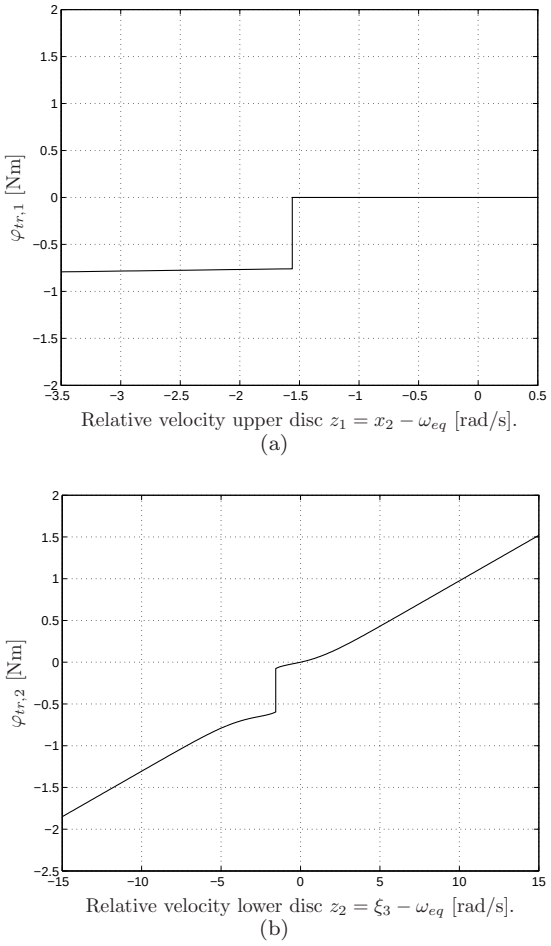

Figure 6.15: Transformed friction laws $\varphi_{tr,1}$ and $\varphi_{tr,1}$ for $u_c = 1.0$ V and $\omega_{eq} = 1.6 rad/s$.

Consider system (6.11). The circle criterion controller design presented in Corollary 5.2.4 involves the following linear state-feedback law:

$$v = K\xi, \tag{6.17}$$

where $K = [k_1 \quad k_2 \quad k_3]$ is the feedback gain. In order to guarantee that the closed-loop system (6.11), (6.17) is absolutely stable using Corollary 5.2.4, firstly, the set-valued nonlinearities ($\varphi_{tr,1}$, $\varphi_{tr,2}$) in the feedback loop must be monotone and lie within the sector $[0 \ \infty]$ and, secondly, the linear part of this system should be strictly passive. Based on Figure 6.15, both $\varphi_{tr,1}$, $\varphi_{tr,2}$ are

monotone and belong to the sector [0 ∞] (since that is how we transformed the nonlinearities). By using standard numerical LMI solvers (i.e the numerical solver LMITOOL for MATLAB [38]) we did not succeed in finding a feasible solution to the LMIs (5.30) with the system matrices defined in (6.8), (6.9).

As an extension, we apply a partial feedback cancellation of the friction at the upper disc. The term 'partial' refers to the fact that we only cancel the 'Coulomb' part of the friction at the upper disc. Next, we study whether the new system can be rendered absolutely stable by means of feedback. This study is based on results presented in [5] and [6]. The works [5] and [6] consider Lur'e-type systems with a single nonlinearity in the feedback loop and provide feasibility conditions for controllers based on the circle criterion.

Consider now the new control law

$$v = v_{control} + v_{comp}, \tag{6.18}$$

$$v_{control} = K\xi, \tag{6.19}$$

$$v_{comp} \in \begin{cases} \frac{1}{k_m}(T_{su} + \Delta T_{su}\text{sgn}(\xi_2 + \omega_{eq}) + b_u|\xi_2 + \omega_{eq}| \\ \qquad +\Delta b_u(\xi_2 + \omega_{eq}))\text{sgn}(\xi_2 + \omega_{eq}) - \frac{1}{k_m}T_{fu}(\omega_{eq}) \\ \text{for } \xi_2 \neq -\omega_{eq} \\ \\ \frac{1}{k_m}\left[-T_{su} + \Delta T_{su} - T_{fu}(\omega_{eq}), T_{su} + \Delta T_{su} - T_{fu}(\omega_{eq})\right] \\ \text{for } \xi_2 = -\omega_{eq}. \end{cases} \tag{6.20}$$

where v_{comp} is the partial friction cancellation term. For more information about this friction compensation, see Appendix D.2. The reason for canceling part of the friction at the upper and not part of the friction at the lower disc is because the control action can only be applied to the upper disc (i.e. collocated vs non-collocated friction). By applying the control law (6.18)-(6.20) in system (6.2)-(6.6) and by using the technique of loop transformation as employed in (6.12), the system takes the following form:

$$\begin{aligned} \dot{\xi} &= A_{tr2}\xi + Bv_{control} + G_{tr}\tilde{w} \\ z &= H_{tr}\xi \\ \tilde{w} &\in -\varphi_{tr,2}(z), \end{aligned} \tag{6.21}$$

with $\varphi_{tr,2} : \mathbb{R} \to \mathbb{R}$ defined in (6.12). The system matrices A_{tr2}, G_{tr} and H_{tr} are given by

$$A_{tr2} = \begin{bmatrix} 0 & 1 & -1 \\ -\frac{k_\theta}{J_u} & -\frac{1}{J_u}(b_u - \Delta b_u) & 0 \\ \frac{k_\theta}{J_l} & 0 & \frac{m}{J_l} \end{bmatrix}, \qquad G_{tr} = \begin{bmatrix} 0 \\ 0 \\ \frac{1}{J_l} \end{bmatrix}, \tag{6.22}$$

$$H_{tr} = \begin{bmatrix} 0 & 0 & 1 \end{bmatrix}. \tag{6.23}$$

For more information on the coordinate and loop transformations, see Appendix D. Next, we are going to apply the feasibility conditions presented in [5] and [6] to system (6.21).

Consider system (6.21) and transform it into a normal form by a state and feedback transformation.

$$\begin{aligned} \dot{y}_1 &= y_2 + g_1\tilde{w} \\ \dot{y}_2 &= y_3 + g_2\tilde{w} \\ \dot{y}_3 &= \tilde{v} + g_3\tilde{w}, \end{aligned} \tag{6.24}$$

where $\tilde{v}$ is the new input and $g_1 = \frac{1}{J_l}$, $g_2 = \frac{m}{J_l^2}$ and $g_3 = \frac{1}{J_l}\Big(\frac{m^2}{J_l^2} - \frac{k_\theta}{J_l}\Big)$.
The coordinate transformation is applied according to the following definitions:

$$\begin{aligned} y_1 &= \xi_3 = z \\ y_2 &= \tfrac{k_\theta}{J_l}\xi_1 + \tfrac{m}{J_l}\xi_3 \\ y_3 &= \tfrac{k_\theta m}{J_l^2}\xi_1 + \tfrac{k_\theta}{J_l}\xi_2 + \Big(\tfrac{m^2}{J_l} - \tfrac{k_\theta}{J_l}\Big)\xi_3. \end{aligned} \tag{6.25}$$

The expression for the new control input $\tilde{v}$ is:

$$\begin{aligned} \tilde{v} &= \tfrac{k_\theta k_m}{J_l J_u} v_{control} + \tfrac{k_\theta}{J_l}\Big(\tfrac{m^2}{J_l^2} - \tfrac{k_\theta}{J_l} - \tfrac{k_\theta}{J_u}\Big)\xi_1 \\ &+ \tfrac{k_\theta}{J_l}\Big(\tfrac{\Delta b_u}{J_u} - \tfrac{b_u}{J_u} + \tfrac{m^2}{J_l}\Big)\xi_2 + \tfrac{m}{J_l^2}\Big(\tfrac{m}{J_l} - 2k_\theta\Big)\xi_3. \end{aligned} \tag{6.26}$$

If the conditions of the circle criterion as in (5.30) are feasible for system (6.21) with the linear state-feedback control law (6.19), then the following conditions must be satisfied: $g_1 > 0$ and $g_2 < 0$, see [5] and [6]. The circle criterion design for the system (6.21) with a linear state-feedback control law (6.19) is not feasible because $g_2 > 0$. This is caused by 1) the negative damping term $m\xi_3$ (actually $m\xi_3$ is due to the compensation of the negative damping (Stribeck effect) in the friction of the lower disc needed to render the nonlinearity monotone) in system (6.21), 2) the absence of a damping element in the link between the upper disc and the lower disc.

The latter exposition explains that a controller design based on the circle-criterion is not feasible for solving the stabilization problem for the rotor dynamic system with friction.

Consider now the case where there is damping in the link between the upper disc and the lower disc. Then, the dynamics of the rotor dynamics system is described as follows:

$$\begin{aligned} J_u\ddot{\theta}_u + k_\theta(\theta_u - \theta_l) + b_a(\dot{\theta}_u - \dot{\theta}_l) + T_{fu}(\dot{\theta}_u) - k_m u &= 0 \\ J_l\ddot{\theta}_l - k_\theta(\theta_u - \theta_l) - b_a(\dot{\theta}_u - \dot{\theta}_l) + T_{fl}(\dot{\theta}_l) &= 0, \end{aligned} \tag{6.27}$$

with b_a the coefficient of the damping in the link between the upper disc and the lower disc. By transforming system (6.27) into state-space form, applying

the control law (6.18)-(6.20) in the new system and using the technique of loop transformation as employed in (6.12), the system takes the following form:

$$\begin{aligned} \dot{\xi} &= A_{tr3}\xi + Bv_{control} + G_{tr}\tilde{w} \\ z &= H_{tr}\xi \\ \tilde{w} &\in -\varphi_{tr,2}(z), \end{aligned} \tag{6.28}$$

with the system matrix A_{tr3} given by

$$A_{tr3} = \begin{bmatrix} 0 & 1 & -1 \\ -\frac{k_\theta}{J_u} & -\frac{1}{J_u}(b_u - \Delta b_u + b_a) & \frac{b_a}{J_u} \\ \frac{k_\theta}{J_l} & \frac{b_a}{J_l} & \frac{1}{J_l}(m - b_a) \end{bmatrix}. \tag{6.29}$$

By applying in (6.28) the same transformations as in system (6.21) we derive the following form for g_1 and g_2:

$$g_1 = \frac{1}{J_l},\ g_2 = \frac{m - b_a}{J_l^2}.$$

It is obvious that for $b_a > m$ it holds that $g_2 < 0$. Consequently, the circle criterion design for the system (6.28) with a linear state-feedback control law (6.19) is feasible.

In the following, we will use a Popov-based controller design to render the rotor dynamic system absolutely stable.

6.3.3 Output-feedback controller based on the Popov criterion

In this section, we aim to render the rotor dynamic system absolutely stable by using an output-feedback controller based on the Popov criterion. Once again, this output-feedback controller consists of a state-feedback controller that uses the system state estimates of the observer proposed in Section 6.3.1. First, we will apply partial feedback cancellation of the friction at the upper disc. Next, we will show that there exists a control gain matrix that ensures that the controlled system is absolutely stable. Finally, we will apply the proposed output-feedback controller to the rotor dynamic system and we evaluate its performance in both simulations and experiments. To examine the robustness properties of this controller with respect to variations in the friction characteristics, we use two properly chosen friction configurations and we check whether there exists a unique asymptotically stable equilibrium for the closed-loop system for both friction characteristics. Moreover, due to the fact that the control action applied to the motor of the system is limited to ±5V, we will also study the influence of the saturated control action to the system based on simulations and experiments.

Consider the system (6.21)-(6.23), the control law

$$v_{control} = K\hat{\xi} = K(\xi - e), \tag{6.30}$$

where $K = [k_1 \quad k_2 \quad k_3]$, and the dynamics of the observer error e given in (E.2). Note that

$$e = \xi - \hat{\xi} = x - x_{eq} - \hat{x} + x_{eq} = x - \hat{x}. \tag{6.31}$$

The system (6.21)-(6.23), (6.30) satisfies all the conditions in the Assumptions 5.2.1 and 5.3.1 and the observer error dynamics (E.2) is GES as it is shown in Section 6.3.1. Therefore, by applying Theorem 5.3.3 to the interconnected system (E.2), (6.21)-(6.23), (6.30) we can conclude that $(\xi, e) = (0, 0)$ is a globally asymptotically stable equilibrium point for this system for every constant input u_c, as long as the matrix inequality (5.35) is feasible, i.e,

$$\begin{bmatrix} (A_{tr2} + BK)^T P + P(A_{tr2} + BK) & PG_{tr} - \tilde{H}^T \\ G_{tr}^T P - \tilde{H} & -\tilde{D} - \tilde{D}^T \end{bmatrix} < 0, \tag{6.32}$$

for $P = P^T > 0$ and $\tilde{D}$ and $\tilde{H}$ defined by (5.10).

By using the LMITOOL of MATLAB [38] we can solve the matrix inequality (6.32) for a given K and η. Due to the fact that this LMI-toolbox can only solve semi-definite LMIs we add the square matrix

$$\begin{bmatrix} -Q_P & 0_{3\times 1} \\ 0_{1\times 3} & 0 \end{bmatrix}, \tag{6.33}$$

with $Q_P = Q_P^T$ a positive definite matrix of a proper dimension, in the right-hand side of (6.32).

In the following, we solve matrix inequality (6.32) (including Q_P) for chosen K and η and for the system parameters taken from Table 6.1. The derived solution is:

$$K_1 = \begin{bmatrix} 15.9 & 1.57 & 27.6 \end{bmatrix}, \qquad \eta_1 = 10,$$

$$P_1 = \begin{bmatrix} 3.6243 & 0.4311 & 6.3725 \\ 0.4311 & 0.0702 & 0.7414 \\ 6.3725 & 0.7414 & 11.6411 \end{bmatrix}, \quad Q_{P_1} = \begin{bmatrix} 16.6997 & 2.2968 & 29.1096 \\ 2.2968 & 0.3522 & 3.9707 \\ 29.1096 & 3.9707 & 50.8145 \end{bmatrix}. \tag{6.34}$$

The eigenvalues of P_1 are 15.2, 0.108, 0.0175 and the eigenvalues of Q_{P_1} are 67.8, 0.0508, 0.0076.

6.3.4 Simulations for friction characteristic I

In this section, it will be shown in simulations, that stability of the closed-loop system around the set-point is achieved. Moreover, due to the fact that the

control input is limited to $\pm 5V$, control input saturation may occur. In the following exposition, it will also be shown in simulations, that this fact does not significantly influence the closed-loop system stability around the set-point. The gains used for the observer that is included in the output-feedback controller are L_2, N_2 (see (E.4)). These gains result in an observer error with smaller amplitude and faster convergence to zero than the observer error obtained using the gains L_1, N_1 (see (E.3)), as discussed in Section 6.3.1.

In Figure 6.16, we depict the total control input $u = u_c + v$ and in Figure 6.17, the state variables of system (6.2) for constant voltage input $u_c = 1.8$V and initial conditions $x(0) = \hat{x}(0) = [0\ 0\ 0]^T$. The control action v is given by (6.18)-(6.20) or by $v = v_{comp} + K_1(x - x_{eq})$, with $x_{eq} = [\alpha_{eq}\ \omega_{eq}\ \omega_{eq}]$. The numerical values of α_{eq} and ω_{eq} for $u_c = 1.8$V are 1.55rad and 3.15rad/s, respectively. More specifically, in these figures two graphs are depicted. The graph with the dashed curve corresponds to a control input limited by $\pm 5V$ and the other graph, with the solid curve, corresponds to a non-saturated control input. In Figure 6.18, we depict the absolute value of the components of the control error $x - x_{eq}$ for the saturated and non-saturated control input. Based on the depicted results in Figures 6.17 and 6.18, the solutions converge to the system equilibrium both for the saturated and non-saturated case. The only difference between these cases is that the solution of the system with the saturated input requires more time to reach the equilibrium than that of the system with the non-saturated input. Note that, of course the satisfaction of the conditions of Theorem 5.3.4 only guarantees GAS of $(\xi, e) = (0, 0)$ for the unsaturated case.

Similar results to those depicted in Figures 6.16 and 6.17 are given in Figures 6.19 and 6.20, respectively. The constant input related to the results depicted in this figure is $u_c = 4$V and the initial conditions are $x(0) = \hat{x}(0) = [0\ 0\ 0]^T$ (in terms of system (6.2)). Once again, these figures show that the solutions of both systems converge to the same steady state response which is an equilibrium (the desired set-point). Again, the solution related to the system with the saturated input takes more time until it reaches the system equilibrium than the solution of the system with the non-saturated input. Note that for both $u_c = 1.8$V and $u_c = 4.0$V, the open-loop system exhibits stick-slip limit cycling, see Figure 6.6. Clearly the proposed control strategy suppresses such undesirable limit cycling.

6.3.5 Experiments for friction characteristic I

In Figures 6.21(a)-6.21(b), the bifurcation diagrams of ω_l and α for bifurcation parameter u_c are depicted. The depicted results for ω_l and α involve the experimental steady-state responses of the closed-loop system. The control input u is limited to ± 5V. In these figures, the marks $\circ$ and $\times$ represent experimental results and the solid line simulations. More specifically, $\circ$ depicts stable limit

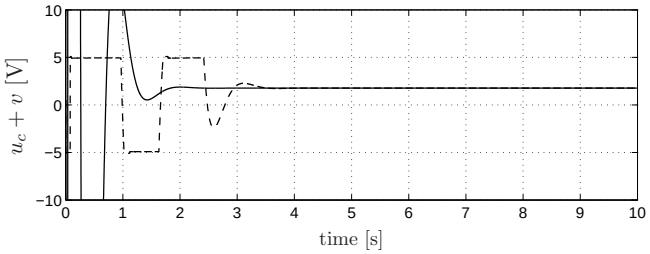

Figure 6.16: Total control input voltage of the closed-loop system with controller with gain $K_1 = [15.9 \quad 1.57 \quad 27.6]$ *switched on at* $t = 0$ *s; The solid line corresponds to an unsaturated control input voltage and the dashed line corresponds to a saturated control input voltage; observer with gains* L_2 *and* N_2*; the constant input voltage is* $u_c = 1.8$ *V; the equilibrium values are* $\alpha_{eq} = 1.55$ *rad and* $\omega_{eq} = 3.15$ *rad/s.*

---

cycles and $\times$ depicts stable equilibria. Actually, $\circ$ depicts the maximum and minimum value of ω_l and α over one period T of the steady-state solution. The solid lines represent the simulated responses of ω_l and α which represent globally asymptotically stable equilibrium branches (as guaranteed by the Theorem 5.3.3). Based on these figures, the equilibrium branches of the real system and the model responses are very similar for the input range $u_c \in [1.4,\ 5]V$. Moreover, in the range $u_c \in [1.3,\ 1.5]V$ it is shown that the experimental system has two stable solutions, namely, a stable equilibrium and a stable limit cycle. On the other hand, the model has a unique solution; a stable equilibrium. Finally, for input voltages u_c below $1.3V$ the experimental system exhibits only stable limit cycles. Based on this analysis, it is clear that on a model level we can achieve a unique equilibrium branch for the whole input range $u_c \in [0,\ 5]V$, as guaranteed by the theory. On the other hand, this is not possible in practice. A reason for this fact can be the presence of unmodeled position dependent friction in the system or noise in the measurement devices.

In Figures 6.22(a)-6.22(b), we compare the experimental bifurcation diagrams of the open-loop system with the experimental bifurcation diagram of the closed-loop system. In these figures, the marks $\circ$, $\times$ represent closed-loop results and the marks $*$, $+$ open-loop results. The aforementioned diagrams show that the output-feedback controller significantly extends the region with only stable equilibria. For the open-loop system, this region covers the constant input voltages $u_c \in [4.5,\ 5.0]$V. The closed-loop system extends the region with only stable equilibria to the constant input voltages $u_c \in [1.5,\ 5.0]$V. Furthermore, the closed-loop limit cycles are different from those of the open-loop system. This is to be expected since the control action changes the dynamics of the closed-loop system with respect to those of the open-loop system.

For a better understanding of the presented results, we will also provide

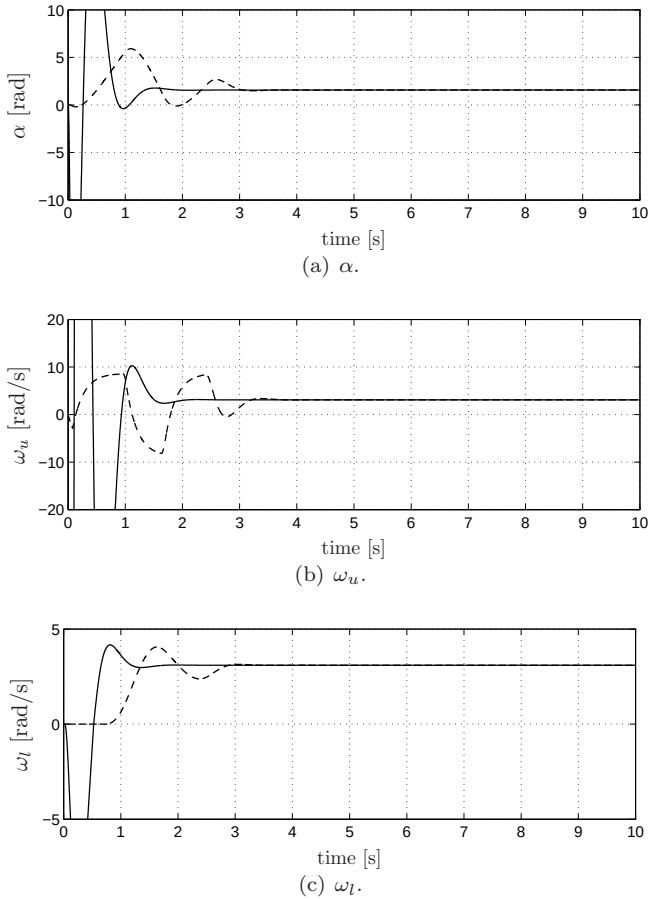

(a) α.

(b) ω_u.

(c) ω_l.

Figure 6.17: Responses of the closed-loop system with controller with gain $K_1 = [15.9 \quad 1.57 \quad 27.6]$ *switched on at* $t = 0$ *s, for input voltage unsaturated (solid line) and for input voltage saturated (dashed line); observer with gains* L_2 *and* N_2*; the constant input voltage is* $u_c = 1.8$ *V; the equilibrium values are* $\alpha_{eq} = 1.55$ *rad and* $\omega_{eq} = 3.15$ *rad/s.*

time responses of the state variables of the rotor dynamic system for a number of constant voltage inputs u_c.

In Figures 6.23, 6.24 the total input $u_c + v$ and the state variables of the experimental rotor dynamic system are depicted, respectively, for constant voltage input $u_c = 2.5V$. As we have already mentioned, the total input is saturated ($u_c \in [-5,\ 5]$V). Initially, the open-loop system is in steady-state and the observer is switched on. Note that, we can also switch on both the controller

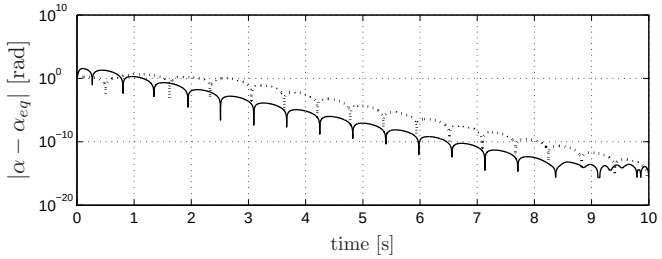

(a) $|\alpha - \alpha_{eq}|$.

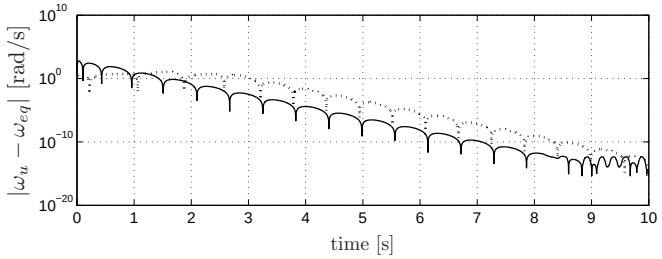

(b) $|\omega_u - \omega_{eq}|$.

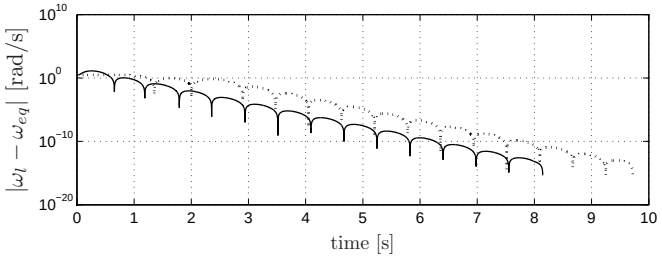

(c) $|\omega_l - \omega_{eq}|$.

Figure 6.18: Control error for closed-loop system with controller with gain $K_1 = [15.9 \quad 1.57 \quad 27.6]$ *switched on at* $t = 0$ *s, for input voltage unsaturated (solid line) and for input voltage saturated (dotted line); observer with gains* L_2 *and* N_2*; the constant input voltage is* $u_c = 1.8$ *V and the equilibrium values are* $\alpha_{eq} = 1.55$ *rad and* $\omega_{eq} = 3.15$ *rad/s.*

and the observer at the same time and the controller will still work. Nevertheless, we have not extensively studied this situation because a large initial observer error will lead to a violent controller reaction in order to stabilize the system. Such controller reaction is undesirable for the system's safety because it may lead to a damage in the motor. In the present study, we will only focus

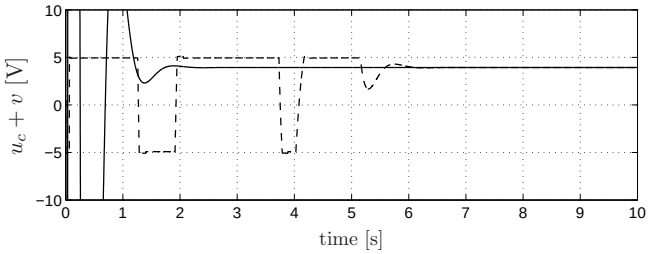

Figure 6.19: Total control input voltage of the closed-loop system with controller with gain $K_1 = [15.9 \quad 1.57 \quad 27.6]$ switched on at $t = 0$ s; The solid line corresponds to an unsaturated control input voltage and the dashed line corresponds to a saturated control input voltage; observer with gains L_2 and N_2; the constant input voltage is $u_c = 4.0$ V; the equilibrium values are $\alpha_{eq} = 1.52$ rad and $\omega_{eq} = 7.06$ rad/s.

---

on the case where the initial conditions of the open-loop system are chosen such that the system converges to a stable limit cycle (see α and ω_l in Figures 6.24(a) and 6.24(c), respectively). At $t = 5$s we switch on the controller. Then, we wait until the closed-loop system reaches its steady-state. This figure shows that the closed-loop steady-state response is a stable equilibrium. The values of this stable equilibrium are equal with the equilibrium values of system (6.2) for $u_c = 2.5V$. In Figure 6.25, the absolute value of the components of the control error $x - x_{eq}$ is depicted. In this figure, it is shown that the control error has a non-zero steady-state response with very small amplitude. This reveals the presence of small fluctuations in the steady-state solution of the experimental system.

Similar results to those depicted in Figures 6.23, 6.24 are given in Figure 6.26. In this figure the steady-state response of the open-loop system is a limit cycle. For this case the controller is switched on at $t = 5$s and the observer 10s earlier such that it reaches its steady state before the controller is switched on. In Figure 6.26, we depict the total control input and all state variables for a constant input of $4V$. The closed-loop system reaches its steady-state, which is a stable equilibrium, approximately, $12s$ after we switch on the controller. Once again, this closed-loop equilibrium is almost equal to the equilibrium of system (6.1) for $u_c = 4$V. The difference between the two equilibria is a small fluctuation similar as in the results for the case with a constant input $u_c = 2.5V$. In Figures 6.27 and 6.29, we focus on the total system input and at the velocity of the lower disc for constant inputs $u_c = 1.4V$ and $u_c = 0.9V$. In Figure 6.27, it is shown that the closed-loop steady-state response ω_l fluctuates around the equilibrium value ω_{eq}. This fluctuation is more dominant than in the cases of $u_c = 2.5$ and $u_c = 4V$. In order to gain insight in this phenomenon, we perform a frequency-domain analysis of the signals $\omega_l(t)$. More specifically,

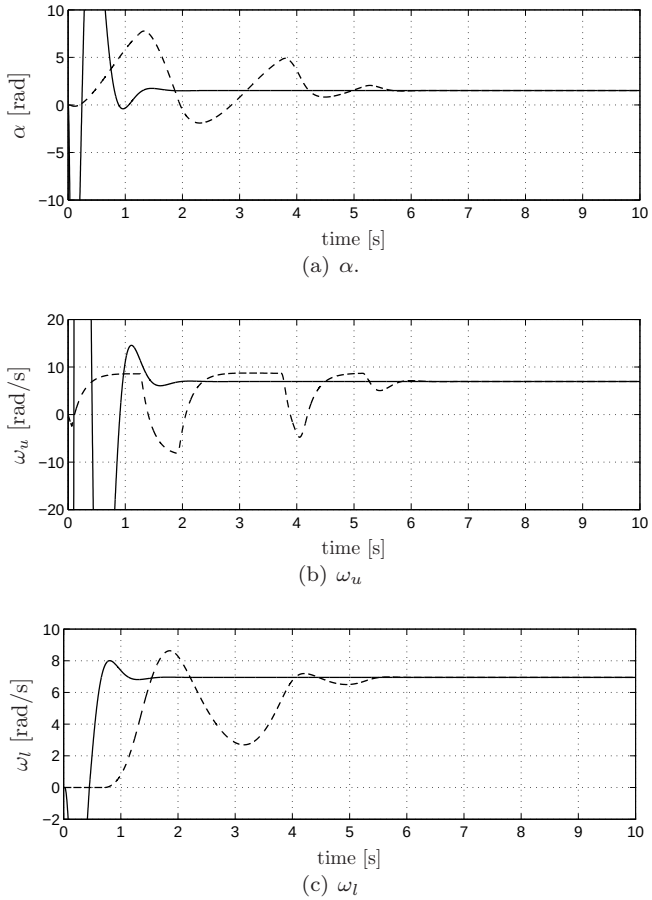

(a) α.

(b) ω_u

(c) ω_l

Figure 6.20: Responses of the closed-loop system with controller with gain $K_1 = [15.9 \quad 1.57 \quad 27.6]$ *switched on at* $t = 0$ *s, for input voltage unsaturated (solid line) and for input voltage saturated (dashed line); observer with gains* L_2 *and* N_2*; the constant input voltage is* $u_c = 4.0$ *V and the equilibrium values are* $\alpha_{eq} = 1.52$ *rad and* $\omega_{eq} = 7.06$ *rad/s.*

---

we compute the power spectral density of the signals $\omega_l(t)$. Once again, the last 50s of the signal history is recorded in order to asses steady-state properties. The results of this analysis are shown in Fig 6.28. The power spectral density of the observed velocity of the lower disc in this figure shows that the rotational frequency (depicted with a vertical dashed line) is dominant. The dominance of the rotational frequency indicates a position-dependent friction acting on the lower disc. Moreover, a second dominant spectral component is present

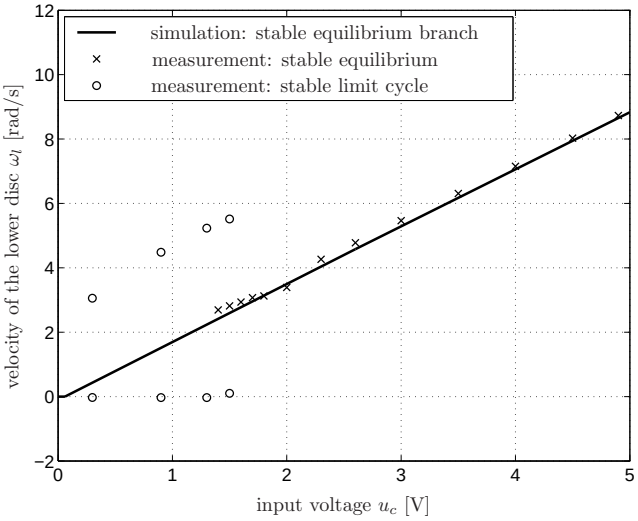

(a) Bifurcation diagram for the velocity of the lower disc.

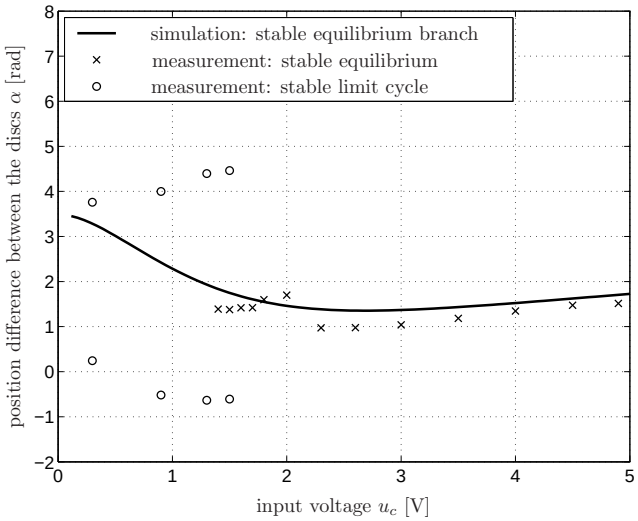

(b) Bifurcation diagram for the position difference between the upper and the lower disc.

Figure 6.21: Experimental bifurcation diagrams of the closed-loop system with control gain $K_1 = [15.9 \quad 1.57 \quad 27.6]$ *for positive input voltages; observer gains are* L_2 *and* N_2.

in the signal at 0.22Hz. This frequency is close to the mechanical resonance

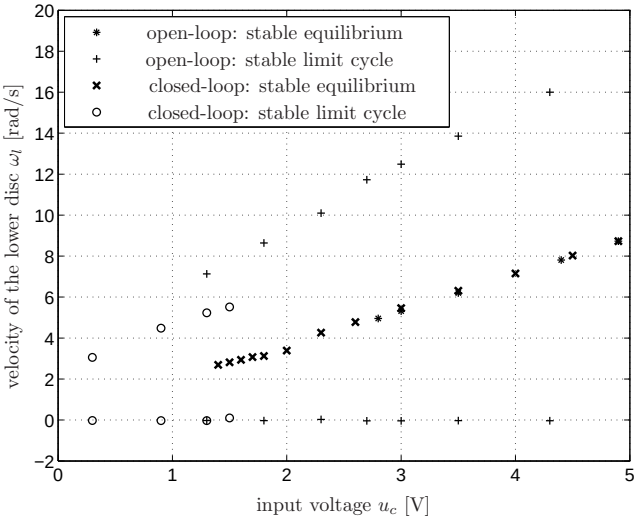

(a) Bifurcation diagram for the velocity of the lower disc.

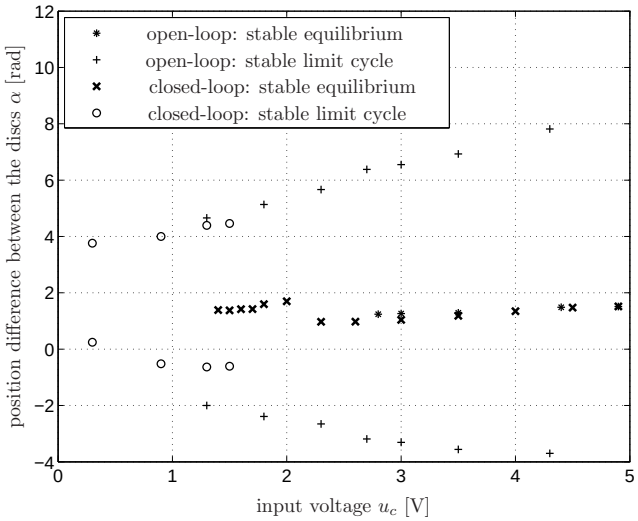

(b) Bifurcation diagram for the position difference between the upper and the lower disc.

Figure 6.22: Experimental bifurcation diagrams of the closed-loop system with control gain $K_1 = [15.9 \quad 1.57 \quad 27.6]$ *for positive input voltages; observer gains are* L_2 *and* N_2*; comparison with the experimental bifurcation diagram of the open-loop system.*

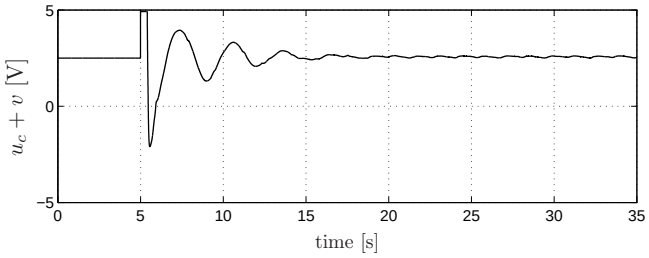

Figure 6.23: Total control input voltage of the closed-loop system response with control gain $K_1 = [15.9 \quad 1.57 \quad 27.6]$ switched on at $t = 5$ s. The constant input voltage is $u_c = 2.5V$, the equilibrium values are $\alpha_{eq} = 1.36$ rad and $\omega_{eq} = 4.40$ rad/s and the observer gains are L_2 and N_2.

frequency of the system, see also [86]. Both frequencies are present in all the measured signals $\omega_l(t)$. The combined results presented in Figures 6.23-6.27 lead to the conclusion that the smaller the constant input the larger the influence of the position-dependent friction acting on the lower disc on the steady-state response ω_l. Finally, in Figure 6.29, we show that the closed-loop rotor dynamic system exhibits limit cycling for $u_c = 0.9$. This implies that the controller is not able to eliminate the limit cycles for low voltages due to the presence of the position-dependent friction in the lower disc.

Remark 6.3.1 Theoretically, the output-feedback controller proposed in Section 6.3.3 renders the rotor dynamic system absolutely stable for any friction model of the form (6.5), as long as this friction model is a monotone set-valued nonlinearity in the sector $[0 \ \infty]$ (after the transformation as used before) and the input $w \in \varphi(z)$ is linearly bounded by z. In Appendix F, this robustness property is also shown experimentally. For this purpose, the friction of the lower disc is changed by applying an additional normal force on the brake that creates an adapted friction characteristic. Moreover, the output-feedback controller is applied, once more, to the system, see Figure 6.5 for the adapted friction characteristic II.

6.4 Summary

In this chapter, we implemented a Popov criterion-based output-feedback controller design on an experimental rotor dynamic setup. The setup can be considered as a benchmark system for mechanical motion systems with flexibilities and friction. This setup consists of two inertias, a flexibility and discontinuous friction acting on both inertias. An actuator drives one of these inertias.

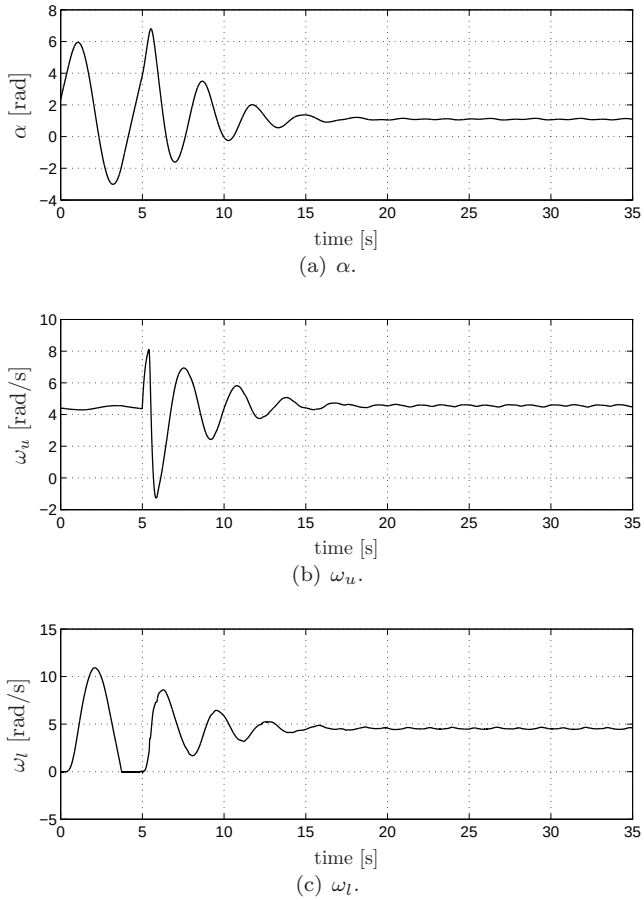

(a) α.

(b) ω_u.

(c) ω_l.

Figure 6.24: Closed-loop system response with control gain $K_1 = [15.9 \quad 1.57 \quad 27.6]$ *switched on at* $t = 5$ *s. The constant input voltage is* $u_c = 2.5V$*, the equilibrium values are* $\alpha_{eq} = 1.36$ *rad and* $\omega_{eq} = 4.40$ *rad/s and the observer gains are* L_2 *and* N_2*.*

Due to the presence of discontinuous friction this setup exhibits complex dynamical phenomena such as coexistence of steady-state solutions, discontinuous bifurcation points and stick-slip limit cycling. Especially the limit cycling is considered to be an undesirable phenomenon because it causes kinetic energy dissipation, excessive wear of machine parts and inferior tracking performance.

Application of the proposed control strategy on a model-level shows that indeed the limit-cycling is eliminated and a desired constant velocity solution is globally asymptotically stabilized. Moreover, the fact that the controller

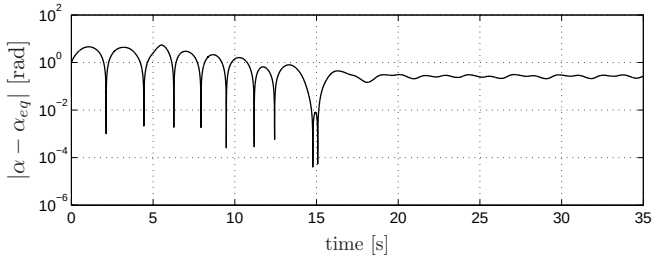

(a) $|\alpha - \alpha_{eq}|$.

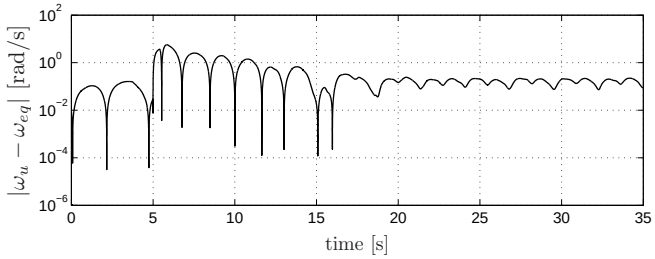

(b) $|\omega_u - \omega_{eq}|$.

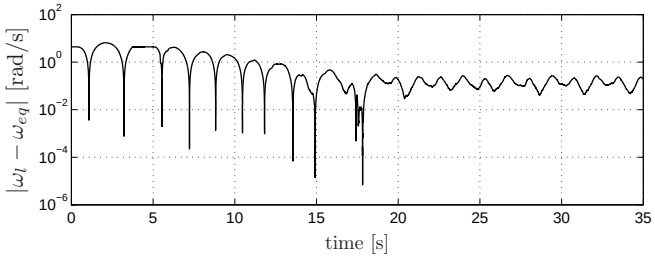

(c) $|\omega_l - \omega_{eq}|$.

Figure 6.25: Absolute value of the control error variables of the closed-loop system with control gain $K_1 = [15.9 \quad 1.57 \quad 27.6]$*; the controller is switched on at* $t = 5$ *s. The constant input voltage is* $u_c = 2.5$ *V, the equilibrium values are* $\alpha_{eq} = 1.36$ *rad and* $\omega_{eq} = 4.40$ *rad/s and the observer gains are* L_2 *and* N_2*.*

---

design guarantees the absolute stability of the closed-loop system implies the robustness of the stability properties with respect to changes in the friction characteristics (which are inevitable in practice). Moreover, such robustness is also shown to be favorable from the perspective of stabilizing a range of set-points with a single controller. By applying the aforementioned output-feedback controller design to the experimental system, we are able to eliminate

the limit cycling for a large range of constant inputs.

The implementation of the proposed strategy on the experimental system shows that the experimental results agree with the simulation results to great extent. The implemented controller eliminates the stable limit cycles for every constant input within a given range and stabilizes the closed-loop system around a velocity equilibrium branch. Nevertheless, the presence of unmodelled position-dependent dynamics in the friction model limits the controller's performance for very small constant inputs. This is reflected by the fact that the controller is not able to entirely eliminate the stick-slip limit cycles for constant inputs below a certain value.

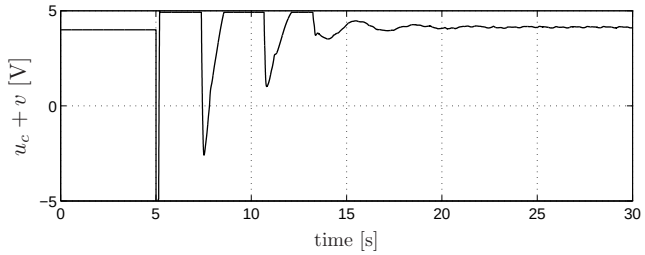

(a) $u_c + v$

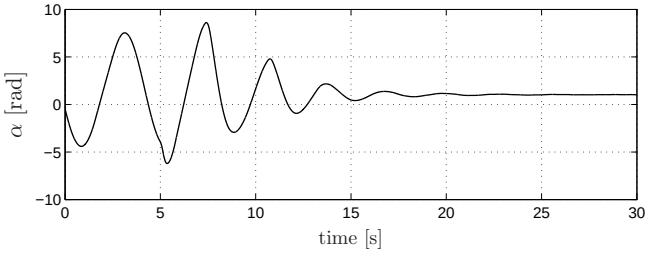

(b) α.

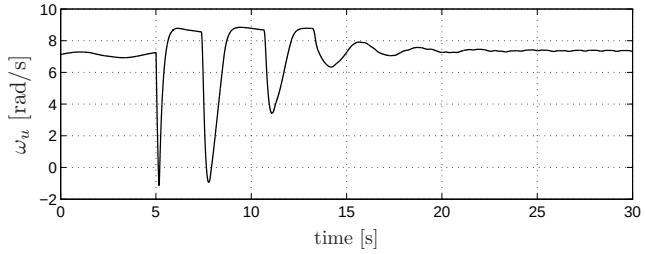

(c) ω_u.

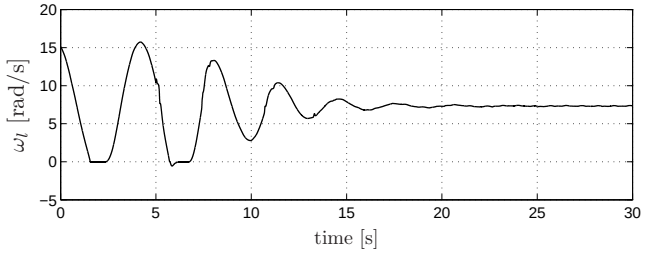

(d) ω_l.

Figure 6.26: Total control input voltage and closed-loop system response with control gain $K_1 = [15.9 \quad 1.57 \quad 27.6]$ *switched on at* $t = 5$ *s; the constant input voltage* $u_c = 4.0$ *V, the equilibrium values are* $\alpha_{eq} = 1.52$ *rad and* $\omega_{eq} = 7.06$ *rad/s; observer gains are* L_2 *and* N_2.

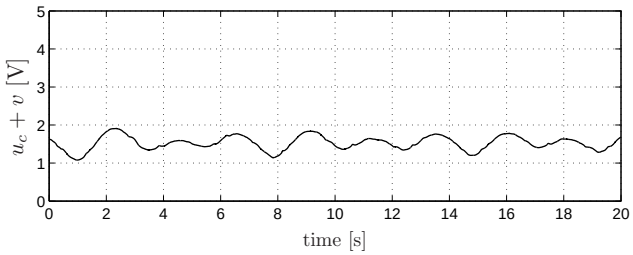

(a) $u_c + v$.

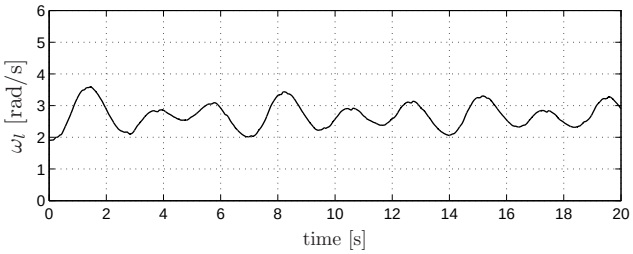

(b) ω_l.

Figure 6.27: Closed-loop system response with control gain $K_1 = [15.9 \quad 1.57 \quad 27.6]$*; the constant input voltage is* $u_c = 1.4$ *V, the equilibrium values are* $\alpha_{eq} = 1.83$ *rad and* $\omega_{eq} = 2.43$ *rad/s; observer gains are* L_2 *and* N_2.

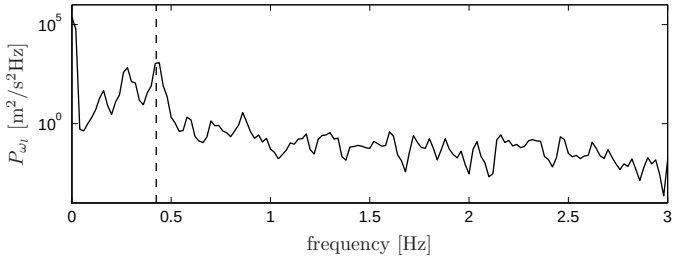

Figure 6.28: Power spectral density analysis of the equilibrium response ω_l *of the rotor dynamic system for the input voltage* $u_c = 1.4$ *V.*

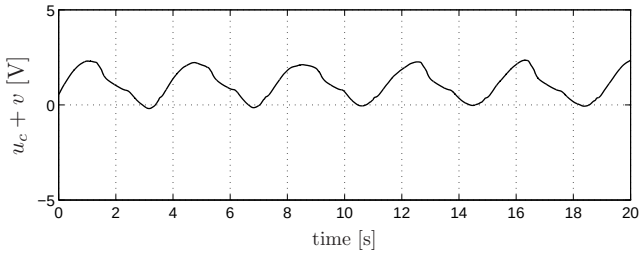

(a) $u_c + v$.

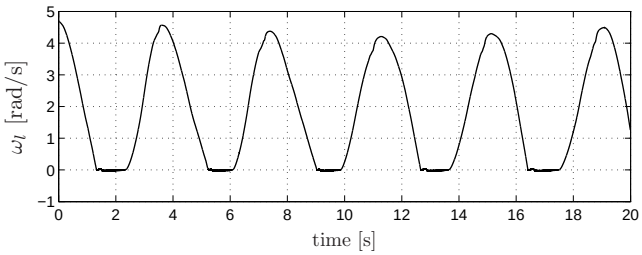

(b) ω_l.

Figure 6.29: Closed-loop system response with control gain $K_1 = [15.9 \quad 1.57 \quad 27.6]$*; the constant input voltage is* $u_c = 0.9$ *V, the equilibrium values are* $\alpha_{eq} = 2.42$ *rad and* $\omega_{eq} = 1.52$ *rad/s; observer gains are* L_2 *and* N_2.

7

Conclusions and Recommendations

7.1 Conclusions

In this thesis, observer-based output-feedback controller design for classes of non-smooth systems have been developed. Firstly, output-feedback controllers aiming at disturbance rejection for continuous-time PWA systems have been designed. Secondly, output-feedback controllers for the stabilization of Lur'e type systems with set-valued nonlinearities (in particular mechanical motion systems with non-collocated friction and actuation) have been developed. In addition to that, the proposed controller design have been implemented on experimental setups to show the strengths and weaknesses of the proposed output-feedback controllers beyond their theoretical importance and demonstrate the value of non-smooth modeling and observer-based controllers for engineering systems in practice.

7.1.1 Disturbance attenuation for continuous PWA systems via output feedback

An observer-based output-feedback controller design that aims at disturbance attenuation for periodically excited PWA systems has been developed. This design is based on the notion of uniform convergence which has been exploited for a number of reasons: 1) stabilize a PWA system, 2) design observer-based output-feedback controllers, 3) develop bounds and performance measures for the system's input and output. In particular, the fact that a uniformly convergent system has a unique globally asymptotically stable steady-state solution for bounded disturbance signals has been essential to our design. Finally, the proposed observer-based output-feedback controller design has been implemented on a setup with PWL restoring characteristics and it has proven to be suitable for attenuating periodic disturbances acting on the setup.

First, state-feedback controllers have been used to render the closed-loop of a PWA system (quadratic) convergent and to attain disturbance attenuation.

Next, output-based controllers have been developed, as often in practice the whole state is not available for feedback. These output-feedback controllers consist of an interconnection of model-based observers and a state-feedback that uses the estimated state of the observers as its input. Furthermore, it has been shown that the 'separation principle' holds in this case in the sense that input-to-state convergent closed-loop systems can be obtained by separately designing the observer and the state-controller controller.

Moreover, an asymptotic ultimate bound for the control action induced by these controllers has been provided. This bound holds for a given bound on the disturbances and for a compact set of initial conditions. Such a guaranteed bound on the control action is very important for the implementation of the proposed controller design strategy on real mechanical systems with PWA characteristics as one always has to deal with actuation limitations in practice.

To compare the disturbance attenuation properties of different control laws, performance measures have been proposed. These performance measures consist of (i) asymptotic ultimate bounds on the output for all disturbance signals included in a given bounded set. This measure does not discriminate between particular shapes or classes of disturbances, such as harmonic functions, (ii) frequency response functions that provide 'nonlinear Bode-like' plots for the class of harmonic disturbances, (iii) quantitative performance measures, based on these Bode-like plots, that capture 'worst case' or 'averaged' information of the steady-state responses in a single number (which allows for quantitative performance comparisons between different controller design).

Finally, the proposed observer-based output-feedback controller design has been implemented experimentally on a setup with PWL restoring characteristics (a flexible beam with flexible one-sided stop and mass-unbalance excitation). Based on the theoretical developments and the performed experiments, it has been shown that the proposed observer-based output-feedback controller can render the setup convergent and attenuate the vibrations induced by periodic excitations.

7.1.2 Stabilization of Lur'e type systems with set-valued nonlinearities

An observer-based output-feedback controller design has been proposed for the stabilization of Lur'e type systems with set-valued nonlinearities in the feedback loop. This design is based on the notion of the absolute stability. This notion has been exploited, firstly, to stabilize a system of the considered type, secondly, to design observer-based output-feedback controllers and, finally, to provide robustness to the controlled system with respect to uncertainties in the set-valued nonlinearities. In particular, the fact that an absolutely stable Lur'e type system has a unique globally asymptotically stable equilibrium for every set-valued nonlinearity that belong to a certain sector (in our case $[0, \infty]$)

has been essential in to our design. Moreover, the proposed observer-based output-feedback controller design has been successfully implemented on an experimental rotor dynamics setup with non-collocated friction and actuation.

First, state-feedback controllers have been used to render the closed-loop of a Lur'e type system with set-valued nonlinearities absolutely stable. One of the controllers achieves absolute stability for the closed-loop system when the closed-loop system satisfies the circle criterion. Due to the fact that some systems may not satisfy the circle criterion, alternative design strategy has been proposed. The conditions imposed on the circle criterion are relaxed by a loop transformation with a dynamic multiplier. In this way we were able to derive an extension of the wellknown Popov criterion that applies to Lur'e type systems with set-valued nonlinearities in the feedback loop. Using these new theoretical results we were able to render the closed-loop system absolutely stable.

Next, output-based controllers have been developed by using these two criteria, as often in practice the whole state is not available for feedback. As for the PWA systems, these output-based controllers consist of an interconnection of model-based observers and a state-feedback controller that uses the estimated state of the observers as its input. Once again, it has been proven that the 'separation principle' holds in both cases in the sense that asymptotically stable closed-loop systems have been obtained by separate observer and controller designs. More specifically, the separation principle has proven to hold for a combination of strictly passive Lur'e type systems with set-valued nonlinearities in the feedback loop with an observer with exponentially stable error dynamics.

The proposed observer-based output-feedback controllers have been tested on an experimental rotor dynamics setup with non-collocated friction and actuation. This setup consists of two inertias subject to friction and a flexible element between the inertias (see Figure 6.1(a)). Due to the presence of friction this system exhibits limit cycling. For this set, commonly applied friction compensation techniques cannot be used. The reason is the non-collocatied nature of the friction and actuation. Based on simulations, it has been shown that the circle criterion design is not feasible. It has been proven that the absence of damping in the flexible connection between the inertias is responsible for this fact. However, the design based on the extended version of the Popov criterion has proven to be effective, in the sense that it was able to remove the limit cycling and stabilize the system to its equilibrium. Moreover, it has been shown experimentally that the proposed design uses a single control gain to stabilize the system for whole range of set-points (equilibria). Finally, it is worth noting that it has been shown experimentally that the design is indeed robust for uncertainties in the friction characteristics.

7.2 Recommendations

In the first part of this section, we will present some recommendations related to the theoretical and experimental results for continuous PWA systems as presented in this thesis (see Chapter 3 and 4).

- In the performance-based controller design strategy, we guarantee, firstly, that a continuous PWA system in closed-loop with a linear static state-feedback law is uniformly convergent as long as a set of constraints, given in LMI form, are satisfied. Secondly, we guarantee that the control input is bounded for bounded disturbances and a compact set of initial conditions. To compute gain matrices of the controllers that satisfy the above two properties and provides 'optimal' performance in terms of disturbance attenuation, we follow a brute force approach that just generates many controllers satisfying the LMI constraints after which we evaluate their performance using the measures in Section 3.5.2. An interesting extension of this work would be the formulation of the presented performance-based controller design strategy in terms of an optimization problem. In such a problem setting, the proposed performance measures can be used as objective functions and the convergence property together with the control input saturation as LMI-based constraints for the optimization problem. Such an approach may be more efficient in constructing a high performance controller, although at the moment it is an open question how to tackle such a complex optimization problem.

- In this work, we have chosen a linear state feedback control law for the purpose of our design. Such choice allows us to check whether the closed-loop system is convergent by using the developed LMI conditions. It would be interested to examine whether a dynamic control law could also be used in the considered systems. Such control law could result in a controller dynamics that incorporates specific controller specifications for every excitation frequency which, in turn, could result in a better disturbance attenuation.

- It is important to mention that the disturbance attenuation approach considered in this thesis is applicable to continuous PWA systems with many switching modes. The fact that this approach has been successfully implemented in experiments encourages us to apply it to more advanced and complex engineering systems.

- In this thesis we have used conditions that guarantee convergence for continuous PWA systems. Conditions for convergence also exist for discontinuous PWA systems. Therefore, it is very interesting to extend this work in that direction.

In the second part of this section, we will present some recommendations related to the theoretical and experimental results for Lur'e type systems with set-valued nonlinearities presented in Chapter 5 and 6.

- The Lur'e type systems we consider in this work consist of a linear part in the forward loop and set-valued nonlinearities in the feedback loop. In the state feedback controller design based on the Popov criterion, the requirement of strict passivity of the linear part of the closed-loop system is relaxed by using a dynamic multiplier. More specifically, the multiplication of the transfer function of the linear part with a dynamic multiplier and the multiplication of the inverse of this multiplier with the set-valued nonlinearities in the feedback loop result in a new linear system and new set-valued nonlinearities. The requirements for absolute stability for the new system are the strict passivity of the new linear part and the passivity of the new system in the feedback path (which is now a dynamical system with a set-valued output map). An interesting extension of this work is to relax the requirements of strict passivity to requirements for passivity by using another multiplier than the first order multiplier used here. This would extend the applicability of the Popov criterion design to a broader class of systems. Moreover, the Popov criterion controller design is only applicable to Lur'e type systems with time-independent nonlinearities. The extension of this design for time-dependent nonlinearities could be of interest (see [13]), although it still has to be generalized to the case of set-valued mappings.

- For the implementation of the Popov criterion-based output-feedback controller on the rotor dynamic system we had to partially compensate the friction acting at the upper disc. It is of great interest to design an output-feedback controller for the uncompensated system due to the fact that overcompensation and undercompensation can lead to undesirable dynamic phenomena in the rotor dynamic system.

- For the implementation of the proposed model-based observer design to the rotor dynamic system we use as observer output injection signal the measured difference between the positions of the upper and lower disc (see Figure 6.1(a)). It would be interesting to study under which conditions we can use as output injection signal only the position of the upper disc. This would be of interest especially for rotary drilling systems (see Figure 1.2) since in such systems down-hole measurements are hardly feasible.

- The output-feedback designs presented in this work use model-based observers. It has been shown experimentally that these observers are robust with respect to changes in the friction characteristics. However, it has not been proven whether they are robust with respect to unmodelled changes

in the set-valued nonlinearities. It is of great importance to design observers and output-feedback controllers with such robustness property.

- In this work, we have proposed observer and controller designs for non-smooth PWA systems described by differential equations with a continuous though non-smooth vectorfield and Lur'e type systems with set-valued nonlinearities. Both the observer and controller designs for the latter class of systems are based on the Popov and circle criterion. It would be interested to extend these designs also to non-smooth systems with jumps in the state variables.

A

Lyapunov function matrices

In this appendix, the matrices P characterizing the Lyapunov function used to design the four different controllers applied in the simulation and experimental results in Chapter 4 are presented.

The controller design matrices P_{HG}, P_{EI}, $P_{IS,1}$ and $P_{IS,2}$ are:

$P_{HG} =$

$$\begin{pmatrix} 8023,412 & 89,034 & -1625,452 & 92,438 & 4,650 & -0,193 & 0,252 & 0,122 \\ 89,034 & 11,129 & -46,768 & -0,526 & 0,094 & -0,003 & 0,001 & 0,003 \\ -1625,452 & -46,768 & 549,501 & -7,886 & -1,205 & 0,048 & -0,0403 & -0,031 \\ 92,438 & -0,526 & -7,886 & 5,443 & 0,0451 & -0,002 & 0,002 & 0,001 \\ 4,650 & 0,094 & -1,205 & 0,045 & 0,004 & -0,000 & 0,000 & 0,000 \\ -0,193 & -0,003 & 0,048 & -0,002 & -0,000 & 0,000 & 0,000 & -0,000 \\ 0,252 & 0,001 & -0,040 & 0,002 & 0,000 & 0,000 & 0,000 & 0,000 \\ 0,122 & 0,003 & -0,031 & 0,001 & 0,000 & -0,000 & 0,000 & 0,000 \end{pmatrix}$$

$P_{EI} =$

$$\begin{pmatrix} 10551,247 & 539,039 & 621,138 & -47,865 & 0,178 & 0,346 & -0,686 & -0,048 \\ 539,039 & 2393,549 & 1257,660 & -866,382 & -0,037 & 0,019 & -0,062 & -0,029 \\ 621,138 & 1257,660 & 829,531 & -378,783 & 0,000 & 0,087 & 0,012 & -0,028 \\ -47,865 & -866,382 & -378,783 & 383,575 & 0,010 & 0,013 & 0,023 & 0,006 \\ 0,178 & -0,037 & 0,000 & 0,010 & 0,001 & 0,001 & 0,000 & -0,000 \\ 0,346 & 0,019 & 0,087 & 0,013 & 0,001 & 0,014 & 0,007 & -0,005 \\ -0,686 & -0,062 & 0,012 & 0,023 & 0,000 & 0,007 & 0,005 & -0,002 \\ -0,048 & -0,029 & -0,028 & 0,006 & -0,000 & -0,005 & -0,002 & 0,002 \end{pmatrix}$$

$P_{IS,1} =$

$$\begin{pmatrix} 1036,701 & 62,312 & 486,638 & -30,836 & -0,003 & -0,075 & 0,151 & -0,025 \\ 62,312 & 3795,354 & 1547,835 & -1369,045 & 0,040 & 0,041 & -0,199 & -0,115 \\ 486,638 & 1547,835 & 927,836 & -583,269 & -0,026 & -0,010 & 0,097 & -0,030 \\ -30,836 & -1369,045 & -583,269 & 677,259 & 0,018 & 0,108 & -0,039 & 0,015 \\ -0,003 & 0,040 & -0,026 & 0,018 & 0,001 & 0,000 & 0,000 & -0,000 \\ -0,075 & 0,041 & -0,010 & 0,108 & 0,000 & 0,023 & 0,009 & -0,008 \\ 0,151 & -0,199 & 0,097 & -0,039 & 0,000 & 0,009 & 0,006 & -0,003 \\ -0,025 & -0,115 & -0,030 & 0,0153 & -0,000 & -0,008 & -0,003 & 0,004 \end{pmatrix}$$

$P_{IS,2} =$

$$\begin{pmatrix}
1295,120 & 37,165 & 595,466 & -26,714 & -0,000 & -0,037 & 0,160 & -0,008 \\
37,165 & 3962,781 & 1609,094 & -1415,891 & 0,044 & 0,084 & -0,289 & 0,002 \\
595,466 & 1609,094 & 1000,766 & -604,060 & -0,021 & 0,047 & 0,079 & 0,031 \\
-26,714 & -1415,891 & -604,060 & 737,074 & 0,017 & 0,023 & -0,116 & 0,010 \\
-0,000 & 0,044 & -0,021 & 0,017 & 0,002 & 0,000 & 0,000 & -0,000 \\
-0,037 & 0,084 & 0,047 & 0,023 & 0,000 & 0,024 & 0,009 & -0,008 \\
0,160 & -0,289 & 0,079 & -0,116 & 0,000 & 0,009 & 0,007 & -0,003 \\
-0,008 & 0,002 & 0,031 & 0,010 & -0,000 & -0,008 & -0,003 & 0,004
\end{pmatrix}.$$

B

Observer design implementations on the PWL beam system

In this Appendix, we design two observers for the PWL beam system by using the theory presented in Section 3.3.1 and we validate their performance based on simulation and experimental results. Firstly, we show that these observers exponentially reconstruct the state of the model that describes the real system (simulations) and, secondly, we show that the observers accurately reconstruct the output and an additional state variable of the real system based on experiments. In the first case, the system output is a transversal displacement of a single point on the beam computed by the model. In the second case, the system output is a measured signal that corresponds to the transversal displacement of the same point on the beam. This signal is measured by a linear displacement transducer mounted on the beam. In order to validate the obtained results we measure the displacement of a second point on the beam.

B.1 Simulation results

In order to design the observer (3.7) or (3.12) for system (4.7a), the observer output injection should be chosen such that the LMIs (3.11) are fulfilled for the first observer and the LMIs (3.14) have to hold for the second observer. By solving the LMIs (3.8) or the LMIs (3.14a)-(3.14b), we can compute the observer gain L for the first observer or the observer gains L_1, L_2 for the second observer, respectively. In the sequel, the observer gains L, L_1, L_2 are chosen such that exponential stability of the observer error dynamics is guaranteed and a balance between fast transient convergence and low sensitivity to model errors and measurement noise is accomplished. This will be explained at the end of this section. A detailed description of the computation of the observer gains is given in the end of this section. The resulting numerical values of the observer gains are

$$L = [93.059\ 89.959\ -225.506\ -7.496\ 4510.783\ 5736.746\ 13937.6\ 547.24]$$

and

$$L_1 = [98.475\ 88.090\ -284.05\ -5.254\ 386.35\ 4626.0\ -18411.0\ 766.50]\,,$$

$$L_2 = [98.781\ 88.212\ -284.35\ -5.2469\ 1910.2\ 5031.8\ -19635.0\ 627.17]\,.$$

In order to validate the observer performance using simulations, two model-based signals (y_A, q_{mid}) that describe the displacements of two points along the beam (point A and the middle of the beam in Figure 4.2(b), respectively) are obtained by means of simulations with model (4.7)-(4.8) and

$$y_A = C_A x \tag{B.1}$$
$$q_{mid} = C_{qmid} x, \tag{B.2}$$

where y_A and q_{mid} are the 68^{th}- and 53^{rd}-DOF of the 111DOF model, respectively. Therefore, $C_A = [\ \tau_{68}^T \quad \underline{0}^T\ ]$ and $C_{qmid} = [\ \tau_{53}^T \quad \underline{0}^T\ ]$, according to (4.8). The numerical values of C_A and C_{qmid} are given by

$$C_A = [-0.317 \quad -0.334 \quad -0.667 \quad -0.3069 \quad 0 \quad 0 \quad 0 \quad 0]$$

and

$$C_{qmid} = [1 \quad 0 \quad 0 \quad 0 \quad 0 \quad 0 \quad 0 \quad 0]\,.$$

By using y_A for observer output injection ($y = y_A$), the observers provide estimates of the full state ($\hat{x}$) and consequently also of the displacement ($\hat{q}_{mid} = C_{qmid}\hat{x}$) of the middle point of the beam. By comparing the signals q_{mid} and $\hat{q}_{mid}$, we validate the observer state reconstruction. The initial conditions for the model and the observers are $x_0 = 10^{-4}\,[1,\ 1,\ 1,\ 1,\ 1,\ 1,\ 1,\ 1]^T$ and $\hat{x}_0 = 100x_0$. Note that the focus here is on the open-loop system of the piecewise linear beam (i.e. (4.7) for $u = 0$).

In the sequel, we will illustrate model estimations, observer estimations and observer errors for both observers for different excitation frequencies and excitation amplitudes.

In Figures B.1(a), B.1(b) and B.2(a), B.2(b), y_A is compared with $\hat{y}_A$ for $\frac{\omega}{2\pi} = 43$Hz, $R = 74$N and $\frac{\omega}{2\pi} = 20$Hz, $R = 16$N, respectively. In these figures, $\hat{y}_{A,L}$ is the estimation based on the observer (3.7) and $\hat{y}_{A,(L_1,L_2)}$ is the estimation based on the observer (3.12).

Moreover, in Figures B.1(c), B.1(d) and B.2(c), B.2(d), q_{mid} is compared with $\hat{q}_{mid}$ for $\frac{\omega}{2\pi} = 43$Hz, $R = 74$N and $\frac{\omega}{2\pi} = 20$Hz, $R = 16$N, respectively. In these figures, $\hat{q}_{mid,L}$ is the estimation based on the observer (3.7) and $\hat{q}_{mid,(L_1,L_2)}$ is the estimation based on the observer (3.12). Similar notations will be used for other validations. In Figures B.3(a) and B.3(b), it is shown that the model and the observers do not switch dynamics (e.g pass through $q_{mid} = 0$ and $\hat{q}_{mid} = 0$) simultaneously. Nevertheless, both converge to the same steady-state solution as shown in Figures B.1(b), B.1(d) and B.2(b), B.2(d), as guaranteed by Theorems 3.3.1 and 3.3.2.

Furthermore, in Figures B.1(e), B.1(f) and B.2(e), B.2(f), we compare the norm of the observer errors $e_{o,L} = \hat{x}_L - x$ and $e_{o,(L_1,L_2)} = \hat{x}_{(L_1,L_2)} - x$ with each other and we provide an upper bound for $\|e_{o,(L_1,L_2)}\|$ based on (3.15), for $\frac{\omega}{2\pi} = 43$Hz, $R(\omega) = 74$N and $\frac{\omega}{2\pi} = 20$Hz, $R(\omega) = 16$N, respectively. Based on these figures, both observer errors converge to zero for both considered excitation frequencies, as guaranteed by the theory. Moreover, $\|e_{o,(L_1,L_2)}\|$ indeed satisfies the bound as in (3.15).

Remark B.1.1 The steady-state solution of the displacements q_{mid} and $\hat{q}_{mid}$ for an excitation frequency of 43Hz is a $\frac{1}{2}$ subharmonic solution (Figures B.1(a), B.1(b)), while for an excitation frequency of 20Hz it is a harmonic solution (Figures B.2(a) and B.2(b)), see [58].

Remark B.1.2 Note that similar results are obtained if we use any other signal y as output injection, as long as the LMIs (3.8) and (3.14a)-(3.14b) are satisfied.

Remark B.1.3 If we compare the two observers based on simulation results we realize that they both provide good estimations of the system state and output, since the observer error converges to zero. Based on Figures B.1(f) and B.2(f), we notice that $e_{o,(L_1,L_2)}$ converges to zero faster than $e_{o,L}$. This is probably due to the switching structure of the observer. From these figures, note that the provided bound is only suitable for $e_{o,(L_1,L_2)}$.

B.2 Experimental results

In order to validate the observer performance using experimental results, we measure two signals $(y_{A,m}, q_{mid,m})$ that describe the displacements of the point A and middle point of the beam. These two signals are measured by two linear variable displacement transducers. By using $y_{A,m}$ as observer output injection, the observers construct an estimation of the full state $(\hat{x})$ of the real system and consequently also an estimation of the displacement $\hat{q}_{mid}$ of the middle point. By comparing $q_{mid,m}$ with $\hat{q}_{mid}$, an experimental validation for the observer state reconstruction is performed. The initial conditions for the model are the same as in the case of simulations. The observer error initial conditions, which can be computed by using the position measurements by the LVDTs for q_{mid} and y_A, are:

$$e_{o,qmid,L} = 13.1 \cdot 10^{-4}\text{m and } e_{o,y_A,L} = 12.1 \cdot 10^{-4}\text{m for 43Hz,}$$

$$e_{o,qmid,(L_1,L_2)} = 12.8 \cdot 10^{-4}\text{m and } e_{o,y_A,(L_1,L_2)} = 12.3 \cdot 10^{-4}\text{m for 43Hz,}$$

$$e_{o,qmid,L} = 5.3 \cdot 10^{-4}\text{m and } e_{o,y_A,L} = 4.05 \cdot 10^{-4}\text{m for 20Hz,}$$

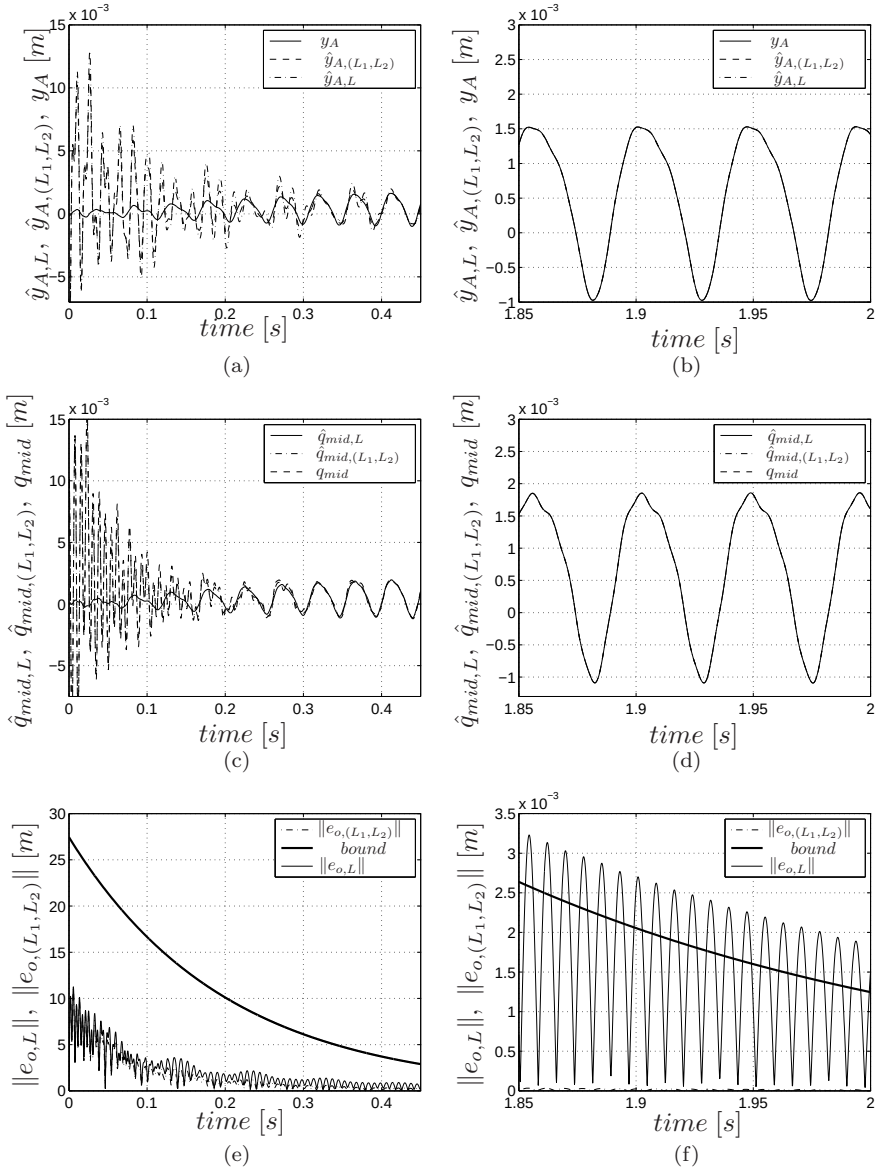

Figure B.1: (a) Model prediction y_A $[m]$ and observer reconstruction $\hat{y}_A$ $[m]$ based on (3.7) *($\hat{y}_{A,L}$) and* (3.12) *($\hat{y}_{A,(L_1,L_2)}$) for excitation frequency $\frac{\omega}{2\pi} = 43Hz$ and excitation amplitude $R = 74N$; (b) Zoomed version of (a) in steady-state; (c) Model prediction q_{mid} $[m]$ and observer reconstruction $\hat{q}_{mid}$ $[m]$ based on* (3.7) *($\hat{q}_{mid,L}$) and* (3.12) *($\hat{q}_{mid,(L_1,L_2)}$); (d) Zoomed version of (c) in steady-state; (e) The norm of the observer error e_o $[m]$ of* (3.7) *($\|e_{o,L}\|$) and* (3.12) *($\|e_{o,(L_1,L_2)}\|$) and the observer error bound* (3.15)*; (f) Zoomed version of (e).*

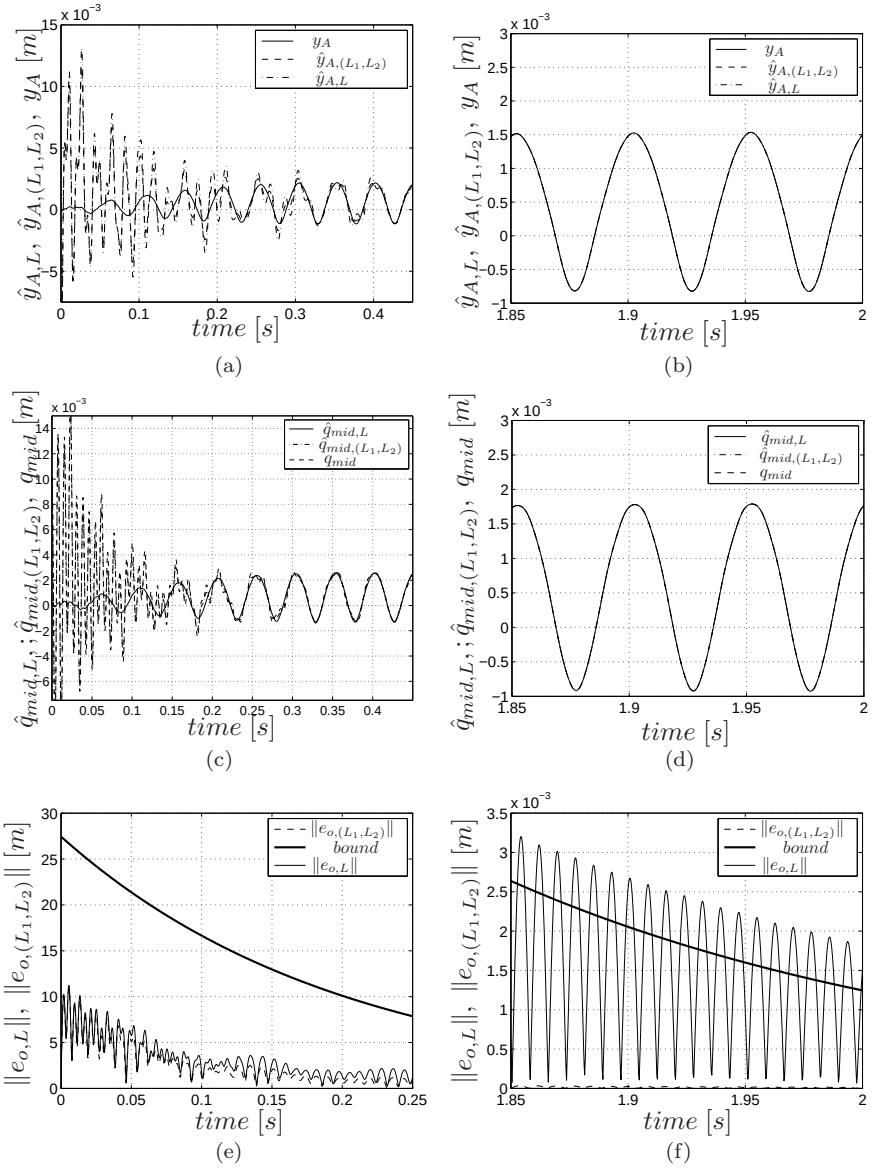

Figure B.2: (a) Model prediction y_A $[m]$ and observer reconstruction $\hat{y}_A$ $[m]$ based on (3.7) *($\hat{y}_{A,L}$) and* (3.12) *($\hat{y}_{A,(L_1,L_2)}$) for excitation frequency $\frac{\omega}{2\pi} = 20Hz$ and excitation amplitude $R = 16N$; (b) Zoomed version of (a) in steady-state; (c) Model prediction q_{mid} $[m]$ and observer reconstruction $\hat{q}_{mid}$ $[m]$ based on* (3.7) *($\hat{q}_{mid,L}$) and* (3.12) *($\hat{q}_{mid,(L_1,L_2)}$); (d) Zoomed version of (c) in steady-state; (e) The norm of the observer error e_o $[m]$ of* (3.7) *($\|e_{o,L}\|$) and* (3.12) *($\|e_{o,(L_1,L_2)}\|$) and the observer error bound* (3.15)*; (f) Zoomed version of (e).*

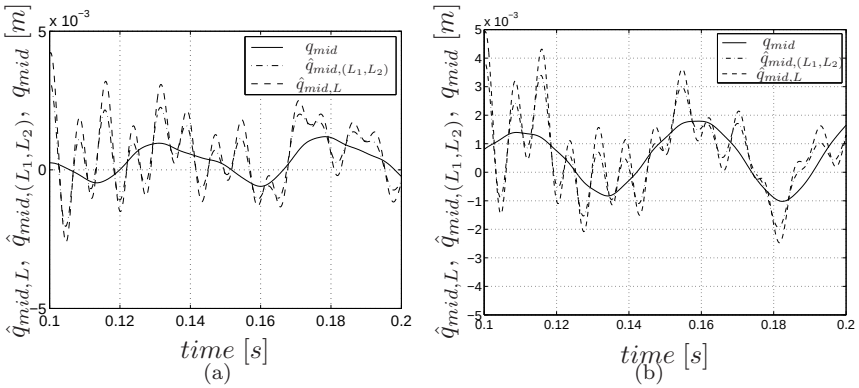

Figure B.3: Model prediction q_{mid} $[m]$ and observer reconstruction $\hat{q}_{mid}$ $[m]$ based on (3.7) *($\hat{q}_{mid,L}$) and* (3.12) *($\hat{q}_{mid,(L_1,L_2)}$): (a) $\frac{\omega}{2\pi} = 43Hz$ and $R = 74N$; (b) $\frac{\omega}{2\pi} = 20Hz$ and $R = 16N$.*

$e_{o,qmid,(L_1,L_2)} = 5.2 \cdot 10^{-4}$m and $e_{o,y_A,(L_1,L_2)} = 4.2 \cdot 10^{-4}$m for 20Hz.

We will now illustrate observer estimations, measured signals and observer errors, for both observers, (3.7) and (3.12), for different excitation frequencies and excitation amplitudes.

In Figures B.4(a) and B.6(a), $\hat{q}_{mid}$ is compared with $q_{mid,m}$ for $\frac{\omega}{2\pi} = 43$Hz, $R = 74$N and $\frac{\omega}{2\pi} = 20$Hz, $R = 16$N, respectively. In these figures, $\hat{q}_{mid,L}$ is the estimation based on the observer (3.7) and $\hat{q}_{mid,(L_1,L_2)}$ is the estimation based on the observer (3.12). Furthermore, in Figures B.4(c), B.5(a) and B.6(c), B.7(a), we compare the observer errors $e_{o,qmid,L} = \hat{q}_{mid,L} - q_{mid,m}$ and $e_{o,qmid,(L_1,L_2)} = \hat{q}_{mid,(L_1,L_2)} - q_{mid,m}$ for $\frac{\omega}{2\pi} = 43$Hz, $R = 74$N and $\frac{\omega}{2\pi} = 20$Hz, $R = 16$N, respectively. In Figures B.4(c) and B.6(c), $e_{qmid,L}$ and $e_{qmid,(L_1,L_2)}$ are depicted in a transient, while in Figures B.5(a) and B.7(a) they are depicted in steady-state.

In Figures B.4(b) and B.6(b), $\hat{y}_A$ is compared with $y_{A,m}$ for $\frac{\omega}{2\pi} = 43$Hz, $R = 74$N and $\frac{\omega}{2\pi} = 20$Hz, $R = 16$N, respectively. In these figures, $\hat{y}_{A,L}$ is the estimation based on the observer (3.7) and $\hat{y}_{A,(L_1,L_2)}$ is the estimation based on the observer (3.12). Furthermore, in Figures B.4(d), B.5(b) and B.6(d), B.7(b), we compare the observer errors $e_{o,y_A,L} = \hat{y}_{y_A,L} - y_{A,m}$ and $e_{o,y_A,(L_1,L_2)} = \hat{y}_{A,(L_1,L_2)} - y_{A,m}$ for $\frac{\omega}{2\pi} = 43$Hz, $R = 74$N and $\frac{\omega}{2\pi} = 20$Hz, $R = 16$N, respectively. In Figures B.4(d) and B.6(d), $e_{A,L}$ and $e_{y_A,(L_1,L_2)}$ are depicted in a transient phase, while in Figures B.5(b) and B.7(b) they are depicted in steady-state.

Clearly, both observers accurately reconstruct the behavior of the real system. The fact that $e_{o,L}$ and $e_{o,(L_1,L_2)}$ do not converge to zero exactly but

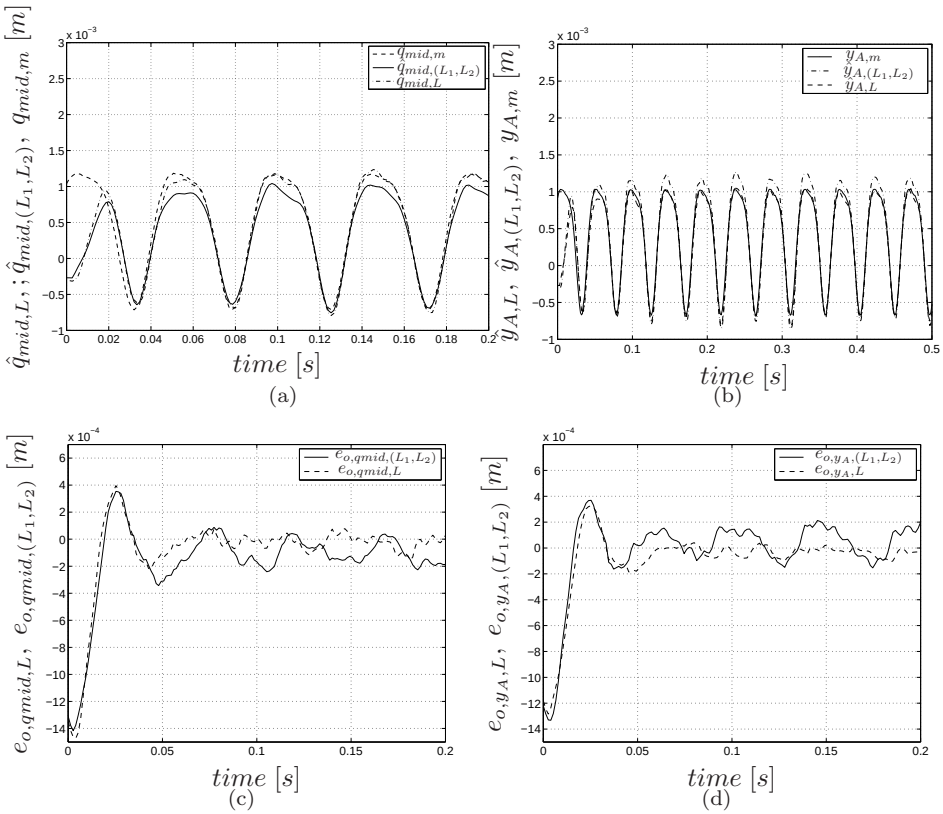

Figure B.4: (a) Observer reconstruction $\hat{q}_{mid}$ [m] based on (3.7) ($\hat{q}_{mid,L}$) and (3.12) ($\hat{q}_{mid,(L_1,L_2)}$) and measured signal $q_{mid,m}$ [m] for excitation frequency $\frac{\omega}{2\pi} = 43Hz$ and excitation amplitude $R = 74N$; (b) Observer reconstruction $\hat{y}_A$ [m] based on (3.7) ($\hat{y}_{A,L}$) and (3.12) ($\hat{y}_{A,(L_1,L_2)}$) and measured signal $y_{A,m}$ [m]; (c) observer error $e_{o,qmid}$ [m] of (3.7) ($e_{o,qmid,L}$) and (3.12) ($e_{o,qmid,(L_1,L_2)}$) in transient; (d) observer error e_{o,y_A} [m] of (3.7) ($e_{o,y_A,L}$) and (3.12) ($e_{o,y_A,(L_1,L_2)}$) in transient.

---

to a steady-state solution with small 'amplitude' (see Figures B.5(a), B.5(b), B.7(a) and B.7(b)) is due to (inevitable) model mismatch and due to noise in the measured signals. In both observers, the steady-state observer error has the same order of magnitude, although the errors $e_{o,L}$ appear to be somewhat smaller than e_{o,L_1,L_2} in steady-state.

The steady-state observer error is a measure for the performance of the observers with the computed observer gains (L_1, L_2) or L. Namely, it reflects the

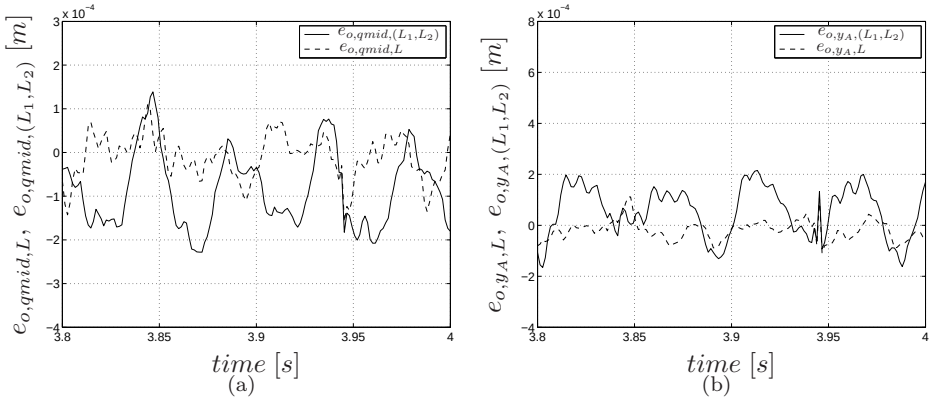

Figure B.5: (a) observer error $e_{o,qmid}$ $[m]$ of (3.7) *($e_{o,qmid,L}$) and* (3.12) *($e_{o,qmid,(L_1,L_2)}$) in steady-state; (b) observer error e_{o,y_A} $[m]$ of* (3.7) *($e_{o,y_A,L}$) and* (3.12) *($e_{o,y_A,(L_1,L_2)}$) in steady-state.*

steady-state sensitivity to model errors and measurement noise. To investigate the influence of the choice of the observer gains on these performance criteria, we compute different observer gains that satisfy the LMI constraints (3.8) or (3.14a)-(3.14b) by varying the constant α. For the obtained observer gains L or (L_1, L_2), we can measure the magnitude of $e_{o,L}$ or $e_{o,(L_1,L_2)}$ in steady-state and the time (called settling time t_s) required for $e_{o,L}$ or $e_{o,(L_1,L_2)}$ to converge to its steady-state.

This knowledge can then be used to asses the effect of the choice of the observer gain on both the transient performance and the steady-state sensitivity to modelling errors and measurement noise. It is exactly the trade off between such transient and steady-state performance that determines the ultimate choice for the observer gains. Clearly, the desired balance between transient and steady-state performance heavily depends on the performance requirements for the system under study. The specific observer gains used in this thesis are obtained by balancing such transient and steady-state performance for the PWL beam system. The presented observer will be used for control purposes. Therefore, the choice of the observer gains should be such that the observer is faster than the controller and the observer error as small as possible in steady-state.

In order to further reduce the model errors and the measurement noise in the system aiming at even higher steady-state observer performance, we could use more accurate (more complex) models to describe the system dynamics. Furthermore, higher precision encoders are needed in order to decrease the measurement noise in the signals that are used to recover the system state.

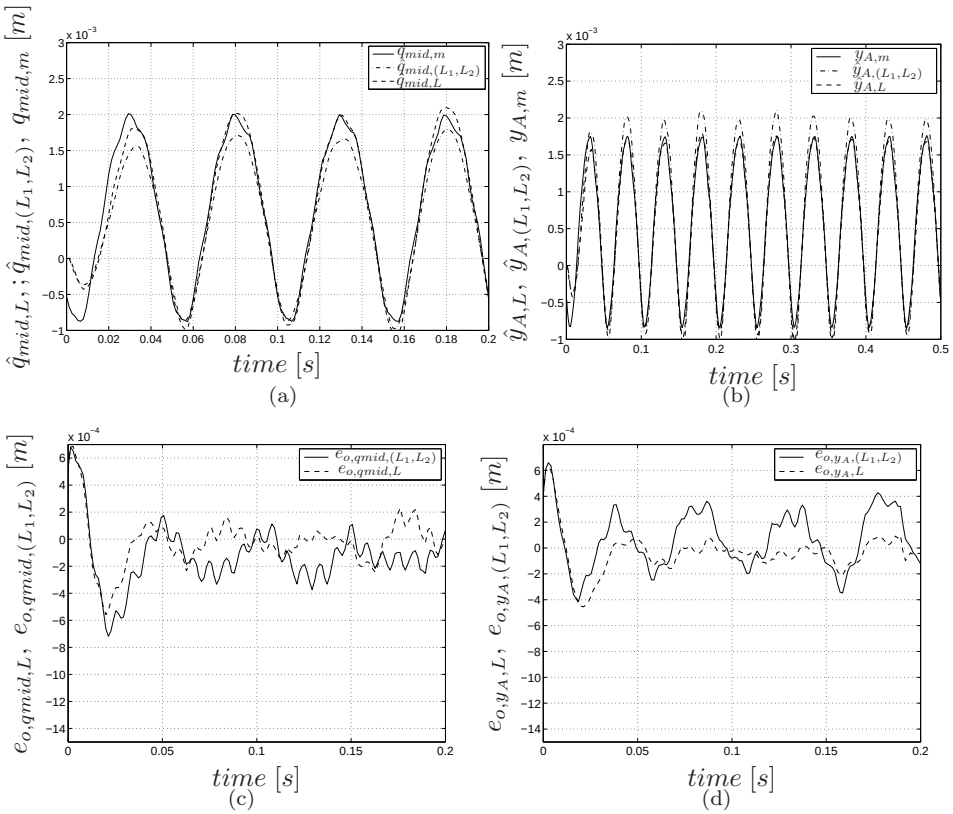

Figure B.6: (a) Observer reconstruction $\hat{q}_{mid}$ $[m]$ based on (3.7) *($\hat{q}_{mid,L}$) and* (3.12) *($\hat{q}_{mid,(L_1,L_2)}$) and measured signal $q_{mid,m}$ $[m]$ for excitation frequency $\frac{\omega}{2\pi} = 20Hz$ and excitation amplitude $R = 16N$; (b) Observer reconstruction $\hat{y}_A$ $[m]$ based on* (3.7) *($\hat{y}_{A,L}$) and* (3.12) *($\hat{y}_{A,(L_1,L_2)}$) and measured signal $y_{A,m}$ $[m]$ (c) observer error $e_{o,qmid}$ $[m]$ of* (3.7) *($e_{o,qmid,L}$) and* (3.12) *($e_{o,qmid,(L_1,L_2)}$) in transient; (d) observer error e_{o,y_A} $[m]$ of* (3.7) *($e_{o,y_A,L}$) and* (3.12) *($e_{o,y_A,(L_1,L_2)}$) in transient.*

The drawback of aiming at more accurate models is that, in most of the cases, it will lead to models of higher order and/or higher complexity. As a result, the calculation of the observer responses becomes (too) computationally expensive. This is not favorable for the on-line implementation of the observers in real systems. The drawback of using high precision encoders in a real system is that they are generally expensive.

In Section 4.4, we will use the switching observer (3.12) for the PWL beam

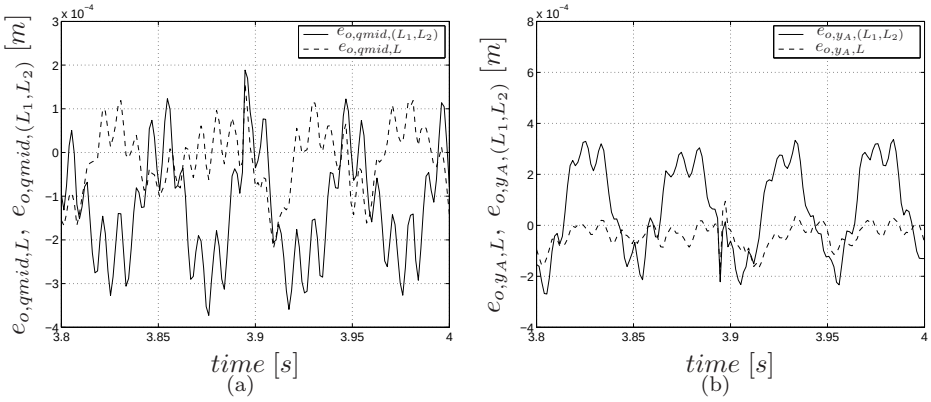

Figure B.7: (a) observer error $e_{o,qmid}$ $[m]$ of (3.7) *($e_{o,qmid,L}$) and* (3.12) *($e_{o,qmid,(L_1,L_2)}$) in steady-state; (b) observer error e_{o,y_A} $[m]$ of* (3.7) *($e_{o,y_A,L}$) and* (3.12) *($e_{o,y_A,(L_1,L_2)}$) in steady-state.*

---

system in an output-feedback control design. As we have already mentioned, for the given system, this observer yields somewhat higher steady-state error levels compared to the observer (3.7). However, observer (3.12) yields, in turn, faster transients, which is a favorable property when combining the observer with a controller in an output feedback scheme. We will show, in Section 4.4, that the accuracy of this observer is high enough for the control purposes in the examined application.

C

Saturated control action on the PWL beam system

As shown in Section 4.4.2, using an actuator with $u_{max} = 650N$ the PWL beam system can be rendered (locally) uniformly convergent while the actuator constraints will be respected if the controller is activated when the system resides in any open-loop steady-state solution or when the system is at rest. Nevertheless, the available actuator in the PWL beam system, can only provide a control action limited to $u_{max} = 75N$ for frequencies in the range of $\frac{\omega}{2\pi} \in$ [10 60]Hz. It is obvious that in this case the control input will be saturated even when using control gains $K_{IS,1}$ and $K_{IS,2}$, see Figure 4.8. Therefore, it will be examined by means of simulations whether such control action can still render the PWL beam system convergent and attenuate the periodic disturbances acting on the system for initial conditions as mentioned above.

In the present study, we will use the control gain matrices $K_{IS,1}$ and $K_{IS,2}$. Firstly, we will compute the control input (without saturation) provided to the closed-loop system in steady-state (denoted by $\bar{u}(t)$). In case $\|\bar{u}(t)\| > u_{max}$ for some t and some $\frac{\omega}{2\pi} \in$ [10 60]Hz, then the control gain matrix related to this control input is rejected. On the other hand, if it holds that $|\bar{u}(t)| \leq u_{max}$ for all t and all $\frac{\omega}{2\pi} \in$ [10 60]Hz, then we investigate further whether the control gain matrix related to this control input can 1) render the system (locally) convergent, 2) attenuate the periodic disturbances acting on the system, by performing further simulations.

In Figure C.1, we depict $\max_{t\in[0\ T]} |\bar{u}(t)|$ for all $\frac{\omega}{2\pi} \in$ [10 60]Hz for both $K_{IS,1}$ and $K_{IS,2}$ together with the upper bound $u_{max} = 75\ N$. In this figure, it is shown that $|\bar{u}^{IS,1}(t)| \leq u_{max}$ for all $t \in [0\ T], \frac{\omega}{2\pi} \in$ [10 60]Hz. On the other hand, $|\bar{u}^{IS,2}(t)| > u_{max}$ for some $t \in [0\ T]$ and $\frac{\omega}{2\pi} \in$ [10 60]Hz. Consequently, $K_{IS,1}$ could eventually render the system (locally) convergent, while $K_{IS,2}$ cannot (at least not with the same steady-state solutions as for the unsaturated system). Note that the control action related to the control gain $K_{IS,2}$ saturates only for $\frac{\omega}{2\pi} \in [53,\ 55]$Hz. In case we are interested in frequencies outside this region, $K_{IS,2}$ might be of interest as well to further investigate its convergence and disturbance attenuation properties . The fact that $|\bar{u}^{IS,2}(t)| > u_{max}$ for some $t \in [0\ T]$ and $\frac{\omega}{2\pi} \in$ [10 60]Hz for $K_{IS,2}$ implies that $X_{cl} \nsubseteq S$ and, therefore, $X_{cl} \nsubseteq \Theta_\rho$ (where again X_{cl} is a set including all closed-loop steady-state solutions). This is graphically illustrated in Figure

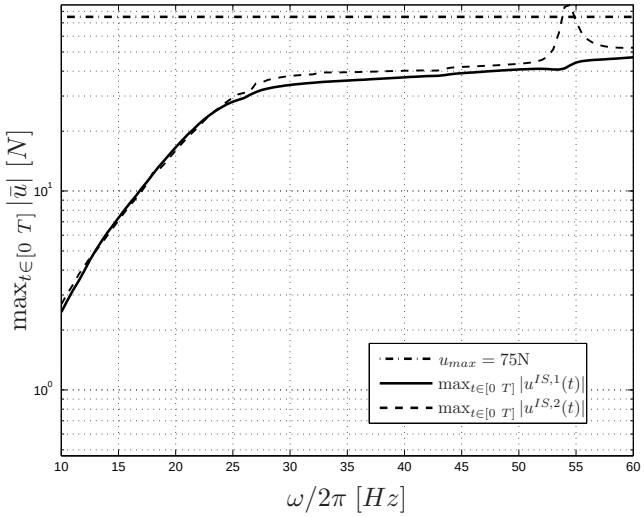

Figure C.1: u_{max} (dash-dotted line), $\max_{t\in[0\ T]} |\bar{u}^{IS,1}(t)|$ (solid curve) and $\max_{t\in[0\ T]} |\bar{u}^{IS,2}(t)|$ (dashed curve) for the interconnected system in steady-state.

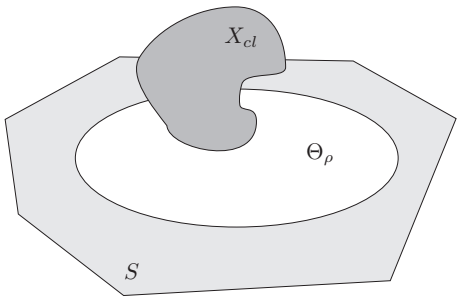

Figure C.2: Graphical illustration of the situation where $X_{cl} \nsubseteq S$ and $X_{cl} \nsubseteq \Theta_\rho$ for the PWL beam system for control gain $K_{IS,2}$, $u_{max} = 75N$, and $R = 144N$.

C.2. More specifically, in this figure we depict X_{cl} by a polyhedral with dark grey color, Θ_ρ by an ellipsoid with white color and S by a polyhedral with light grey color. It is clear that the polyhedral X_{cl} is not included in the ellipsoid Θ_ρ nor in the polyhedral S.

In the sequel, we will numerically compute the responses of the closed-loop system with $K = K_{IS,1}$, firstly, for the case where there is saturation in the control input and, secondly, in the case where there is no saturation in the

control input. Moreover, based on these responses we will examine whether the saturated control action renders the closed-loop system convergent. The initial conditions $x_0 \in X_0 \not\subseteq \Theta_\rho$ and the saturated control action is given by $u(t) = \min\{|K_{IS,1}x(t)|, u_{max}\}\text{sign}(K_{IS,1}x(t))\ \forall t$. In Figures C.3(a)-C.3(c),

$$\max_{t\in[0\ T]} |\bar{q}^{\omega}_{mid}(t)|/R(\omega),\ \max_{t\in[0\ T]} |\bar{q}^{\omega}_{act}(t)|/R(\omega) \text{ and } \max_{t\in[0\ T]} |\bar{y}^{\omega}_{A}(t)|/R(\omega)$$

are plotted for the closed-loop system. In these figures, the solid curves correspond to the responses of the closed-loop system where the control action does not saturate and $u_{max} = 650$N, and the dashed curves correspond to the responses of the closed-loop system where the control action saturates and $u_{max} = 75$N. Based on these curves, the system with saturated control action exhibits the same steady-state responses as the one without saturated control action. Recall in this respect that, for the control gain $K_{IS,1}$, the control action does not exceed $u_{max} = 75$N in steady-state.

For a better understanding of this phenomenon, time responses of q_{mid}, q_{act}, y_A and u are given in Figures C.4 and C.5. In these figures, the dashed curves correspond to responses for the saturated system, while the solid curves correspond to responses for the non-saturated system. The excitation frequencies and amplitudes in Figures C.4 and C.5 are 21Hz, $R = 18$N and 43Hz, $R = 50$N, respectively. Figures C.4(d) and C.5(d) do indeed show that in steady-state no saturation occurs, which guarantees that the globally asymptotically stable steady-state solutions of the non-saturated system are also (at least locally) asymptotically stable steady-state solutions of the saturated system. Moreover, these figures show that for considerably deviating initial conditions, solutions of the saturated system still converge to these steady-state solutions (although this cannot be guaranteed in general). The latter results indicate that despite the actuator saturation, the control design with gains $K_{IS,1}$ may still perform well in practice. Note that the results in Figures C.4 and C.5 correspond to two test-cases in which the exited open-loop system resides in the harmonic and $\frac{1}{2}$-subharmonic resonances which are (concerning actuator saturation) two critical cases (see also Figure 4.8).

At this point, we will give a graphical illustration of the situation where the control action, related to $K_{IS,1}$, is saturated and the saturated closed-loop system still converges to the steady-state solution of the non-saturated closed-loop system. Once again, $u_{max} = 75$N, $R = 144$N and $\rho = 1$. Moreover, the numerical values of the variables γ ($\gamma_{IS,1}$) and μ_{max} that characterize the sets Θ_γ and $\Theta_{\mu_{max}}$ are 53.48 and 72.5, respectively. Consider, hereto, the Figure C.6 where the already defined sets X_{cl}, Θ_ρ, Θ_γ, X_0, $\Theta_{\mu_{max}}$ and S are depicted together with a new set Ω. This set includes all the initial states of the saturated system such that the corresponding solution of this system reaches X_{cl} for some $t \leq t_0$. This set is depicted by a polyhedral with light grey color. The set X_0 is depicted by a polyhedral with dark grey color and the sets X_{cl} and S are depicted by polymorphic shapes with black color and

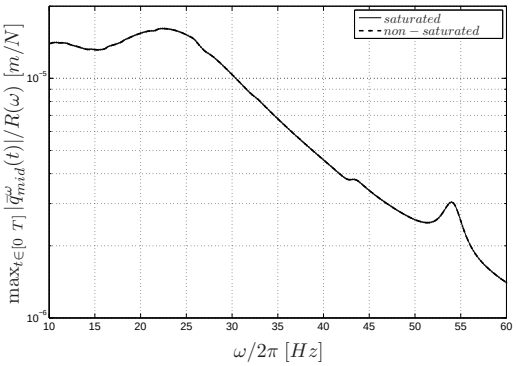

(a) $\max_{t\in[0\ T]} |\bar{q}^{\omega}_{mid}(t)|/R(\omega)$.

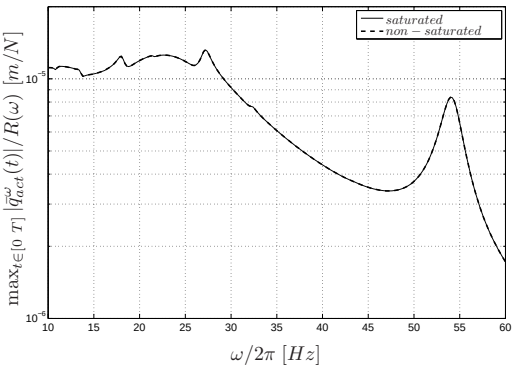

(b) $\max_{t\in[0\ T]} |\bar{q}^{\omega}_{act}(t)|/R(\omega)$.

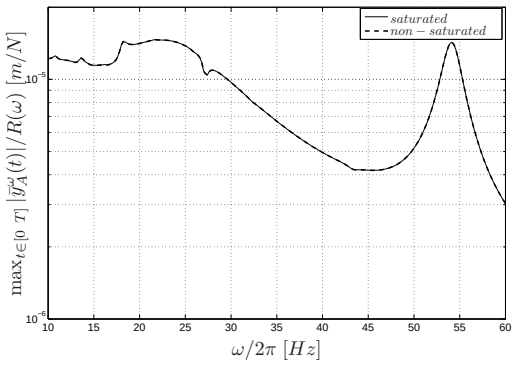

(c) $\max_{t\in[0\ T]} |\bar{y}^{\omega}_{A}(t)|/R(\omega)$.

Figure C.3: (a) $\max_{t\in[0\ T]} |\bar{q}^{\omega}_{mid}(t)|/R(\omega)$*; (b)* $\max_{t\in[0\ T]} |\bar{q}^{\omega}_{act}(t)|/R(\omega)$*; (c)* $\max_{t\in[0\ T]} |\bar{y}^{\omega}_{A}(t)|/R(\omega)$ *non-saturated (solid curve) and saturated (dashed curve) control action.*

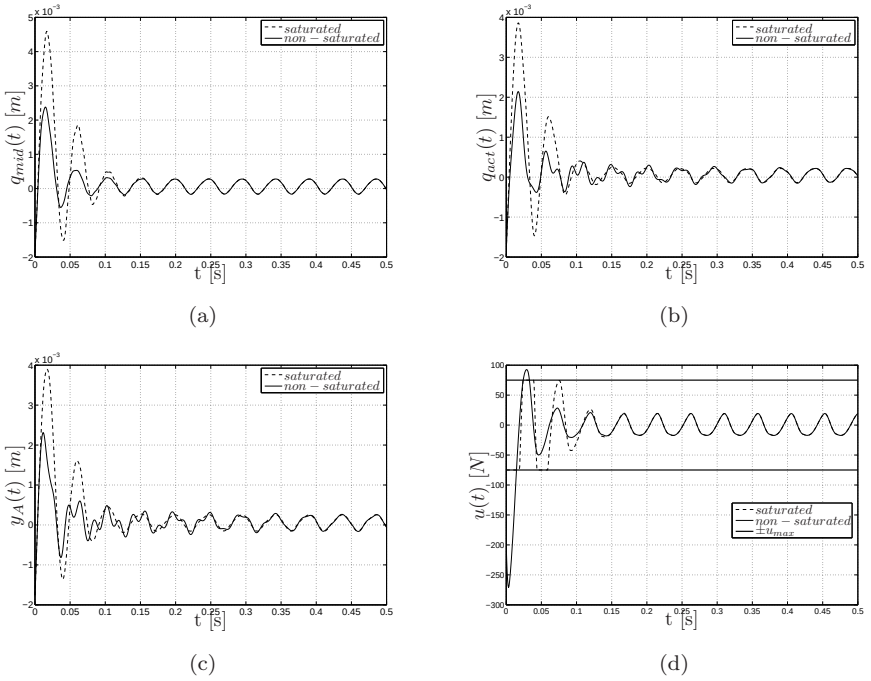

Figure C.4: (a) $q_{mid}(t)$; (b) $q_{act}(t)$; (c) $y_A(t)$ and (d) $u(t)$ for saturated (dashed curves) and non-saturated (solid curves) control action. $\frac{\omega}{2\pi} = 21Hz$, $R = 18N$ and $u_{max} = 75N$ for the saturated case.

thick solid curve, respectively. Once again, X_0 is the set of initial condition for both the saturated and non-saturated closed-loop systems, X_{cl} represents the set that includes the steady-state solutions ($\bar{x}_{cl}^{\omega}(t)$) of the non-saturated closed-loop system (note that since $X_{cl} \subseteq \Theta_\rho$, these are also steady-state solutions of the saturated system) and S reflects the largest set for which $|u| \leq u_{max}$ (see Section 3.4). Finally, the sets Θ_ρ, Θ_γ and $\Theta_{\mu_{max}}$ are depicted by the ellipsoids with light grey color, white color and dark grey color, respectively. Due to the fact that $\mu_{max} > \gamma > \rho = 1$, Θ_ρ lies inside Θ_γ and Θ_γ inside $\Theta_{\mu_{max}}$. Since $\Theta_\gamma \nsubseteq \Theta_\rho$, we cannot guarantee, based on the theory, that Θ_ρ is PI. Hence, even if $x_0 \in \Theta_\rho$ it is possible that the system will leave Θ_ρ and the actuator may ultimate saturate. Nevertheless, in the examined simulation case, the set of initial conditions X_0 clearly is a subset of the set Ω, since, as it is shown in Figures C.4 and C.5, the control action is saturated (i.e. solutions $x(t)$ are outside S for some $t \geq t_0$) but still the solutions of the saturated system starting from X_0 solutions eventually reach X_{cl}. Therefore, the fact that $\Theta_\gamma \nsubseteq \Theta_\rho$ does

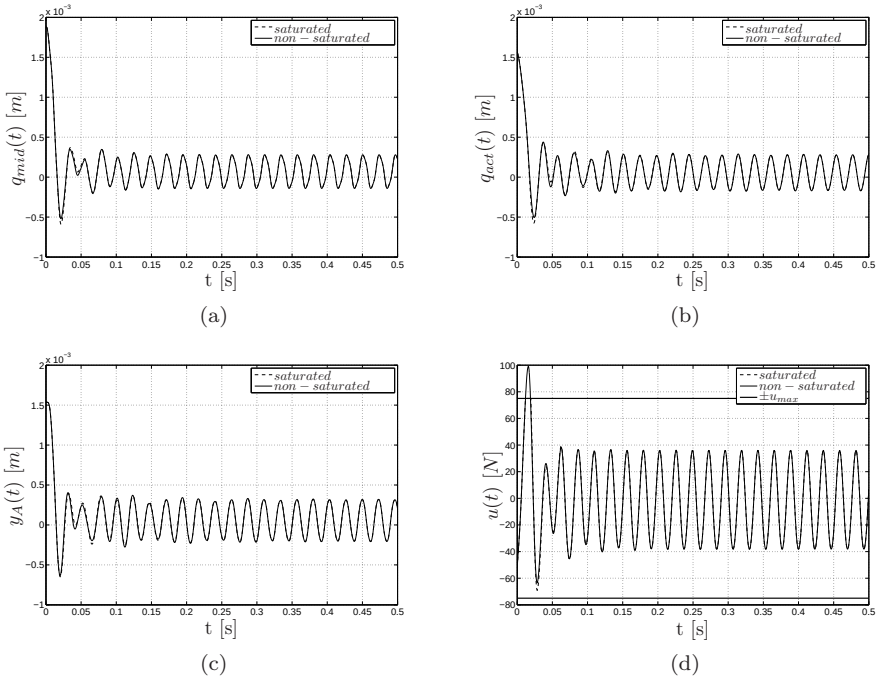

Figure C.5: (a) $q_{mid}(t)$; (b) $q_{act}(t)$; (c) $y_A(t)|$ and (d) $u(t)$ for saturated (dashed curves) and non-saturated (solid curves) control action. $\frac{\omega}{2\pi} = 43Hz$, $R = 50N$ and $u_{max} = 75N$ for the saturated case.

---

not prevent the state of the saturated system to reach the steady-state solution of the non-saturated system. The latter exposition aims to explain why indeed the saturated controller still exhibits satisfactory performance, as shown in simulations, while this is not guaranteed by the theory.

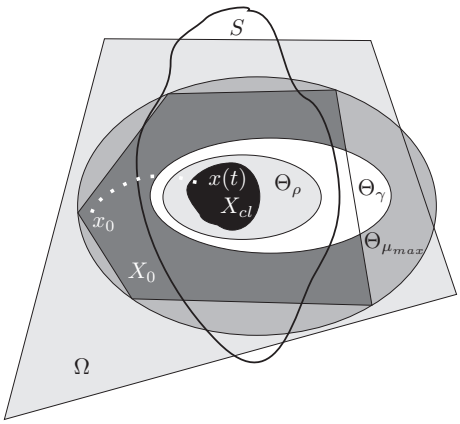

Figure C.6: Graphical illustration of the situation where the control action, related to $K_{IS,1}$, is saturated by 75N and the saturated closed-loop system still converges to the steady-state solution of the non-saturated closed-loop system.

D

Transformations in the model of the rotor dynamic system

In this appendix we will describe in detail the transformations applied to the model of the rotor dynamic system (6.2)-(6.6) in order to derive a new system that belongs to the class of Lur'e-type systems under study. In Section D.1, we apply a coordinate transformation to model (6.2)-(6.6) to transform system it into a Lur'e-type form with two monotone set-valued nonlinearities in the feedback-loop and to guarantee that it has the origin as equilibrium for every constant external input u_c. The set-valued nonlinearities correspond to the friction laws of the upper and lower discs. In Section D.2, we partially compensate the friction in the upper disc and we derive a Lur'e type system with a single (scalar) nonlinearity in the feedback loop. Finally, in Section D.3, we perform a loop transformation to the derived system to render the unique set-valued nonlinearity monotone and apply the proposed control design.

D.1 Coordinate transformation

We consider the rotor dynamic system (6.2)-(6.6). For a constant input voltage u_c, such that x_{eq} is a unique isolated equilibrium point of (6.2)-(6.6), we employ a coordinate transformation. This coordinate transformation ensures that the origin is the unique equilibrium point of the transformed system.

The new states are defined by:

$$\begin{aligned} \xi_1 = x_1 - x_{1eq} &= \alpha - \alpha_{eq} \\ \xi_2 = x_2 - x_{2eq} &= \omega_u - \omega_{eq} \\ \xi_3 = x_3 - x_{3eq} &= \omega_l - \omega_{eq}. \end{aligned} \tag{D.1}$$

The control input is $u = u_c + v = \frac{1}{k_m}[k_\theta \alpha_{eq} + T_{fu}(\omega_{eq})] + v$, where v is the input for the transformed model. The input voltage v will be zero for the

uncontrolled system. The state-space equations of the transformed system are given by

$$\begin{aligned}\dot{\xi}_1 &= \xi_2 - \xi_3 \\ \dot{\xi}_2 &= \tfrac{1}{J_u}[-k_\theta \xi_1 - k_\theta \alpha_{eq} + k_m u_c - T_{fu,tr}(\xi_2) + k_m v] \\ \dot{\xi}_3 &= \tfrac{1}{J_l}[k_\theta \xi_1 + k_\theta \alpha_{eq} - T_{fl,tr}(\xi_3)],\end{aligned} \tag{D.2}$$

with the transformed friction models for the upper disc $T_{fu,tr}(\xi_2)$ and the lower disc $T_{fl,tr}(\xi_3)$ given by (6.13) and (6.15) (see also Figures D.1 and D.2).

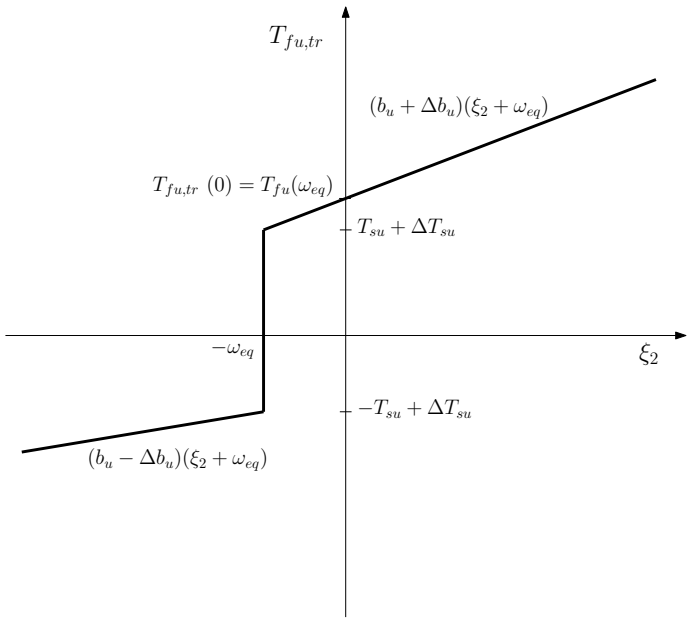

Figure D.1: Transformed upper friction model $T_{fu,tr}(\xi_2)$.

The transformed rotor dynamic model can be written into a form with a linear time-invariant system in the forward path and a set-valued nonlinearity in the feedback part. This form of the model is convenient for application of the circle criterion and the Popov criterion. These criteria will be used for observer and control design in the Chapter 6. The constants $-k_\theta \alpha_{eq} + k_m u_c$ and $k_\theta \alpha_{eq}$ in the right-hand side of the differential equations for ξ_2 and ξ_3 in (D.2), will be added to the friction models $T_{fu,tr}(\xi_2)$ and $T_{fl,tr}(\xi_3)$, see Figures D.1 and D.2 to create new friction models $T_{fu,tr2}(\xi_2)$ and $T_{fl,tr2}(\xi_3)$, see Figures D.3 and D.4. This results in a linear system for which zero input yields zero output, i.e $0 \in T_{fu,tr2}(0)$ and $0 \in T_{fl,tr2}(0)$.

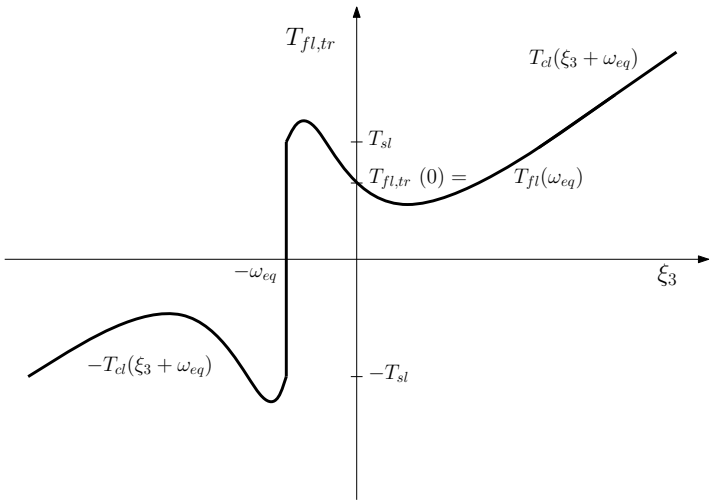

Figure D.2: Transformed lower friction model $T_{fl,tr}(\xi_3)$.

Then the model of the rotor dynamic system can be written as follows,

$$\begin{aligned} \dot{\xi} &= A\xi + Bv + Gw \\ z &= H\xi \\ w &\in -\varphi(z), \end{aligned} \tag{D.3}$$

with $\xi \in \mathbb{R}^3$, $z \in \mathbb{R}^2$, $\boldsymbol{\varphi} : \mathbb{R}^2 \to \mathbb{R}^2$, $w \in \mathbb{R}^2$ and with the matrices given by

$$A = \begin{bmatrix} 0 & 1 & -1 \\ -\frac{k_\theta}{J_u} & 0 & 0 \\ \frac{k_\theta}{J_l} & 0 & 0 \end{bmatrix}, \qquad B = \begin{bmatrix} 0 \\ \frac{k_m}{J_u} \\ 0 \end{bmatrix}, \qquad G = \begin{bmatrix} 0 & 0 \\ \frac{1}{J_u} & 0 \\ 0 & \frac{1}{J_l} \end{bmatrix}, \tag{D.4}$$

$$H = \begin{bmatrix} 0 & 1 & 0 \\ 0 & 0 & 1 \end{bmatrix}, \qquad \boldsymbol{\varphi}(z) = \begin{bmatrix} \varphi_1(z_1) \\ \varphi_2(z_2) \end{bmatrix} = \begin{bmatrix} T_{fu,tr2}(z_1) \\ T_{fl,tr2}(z_2) \end{bmatrix}. \tag{D.5}$$

The set-valued nonlinearities $T_{fu,tr2}(z_1)$, $T_{fl,tr2}(z_1)$ are given by

$$T_{fu,tr2}(z_1) \quad = T_{fu,tr}(z_1) - T_{fu}(\omega_{eq}), \tag{D.6}$$

$$T_{fl,tr2}(z_2) \quad = T_{fl,tr}(z_2) - T_{fl}(\omega_{eq}), \tag{D.7}$$

where $T_{fu,tr}(z_1)$ and $T_{fl,tr}(z_1)$ are given by (6.13) and (6.15), respectively.

Figures D.3 and D.4 show that the upper friction $T_{fu,tr2}$ is monotone, while the lower friction $T_{fl,tr2}$ is not monotone. Therefore both the observer and

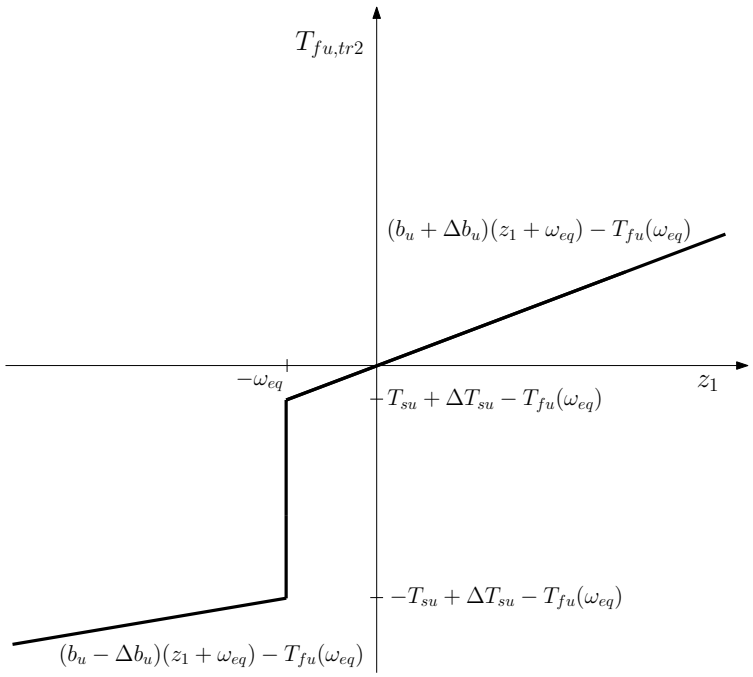

Figure D.3: Transformed upper friction model $T_{fu,tr2}(z_1)$.

control design can not be applied to the current form of the model of the rotor dynamic system. To overcome this problem, we transform the system via loop transformations, such that the lower friction $T_{fl,tr3}$ derived from this transformation, is monotone. The lopp transformation is given by

$$\begin{bmatrix} T_{fu,tr3} \\ T_{fl,tr3} \end{bmatrix} = \begin{bmatrix} T_{fu,tr2} \\ T_{fl,tr2} \end{bmatrix} + M \begin{bmatrix} \xi_2 \\ \xi_3 \end{bmatrix}. \tag{D.8}$$

Herein, the loop transformation matrix M is given by

$$M = \begin{bmatrix} -b & 0 \\ 0 & m \end{bmatrix}, \tag{D.9}$$

where $b = b_u - \Delta b_u$Nms/rad and $m = 0.1$ Nms/rad. Further information for the use of this loop transformation matrix M is given below. The minimum linear damping needed to render the transformed friction $T_{fl,tr3}$ monotone (i.e. to ensure that the derivative of $T_{fl,tr3}$ with respect to ξ_3 is larger or equal to zero $\forall \xi_3 \neq 0$), is less than the chosen value for m. In that way, a certain level of robustness with respect to rendering a changed friction $T^*_{fl,tr3}$ monotone is obtained, where $T^*_{fl,tr3}$ represents the actual friction acting on

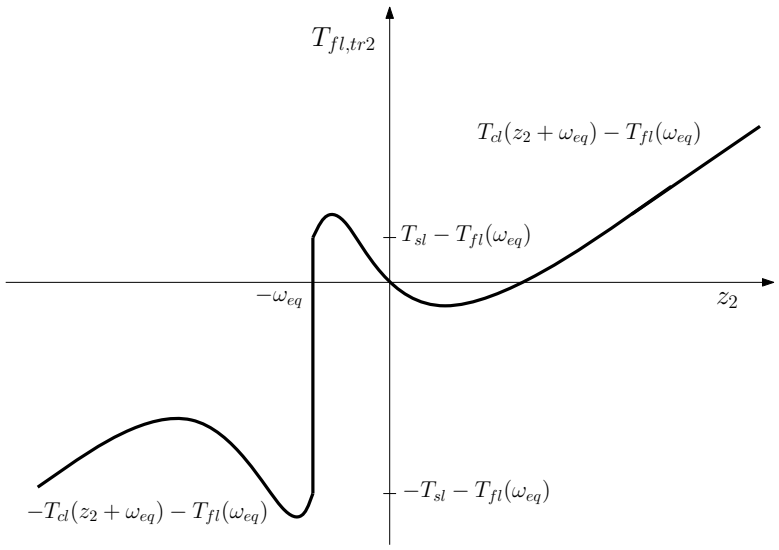

Figure D.4: Transformed lower friction model $T_{fl,tr2}(z_2)$.

the lower disc which may differ from the modeled friction model $T_{fl,tr3}$ (due to unavoidable modeling errors). By including the loop transformation matrix (D.8) in the structure of system (D.3)-(D.5), we obtain the system in (6.11) (with $\varphi_{tr,1}(z_1) = T_{fu,tr3}(z_1)$ and $\varphi_{tr,2}(z_2) = T_{fl,tr3}(z_2)$).

D.2 Friction compensation for the friction at the upper disc

We consider the rotor dynamic system (D.3)-(D.5) in Lur'e form. The Coulomb friction and the asymmetric part of the viscous friction acting on the upper disc (included in the friction map $T_{fu,tr2}$ of system (D.3)) are compensated by applying the following control law v to the rotor dynamic system (D.3):

$$v = v_{comp} + v_{control}, \tag{D.10}$$

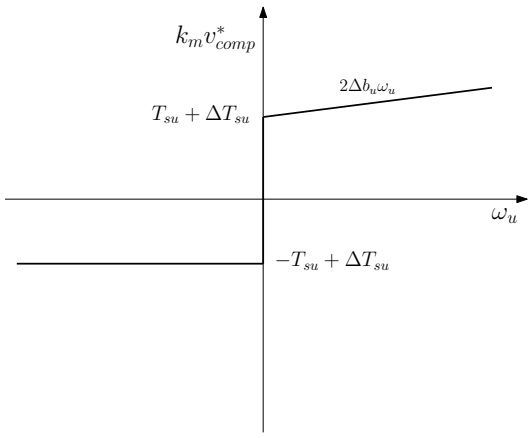

(a) Compensation $k_m v^*_{comp}$ for system (6.2)-(6.6).

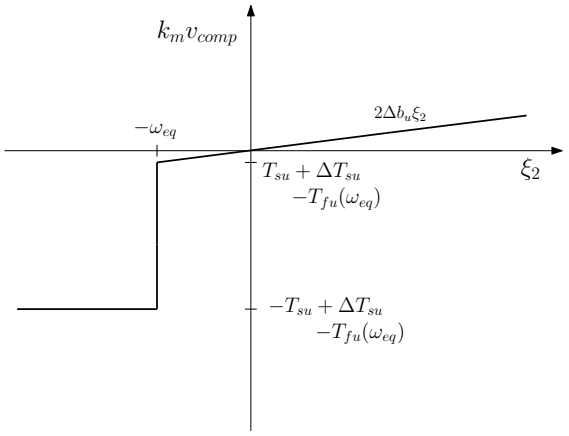

(b) Compensation $k_m v_{comp}$ for system (D.3)-(D.5).

Figure D.5: Compensation for different rotor dynamic models.

with $v_{control}$ as the new control input and where the friction compensation control input v_{comp} is given by

$$v_{comp}(\xi_2) \in \begin{cases} \frac{1}{k_m}(T_{su} + \Delta T_{su}\mathrm{sgn}(\xi_2 + \omega_{eq}) + b_u|\xi_2 + \omega_{eq}| \\ \qquad +\Delta b_u(\xi_2 + \omega_{eq}))\mathrm{sgn}(\xi_2 + \omega_{eq}) - \frac{1}{k_m}T_{fu}(\omega_{eq}) \\ \text{for } \xi_2 \neq -\omega_{eq} \\ \\ \frac{1}{k_m}\left[-T_{su} + \Delta T_{su} - T_{fu}(\omega_{eq}), T_{su} + \Delta T_{su} - T_{fu}(\omega_{eq})\right] \\ \text{for } \xi_2 = -\omega_{eq}. \end{cases} \tag{D.11}$$

The set-valued nonlinearity T_{fu} is described by (6.3) and the equilibrium velocity ω_{eq} is an element of x_{eq} corresponds to an equilibrium of system (6.2)-(6.6). The compensation control law v_{comp} partly compensates the friction acting on the upper disc. The remaining viscous damping $-\frac{1}{J_u}(b_u - \Delta b_u)\xi_2$ will be included in the linear part of the system. The reason for not compensating all the friction acting at the upper disc is that the remaining viscous damping may ultimately help to render the linear part of the system passive, as required in the control designs discussed in Chapters 5 and 6. The compensation $k_m v_{comp}$ for the rotor dynamic system (D.3)-(D.5) is depicted in Figure D.5(b). We show in Figure D.5(a), for clarity, the compensation $k_m v^*_{comp}$ for the rotor dynamic system (6.2)-(6.6) with v^*_{comp} as the compensation control law. The compensation $k_m v^*_{comp}$ represents a torque for this system. The relation between $k_m v_{comp}$ and $k_m v^*_{comp}$ is given by

$$k_m v_{comp} = k_m v^*_{comp} + T_{fu}(\omega_{eq}).$$

After the application of the control law for v in (D.10), the model of the rotor dynamic system (D.3) transforms to:

$$\begin{aligned} \dot{\xi} &= A_{new}\xi + B v_{control} + G_{tr} w \\ z &= H_{tr}\xi \\ w &\in -\varphi_{new}(z) \end{aligned} \tag{D.12}$$

with $\boldsymbol{\xi} \in \mathbb{R}^3$, $v_{control}, w, z \in \mathbb{R}$, $\varphi_{new} : \mathbb{R} \to \mathbb{R}$, and with the matrices and the set-valued nonlinearity φ_{new} in the feedback loop given by

$$A_{new} = \begin{bmatrix} 0 & 1 & -1 \\ -\frac{k_\theta}{J_u} & -\frac{1}{J_u}(b_u - \Delta b_u) & 0 \\ \frac{k_\theta}{J_l} & 0 & 0 \end{bmatrix}, \qquad B = \begin{bmatrix} 0 \\ \frac{k_m}{J_u} \\ 0 \end{bmatrix}, \qquad G_{tr} = \begin{bmatrix} 0 \\ 0 \\ \frac{1}{J_l} \end{bmatrix}, \tag{D.13}$$

$$H_{tr} = \begin{bmatrix} 0 & 0 & 1 \end{bmatrix}, \qquad \varphi_{new}(z) = T_{fl,tr2}(z). \tag{D.14}$$

The set-valued nonlinearity $T_{fl,tr2}$ is given by (D.7).

D.3 Loop transformation of the rotor dynamic system

For the application of the controller based on the Popov criterion to the rotor dynamic system (D.12)-(D.14), the set-valued nonlinearity φ_{new} in the feedback loop has to be monotone. Nevertheless, the set-valued nonlinearity $T_{fl,tr2}$, depicted in Figure D.6, is not monotone. To overcome this problem, the loop transformation presented in (D.8) and (D.9) is applied to the rotor dynamic system (D.12)-(D.14). As we mentioned in Section D.1, the value $m = 0.1$Nms/rad

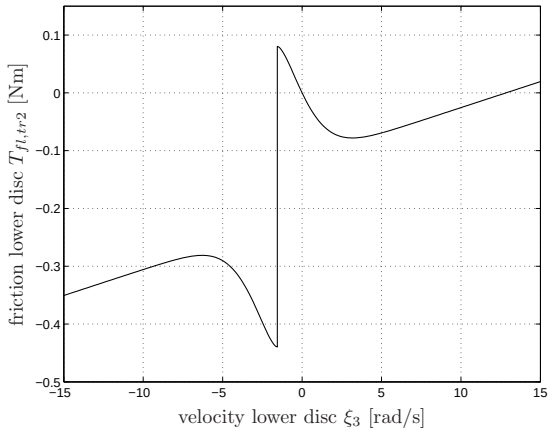

Figure D.6: Model of the friction $T_{fl,tr2}$ acting on the lower disc.

is chosen for the loop transformation, which transforms the friction map $T_{fl,tr2}$ into the monotone friction map $T_{fl,tr3}$. The reason for such choice is also explained in that section. The transformed system is described by (6.21)- (6.23).

E

Observer design implementations on the rotor dynamic system

In this Appendix, we design two observers for the rotor dynamic system given in (6.7) based on the results presented in Section 5.3.1 and we validate their performance based on simulations and experimental results. For the complete state reconstruction of the dynamic rotor system, the difference between the measured angular positions of the two discs is used as an output injection signal. In other words, the output matrix in (6.7) is given by $C = [1\ 0\ 0]$. Once again, these angular positions are measured using incremental encoders. For the validation of the observer for the dynamic rotor system we, firstly, show that the observer can reconstruct the state of the model. Secondly, we show experimentally that this also holds for the state of the real system.

Consider the model-based observer, which is taken of the form as in (5.31),

$$\begin{aligned} \dot{\hat{x}} &= A_{tr}\hat{x} + L(y - C\hat{x}) + G\hat{\bar{w}} + Bu \\ \hat{\bar{w}} &= -\bar{\varphi}(\hat{z}) \\ \hat{z} &= H\hat{x} + N(y - C\hat{x}) \\ \hat{y} &= C\hat{x}, \end{aligned} \tag{E.1}$$

where $\hat{x} \in \mathbb{R}^3$, $\hat{z}, \hat{\bar{w}} \in \mathbb{R}^2$, and $N \in \mathbb{R}^{2\times 1}$, $L \in \mathbb{R}^{3\times 1}$ are the observer gain matrices. The dynamics of the observer error $e = x - \hat{x}$ is then given by

$$\dot{e} = (A_{tr} - LC)e + G(\bar{w} - \hat{\bar{w}}) \tag{E.2a}$$

$$\bar{w} \in -\bar{\varphi}(Hx) \tag{E.2b}$$

$$\hat{\bar{w}} \in -\bar{\varphi}(H\hat{x} + N(y - \hat{y})). \tag{E.2c}$$

The observer will provide estimates for the state variables (i.e. also the velocities of the upper and lower discs). In simulations and experiments, we will compare the estimated values of the state variables with the simulated/measured values. Due to the fact that velocities are not measured directly in the experimental setup and in order to still provide a comparison measure for the estimated velocities provided by the observer (E.1), we will obtain estimates of the velocities of the discs by numerically differentiating the angular positions

of the discs and filtering the resulting signals using a low-pass filter. The high resolution of the encoders allows for accurately computing the aforementioned velocities.

The design of the observer (E.1) for system (6.7) entails finding gains L and N such that the triple $(A_{tr} - LC, G, H - NC)$ is strictly passive. By solving the LMIs in (5.35) using the LMITOOL for MATLAB [38] we can find L, N guaranteeing strict passivity of the triple $(A_{tr} - LC, G, H - NC)$. In the present case, two solutions are computed. The first solution to LMIs (5.35) is given by

$$L_1 = \begin{bmatrix} 13.8 \\ -4.37 \\ -165 \end{bmatrix}, N_1 = \begin{bmatrix} -0.572 \\ -7.07 \end{bmatrix}, P_1 = \begin{bmatrix} 3.1398 & 0.2726 & 0.2474 \\ 0.2726 & 0.4765 & 0.0000 \\ 0.2474 & 0.0000 & 0.0350 \end{bmatrix}. \tag{E.3}$$

for $\nu_1 = 0.154$. The eigenvalues of the matrix in the left-hand side of the second matrix inequality in (5.35) for $P = P_1$, $L = L_1$ and $N = N_1$ are: -1.4899, -4.1335, -70.141. Now we aim at a faster transient response by increasing ν in LMIs (5.35). The second solution to LMIs (5.35) is given by

$$L_2 = \begin{bmatrix} 195 \\ -312 \\ -9080 \end{bmatrix}, N_2 = \begin{bmatrix} -2.22 \\ -37.8 \end{bmatrix}, P_2 = \begin{bmatrix} 63.3492 & 1.0578 & 1.3230 \\ 1.0578 & 0.4765 & 0.0000 \\ 1.3230 & 0.0000 & 0.0350 \end{bmatrix}. \tag{E.4}$$

for $\nu_2 = 2.20$. The eigenvalues of the matrix in the left-hand side of the second matrix inequality in (5.35) for $P = P_2$, $L = L_2$ and $N = N_2$ are: -12.915, -0.6783, -0.0691. For simulation purposes, the input signal u in (6.2) is chosen to be a constant signal, $u = 2V$. At this point, we present simulations for the initial state for the system taken as $x(0) = [0 \;\; 0 \;\; 0]^T$ and for the observer as $\hat{x}(0) = [4 \;\; 4 \;\; 4]^T$. The observer is simulated, once again, using the dedicated technique for systems with set-valued characteristics based on the switch model presented in [80].

Simulation results

The simulation results are depicted in Figures E.1(a)-E.1(c) and E.2(a)-E.2(c). These results show transient responses. When a constant input voltage $u_c = 2$V is applied (i.e a constant torque is applied to the upper disc) stick-slip oscillations (torsional vibrations) occur due to the negative damping in the friction law (6.5) see Figures 6.6 and 6.7. During these oscillations, the velocity ω_l of the lower disc alternates between zero (stick phase) and positive values (slip phase). As guaranteed by the theory, the designed observer is able to provide the correct estimate of the state. In Figures E.1(a)-E.1(c), the responses α, $\hat{\alpha}$, ω_u, $\hat{\omega}_u$ and ω_l, $\hat{\omega}_l$ are shown. Moreover, the absolute values of the elements of the estimation error e are depicted in Figures E.2(a)-E.2(c). The observer estimates for the state variables and the absolute values of the estimation error

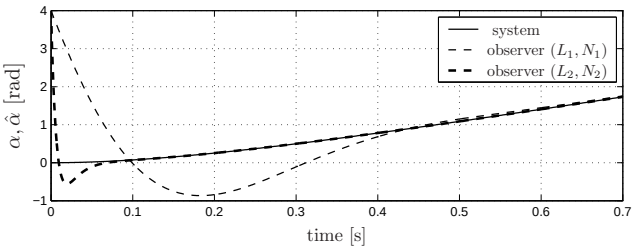

(a) Rotor dynamic system state component α and observer state component $\hat{\alpha}$.

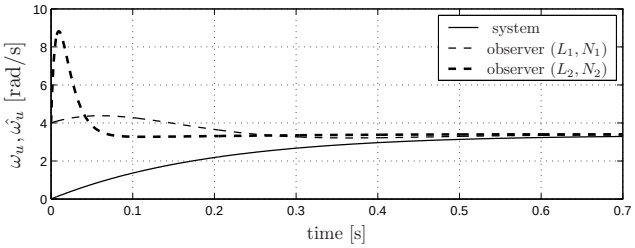

(b) Rotor dynamic system state component ω_u and observer state component $\hat{\omega}_u$.

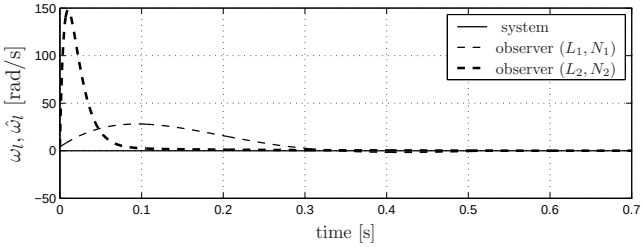

(c) Rotor dynamic system state component ω_l and observer state component $\hat{\omega}_l$.

Figure E.1: Responses of the rotor dynamic system and the two observers with different gains for the input voltage $u_c = 2.0$ V.

values are given for two pairs of observer gains (L_1, N_1) and (L_2, N_2). Based on these figures, the pair (L_2, N_2) leads to a faster transient convergence of the observer estimate to the system state than the pair (L_1, N_1). This is to be expected since the rate of the observer error to zero (given in (5.33)) related to the pair (L_2, N_2) ($\frac{\lambda_{min}(\nu_2 I)}{\lambda_{min}(P_2)} = 349.82$) is larger than this related to the pair (L_1, N_1) ($\frac{\lambda_{min}(\nu_1 I)}{\lambda_{min}(P_1)} = 10.72$). However, the pair (L_2, N_2) gives rise to larger transients errors than this of the pair (L_1, N_1).

The (squared) vector norm of the estimation error $\|e\|_2^2$ for the two observer

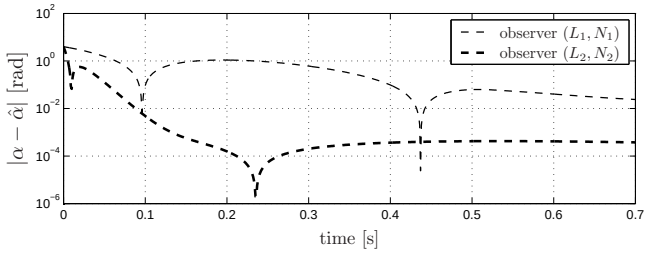

(a) Observer error $|\alpha - \hat{\alpha}|$.

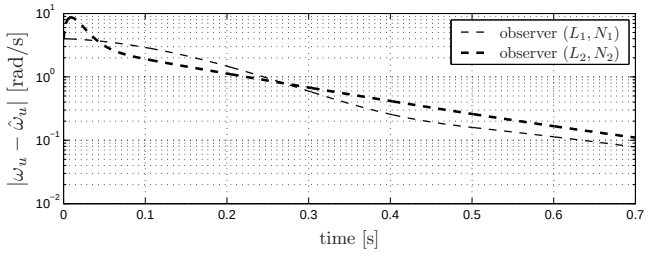

(b) Observer error $|\omega_u - \hat{\omega}_u|$.

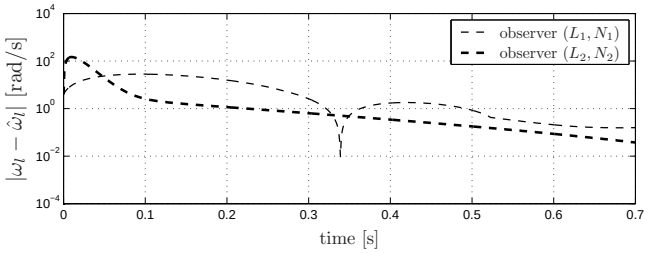

(c) Observer error $|\omega_l - \hat{\omega}_l|$.

Figure E.2: Observer error responses for different observer gains for the input voltage $u_c = 2.0\ V$.

gains together with an upper bound for the observer error, as given in (5.33), are depicted in Figures E.3(a), E.3(b). The constant input is $u_c = 2V$ and the time interval of the simulations is [0, 5]s. These figures show that the provided error bound is conservative and that the estimation error converges to zero.

In Figure E.4(a), we depict the responses $\hat{\omega}_l$, ω_l, and in Figure E.4(b) we depict the observer error $|\omega_l - \hat{\omega}_l|$ for (L_1, N_1) and for $u_c = 3.5V$. The initial condition for the rotor dynamic system is $x(0) = [3.5 \quad 6 \quad 0]^T$ and for the observer $\hat{x}(0) = [4 \quad 4 \quad 4]^T$. Note that the choice for $x(0)$ leads the system to exhibit limit cycling. Based on the results of Figure E.4, the observer is able to estimate the rotor dynamic state for both slip and stick phase.

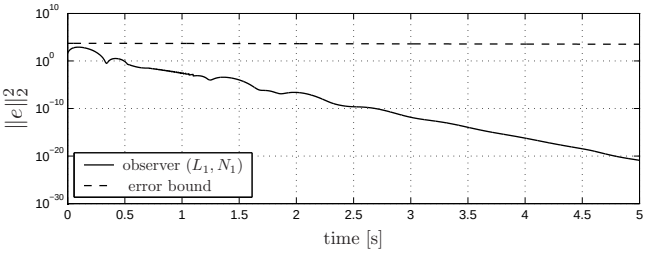

(a) Observer error of observer with gains L_1 and N_1.

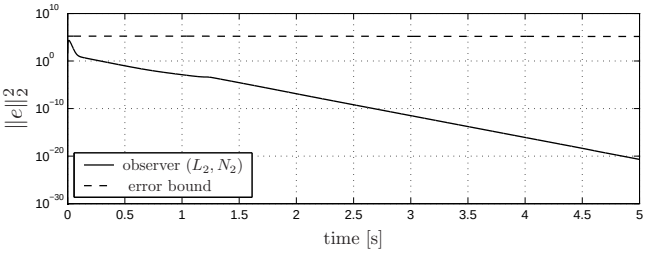

(b) Observer error of observer with gains L_2 and N_2.

Figure E.3: Squared vector norm of (and a bound for) the observer error of the two observer gains for the input voltage $u_c = 2.0V$.

In Figures E.5(a)-E.5(c), we depict the observer estimates $\hat{\alpha}_l$, $\hat{\omega}_u$ and $\hat{\omega}_l$ for the observer gain (L_1, N_1) and the corresponding responses α_l, ω_u and ω_l. In these figures, the input voltage u_c is changed from $2.7V$ to $2.2V$ at $t = 0.25s$. The initial condition $x(0)$ are the equilibrium values corresponding to the input voltage $u_c = 2.7$V i.e. $x(0) = x_{eq} = [1.35\ 4.62\ 4.62]$ and the initial condition $\hat{x}(0)$ is $\hat{x}(0) = [0\quad 3\quad 3]^T$. As guaranteed by the theory, the observer error converges to zero despite the sudden change in the input u_c.

Experimental results

As it was mentioned in the beginning of Subsection 6.3.1, the response α of the experimental setup is measured and the responses ω_u, ω_l are computed (using numerical differentiation of the measured displacements of the upper and lower discs). We use the same input voltage ($u = 2V$) as for the first simulation results. The measured state component α and the observer estimate $\hat{\alpha}$ for (L_1, N_1) and (L_2, N_2) are depicted in Figures E.6(a) and E.9(a), respectively. The absolute value of the observer error $|\alpha - \hat{\alpha}|$ and the observer error $\alpha - \hat{\alpha}$ for (L_1, N_1) and (L_2, N_2) are depicted in Figures E.6(b), E.6(c) and E.9(b), E.9(c), respectively. Finally, the computed state components ω_u, ω_l and the estimated state components $\hat{\omega}_u$, $\hat{\omega}_l$ are depicted in Figures E.7 and E.8 for (L_1, N_1).

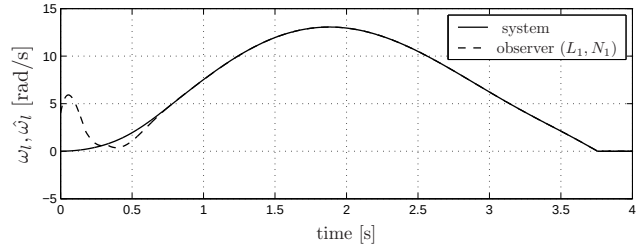

(a) Rotor dynamic system state component ω_l and observer state component $\hat{\omega}_l$.

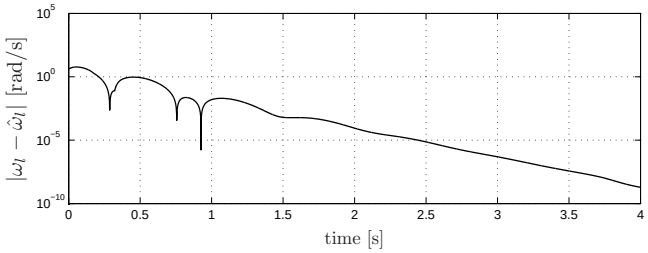

(b) Observer error $|\omega_l - \hat{\omega}_l|$.

Figure E.4: Response of the rotor dynamic system and the observer with the gains L_1 and N_1 for the input voltage $u_c = 3.5$ V.

The experimental results show that the designed observer is able to provide accurate estimates of the state of the experimental setup. The observer error related to α does not converge to zero exactly, but oscillates between 0.01 and -0.03rad for (L_1, N_1) and between $5 \cdot 10^{-4}$ and $-8 \cdot 10^{-4}$rad for (L_2, N_2). This error is small compared to the magnitude of the state, but larger than in the simulation results. The residual error can be attributed to (inevitable) model errors and sensor imperfections.

The mismatch between the observer behavior and the dynamic rotor system behavior in steady-state (see the remaining observer error in Figures E.6(c) and E.9(c) and the transient convergence speed (see Figures E.6(b) and E.9(b)) form the guideline for the evaluation of the computed observer gains (L_1, N_1) and (L_2, N_2). Namely, the observer design aims at a fast transient convergence and low sensitivity to model errors and measurement noise. More specifically, we compute different observer gains that satisfy the LMI constraints (5.35) by varying the constant ν, respectively. For every pair of observer gains (L, N) we can measure the magnitude of the observer error in steady-state and the time required for this error to converge to its steady-state. This knowledge can then be used to assess the effect of the choice of the observer gain on both the transient performance and the steady-state sensitivity to modeling errors and measurement noise. This is exactly the trade off between such

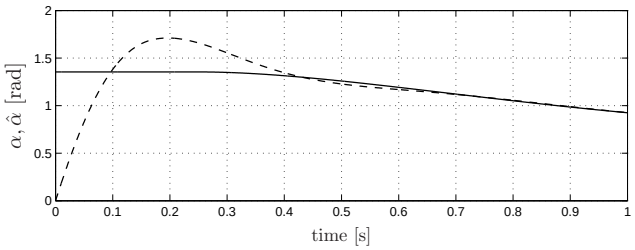

(a) Rotor dynamic system state component α (solid line) and observer state component $\hat{\alpha}$ (dashed line).

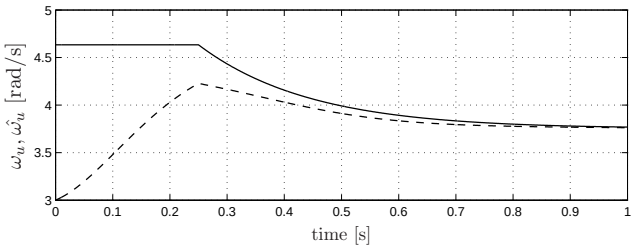

(b) Rotor dynamic system state component ω_u (solid line) and observer state component $\hat{\omega}_u$ (dashed line).

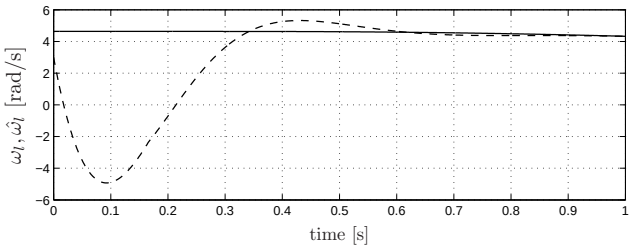

(c) Rotor dynamic system state component ω_l (solid line) and observer state component $\hat{\omega}_l$ (dashed line).

Figure E.5: Responses of the rotor dynamic system and the observer with the gains L_1 and N_1, the input voltage decreases with a step on $t = 0.25$ s from $u_c = 2.7$ V to $u_c = 2.2$ V.

transient and steady-state performance that determines the ultimate choice for the observer gains. From this perspective, the observer gains L_2, N_2 (see (E.4)) are preferable with respect to the observer gains L_1, N_1 (see (E.3)) for the present application, because they result in an observer error with smaller amplitude and faster convergence to zero than the observer error that uses the gains L_1, N_1.

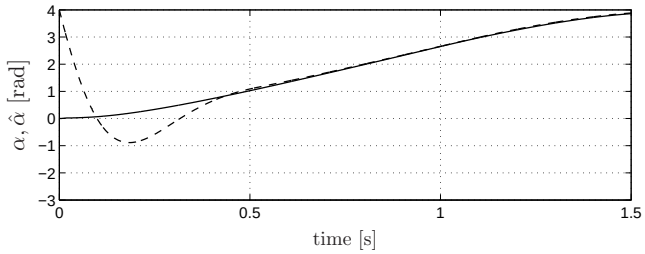

(a) Measured and observed state component α (solid line) and $\hat{\alpha}$ (dashed line), respectively.

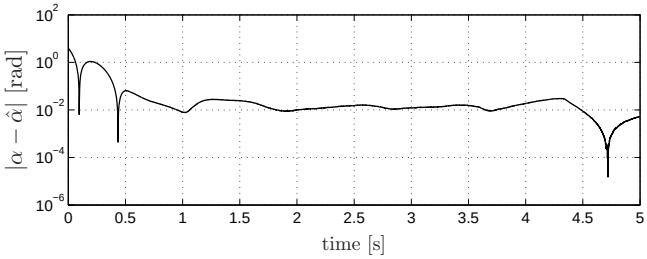

(b) The observer error $|\alpha - \hat{\alpha}|$.

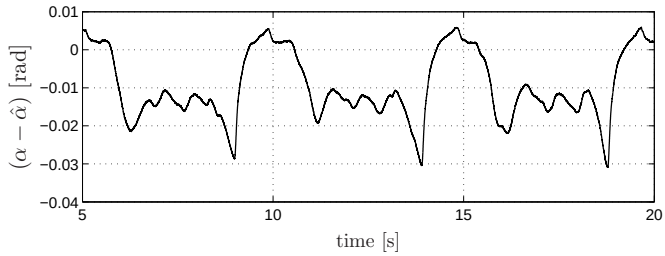

(c) The observer error $(\alpha - \hat{\alpha})$.

Figure E.6: Comparison of the measured state component α with the state component $\hat{\alpha}$ of the observer with the gains L_1 and N_1 for $u_c = 2.0$ V.

In case it is designed to further reduce the effects of model errors and measurement noise in the examined system aiming at even higher steady-state (estimation) performance, we could use more accurate models to describe the system dynamics. Furthermore, encoders with higher precision are needed in order to decrease the measurement noise in the signals that are used to recover the system state. The drawback of aiming at more accurate models is that, in most cases, this will lead to models of higher order and/or higher complexity. As a result, the calculation of the observer responses becomes (too) compu-

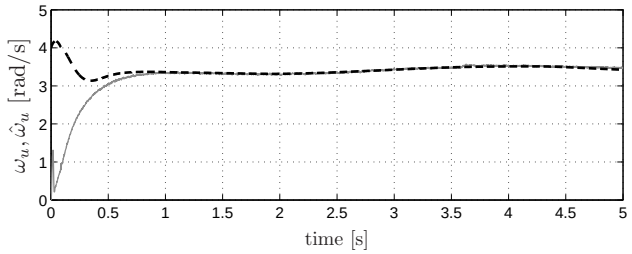

(a) State component ω_u and estimate $\hat{\omega}_u$ for $0 \leq t \leq 5$.

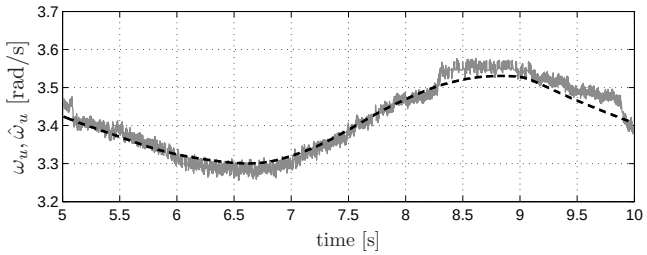

(b) State component ω_u and estimate $\hat{\omega}_u$ for $5 \leq t \leq 10$.

Figure E.7: Comparison of the response $\hat{\omega}_u$ of the observer with the gains L_1 and N_1 (black dashed line) and the response ω_u, derived by numerically differentiating the measured signal θ_u, (grey solid line) for $u_c = 2.0$ V.

tationally expensive. This is not favorable for the on-line implementation of observer designs in real systems. Moreover, the drawback of using high precision encoders is that these are generally expensive and hence often prohibitive in commercial application.

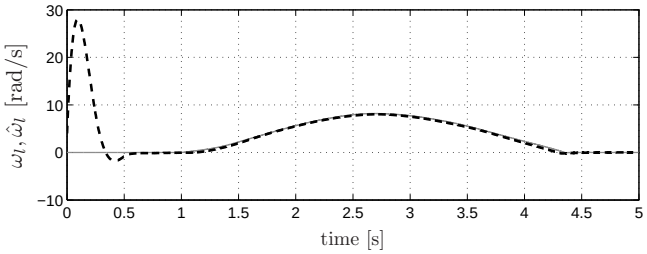

(a) State component ω_l and estimate $\hat{\omega}_l$ for $0 \leq t \leq 5$.

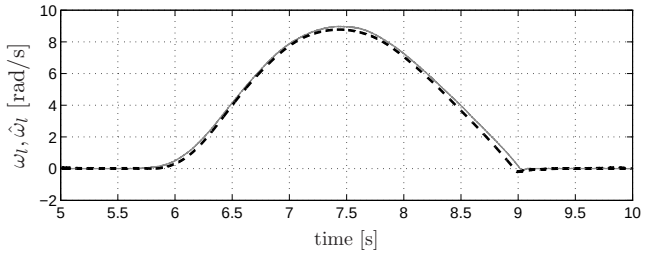

(b) State component ω_l and estimate $\hat{\omega}_l$ for $5 \leq t \leq 10$.

Figure E.8: Comparison of the response $\hat{\omega}_l$ of the observer with the gains L_1 and N_1 (black dashed line) and the response ω_l, derived by numerically differentiating the measured signal θ_l, (grey solid line) for $u_c = 2.0$ V.

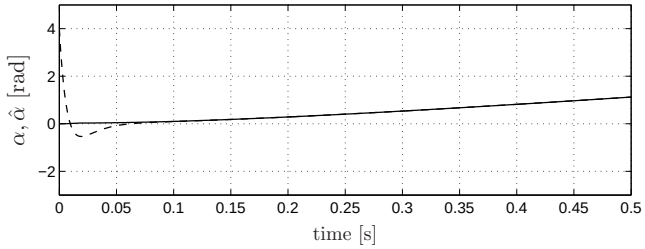

(a) Measured and observed state component α (solid line) and $\hat{\alpha}$ (dashed line), respectively.

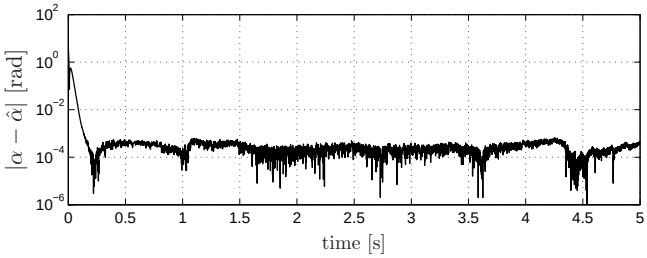

(b) The observer error $|\alpha - \hat{\alpha}|$.

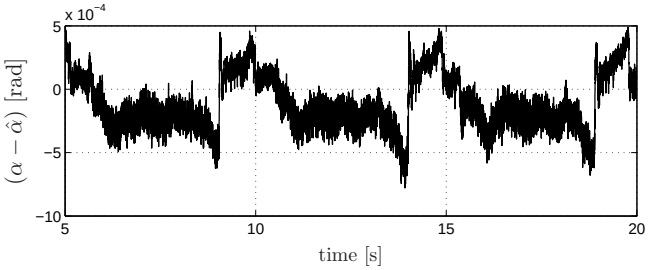

(c) The observer error $(\alpha - \hat{\alpha})$.

Figure E.9: Comparison of the measured state component α with the state component $\hat{\alpha}$ of the observer with the gains L_2 and N_2 for $u_c = 2.0$ V.

F

Simulations-Experiments for friction characteristic II

Theoretically, the output-feedback controller proposed in Section 6.3.3 renders the rotor dynamic system absolutely stable for any friction model of the form (6.5), as long as this friction model is a monotone set-valued nonlinearity in the sector $[0\ \infty]$ (after the transformation as used before). We will show this robustness property also experimentally. For this purpose, we will change the friction of the lower disc by applying an additional normal force on the brake that creates an adapted friction characteristic and we will apply the output-feedback controller again to the system, see Figure 6.5 for the adapted friction characteristic II.

Consider the system (6.2)-(6.6) with parameter values taken from Table 6.2 (friction characteristic II). As mentioned in Section 6.3, by performing the loop transformation, this system can be written in a Lur'e type form that consists of a linear part and a monotone set-valued nonlinearity in the feedback loop. This system is described by (6.11) with system matrices given by (6.8) and (6.9). As long as the value of m is larger than the maximal negative slope of the graph related to friction (6.5), (6.6) with friction characteristic II (see Figure 6.5) then the resulting nonlinearity $\varphi_{tr,1}$ in (6.12) is still monotone and such changes in the values of the friction (6.5), (6.6) do not influence the linear part of the system.

By using the observer (E.1), the state variables of the rotor dynamic system are estimated. As the calculation of the observer gains $(L,\ N)$ based on the matrix inequality (5.35), only depends on the linear system matrices and the control gain K, the solutions $(L_2,\ N_2)$ and K for the system with friction characteristic I is also applicable to the system with friction characteristic II.

In Figures F.1(a)-F.1(b), the bifurcation diagrams of ω_l and α for bifurcation parameter u_c are depicted. The responses ω_l and α are the steady-state responses of the closed-loop system with friction characteristic II. The control input u is limited to $[-5,\ 5]$V. In these figures, the marks $\circ$ and $\times$ represent experimental results and the solid line simulations. More specifically, $\circ$ depicts the maximum and minimum value of the state on the stable limit cycles and $\times$ depicts stable equilibria. The solid lines represent the model-based globally asymptotically stable equilibrium branches for ω_l and α. These figures show that the equilibrium branches of the experimental system and the model re-

sponses correspond well for the input range $u_c \in [1.5,\ 5]$V. Moreover, in the range $u_c \in [1.5,\ 1.75]$V it is shown that the experimental system has two stable steady-state solutions: a stable equilibrium and a stable limit cycle. On the other hand, the model has a unique steady-state solution: a stable equilibrium (as guaranteed by the theory). Finally, for input voltages below 1.5V the experimental system exhibits only stable limit cycles and the model only stable equilibria. Based on this analysis, it is clear that on simulation level we can achieve a unique globally asymptotically stable equilibrium branch for the whole input range $u_c \in [0,\ 5]$V, as guaranteed by the theory. On the other hand, this appears not to be possible in practice. Again, a possible reason for this fact is the presence of position-dependent (unmodeled) friction or noise in the measurement devices.

In Figures F.2(a)-F.2(b), we compare the experimental bifurcation diagrams of the open-loop system with the experimental bifurcation diagram of the closed-loop system. In these figures, the marks $\circ$, $\times$ represent closed-loop results and the marks $*$, $+$ open-loop results. The aforementioned diagrams show that the output-feedback controller significantly extends the region in which only stable equilibria occur. For the open-loop system, this region covers the constant input voltages $u_c \in [4.0,\ 5.0]$V. The closed-loop system extends the region with only stable equilibria to the constant input voltages in $u_c \in [1.75,\ 5.0]$V.

Based on Figures 6.21, 6.22, F.1 and F.2, we conclude that the output-feedback controller (6.30) with control gain given in (6.34) is able to render the rotor dynamic system with friction characteristics I and II (see Figure 6.5) stable. This robustness property with respect to changes in the friction characteristics is guaranteed by the absolute stability of the closed-loop system. Such robustness property is crucial in practice since changes in friction characteristics due to temperature variations, humidity changes, wear or contamination of the lubricants is inevitable.

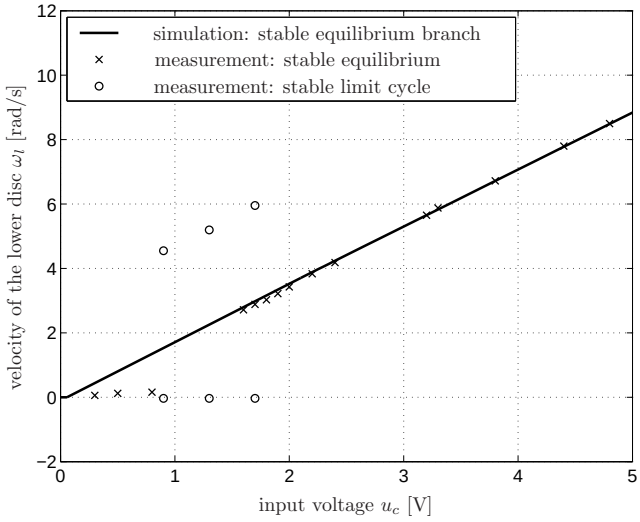

(a) Bifurcation diagram with the velocity of the lower disc.

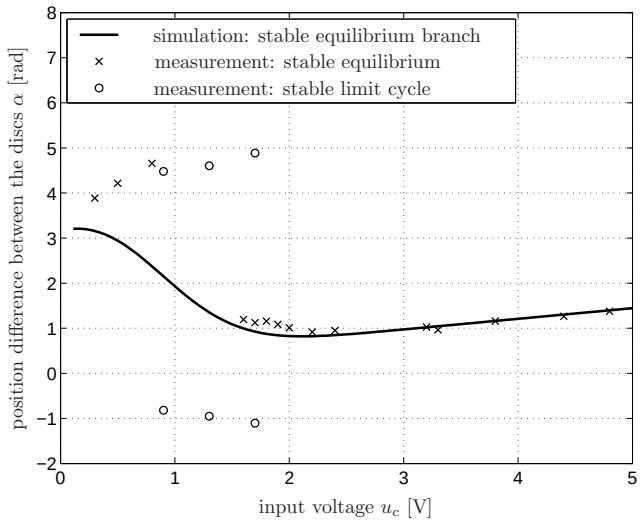

(b) Bifurcation diagram with the position difference between the upper and the lower disc.

Figure F.1: Bifurcation diagrams of the closed-loop system with control gain $K_1 = [15.9 \quad 1.57 \quad 27.6]$ *for positive input voltages (friction characteristic II for friction at the lower disc); observer gains are* L_2 *and* N_2.

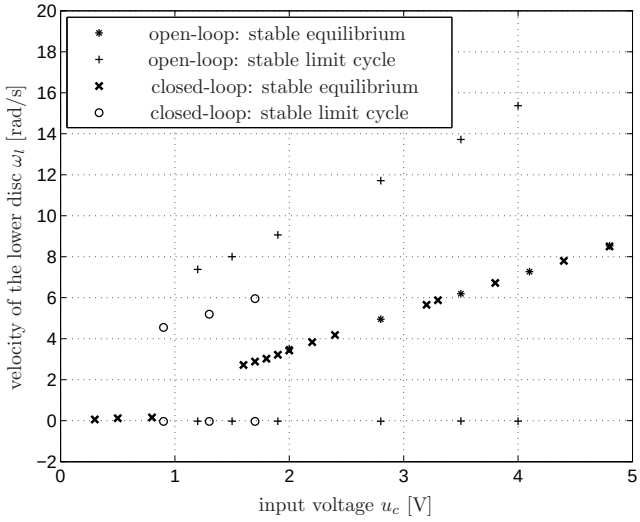

(a) Bifurcation diagram with the velocity of the lower disc.

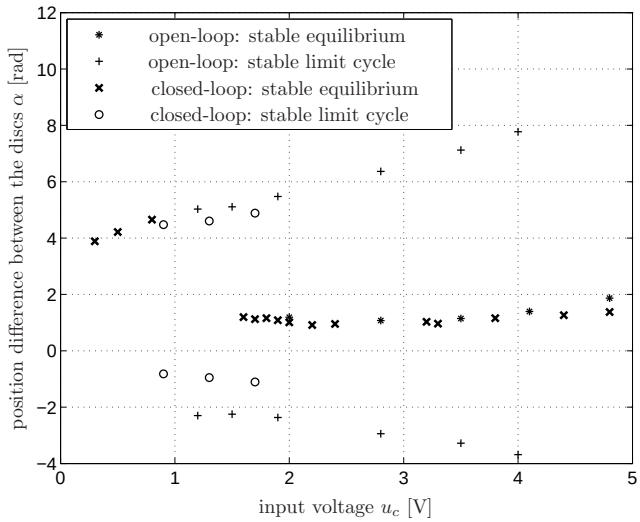

(b) Bifurcation diagram with the position difference between the upper and the lower disc.

Figure F.2: Bifurcation diagrams of the open-loop and closed-loop system with control gain $K_1 = [15.9 \quad 1.57 \quad 27.6]$ *for positive input voltages (and using friction characteristic II for friction at the lower disc).*

Bibliography

[1] F. Abbasssian and V.A. Dunayevsky. Application of stability approach to torsional and lateral bit dynamics. *SPE Drilling and Completion*, 13(2):99–107, 1998.

[2] F. Al-Bender, V. Lampaert, and J. Swevers. Modeling of dry sliding friction dynamics: From heuristic models to physically motivated models and back. *Chaos*, 14(2):446–460, 2004.

[3] Y. Altintas. *Manufacturing automation*. Cambridge University Press, Cambridge, UK, 2000.

[4] D. Angeli. A Lyapunov approach to incremental stability properties. *IEEE Trans. Automatic Control*, 47(3):410–421, 2002.

[5] M. Arcak and P. Kokotović. Feasibility conditions for circle criterion designs. *Systems and Control Letters*, 42(5):405–412, April 2001.

[6] M. Arcak, M. Larsen, and P. Kokotović. Circle and Popov criteria as tools for nonlinear feedback design. *Automatica*, 39(4):643–650, April 2003.

[7] B. Armstrong-Hélouvry. *Control of Machines with Friction*. Kluwer Academic Publishers, 1991.

[8] B. Armstrong-Hélouvry, P. Dupont, and C. Canudas de Wit. A survey of models, analysis tools and compensation methods for the control of machines with friction. *Automatica*, 30(7):1083–1138, 1994.

[9] U.M. Ascher, R.M.M. Mattheij, and R.D. Russel. Numerical solution of boundary value problem for ordinary differential equations. *Society for Industrial and Applied Mathematics*, 1995.

[10] J.-P. Aubin and A. Cellina. *Differential inclusions*. Springer-Verlag, Berlin, 1984.

[11] A. Bemporad, A. Garulli, S. Paoletti, and A. Vicino. Data classification and parameter estimation for the identification of piecewise affine models. In *Conf. on Decision and Control*, volume 1, pages 20– 25, Atlantis, Paradise Island, Bahamas, 2004.

[12] S. Bennett. *History of Control Engineering*. Peter Perigrinos, Sterenge, 1979.

[13] P.A. Bliman and A.M. Krasnosel'skii. Popov absolute stability criterion for time-varying multivariable nonlinear systems. In *Proc. of the 5th European Control Conference*, Karlsruhe, Germany, 1999.

[14] J.H. Bonsel, R.H.B. Fey, and H. Nijmeijer. Application of a dynamic vibration absorber to a piecewise linear beam system. *Nonlinear Dynamics*, 37:227–243, 2004.

[15] S. Boyd, El Ghaoui, E. Feron, and V. Balakrishnan. *Linear Matrix Inequalities in Control Theory*, volume 15 of *Studies in Applied Mathematics*. SIAM, 1994.

[16] H. Brézis. *Operateurs Maximaux Monotones*. North-Holland/American Elsevier, Amsterdam, 1973.

[17] B. Brogliato. *Nonsmooth Mechanics: Models, Dynamics and Control*. Springer-Verlag, Berlin, 1999.

[18] B. Brogliato. On the control of nonsmooth complementarity dynamical systems. *Philosophical Transactions of the Royal Society series A (Mathematical, Physical and Engineering Sciences)*, 359(1789):2369–2384, 2001.

[19] B. Brogliato. Absolute stability and the Lagrange-Dirichlet theorem with monotone multivalued mappings. *System and Control Letters*, 51:343–353, 2004.

[20] B. Brogliato, A. Daniilidis, C. Lemarchal, and V. Acary. On the equivalence between complementarity systems, projected systems and unilateral differential inclusions. *Systems and Control letters*, 55:45–51, 2006.

[21] J.M.W. Brownjohn. Obsevations on non-linear dynamic characteristics of suspension bridges. *Earthquake engineering and structural dynamics*, 23:1351–1367, 1994.

[22] D. Bryja and P. Sniady. Stochastic non-linear vibrations of highway suspension bridge under inertial sprung moving load. *Journal of sound and vibration*, 216:507–519, 1998.

[23] M. Camlibel and J. Schumacher. Existence and uniqueness of solutions for a class of piecewise linear dynamical systems. *Linear Algebra and its Applications*, 351:147–184, 2002.

[24] M.K. Camlibel, W.P.M.H. Heemels, and J.M. Schumacher. On linear passive complementarity systems. *European Journal of Control*, 8(3):220–237, 2002.

[25] C. Canudas de Wit and C.C. Ge. Adaptive friction compensation for systems with generalized velocity/position friction dependency. In *Proc. of the* 36^{st} *IEEE Conf. on Decision and Control*, volume 3, pages 2465–2470, San Diego, USA, 1997.

[26] C. Canudas de Wit, P. Noel, A. Aubin, and B. Brogliato. Adaptive friction compensation in robot manipulators: Low-velocities. *International Journal of Robotics Research*, 10(3):189–199, 1991.

[27] Ch. G. Cassandras and J. Lygeros. *Stochastic Hybrid Systems*. Control engineering series, CRC Taylor & Francis, 2006.

[28] E. Cataldi and Ch. Glocher. Curve squealing of railroad vehicles. In *Proc. of the 5th EUROMECH Nonlinear Oscillations Conference*, volume 17, pages 1970–1976, Eindhoven, The Netherlands, 2005.

[29] E. Coddington and N. Levinson. *Theory of Ordinary Differential Equations*. McGraw-Hill, New York, 1955.

[30] R.R. Craig, Jr. A review of time-domain and frequency-domain component mode synthesis methodes, combined experimental/analytical modeling of dynamic structural systems using substructure synthesis. *ASME Applied Mechanics AMD-67, New York*, pages 1–31, 1985.

[31] C. Canudas de Wit, A. Miguel, F. Corchero, F.R. Rubio, and E. Navarro-Lpez. D-oskil: a new mechanism for suppressing stick-slip in oil well drillstrings. In *Proc. of the 44th IEEE Conf. on Decision and Control, and the European Control Conf.*, pages 493–499, Seville, Spain, 2005.

[32] B.P. Demidovich. *Lectures on stability theory (in Russian)*. Nauka, Moscow, 1967.

[33] S.H. Doole and S.J. Hogan. A piecewise linear suspension bridge model: Nonlinear dynamics and orbit continuation. *Dynamics and Stability of Systems*, 11(1):19–47, 1996.

[34] A. Doris, C.G.M. de Bont, R. Wouters, N. van de Wouw, and H. Nijmeijer. Active disturbance attenuation for an experimental piecewise linear beam system. In *1st IFAC Conf. on Analysis and Control of Chaotic Systems.*, Reims, France, 2006.

[35] A. Doris, A. Juloski, M. Heemels, N. van de Wouw, and H. Nijmeijer. Switching observer design for an experimental piece-wise linear beam system. In *Proc. of the 16th IFAC conf.*, Prague, Czech Republic, 2005.

[36] A. Doris, J.Lj. Juloski, N. Mihajlović, M. Heemels, N. van de Wouw, and H. Nijmeijer. Observer design for experimental non-smooth and discontinuous systems. *submitted*.

[37] A. Doris, N. van de Wouw, and H. Nijmeijer. Disturbance attenuation for a periodically excited piece-wise linear beam system. In *Proc. of the ENOC Conf.*, volume 1, pages 301–310, Eindhoven, The Netherlands, 2005.

[38] El Ghaoui and J.L. Commeau. LMITOOL: a package for LMI optimization in Scilab user's guide. 1999. web site: http://robotics.eecs.berkeley.edu/ elghaoui/lmitool/lmitool.html.

[39] G. Feng, G. P. Lu, and S. S. Zhou. An approach to H_∞ controller synthesis of piece-wise linear systems. *International Press communications in information and systems*, 2(3):245–254, 2002.

[40] G. Ferrari-Trecate, F.A. Cuzzola, D. Mignone, and M. Morari. Analysis of discrete-time piecewise affine and hybrid systems. *Automatica*, 38(12):2139–2146, 2002.

[41] R.H.B. Fey. *Steady-state behaviour of reduced dynamic systems with local nonlinearities*. PhD thesis, Eindhoven University of Technology, Einhoven, The Netherlands, 1992.

[42] A. F. Filippov. *Differential Equations with Discontinuous Righthand Sides*. Mathematics and its Applications. Kluwer, Dordrecht, The Netherlands, 1988.

[43] B. Friedlan and S. Mentzelopoulou. On adaptive friction compensation without velocity measurements. volume 2, pages 1076–1081, Dayton, OH, USA, 1992.

[44] V. Fromion, S. Monaco, and D. Normand-Cryot. A possible extension of H_∞ control to the nonlinear context. In *Proc. of the* 34^{th} *IEEE Conf. on Decision and Control*, pages 975–980, New Orleans, Louisiana, USA, 1995.

[45] V. Fromion, S. Monaco, and D. Normand-Cyrot. Asymptotic properties of incrementally stable systems. *IEEE Trans. Automatic Control*, 41:721–723, 1996.

[46] V. Fromion, S. Monaco, and D. Normand-Cyrot. A link between input-output stability and Lyapunov stability. *Systems and Control Letters*, 27:243–248, 1996.

[47] V. Fromion, G. Scorletti, and G. Ferreres. Nonlinear performance of a PI controlled missile: an explanation. *Int. J. Robust Nonlinear Control*, 9:485–518, 1999.

[48] Ch. Glocker. *Set-valued force laws: dynamics of nonsmooth systems*. Springer-Verlag, Berlin, 2001.

[49] Ch. Glocker. Newton's and poisson's impact law for the non-convex case of re-entrant corners. complementarity, duality and symmetry in nonlinear mechanics. In *Proc. of the IUTAM Symposium*, volume 6, pages 101–125, Kluwer Akad. Publ., 2004.

[50] Ch. Glocker and Ch. Studer. Formulation and preparation for numerical evaluation of linear complementarity systems in dynamics. *Multibody System Dynamics*, 13(4):447–463, 2005.

[51] D. Goodall and E. Ryan. Feedback controlled differential inclusions and stabilization of uncertain dynamical systems. *Journal on Control and Optimization*, 26(6):14311441, 1988.

[52] G.W. Halsey, A. Kyllingstad, and A. Kylling. Torque feedback used to cure slip-stick motion. In *63rd SPE Annual Technical Conf. and Exhibition*, pages 277–282, 1988.

[53] C. H. Hansen and S. D. Snyder. *Active Control of Noise and Vibration*. Spon Press (UK), 1997.

[54] A. Hassibi and S. Boyd. Quadratic stabilization and control of piece-wise linear systems. In *Proc. of the American Control Conf.*, volume 1, pages 3659–3664, Philadelphia PA., USA, 2005.

[55] W.P.M.H. Heemels, A.Lj. Juloski, and B. Brogliato. Observer and control design for Lure's systems with multivalued mappings. In *Proc. of the 16th IFAC World Congress 2005*, Prague, Czech Republic, 2005.

[56] W.P.M.H. Heemels, J.M. Schumacher, and S. Weiland. Well-posedness of linear complementarity systems. In *in Proc. of the IEEE Conference on Decision and Control*, pages 3037–3042, Phoenix, United States, 1999.

[57] M. Heertjes, N. van de Wouw, E. Pastink, A. Pavlov, H. Nijmeijer, and M. Steinbuch. Performance of variable-gain controlled optical storage drives. In *Proc. of the American Control Conf.*, pages 6–12, Minneapolis, Minnesota, USA, 2006.

[58] M.F. Heertjes. *Controlled Stabilization of Long-Term Solutions in a Piece-wise Linear Beam System*. PhD thesis, Eindhoven University of Technology, Einhoven, The Netherlands, 1999.

[59] M.F. Heertjes and M. Steinbuch. Stability and performance of variable gain controllers with application to a DVD storage drive. *Automatica*, 40:591–602, 2004.

[60] R.H.A. Hensen. *Controlled mechanical systems with friction*. PhD thesis, Eindhoven University of Technology, Eindhoven, The Netherlands, 2002.

[61] D.J. Inman, M. Ahmadian, and R.O. Claus. Suppressing plate vibrations with smart materials. In *Proc. of the 71st Shock and Vibration Symposium*, Arlington, 2000.

[62] D.J. Inman and T. Hegewald. Simultaneous active damping and health monitoring of aircraft panels. *International Congress on Sound and Vibration*, 12:775–783, 2000.

[63] A. Isidori. *Nonlinear Control Systems*. 3rd edition, Springer-Verlag, New York, USA, 1995.

[64] M. Janković, M. Larsen, and P. Kokotović. Master-slave passivity design for stabilization of nonlinear systems. In *Proc. of the American Control Conference*, volume 2, pages 769–773, San Diego, California, USA, June 1999.

[65] J.D. Jansen. Non-linear rotor dynamics as applied to oilwell drillstring vibrations. *Journal of Sound and Vibration*, 144(1):115–135, 1991.

[66] J.D. Jansen and L. van den Steen. Active damping of self-excited torsional vibrations in oil well drillstrings. *Journal of Sound and Vibration*, 174(4):647668, 1995.

[67] M. Johansson and A. Rantzer. Computation of piecewise quadratic Lyapunov functions for hybrid systems. *IEEE transactions on automatic control*, 43(4):555–559, 1998.

[68] R. Johansson and A. Rantzer. *Nonlinear and Hybrid Systems in Automotive Control*. Springer, 2002.

[69] A. Juloski. *Observer Design and Identification Methods for Hybrid Systems: theory and experiments*. PhD thesis, Eindhoven University of Technology, Eindhoven, The Netherlands, 2004.

[70] A. Juloski, M. Heemels, and S. Weiland. Observer design for a class of piecewise affine systems. In *Proc. of IEEE Conf. Decision and Control*, volume 3, pages 2606–2611, Las Vegas, Nevada, USA, 2002.

[71] A.Lj. Juloski, W.P.M.H. Heemels, and G. Ferrari-Trecate. Data-based hybrid modelling of the component placement process in pick-and-place machines. In *Control Engineering Practice*, volume 12(10), Sointhold, France, 2004.

[72] H.K. Khalil. *Nonlinear systems, 3nd ed.* Prentice Hall, New Jersey, 2002.

[73] A.N. Kolmogorov and S.V. Fomin. *Introductory real analysis*. Prentice Hall, 1970.

[74] M.V. Kothare, V. Balakrishnan, and M.A. Morari. Robust constrained model predictive control using linear matrix inequalities. In *Proc. of the American Control Conf.*, Baltimore, Meryland, USA, 1994.

[75] N.E. Leonard P. Krishnaprasad. Adaptive friction compensation for bidirectional low-velocity position tracking. In *Proc. of the* 31^{st} *IEEE Conf. on Decision and Control*, pages 267–273, Arizona, USA, 1992.

[76] H.G. Kwatny, C. Teolis, and M. Mattice. Variable structure control of systems with uncertain nonlinear friction. *Automatica*, 38(7):1251–1256, 2002.

[77] D. C. Lalanne. *Mechanical Vibration and Shock*, volume III. New York, 2002.

[78] R.I. Leine, D.H. Campen, and W.J.G. Keultjes. Stick-slip whirl interaction in drilling-string dynamics. *ASME Journal of Vibration and Acoustics 124*, 124(2):209–220, 2002.

[79] R.I. Leine and Ch. Glocker. A set-valued force law for spatial coulomb-contensou friction. *European Journal of Mechanics A/Solids*, 22:193216, 2003.

[80] R.I. Leine and H. Nijmeijer. *Dynamics and Bifurcations in Non-Smooth Mechanical Systems*. Springer-Verlag, 2004.

[81] G.A. Leonov, D.V. Ponomarenko, and V.B. Smirnova. *Frequency-domain methods for nonlinear analysis - theory and applications*. World Scientific, Singapore, 1996.

[82] D. Liberzon. *Switching in systems and control*. Birkhauser, Boston, 2003.

[83] J. Lygeros, K. H. Johansson, S. N. Simic, J. Zhang, and S. Sastry. Dynamical properties of hybrid automata. *IEEE Transactions on Automatic Control*, 48:2–17, 2003.

[84] N. Mallon, N. van de Wouw, D. Putra, and H. Nijmeijer. Friction compensation in a controlled one-link robot using reduced-order observer. *IEEE Transactions on Control Systems Technology*, 14(2):374–383, 2006.

[85] M. Meijboom. Non-model-based friction compensation of a system with non-collocated friction. Master's thesis, Technische Universiteit Eindhoven, Eindhoven, DCT nr. 2005.99, July 2005.

[86] N. Mihajlović. Torsional and lateral vibrations in flexible rotor systems with friction. *PhD thesis, Eindhoven University of Technology.*, 2005.

[87] N. Mihajlović, A. A. van Veggel, N. van de Wouw, and H. Nijmeijer. Analysis of friction-induced limit sysling in an experimental drill-string system. *ASME Journal of Dynamic Systems, Measurements and Control*, 126(4):709–720, 2005.

[88] N. Mihajlović, N. van de Wouw, M.P.M. Hendriks, and H. Nijmeijer. Friction-induced limit cycling in flexible rotor systems: an experimental drill-string set-up. *Nonlinear Dynamics*, 6(3):273–291, 2006.

[89] J.J. Moreau. *Standard inelastic shocks and the dynamics of unilateral constraints*. Number 288. Unilateral Problems in Structural Analysis, Springer Verlag, 1985.

[90] J.J. Moreau. *Bounded variation in time*. In J.J Moreau, P.D. Panagiotopoulos, and G. Strang, editors, Topics in Nonsmooth mechanics, Birkhuser, Basel, 1988.

[91] J.J. Moreau and P.D. Panagiotopoulos. *Unilateral contact and dry friction in finite freedom dynamics*. Number 302. Springer Verlag, 1988.

[92] E.M. Navarro-Lopez and R. Suarez. Practical approach to modelling and controlling stick-slip oscillations in oilwell drillstrings. In *Proc. of ICCA*, volume 2, pages 1454–1460, 2004.

[93] E.M. Navarro-Lopez and R. Surez-Cortez. Practical approach to modelling and controlling stick-slip oscillations in oilwell drillstrings. In *Proc. IEEE International Conf. on Control Applications*, volume 2, pages 1454–1460, Taipei. Taiwan, 2004.

[94] I. Necoara, B. De Schutter, W.P.M.H. Heemels, s. Weiland, M. Lazar, and T.J.J van den Boom. Control of pwa systems using a stable receding horizon method. In *Proc. of the 16th IFAC conf.*, pages 1–6, Prague, Czech Republic, 2005.

[95] H. Nijmeijer and A. van der Schaft. *Nonlinear Dynamical Control Systems*. Springer-Verlag, New York, USA, 1990.

[96] H. Olsson and K.J. Astrom. Friction generated limit cycles. In *Proc. of Control Applications*, pages 798–803, Dearborn, 1996.

[97] H. Olsson, K. J. strm, C. Canudas de Wit, M. Gafvert, and P. Lischinsky. Friction models and friction compensation. *European Journal of Control*, 4(3):176–195, 1998.

[98] A. Pavlov, A. Pogromsky, N. van de Wouw, and H. Nijmeijer. Convergent dynamics, a tribute to Boris Pavlovich Demidovich. *Systems and Control Letters*, 52:257–261, 2004.

[99] A. Pavlov, A. Progromsky, N. van de Wouw, and H. Nijmeijer. On convergence properties of piecewise affine systems. In *Proc. of the 5th EUROMECH Nonlinear Oscillations Conference (ENOC)*, Eindhoven, The Netherlands, 2005.

[100] A. Pavlov, N. van de Wouw, and H. Nijmeijer. Convergent piecewise affine systems: analysis and design part I: continuous case. In *Proc. of the 44th IEEE Conference on Decision and Control and European Control Conference ECC*, pages 5391–5396, Sevilla, Spain, 2005.

[101] A. Pavlov, N. van de Wouw, and H. Nijmeijer. Frequency response functions and bode plots for nonlinear convergent systems. In *Proc. of the 45th IEEE Conference on Decision and Control*, pages 3765–3770, San Diego, USA, 2006.

[102] A. Pavlov, N. van de Wouw, and H. Nijmeijer. *Uniform Output Regulation of Nonlinear Systems*. Birkhäuser, Berlin, 2006.

[103] A.V. Pavlov, A.Y. Pogromsky, N. van de Wouw, and H. Nijmeijer. On convergence properties of piecewise affine systems. *International Journal of Control*, accepted, 2007.

[104] D.R. Pavone and J.P. Desplans. Application of high sampling rate downhole measurements for analysis and cure of stick-slip in drilling. In *SPE Annual Technical Conf. and Exhibition*, pages 335–345, 1994.

[105] F. Pfeiffer and Ch. Glocker. *Multibody Dynamics with Unilateral Contacts*. John Wiley & Sons, New York, 1996.

[106] F. Pfeiffer and Ch. Glocker. *IUTAM Symposium on Unilateral Multibody Contacts*, volume 72. SOLID MECHANICS AND ITS APPLICATIONS,Kluwer Academic Publishers, 1999.

[107] F. Pfeiffer and M. Hajek. Stick-slip motions in turbine blade dampers. *Philosophical Transactions of the Royal Society of London, No.1651*, 338:503–517, 1992.

[108] D. Putra. Control of limit cycling in friction mechanical systems. *PhD thesis, Eindhoven University of Technology.*, 2004.

[109] A. Rantzer and M. Johansson. Piece-wise linear quadratic optimal control. *IEEE transactions on automatic control*, 45(4):629–637, 2000.

[110] F. Ricciardelli. Prediction of the response of suspension and cable-stayed bridge towers to wind loading. *Journal of wind engineering and industrial aerodynamics*, 64:145–159, 1996.

[111] R.T. Rockafellar and R.J.B. Wets. *Variational Analysis*. Springer, 1997.

[112] L. Rodrigues, A. Hassibi, and J.P. How. Output feedback controller synthesis for piecewise-affine systems with multiple equilibria. In *Proc. of the American control conf.*, pages 1784–1789, 2000.

[113] L. Rodrigues and J.P. How. Observer-based control of piecewise-affine systems. In *Proc. of the 40th IEEE Conf. of Decision and Control*, volume 76, pages 459–477, Orlando, Florida USA, 2001.

[114] E. Ryan. A universal adaptive stabilizer for a class of nonlinear systems. *Systems & Control Letters*, 16(3):209–218, 1991.

[115] P. Sananikone, O. Kamoshima, and D.B. White. A field method for controlling drillstring torsional vibrations. In *IADC/SPE Drilling Conf.*, pages 443–452, 1992.

[116] S. Sastry. *Nonlinear systems: Analysis, Stability and Control*. Springer, New York, 1999.

[117] S. Sastry and T.A. Henzinger. *Hybrid Systems: Computation and Control*. Number 1386. Springer Verlag, 1985.

[118] E.B. Sontag. A Remark on the Converging-Input Converging-State Property. *IEEE Transactions on Automatic Control*, 48(2):313–314, 2003.

[119] E.D. Sontag. Non-linear regulation: the piecewise linear approach. *IEEE Transactions on Automatic Control.*, 26:346–357, 1981.

[120] E.D. Sontag. On the input-to-state stability property. *European J. Control*, 1:24–36, 1995.

[121] S. Tafazoli and C.W. de Silva P.D. Lawrence. Friction estimation in a planar electrohydrolic manipulator. In *Proc. of the IEEE ACC*, volume 5, pages 3294–3298, Baltimore, USA, 1994.

[122] H.G. Tanner and K.J. Kyriakopoulos. Backstepping for nonsmooth systems. *Automatica*, 39(7):12591265, 2003.

[123] A. Taware, G. Tao, N. Pradhan, and C. Teolis. Friction compensation for a sandwich dynamic system. *Automatica*, 39(3):481–488, 2003.

[124] J.M.T. Thompson and H.B. Stewart. Nonlinear dynamics and chaos; geometrical methods for engineers and scientists. *John Wiley and Sons Ltd.*, 1986.

[125] J. Tlusty. *Manufacturing processes and equipment*. Prentice Hall, Upper Saddle River, NJ, USA, 2000.

[126] W. van Bokhoven. *Piecewise linear modeling analysis*. Kluwer Academic Publisher, 1981.

[127] D.H. van Campen, R.H.B. Fey, F.P.H. van Liempt, and A. de Kraker. Steady-state behaviour of a solar array system with elastic stops. *In F.C. Moon, editor, Proc:IUTAM Symposium on New Applications of Nonlinear and Chaotic Dynamics in Mechanics, Kluwer Academic Publishers.*, pages 303–312, 1998.

[128] N. van de Wouw and R.I. Leine. Attractivity of equilibrium sets of systems with dry friction. *Nonlinear Dynamics*, 35:65–82, 2004.

[129] N. van de Wouw, N. Mihajlović, and H. Nijmeijer. Friction-induced limit cycling in flexible rotor systems: An experimental drill-string set-up. In *Proc. of IDETC/CIE ASME 2005 International Design Engineering Technical Conf. & Computers and Information in Engineering Conf.*, Long Beach, California, USA, 2005.

[130] A. van der Schaft and H. Schumacher. *An Intruduction to Hybrid Dynamical Systems*, volume 251. Lect. Notes in Contr. and Inform. Sci. Springer Verlag, 2000.

[131] J.A. Imura van der Schaft. Characterization of well-posedness of piecewise-linear systems. *IEEE Transactions on Automatic Control*, 45:1600–1619, 2000.

[132] E.L.B. Van der Vorst. *Long terms dynamics and stabilization of nonlinear mechanical systems*. Einhoven, The Netherlands, 1996.

[133] M. Vidyasagar. *Nonlinear Systems Analysis*. Prentice Hall, Engelwood Cliffs, New Jersey, 1993.

[134] C. Walrath. Adaptive bearing friction compensation based on recent knowledge of dynamic friction. *Automatica*, 20(6):712–727, 1984.

[135] J.T. Wen. Time domain and frequency domain conditions for strict positive realness. *IEEE Transactions on Automatic Control*, 33(10):988–992, 1988.

[136] J. Willems. *Stability theory of Dynamical Systems*. Thomas Nelson and Sons Ltd., London, 1970.

[137] Yakubovich and G.A. Leonov. *Stability of stationary sets in control systems with discontinuous nonlinearities*. World Scientific, 2004.

[138] V.A. Yakubovich. Matrix inequalities method in stability theory for nonlinear control systems: I. absolute stability of forced vibrations. *Automation and Remote Control*, 7:905–917, 1964.

Summary

In this thesis, the focus is on two control problems for non-smooth systems. Firstly, the disturbance attenuation problem for piecewise linear (PWL) and piecewise affine (PWA) systems is studied. Here, we focus on applications in the field of perturbed flexible mechanical systems with PWL restoring characteristics. Secondly, the stabilization problem for Lur'e type systems with set-valued nonlinearities is examined. In the latter context, the focus is on the application area of mechanical systems with set-valued friction characteristics, where the friction is non-collocated with the control action. In this thesis, in order to deal with both the disturbance attenuation problem and the stabilization problem, observer-based output-feedback control strategies are proposed.

More specifically, the disturbance attenuation problem for perturbed PWL and PWA mechanical systems is an important control problem. Namely, the attenuation of the disturbances acting on these systems is important because it avoids damages to the structures and allows for increased system performance. Classical examples of mechanical systems with PWL and PWA restoring characteristics are tower cranes, suspension bridges, snubbers on solar panels on satellites, floating platforms for oil exploration, etc.

Therefore, a controller design strategy is proposed for a class of perturbed PWL/PWA systems based on the notions of convergence and input-to-state convergence. The control design aims at the performance of such control designs in terms of disturbance attenuation for the specific class of periodic disturbances and the more general class of bounded disturbances. Roughly speaking, a system that is convergent, has, for each bounded disturbance, a unique globally asymptotically stable steady-state solution that is bounded for all time. A system is input-to-state convergent for a class of bounded disturbances if it is convergent and ISS with respect to the system's unique steady-state solution. The input-to-state convergence property is instrumental in constructing output-feedback schemes. In the present work, we render a system convergent by means of feedback.

To guarantee the practical applicability of the convergence-based controllers, a saturation constraint is proposed that provides a guaranteed upper bound on the control input, given an upper bound for the disturbances and a set of initial conditions. Next, an ultimate bound for the system state given a bound on the disturbances is proposed. Finally, performance measures based on computed steady-state responses for a specific class of disturbances (in our case harmonic disturbances) are presented. The motivation for the choice of harmonic disturbances lies in the fact that in engineering practice many disturbances can be approximated by a finite sum of harmonic signals (or are even harmonic as in

systems with mass-unbalance). The ultimate objective of this part of the thesis is the implementation of the controller design strategy in an experimental environment, which implies that only measurements of a limited number of state variables will be available. Therefore, observers for PWL/PWA systems are used and a result that combines the controller and the observer in an output-feedback strategy is provided. The convergent-based controller design strategy is applied to an experimental piecewise linear system and its effectiveness is shown in experiments.

The stabilization of mechanical systems with friction is another challenging unsolved control problem because the presence of friction can induce unwanted phenomena such as self-sustained vibrations, chatter and squeal. These phenomena are unwanted in many engineering applications because they can destabilize a system and/or limit the system performance. Classical examples of mechanical systems with friction are industrial robots, drilling rigs, turbine blade dampers, accurate mirror positioning systems on satellites, printers and many more.

Therefore, a control design strategy is proposed for a class of discontinuous systems; namely Lur'e systems with set-valued mappings. Here the focus is on the application area of mechanical systems with discontinuous friction. These systems exhibit unwanted (stick-slip) limit cycling which we aim to avoid entirely by the control design. In this work, we consider the problem of non-collocated friction and actuation, which rules out the application of common friction compensation techniques. The control design strategy proposed here is based on the notion of passivity and the Popov criterion. In addition to that, it is shown that the resulting closed-loop system is robust with respect to uncertainties in the discontinuous friction model under some mild constraints for the model that describes the friction. Once again, the aim is to implement this strategy on a mechanical experimental set-up with limited measurements. Therefore, an observer for Lur'e systems with multi-valued mappings is used as a state estimator and a result that combines the controller and the observer in an output-feedback strategy is provided. The passivity-based controller design strategy is implemented on a dynamic rotor system with friction in one of its components. The implemented output-feedback controller is evaluated in both simulations and experiments.

Generally speaking, to show the strengths, weaknesses and potential of output-feedback controllers beyond their theoretical importance, it is indispensable to evaluate them in experimental and industrial setups. As such the presented case studies can be considered as benchmarks for the proposed observer-based controller designs for non-smooth and discontinuous systems. The value of non-smooth and discontinuous models and observer-based controllers is also evidenced by this work, as it demonstrates the effectiveness for real-life applications.

Output-feedback design for non-smooth mechanical systems:
Control synthesis and experiments

Samenvatting

Dit proefschrift betreft de studie van een tweetal regelproblemen voor niet-gladde en discontinue dynamische systemen. Eerst wordt het storingsonderdrukking-probleem voor stuksgewijs affiene en stuksgewijs lineaire systemen bestudeerd. Hierbij richten we ons met name op toepassingen van flexibele mechanische systemen met stuksgewijs lineaire stijfheidkarakteristieken en externe tijdsvariërende excitaties. Als tweede wordt het stabilisatieprobleem voor Lur'e systemen met meerwaardige niet-lineariteiten bestudeerd. Hierbij concentreren we ons op het applicatiegebied van mechanische systemen met wrijvingskarakteristieken beschreven door meerwaardige functies, waarbij de regelactie en de wrijving op verschillende plaatsen in het systeem aangrijpen. Om deze twee problemen aan te pakken, worden in dit proefschrift waarnemergebaseerde uitgangsterugkoppelingen ontworpen.

De storingsonderdrukking voor stuksgewijs lineaire/affiene systemen onder externe excitatie is een belangrijk regelprobleem. De onderdrukking van verstoringen in dergelijke systemen is belangrijk om structuurschade te voorkomen en een hoge systeem (bijv. positionerings) prestatie te kunnen garanderen. Klassieke voorbeelden in deze context zijn hijskranen, hangbruggen, zonnepanelen (op satellieten) met eenzijdige veiligheidsstoppers, drijvende platformen voor de olie-industrie etc.

Als oplossing stellen we een ontwerpstrategie voor regelaars voor stuksgewijs lineaire/affiene systemen voor, welke gebaseerd is op de notie van convergente systemen (en dat van zogenaamde 'ingang-naar-toestand convergentie'). Het doel van het regelaarontwerp is de onderdrukking van, ten eerste, de specifieke klasse van periodieke verstoringen en, ten tweede, de meer generieke klasse van begrensde verstoringen. Een convergent systeem heeft, voor elke begrensde verstoring, een unieke globaal asymptotisch begrensde stabiele limietoplossing. Een systeem heeft de eigenschap van ingang-naar-toestand convergentie voor een klasse van begrensde verstoringen als het convergent is en het ingang-naar-toestand stabiel is met betrekking tot de unieke limietoplossing. De eigenschap van ingang-naar-toestand convergentie is met name bruikbaar bij het ontwerpen van een uitgangsterugkoppeling. In dit proefschrift, maken we een dynamisch systeem convergent door terugkoppeling.

Met het oog op de praktische toepassing van deze convergentiegebaseerde regelaars, wordt een beperking op de regelingang in rekening gebracht die garandeert dat een gegeven bovengrens op de regelactie niet wordt overschreden (gegeven een bovengrens voor de verstoringen en een verzameling van begincondities). Verder wordt, gegeven een bovengrens voor de verstoringen, een bovengrens voor de grootte van de toestandsrespons afgeleid. Bovendien, worden

prestatiematen gepresenteerd gebaseerd op limietoplossingen voor de klasse van harmonische verstoringen. De studie van deze specifieke klasse van verstoringen wordt gemotiveerd door het feit dat in de praktijk verstoringen vaak harmonisch zijn (denk aan verstoringen als gevolg van massaonbalans-gerelateerde excitaties) of benaderd kunnen worden door een eindige som van harmonische componenten. Het uiteindelijke doel van dit deel van het proefschrift is de implementatie van de ontwikkelde regelaars in een experimentele omgeving, waarin doorgaans slechts een beperkt aantal toestanden gemeten kunnen worden. Daarom worden waarnemers gebruikt die, samen met de ontwikkelde regelaars, een uitgangsterugkoppeling vormen. De convergentiegebaseerde regelaars zijn toegepast op een laboratorium opstelling die gemodelleerd kan worden als een stuksgewijs lineair systeem en de verbeterde prestatie van deze regelaar is in experimenten aangetoond.

De stabilisatie van mechanische systemen met wrijving is een ander uitdagend (en onopgelost) regelprobleem, aangezien wrijving ongewenste trillingen kan veroorzaken. Deze trillingen zijn ongewenst omdat ze een systeem kunnen destabiliseren en/of de prestatie kunnen beperken. Klassieke voorbeelden zijn industriële robots, rotorinstallaties, dempers voor turbinesystemen, positioneringssystemen voor spiegels op satellieten, printers en vele andere.

Daarom ontwikkelen we in dit proefschrift een regelstrategie voor een klasse van discontinue systemen, namelijk Lur'e systemen met meerwaardige niet-lineariteiten. Hierbij ligt de focus op de toepassing in mechanische systemen met discontinue wrijvingskarakteristieken. Dergelijke systemen kunnen ongewenste 'stick-slip' trillingen vertonen welke door middel van een goed ontworpen regelaar geheel onderdrukt dienen te worden. In het proefschrift, beschouwen we bovendien het probleem waarbij de actuatie en de wrijving niet op dezelfde plaats in het systeem aangrijpen. Daardoor is de toepassing van standaard wrijvingscompensatietechnieken niet mogelijk. De voorgestelde regelstrategie is gebaseerd op de notie van passiviteit en het Popov-criterium. Bovendien laten we zien dat het geregelde system robuust is met betrekking tot onzekerheden in het wrijvingsmodel (onder milde aannames met betrekking tot het wrijvingsmodel). Wederom ligt het uiteindelijke doel bij de implementatie van de ontwikkelde regelaars in een experimentele omgeving met beperkte toestandsmetingen.
Daarom wordt een waarnemer voor Lur'e systemen met meerwaardige niet-lineariteiten gebruikt en een resultaat voorgesteld, dat deze waarnemer combineert met de ontworpen regelaar tot een uitgangsterugkoppeling. De regelstrategie is geïmplementeerd op een rotor-dynamisch systeem met wrijving. De prestatie van de ontwikkelde regelstrategie is aangetoond in zowel simulaties als experimenten.

Om de voordelen, nadelen en de potentie van uitgangsterugkoppeling-regelaars voor niet-gladde en discontinue systemen aan te tonen is het onontbeerlijk deze regelaars te evalueren in experimentele en industriële systemen. De in dit

proefschrift gepresenteerde studies kunnen als 'benchmarks' voor de ontworpen regelaars voor niet-gladde systemen beschouwd worden. De waarde van niet-gladde modellen en de ontworpen regelaars wordt door dit werk benadrukt, daar het de effectiviteit ervan in toepassingen aantoont.

Acknowledgments

At the end of this thesis I would like to thank all the people who supported me to complete this work.

Firstly, I would like to thank my promotor Prof. Henk Nijmeijer for giving me the opportunity to do a Ph.D. in the field of control for non-smooth systems. His constructive criticism for my work and my personality helped me to improve as a researcher and as a person. My special words of gratitude are to my supervisor and very good friend Dr. Nathan van de Wouw. Nathan thank you for your time, effort, patient and understanding. I consider myself very lucky for the fact that you were the supervisor my Ph.D. work.

I would also like to thank my second supervisor Dr. Maurice Heemels for his useful advices and comments on my thesis. His expertise in mathematics helped me to significantly improve this thesis.

I would like to thank the members of my core committee dr. Bernard Brogliato, Prof. Daniel Rixen and Prof. Maarten Steinbuch for their time to read my thesis and their useful comments.

A special thanks goes to the master students JanKees de Bruin, Niels de Bont and Ron Wouters for their valuable contribution in the experimental part of my Ph.D. work.

Many thanks to Ronald, Wilbert, Niels, Nenad, Marieke, Björn and Rob for being good friends and colleagues. I would also like to thank Ram for his friendship and his valuable help in the DISC courses.

My gratitude goes to my very good friends Effie, Eleni, Athon, Thomas, Mark, Mircea and George for being always next to me in the difficult moments of the last four years.

I would like to thank Eirini, Maria, Melina, Iciar, Arianna, Samuil and Natasha for all the good times we had together.

I am very grateful to my brother Konstantinos who has always been a bright example for me and whose advises were more than valuable in my life. I would also like to thank Eva for her understanding and encouragement in finishing my thesis. A special thanks goes to my brother Kyriakos for his company and his endless enthusiasm to help me in all sorts of difficulties I faced in my life.

Last but not least, I am entirely indebted to my parents Ioannis and Aikaterini for their support, love and for all the sacrificies they made for me and my brothers.

Curriculum vitae

Apostolos Doris was born in Thessaloniki, Greece the 31^{st} of July 1976. Upon completion of his studies at the 21^{st} Gymnasium of Thessaloniki in 1994, he started his academic career in Forestry at the Technological Education Institute of Karpenisi, Greece. In 1995, he moved to the University of Ioannina to study Physics. In 1996, he started his studies in the Mechanical Engineering Department of Aristotle University of Thessaloniki. He received his master degree with specialization in Dynamics of Mechanical systems in March 2002. In September 2002, he was employed as a research scientist in the Dynamics and Control Group of the Department of Mechanical Engineering in the Technical University of Eindhoven, The Netherlands. Since April 2003, he is a Ph.D. student in that group. The results of his Ph.D. research are given in this thesis.